Uranium series, major and trace element geochemistry of lavas from Tenerife and Lanzarote, Canary Islands

Thesis

UNRESTRICTED

Uranium Series, Major and Trace Element Geochemistry of Lavas from Tenerife and Lanzarote, Canary Islands

A thesis presented for the degree of Doctor of Philosophy

by

LOUISE ELANA THOMAS

B.Sc. (Hons.) *London* 1993

Department of Earth Sciences

The Open University

October 1998

But when, in forming a theory of the earth, a geologist shall indulge his fancy in framing, without evidence, that which had preceded the present order of things, he then either misleads himself, or writes a fable for the amusement of his reader.

James Hutton 1726 -1797 'a private gentleman' and physican
Theory of the Earth vol I 280-281 vol ii 540-564 1795.

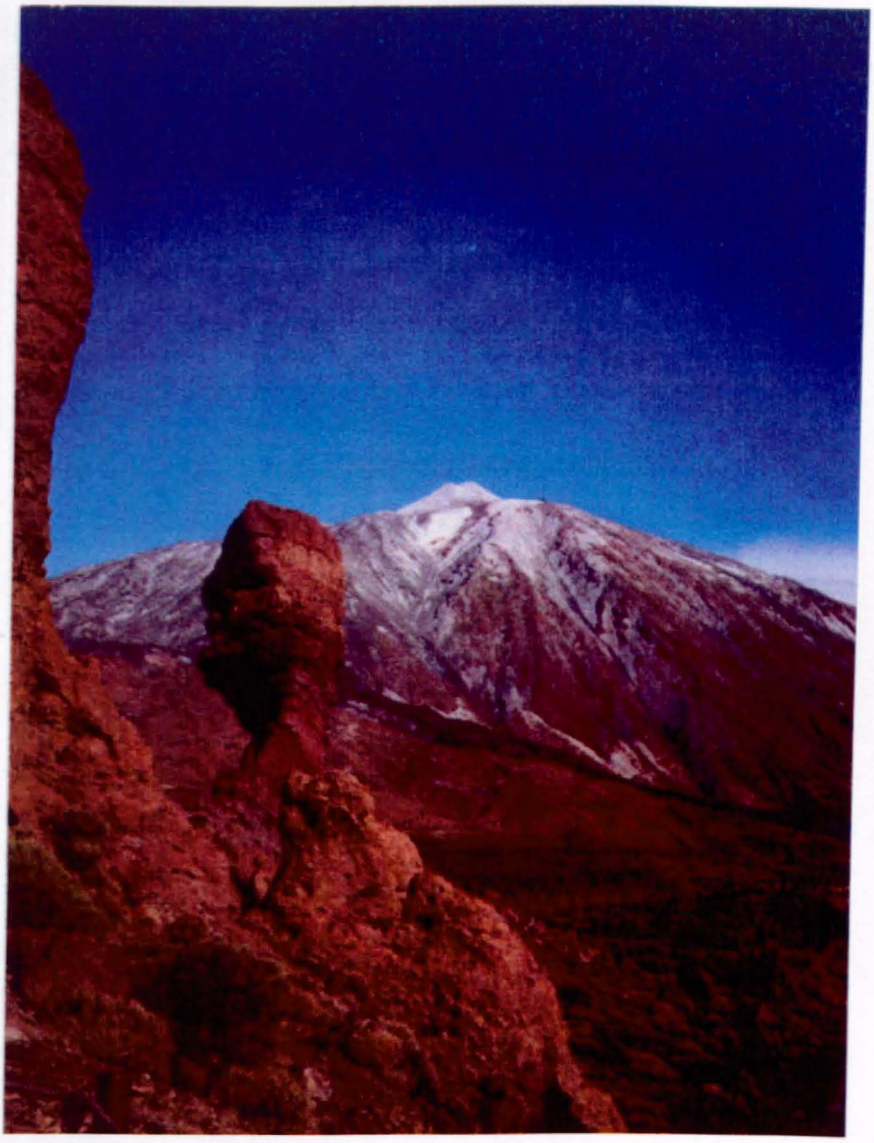

Plate I

Mt Teide towering above the Roques de Garçia
The dark brown lavas flows in the foreground are part of the 1492 eruption

Abstract

Ocean Islands Basalts provide important windows into the compositional variations of the Earth's mantle, which in turn constrains models for mantle convection and evolution.
The Canary Islands show contrasting styles of eruption and evolution of magmas in an ocean island setting. U-Th-Ra disequilibria have been used to constrain rates and timescales of melt generation and differentiation beneath ocean islands, and to estimate the buoyancy flux, potential mantle temperature and the depth and degree of melting. The Canary Islands provide a rare opportunity to observe U-Th-Ra disequilibrium, because they are underlain by a region of low buoyancy flux, and were expected to show significant disequilibrium.

Tenerife is underlain by numerous magma chambers, in which magmas have time to differentiate from basanites to phonolites, erupting to form large strato-volcano complexes. The fissure and small vent eruptions of unusually primitive basanites and alkali basalts from Lanzarote show little evidence of magma chambers, unless of substantial size and longevity at depth. The U-Th results indicate that lavas underwent rapid transport from the melt region.

The historic and recent pre-historic eruptions (1824, 1730-36, Corona) from Lanzarote have some of the most primitive compositions found on oceanic islands with low SiO_2 contents (< 51 %), Mg numbers of 67-74 and high Cr and Ni contents. The rocks are restricted in Sr, Nd and Pb isotopes, being displaced from MORB towards the HIMU OIB field. The major and trace elements have been modelled by mixing a deep smaller degree (1%) melt and a shallower larger degree (4%) melt. Negative K anomalies were observed in the small degree melts indicating that melt generation may have continued at a shallow level, perhaps to within the lithospheric mantle with melting in the presence of residual phlogopite. The Lanzarote source was modelled as a mixture of HIMU and EMII asthenospheric mantle, with a small contribution from a shallow, lithospheric source. Thermal erosion of the lithospheric mantle is required for melting at depths (58 and 73 km) modelled from the major and trace elements. The Lanzarote lavas exhibit significant ($^{230}Th/^{238}U$) disequilibrium with ^{230}Th excesses of 6 - 81%. This was modelled by dynamic melting giving a calculated melt rate of 0.125×10^{-3} $kg.m^{-1}.yr^{-1}$, a timescale of melt generation (matrix transfer time) of 270 ka for the 1% melt and 1,100 ka for the 4 % melt. A consistent upwelling rate of 1 $cm.yr^{-1}$ and an assumption that the melting process has remained consistent over tens of km at depth.

The Teide-Pico Viejo complex lavas have undergone fractionation and mixing to form compositions from basanite to phonolite. Crystallising phases differ in the Pico Viejo series, where amphibole is dominant in the more evolved lavas, and Pico Teide series, where olivine in the major control. The more evolved lavas require assimilation and fractional crystallisation to explain the range in $^{87}Sr/^{86}Sr$. ($^{230}Th/^{238}U$) ranges from 1.004-1.39 and gives information regarding the timescales of differentiation within the magma chambers, not least because the youngest mafic rocks have the highest ($^{230}Th/^{238}U$) and the most evolved phonolites have the lowest. The timescale of differentiation from basanite to phonolite is of the order of 150,000 years, which links to the periodicity of the eruption cycles on the island. A Ra-Th 'pseudo' whole rock isochron gave an age of fractionation for the Montaña Blanca eruption of 2.3 ka ± 80, which is a maximum of 300 years prior to eruption, indicating that fractionation of plagioclase as a possible trigger of an eruption.

Acknowledgements

Firstly many thanks go to my supervisors Chris Hawkesworth and Peter van Calsteren, for their unflappable calm during the last three years and 10 months, their supervisory 'chats' have kept this PhD on the right (-ish) road! Chris has always been there with "have you thought about?" when you thought you'd thought about everything there was to think about. Peter has been a god of many a dynamic melting model and of course, where would the mass specs. be without you. Seriously though, without your continuous help and encouragement this project would not have been possible.

Secondly many thanks to my examiners Steve Blake and Ray MacDonald for thoroughly going through this thesis and for helpful comments and suggestions.
Thanks to David Peate, Simon Turner and Nick Rogers who were always available for chats, to bounce numerous ideas off, and who understood when Radium didn't work or when the Th 'U' wouldn't run.

A big thanks to Mabs, Peter and Jo who make the lab THE most happening place to be (*certainly in the case of chocolate, ice cream, wine and the infamous brownie competition....*), and of course fellow U-Th silicates workers including Pete, Rob, Dave, Thomas, Simon, Yiming, Rhino, Georg, and those who had the common sense to stay away from the U-Th lab, but not quite away from the other chemistry labs, Linda (*my fellow chocolate lab party person*), Helen, Elric and Johnny (*also my long-suffering housemate - cheers babe*), and those of the Re-Os and Sm-Nd posses Jessica (*good escape there !*), Anthony, Ian, Mark, Aussie Bruce and Yvonne; and Derek, Christophe and Gav. Good luck to the next generation of U-Th silicate people, Bruce, Cheryl, and Yvonne. I hope the lab is kind to you!

Fieldwork in Lanzarote was ably assisted by Peter and Corrie (who devoted her half-term holiday) and thanks to Giray Ablay for fieldwork in Tenerife and discussion on the results that followed (*and for changing the nomenclature of the samples in late September 1998*!). Giray is also to be thanked, along with Joan Marti for the expansion of my knowledge of Canarian restaurants and specialities of the food and drink varieties. Thanks also go to AGU and CSIC (Barcelona) for funding a Tenerife conference/workshop each.

To those who lurk downstairs, many thanks go to John H. for money matters, Peter W. and John W. for XRF analysis, Kay and Brian for thin sections, Nick for INAA analyses, and Mike Henty (*for making sure that I spent money on minerals*). To those who live upstairs, many thanks to Andy and John in Cartography for those last minute slides, Janet for those calming comments, Rita and Anita.

These acknowledgements would not be complete without a large helping of thanks to my officemates past and present, Adam (*no, I am not the secretary!*), the kiwis Paul and Bill, Christophe, Sair, Rob (*sarcastic comments!*) Helen (*how much coffee!*) and Georg (*whose Germanic antics have aided writing up!*). Not forgetting of course the many people who brightened life at the OU, and outside including those mentioned above and Liz, Sarah and Jane, Mark, Tubbs, and Sair. Cheers to Jus, Andy and Charlotte for dragging me away from Milton Keynes occasionally and for actually managing to survive a visit and returning more than once.

Finally most of all thanks to my parents, for the love, understanding and much needed support they've given me over the years: (thanks to my Mum for providing a lifetime's encouragement, and Dad for persuading me in his usual fashion that maybe I shouldn't give up on chemistry ...). Ta to Cris my brother, for not having a clue about what I'm doing... good luck in the navy babe.) And last but not least love and thanks to Nick for just being there, and putting up with me over the last two and a half years.

CHAPTER ONE

INTRODUCTION TO IDEAS AND CONCEPTS.....1

List of Figures

Chapter 1

Chapter 2

Chapter 3

Chapter 4

List of Tables

Table of Plates

CHAPTER ONE

Introduction to Ideas and Concepts

1.1. Thesis Structure

This thesis consists of five chapters, commencing with a basic introduction (Chapter 1) which introduces some of the concepts and ideas that are in use throughout, to gain insights into ocean island magmatism and U-series isotopes. This chapter introduces the locations and models of intraplate ocean island magmatism and a comparison with what is believed to be the better understood scenario of Mid Ocean Ridge magmatism. It deals with definitions of the mantle sources (such as asthenosphere and lithosphere), that are widely used in discussion of oceanic magmatism and the different contributing factors to mantle 'source' composition, such as subducted slab material and sediments. This chapter provides an introduction to the types of melting models, which are used routinely for Mid Ocean Ridge Basalts (MORB), such as batch and fractional melting, mixing and dynamic melting models. These models have been modified by various authors (e.g. Williams and Gill, 1989; Spiegelman and Elliott, 1993; van Calsteren and Hawkesworth (in prep.), 1999) to allow modelling of Ocean Island Basalts (OIB), in an attempt to understand the processes of melt generation and differentiation. The use of U-series isotopes in assessing the rates and timescales of melting is also examined. A section looking at magma chambers and magma chamber processes is also included here, as the presence of a magma chamber causes a major difference in the types of modelling which can be applied to the rocks. Finally, the region of study: the Canary Islands is introduced, the geological setting and evolution is discussed along with the debate of the origin of the Canaries.

Chapter 2 consists of a detailed account of the analytical techniques used for U-Th isotope measurements and the development of the techniques for the analysis of Radium. A

brief introduction to the radioactive decay scheme is presented, along with the equations and Equiline or Isochron diagrams used for the U-Th-Ra system.

Descriptions of the individual sample localities, mineralogy and petrology are presented in Appendix B.

Chapter 3 has been re-written from a paper: Melt Generation beneath Ocean Islands: a U-Th-Ra isotope study from Lanzarote in the Canary Islands. L.E. Thomas, C.J. Hawkesworth, P. van Calsteren, S. P. Turner and N.W. Rogers, accepted in March 1999 to the Allègre special volume of Geochimica et Cosmochimica Acta. This chapter includes location maps and a detailed geological evolution from Miocene to present day and deals with the geochemistry of an unusually primitive suite of samples from Lanzarote. Their major, trace element and isotopic geochemistry (Data tables in Appendix A) is discussed in detail and modal dynamic melting models are used in an attempt to model the results.

Chapter 4 presents the major, trace element and isotopic geochemistry of the Teide-Pico Viejo complex of Tenerife. An interpretation of the petrogenesis of the suite of rocks ranging in composition from basanite to phonolite has been recently presented by Ablay et al. (1998); however the isotopic geochemistry and in particular the U-Th and Th-Ra data result in a different slant to that previously reported. The story of Tenerife is very different from that of Lanzarote, not least due to the presence of magma chambers underlying the complex, which have been active in mixing and the evolution of magmas through time. Although presented in journal format, this chapter provides only the basis of a paper to be submitted on the isotopic geochemistry and evolution of the Teide-Pico Viejo complex in Tenerife.

The final chapter, Chapter 5, integrates the geochemistry of the individual islands, summarises differences and similarities and attempts to develop a consensus model for the evolution of the source of the Canary Islands. The chapter concludes with a summary of the rates and timescales of melting and upwelling and the controls on these processes modelled from the geochemistry of different ocean islands.

Published abstracts relating to this thesis are given in Appendix I.

1.2. Ocean Islands and Mid Oceans Ridges: Windows to the Mantle

Some 90% of present day volcanism is concentrated within or adjacent to zones of plate divergence, such as Mid Ocean Ridges, or convergence, such as subduction zones (Wilson, 1989). However intra-plate volcanism exists and ocean islands and seamounts are evidence of volcanic activity far from plate boundaries. Ocean islands are immense structures rising thousands of metres above the ocean floor. For example the summit of Mount Teide on Tenerife is at 3718 m above sea level, the water depth is between 3-4 km, and it is thought that the subaerial part of Tenerife represents only 8% of its total volume.

The origin of many of these ocean islands was proposed by Wilson (1963) to be a hotspot or plume, where magma rises from a fixed plume of buoyant upwelling mantle, feeding the surface volcanism. Burke and Wilson (1976) identified 122 hotspot ocean island chains (See Figure 1).

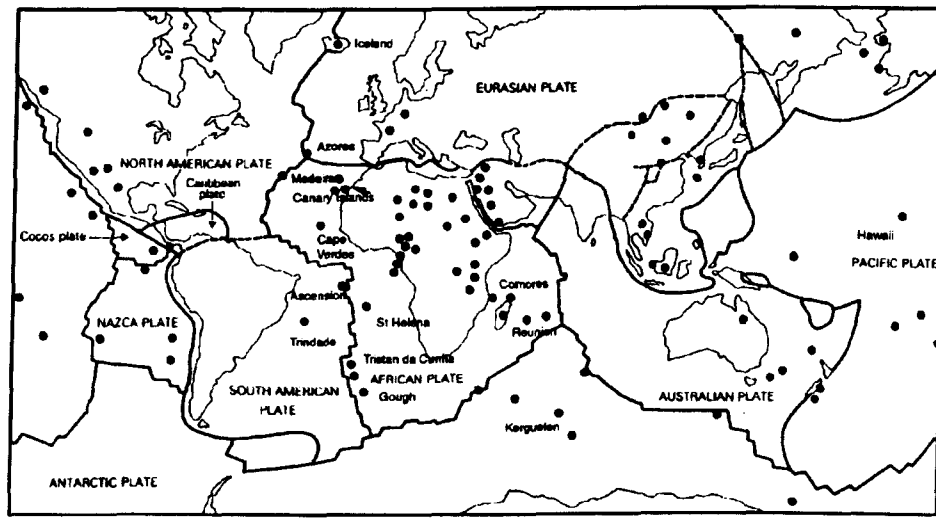

Figure 1.1. Location map of plates and hotspots (modified after Burke and Wilson, 1976; Wilson, 1989)

As the plate moves across the hotspot, the focus of activity shifts to a different position in the overlying plate, and over time forms a volcanic island chain. Such models have become readily accepted for island chains where the plate is rapidly moving across a hotspot, e.g. the Hawaiian-Emperor sea mount chain. However in regions of slower plate movement and hence slower ocean spreading, such as the Atlantic, the model has met with greater debate,

and there are those who propose purely tectonic origins such as rifting for certain ocean island magmatism (Wilson, 1989).

Ocean Island Basalts (OIB) and Mid Ocean Ridges Basalts (MORB) provide important windows into the compositional variations of the Earth's mantle, which in turn constrain models for mantle convection and evolution (e.g. McKenzie and O'Nions, 1995). OIB and MORB volcanism 'sample' the mantle to great depths, because solid state convection transports deep material into the shallow (30 - 100 km) melting region. It remains difficult to determine the depth of sampling of the source components recorded in OIB, but a number of recent studies (Wulff-Pedersen et al., 1996; Class and Goldstein, 1997; Neumann and Wulff-Pedersen, 1997; Thomas et al., 1999) have highlighted that some source components are present at comparatively shallow levels in the lithospheric upper mantle. In order to gain an understanding of the source of ocean islands, it is necessary to take into account the different types of material, which might contribute to the bulk source composition.

In the 1970's geochemists developed the idea of a chemically layered mantle, with an upper layer, depleted in incompatible elements and a lower fertile layer. It was found that there is a fundamental geochemical difference between MORB which are commonly sourced in mantle regions that are depleted in incompatible elements, and OIB which are less depleted or even enriched in incompatible elements and are inferred to be sourced at least in part from the deeper layer. When mantle material melts, it loses its incompatible elements, such as U and Th, as they preferentially enter the melt. The evidence of chemical heterogeneity in OIB suggests that they cannot be derived from similar sources to MORB and that they may be derived from source regions modified by recycling of the enriched lithospheric or crustal material into the mantle (Hofmann, 1997).

1.2.1. Models of Mantle Convection

Numerous models have been put forward for the structure of the Earth's mantle and for mantle convection. Some retain the concept of a two layer mantle, where the layers are kept separate by an intrinsic compositional density contrast or by a negative pressure-temperature slope at the phase transition at 660 km (Christensen, 1995). Plumes may originate from the base of the upper layer, but contain entrained material from the lower layer

(Allègre and Turcotte, 1985; Galer and O'Nions, 1985). In contrast, other models invoke whole mantle convection (Hart, 1988; Davies, 1990; Hart et al., 1992), where all plumes are generated from the core-mantle boundary and subducted lithosphere (see below) penetrates beneath the discontinuity at 660 km. Hybrid models involve elements of both classes of model, with plumes rising both from the core-mantle boundary and the 660 km discontinuity, and subducted lithosphere entering the convecting layers to different depths (e.g. Stein and Hofmann, 1994; McKenzie, 1985a; Watson and McKenzie, 1991; White and McKenzie, 1995; overview in Hofmann, 1997).

1.3. Source Components

A summary of the different components that may be involved in the source of OIB and how they might be recognised is detailed below. Ocean islands are less depleted and often more enriched in incompatible elements compared to MORB, as illustrated in Figure 1.2

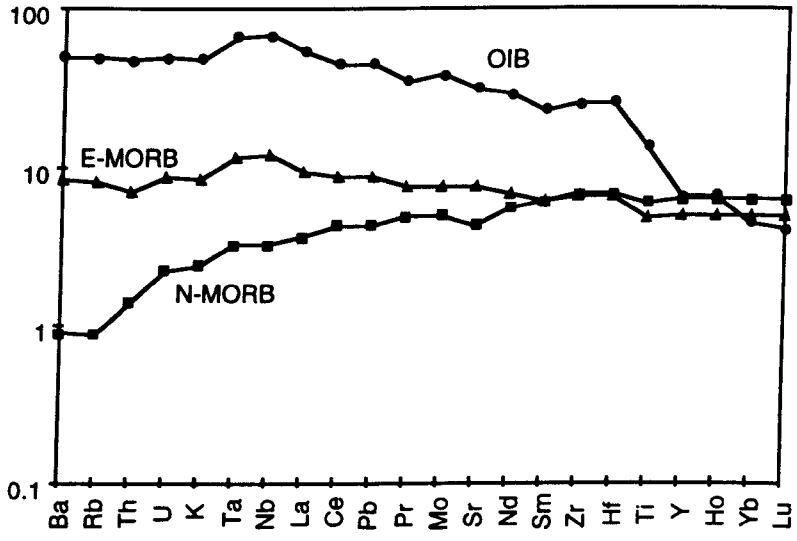

Figure 1.2. Mantle normalised incompatible element and rare earth element plot showing the differences between MORB (N = Normal and E = Enriched) and OIB. (Values for OIB, MORB and Primitive Mantle for normalisation - Sun and McDonough, 1989.)

1.3.1. The Asthenosphere

Mid ocean ridges are controlled largely by the geometry of the plates, and they should sample the upper most mantle, the asthenosphere, which rises passively under the spreading ridge. The depleted asthenosphere is a relatively weak region of the hot mantle (at

or near the melting zone). Its thickness is of the order of 100 km, but it is poorly defined as the internal strength increases gradually with depth. It is characterised by low seismic velocities and low viscosity relative to the overlying lithosphere. Typically N-type MORB are depleted in incompatible elements relative to bulk earth compositions (although P (plume) or E (enriched)-type MORB are the exception with some incompatible trace elements similar or enriched relative to bulk earth compositions). MORB are thought to originate from shallow levels in the asthenosphere, from a mantle reservoir depleted by previous episodes of crust formation. Mantle plumes originate at boundaries in the mantle at either the 660 km discontinuity or the core mantle boundary. Heating lowers the density of the plume relative to the surrounding mantle until it rises upwards. Melting in the mantle occurs in response to decompression both in upwelling mantle plumes and passively rising material at ridges.

A lower undepleted mantle layer is regarded as the major source reservoir of oceanic islands. This material may be primordial mantle, which has not been involved in melting to generate crust (Morgan, 1972). However this simple primordial mantle concept is a gross simplification and as the study of geochemical and isotopic signatures improved over the last 25 years, it became obvious that the OIB source reservoir must be envisaged as a mixture between primordial mantle and other components. The heterogeneity of oceanic magmatism (often best seen in isotopic compositions) has led to a taxonomy of 'source reservoirs', such as EMI, EMII and HIMU. Each of these is characterised by different isotope ratios and is thought to include contributions from different components, such as altered oceanic crust, lithosphere and metasomatised mantle. Perceptions over the origins of these source compositions need to take into account whether they can be generated by intra-mantle enrichment or metasomatic processes, or whether they require a contribution from deeply recycled continental or oceanic crust (Hawkesworth et al., 1979; Cohen and O'Nions, 1993; McKenzie and O'Nions, 1995; Hofmann, 1997).

1.3.2. The Lithosphere

The lithosphere is a term that has been mentioned a number of times already. In general terms, it is the cold outer rigid layer of the Earth that moves around as the tectonic plates. It includes the Earth's crust and a region of underlying mantle, which may be distinguished from the convecting upper mantle on the basis of trace elements and radiogenic

isotopes. The lithosphere is considered to be the part of the Earth that is affected by tectonic processes. It extends to depths of 120 - 150 km, although this varies with extension, compression and the age of the lithosphere and it can be thinned both thermally and mechanically. The term lithosphere (Parsons and McKenzie, 1978; McKenzie and Bickle, 1988; Davies and Richards, 1992 and Davies, 1994) is linked to its strength and, due to the thermal dependence of rheology, it also depends on temperature. In the lithosphere heat transfer is by conduction, whereas it is primarily by convection in the underlying asthenosphere (Figure 1.3). The lithosphere may be regarded as the upper thermal boundary layer of a convecting system, and so the material is isolated, enabling the development of enriched radiogenic isotope signatures in a way that is not possible in the underlying asthenosphere. However the overall geochemical and isotopic signatures for most OIB are thought to have been derived from source regions in the asthenospheric mantle.

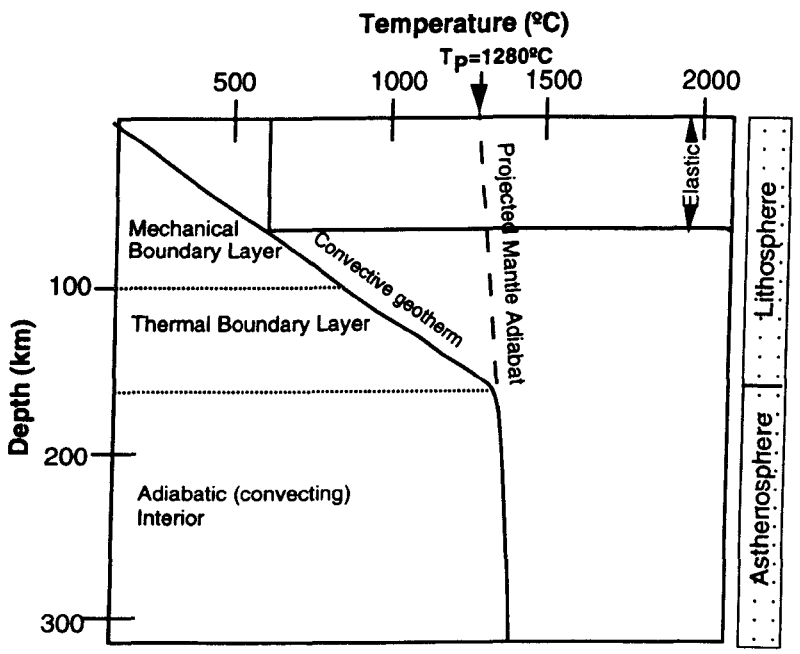

Figure 1.3. illustrates a schematic section through the asthenosphere and lithosphere showing the mechanical and thermal boundaries. The curved solid line is the horizontally averaged thermal structure of old oceanic lithosphere over normal asthenospheric temperature, (Potential temperature = 1280°C).

It is unlikely that any oceanic magmatism is generated totally within the lithosphere; however it is possible that the lithospheric mantle may contribute in the generation of OIB. As melts rise from the asthenosphere they may become trapped within the lithosphere, and may entrain certain geochemical signatures which can be identified in lavas, such as the

evidence of melting in the presence of phlogopite, which is unstable in the upwelling mantle (Mengel and Green, 1989).

During subduction, lithosphere is recycled into the asthenosphere down to the boundary layer at 660 km and perhaps deeper (Hart, 1988). The recycled lithosphere will mix with the asthenosphere, and over time the heterogeneities may be rehomogenized by convection (Allègre and Turcotte, 1986) and so the signature will become modified. At shallower levels subducted lithosphere may influence the source of magmatism, in particular in areas where subduction volcanism gives rise to island arcs.

The age of oceanic lithosphere underlying the Canary Islands varies from 150 Ma in the east to 175 Ma in the west (Verhoef et al., 1991; Roest et al., 1992). Since oceanic lithosphere becomes thermally stabilised after about 70-80 Ma, the depth to the region where isotherms become horizontal, i.e. the base of the lithosphere, is of the order of 100-125 km, and this does not change significantly for oceanic crust older than 70-80 Ma (Parsons and Sclater, 1977; Parsons and McKenzie, 1978).

1.3.3. Crust and Sediments

When the lithosphere is subducted at subduction zones, it takes fresh and altered oceanic crust, overlying sediments and fluid down into the underlying mantle. The main difference between the influences of the altered and unaltered oceanic crust, is that the altered crust would add more hydrous and exotic phases to the melting pot. Any sediment signature may be quickly removed from the source during subduction, as the sediments have a lower melting point; it is common to find sediment signatures in subduction zone volcanics (e.g. Turner et al., 1996).

1.3.4. Metasomatic Activity

Mantle metasomatism can modify the composition of the source reservoir. Metasomatism is the process of changing the bulk chemical composition of a rock, usually by infiltration of a fluid/melt, typically carbonatitic or hydrous fluids. The bulk composition of the metasomatised mantle will depend on the new minerals that form and the partition coefficients between those minerals and the metasomatic agent.

1.3.5. Sea Floor Spreading

Sea floor spreading generates large chemical heterogeneities, by extracting melt from the mantle, and forming a basaltic crust and a refractory residue.

1.3.6. Isotopic Source Components

Zindler and Hart (1986) recognised five end-member isotopic compositions in the mantle, which by a variety of mixing processes they suggested could explain most of the observed radiogenic isotope ratios in MORB and OIB. This has led to an improved understanding of the complexity of OIB; for example, Hoernle et al. (1991) proposed that the Gran Canaria source comprised at least 4 of these mantle components (HIMU, DM, EMI and EMII). These end member compositions are as follows:

a) Depleted Mantle (DM): Depleted mantle is characterised by high $^{143}Nd/^{144}Nd$, low $^{87}Sr/^{86}Sr$ and low $^{206}Pb/^{204}Pb$. It is the dominant component of most MORB and it is thought to occur at shallow levels in the asthenosphere.

b) HIMU Mantle: The μ-value is the ratio $^{238}U/^{204}Pb$. High $^{206}Pb/^{204}Pb$ and $^{208}Pb/^{204}Pb$ ratios observed in some ocean islands are coupled with low $^{87}Sr/^{86}Sr$ and intermediate $^{143}Nd/^{144}Nd$ suggesting a mantle source enriched in U and Th relative to Pb without an associated increase in Rb/Sr. This is a long-lived enrichment and a number of models have been proposed to explain the origin of this mantle reservoir. These include altered oceanic crust (Anderson, 1979), Pb extraction and storage in the lower crust (O'Nions et al., 1979; Cohen et al., 1980), loss of Pb from part of the mantle into the Earth's core (Dupre and Allègre, 1980) and the removal of Pb and Rb by mantle metasomatism (Menzies and Murthy, 1980; Hauri et al., 1993).

c) Enriched Mantle (EM): Enriched mantle is characterised by low $^{143}Nd/^{144}Nd$, variable $^{87}Sr/^{86}Sr$ and high $^{207}Pb/^{204}Pb$ and $^{208}Pb/^{204}Pb$ at a given $^{206}Pb/^{204}Pb$ value.

EM is divided into EMI, which has relatively low $^{87}Sr/^{86}Sr$ and EMII with high $^{87}Sr/^{86}Sr$. A striking EMII anomaly is the DUPAL anomaly identified by Hart (1984). For Pb isotopes this enriched mantle material is identified with respect to a Northern Hemisphere Reference Line (NHRL) defined by linear arrays on $^{207}Pb/^{204}Pb$ - $^{206}Pb/^{204}Pb$ and $^{208}Pb/^{204}Pb$ and $^{206}Pb/^{204}Pb$ plots for MORB and OIB. EMII may represent recycling of continentally derived sediment, continental crust, altered ocean crust or ocean-island crust. An alternative

model is one based on the similarity between subcontinental lithosphere and the enriched mantle features suggesting that the EMII may be due to mixing of the subcontinental lithosphere back into the convecting mantle. EMI has affinities with the lower crust and it might represent recycled lower crustal material, but an alternative hypothesis suggests that it is enriched by carbonatitic mantle metasomatism. Weaver (1991) proposed that EMI and EMII are produced by mixing between HIMU and subducted oceanic sediment.

d) PREMA (PREvalent Mantle reservoir): A surprising number of OIB and continental basalt suites have broadly similar radiogenic isotopes. It has been suggested that they were derived from similar source regions termed PREMA.

e) Bulk Earth: Primary Uniform Reservoir. It can be argued that some mantle material has the composition of bulk silicate earth, the hypothetical composition of homogeneous primitive mantle.

Hart et al. (1992) described another mantle reservoir termed FOZO (FOcus ZOne), which is a mantle reservoir with isotopic characteristics representative of the central or focal zone, but this parental reservoir is rarely sampled in pure form. The FOZO reservoir may be located in the lower mantle. Other locations discussed by Hart et al. (1992) include the upper mantle or within the boundary layer of the core-mantle or the 660 km boundary. These locations have been discarded due to the presence of high $^{3}He/^{4}He$ ratios in FOZO and the need for the reservoir to be over-entrained relative to DM, which would swamp the DM signature.

1.4. Rates and Timescales

Whatever the source characteristics of mantle derived basalts, geochemical signatures arrive at the surface having survived many processes, including partial melting, melt segregation, melt transport and subsequent differentiation to name a few. The effect of a new component introduced into the mantle will change through time, and convection may gradually re-set the isotopes and geochemistry, or the new component may be left untouched away from the convective cells, and only become incorporated millions of years later.

1.4.1. Rates and Timescales of Melt Generation - The Use of U-Series Disequilibrium

The composition of melts produced by decompression melting of the mantle are controlled primarily by the bulk composition of the source, the degree of partial melting and the residual mineralogy. The latter depends on the composition, the temperature of the source and the depths at which melting occurs. The depths of melt generation can be inferred from both major and trace element compositions and the U-series isotopes. However there is a question as to the extent to which melt generation and transport may decouple radiogenic systems from the incompatible element fractionation and hence the two explanations may not coincide.

The presence of U-Series disequilibrium (the fractionation of U from Th having taken place less than 350,000 year ago) in MORB and OIB has been linked to a number of controlling factors. These include the degree and depth of melting, the thickness of the overlying lithosphere lid, the rate of melting and the buoyancy flux (the rate of upwelling in a mantle plume, relative to normal mantle), some of which are interdependent. U-series isotope disequilibrium is generated at depth in the convecting asthenosphere (Chabaux and Allègre, 1994; Bourdon et al., 1996), and in ocean islands excesses of the Th isotopes are most common. These ^{230}Th excesses require Th to be preferentially fractionated into the melts relative to U, and thus a mantle phase which retains U relative to Th during partial melting must be present. Of the two main U and Th bearing mantle phases, only garnet will preferentially retain the U and allow excess Th to be generated (Beattie, 1993b; Hauri et al., 1997). Thus if lavas have excess ^{230}Th melting must have taken place within the garnet stability field. Subduction related island arc magmas tend to have U excess, whilst MORB tend to have excess Th also.

The systematics of short-lived U and Th isotopes are introduced in the next chapter; however, the rate of melting exerts a strong control on (^{230}Th-^{238}U) disequilibrium since the rate limits the time for ^{230}Th ingrowth in the mantle matrix (e.g. McKenzie, 1985). The rate of melt generation depends on the rate of upwelling of the mantle material through the melt zone, and hence on the buoyancy and temperature of the mantle plume.

The degree of (^{230}Th-^{238}U) disequilibrium in MORB is greater in MORB from shallower ridge depths. This has been attributed to more efficient melt extraction (melt

removal from the source region) and more of the melting zone being in the garnet stability field. This is inferred to be because the mantle is hotter (relative to the lithosphere) underneath shallow ridges, so more melting takes place in the garnet stability field resulting in more U-Th isotope disequilibrium in areas of higher mantle temperature. In contrast, OIB has less (^{230}Th-^{238}U) disequilibrium in areas of higher buoyancy flux (i.e. higher mantle temperatures). In other words, (^{230}Th-^{238}U) disequilibrium decreases with increasing mantle temperature in OIB (Cohen and O'Nions, 1993; Chabaux and Allègre, 1994; Sims et al., 1995), and so the controls on OIB and MORB are strikingly different.

1.4.2. Melting Models

Wide varieties of melting models have been used to model major and trace elements in basalts. These include simple batch and fractional models (McKenzie, 1985), but simple batch models do not take into account radioactive decay and they cannot account for U-series isotope disequilibrium, except at unrealistically small degrees of melting < 0.1% (e.g. Elliott, 1997). At degrees of melting consistent with OIB of 1 - 8 %, the U/Th ratio of the melt is similar to that of the source even when significant (^{230}Th-^{238}U) disequilibrium is observed. Hence such disequilibria are better modelled by dynamic melting (e.g. Williams and Gill, 1989), where the melt and the matrix peridotite may continue to interact as the melt migrates towards the surface (Spiegelman and Elliott, 1993; Elliott, 1997). The ingrowth of Th to generate ^{230}Th excesses found commonly in OIB is then linked to the upwelling rate of the mantle matrix, and the matrix must remain in the melting zone for a significant time period to obtain the observed excess Th. A modal dynamic melting model (MDM) developed by van Calsteren and Hawkesworth (1999) has been used during this work to model the Lanzarote lavas. This model is developed from those of Williams and Gill (1989; 1992), Gill (1993), and Spiegelman and Elliott (1993), to allow the integration of the melt fraction through space and time, and the continued interaction between the melt and the matrix as the melt moves through the melting zone.

1.5. Existence of Magma Chambers and their Role in Differentiation

Many mechanisms have been proposed that create the required physical conditions for magmatic differentiation. Many of the earliest observations were based on sampling plutons and other intrusive bodies, and from this the concept of the magma chamber was initially developed (Harker, 1909). A magma chamber provides a convenient location for the majority of the differentiation mechanisms to take place, in such a location, fractional crystallisation can occur, assimilation and/or magma mixing, and accumulation can alter the derived magma composition.

Evidence for the existence of large magma reservoirs beneath the Earth's surface comes from a variety of sources. These include observations from exposed intrusive rocks, where exposed magma chambers can be seen (e.g. the Skaergaard intrusion of east Greenland (Wager and Deer, 1939; McBirney and Noyes, 1979) and the formation of calderas, thought to be the surface expression of collapsed magma chambers. Geophysical evidence can also reveal the presence of magma chambers, as these areas exhibit low P wave velocities and cannot propagate S waves. The size of magma chamber can vary greatly ranging from < 5 km^3 melt pockets beneath mid-ocean ridges (e.g. Burnett et al., 1989) to several hundred cubic kilometres of magma (e.g. Teide-Pico Viejo, Tenerife; (Ablay, 1997) and Long Valley, California (e.g. Hildreth, 1979, 1981). Not all volcanoes show evidence of sub-volcanic magma chambers, e.g. Vesuvius shows no evidence of magma storage within 5 km of the surface (De Natale et al., 1998) and the nature of the reservoirs revealed by geophysical methods is often different to the structures seen in exposed intrusions. Seismic imaging of Kilauea (Ryan, 1987) for example, revealed a complex series of interconnecting dykes and reservoirs.

The perception of a magma chamber is often dependent on the viewpoint of the scientist, a geophysist may see a reservoir bounded by S waves, a geochemist may see layered region of crystal mush and some liquid, even within scientific fields arguments continue. However it is unlikely that the presence of a 'hole' or a hole filled with totally molten rock will suffice. The presence of a magma chamber beneath Lanzarote was thought

to be unlikely (Thomas et al. 1999), as the lavas are primitive in composition and a very rapid throughput of lava would be required to preserve the observed U-Th disequilibria.

Large volume pyroclastic eruptions such as the Bishop Tuff of Long Valley, the Bandas del Sur of Tenerife and the Toba Tuff, Sumatra (Jones, 1993) have also given insight into the evolution of salic magma chambers. Large pyroclastic deposits often associated with caldera collapse are believed to represent the partial draining of magma chambers. Detailed investigations of such deposits identified compositional variation interpreted to reflect internal zonation of the original magma chamber.

One of the most important advances in understanding magmatic processes has been the role of the magma chamber and processes involved within. Convection models have been studied suggesting complex movements within the reservoir. Stratification of the chamber is a common place scenario and the compositional variation due to, for example, crystal fractionation, mixing, accumulation, side wall crystallisation and AFC control the composition of the erupted magma.

1.5.1. Timescales of Magma Chamber Evolution

High precision Rb-Sr isotope dating of lavas from the Long Valley caldera have also been used to investigate the timescales of differentiation (Davies et al. 1994 and Davies and Halliday, 1998). Two rhyolite magma batches were accurately dated and the residence times of the phenocrysts were in the order of 200 ka older than the eruption ages. The differences in residence times were attributed in the different magma batches to different cooling rates at varying depths in the magma chamber. U-Series isotopes can give information regarding the timescales of other magma differentiation processes, in addition to partial melting and mantle upwelling. In the case of Tenerife (this study), St Vincent (Heath et al., 1998), Stromboli and Etna (e.g. Condomines et al., 1987; Volpe et al., 1991), the timescale of magma evolution of crustal level chambers can be inferred, using whole rock and mineral separates analyses. Specifically it is possible to evaluate the time taken for a suite of rocks to differentiate, or the age of eruption, if the observed fractionation of the parent-daughter isotopes took place just prior to eruption.

1.5.2. Previous U-series Studies on the Timescales of Magma Chamber Processes

The majority of U-series studies have been concerned with either the time period between formation of melt and its eruption, or the residence time of magma (and/or phenocrysts) in a magma chamber. This work has presented a wide array of timescales for magmatic processes varying by up to five order of magnitude.

An investigation into the alkali basalt magma chamber of Surtsey (1963-67) and Heimaey (1973) by Sigmarsson (1996) gave residence times in the order of ~10 years, from ^{210}Pb-^{226}Ra-^{230}Th during which 30 % fractional crystallisation from alkali basalt to hawaiite took place. Similarly short time periods have been invoked for the carbonatite lavas of Oldoinyo Lengai in Tanzania (Pyle et al. 1991).

Residence times of 0.5 to 5 ka have been suggested from ^{230}Th-^{226}Ra systematics for Mount Erebus (Kyle et al. 1992) and Mt. St. Helens (Volpe and Hammond, 1991). U-Th-Ra disequilibrium in recent andesite and dacite lavas from Mt Shasta, (Volpe, 1992) indicated fractionation took place < 10 ka and that the mean residence time is in the order of 6-7 ka.

Residence time greater than 20 ka have been identified for a variety of settings, including comendites from Olkaria domes of Kenya (Black et al, 1997) and the calc-alkaline suite from Soufriere, St Vincent (Heath et al., 1998) being in excess of 50 ka. The extensive study of Etna (Condomines et al., 1982; 1988; 1995) has revealed a complex range of timescales and differentiation mechanisms. The main chamber (150-300 km^3) is thought to be undergoing steady state replenishment. Differentiation from hawaiite to mugearite is a rapid process, occurring within the residence time of less than 1500 years, whilst a smaller magma body (0.5km^3) has a significantly shorter residence time of only a few tens of years, as a consequence of magma bypassing the main chamber.

Timescales of magma differentiation have been determined for trachytes of Sao Miguel in the Azores (Widom et al., 1992) and phonolite magmas of the Laacher See in Germany (Bourdon et al. 1994). At Sao Miguel a single magma chamber has been shown to have existed for at least 15 years in which compositional zonation under closed system conditions can occur within 4.6 ka after a preceding eruption. The differentiation from alkali basalt to trachyte by fractional crystallisation took less than 90 ka. Phenocrysts in the

Laacher See phonolites have residence times of 1-2 ka, but the time taken for zonation to occur is in the order of 10-20 ka. The basanite to phonolite fractionation took place over a period of 100 ka.

1.6. Ocean Islands - Current Debates Surrounding the Canaries

This section introduces the Canary Islands and the debates surrounding them. It summarises the geological setting, and provides an answer to the question 'why study the Canaries?'

1.6.1. Location of the Canary Islands

The Canary Islands are a group of seven main volcanic ocean islands and several islets that extend for almost 500 km roughly east-west from approximately 100 km off the NW coast of Morocco in the Northeast Atlantic ocean (Figure 3.1). The eroded remains of Selvagem island, several seamounts and the Conception Bank to the North of Lanzarote also form part of this, the most voluminous and persistent volcanic province in the Atlantic basin (Schmincke, 1982; Araña, 1995). The chain is situated in the Jurassic magnetic quiet zone of the passive African margin, at the edge of the continental slope of Northwest Africa (Banda et al., 1981). The Canary Islands have been well studied over the past century, but as yet, their origin and evolution remain poorly understood relative to more 'typical' ocean island chains, such as the Hawaiian islands.

1.6.2. Origin and Evolution of the Canary Islands

With the advancements of plate tectonics theory, Wilson (1963) proposed a model that both the Hawaiian islands and the Canaries were related to hotspots - buoyant, hot mantle plumes. It seems that the theory of a fixed magma source mantle plume with the oceanic lithosphere plate moving across it, has been accepted for Hawaii, where the Pacific is a fast spreading ocean, whilst the argument for the Canary Islands 'hotspot' has been less readily accepted. The Atlantic is a slow spreading ocean and ocean islands within this setting tend to be in small groups, as opposed to the obvious linear structures of the Hawaiian - Emperor Seamount chain and Tuamotu chain. The debate over the origin of the Canaries still continues with different authors favouring their own theories. Such models include the

modified hotspot model (e.g. Schmincke, 1982; Hoernle et al., 1991; Hoernle and Schmincke, 1993), and those preferring more obvious tectonic control, such as in a rift zone, or faulting caused by deformation within the Atlas Mountains (e.g. Araña and Ortiz, 1991). This debate may in part reflect an incomplete understanding of the geodynamics of the East Atlantic passive margin.

None of the models suggested for Canarian evolution fully explain all the features of the archipelago. The hot spot models flounder against the complex spatial and chemical progression as the islands become younger from east to west (Abdel-Monem et al., 1971), whilst models that do not include a hot-spot encounter problems regarding the geophysical arrangement and the petrological evolution of the islands. The current consensus invokes the co-existence of a hot spot within a complex regional structural framework (Schmincke, 1982, Marinoni and Pasquarè, 1994), with the sites of active volcanism reflecting tectonic control across a relatively static mantle hot spot (Schmincke, 1982). Deformation and extension have occurred along the NE-SW trending South Atlas fault in the Atlas Mountains (Banda et al., 1981) and similar trending structures are found in the eastern Canary Islands, Lanzarote and Fuerteventura.

For those who accept a mantle plume as the source, the type of mantle plume is of considerable interest. There are those who prefer a whole region of upwelling buoyant mantle beneath the whole of the North-west Atlantic (Hoernle et al., 1995). Whilst others invoke a single mantle plume generated at depth, perhaps at the 660 km discontinuity, and upwelling to give each individual island (Araña and Carracedo, 1979).

The Canary Islands are generally assumed to have formed since the Miocene, although Storedtvedt et al. (1979) suggested a much earlier Late Cretaceous origin for the basal intrusives. However, neither age implies any connection with the early opening of the Atlantic Ocean at 200 Ma, and today the islands are ~ 2000 km from the Mid Atlantic Ridge. The Canary Islands have had a complex geological history, and while there is a general E-W progression in the age of the first subaerial activity, the recent volcanic activity is more randomly scattered across the different islands, with all but one of the islands being active in historic or recent prehistoric times. At present the only significant residual thermal anomaly is at Timanfaya on Lanzarote (Arana et al., 1984) and one localised but persistent fumarole in the Teide summit area of Tenerife (Albert et al., 1990).

1.6.3. Tectonic Setting of the Canary Islands

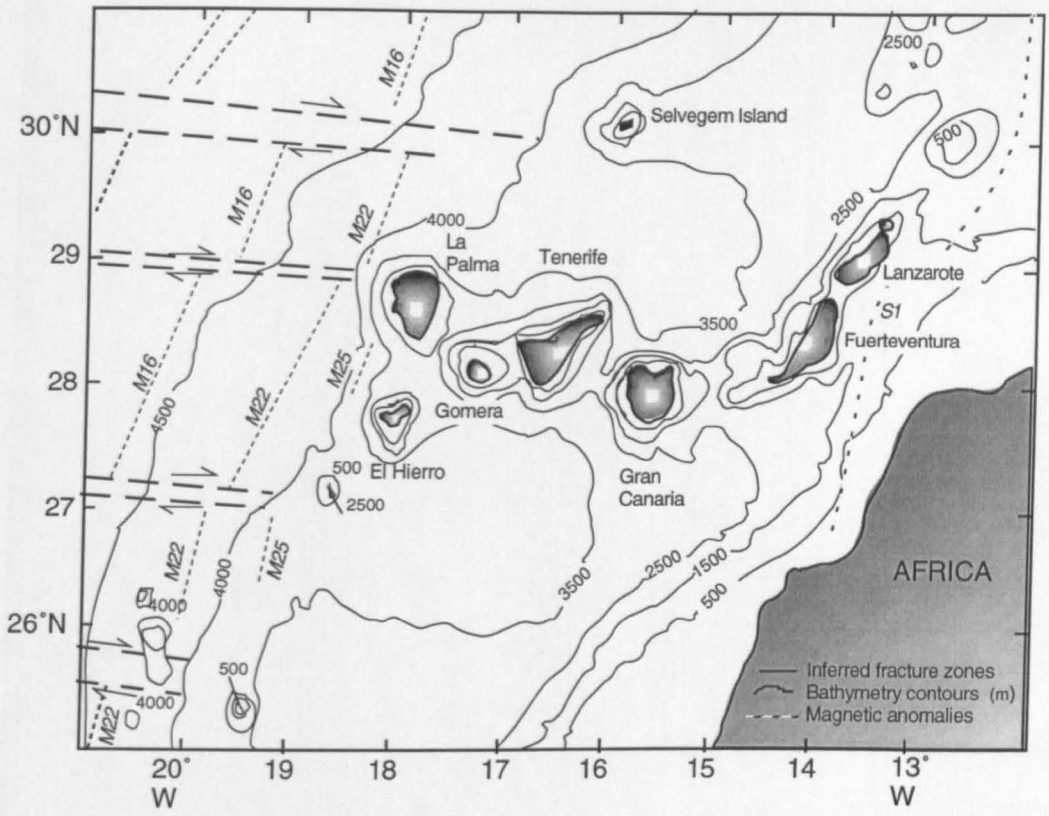

Figure 1.4. shows the tectonic setting of the Canary Islands, and the surrounding bathymetry and magnetic anomalies (after Schmincke, 1982; Coello et al., 1992 and Roest et al., 1992).

1.6.4. Magnetic Anomalies

The Canary Islands are located in the Jurassic magnetic quiet zone situated landwards of the M-series magnetic anomaly M25 (see Figure 1.4). Magnetic anomaly profiles have been analysed to identify M series sea floor spreading and oceanic fracture zones on the African plate (Roest et al., 1992). The magnetic anomalies M22-M25 (145-148 Ma) can be traced towards the western-most islands which are generally believed to rest on oceanic crust (Verhoef et al., 1991; Roest et al., 1992). The eastern islands (including Lanzarote) were thought to be located on transitional lithosphere close to the African continental margin (Banda et al., 1981). This transitional lithosphere may have represented thickened oceanic lithospheric mantle or Palaeozoic-Precambrian basement from the continental crust (e.g. Rothe and Schmincke, 1968; Araña and Ortiz, 1991). On the basis of magnetic anomaly S1 (located between Lanzarote/Fuerteventura and the coast of Africa), Verhoef et al. (1991) and

Roest et al. (1992) placed the edge of the oceanic crust to the east of the Canary Islands. However the influence of some attenuated continental mantle lithosphere cannot be totally refuted beneath the eastern-most islands.

1.6.5. Lithospheric Age and Thickness and Bathymetry

The age of underlying oceanic lithosphere varies from 150 Ma in the east to 175 Ma in the west (Verhoef et al., 1991; Roest et al., 1992). Oceanic lithosphere becomes thermally stabilised after about 70-80 Ma when the depth to the horizontal isotherm is of the order of 100-125 km (Parsons and Sclater, 1977; Parsons and McKenzie, 1978). Thus, the 150-175 Ma old lithosphere of the Canaries should have reached a steady state thickness of 100-125 km, provided that there has been no thermal erosion.

The expected water depths for such lithosphere should be ~ 5 km (Parsons and McKenzie, 1978), and yet those around Lanzarote and Fuerteventura are ~ 1.5 km, although these increase to ~ 3 km around the islands further west (Araña and Carracedo, 1979). These shallower depths may either reflect some combination of the dynamic support by the mantle plume, transition to the African continental lithosphere and/or the thermal erosion of the lithosphere by the plume (Davies, 1994). The crustal thickness beneath the Canary Islands varies systematically from 10-15 km in the east to 7-10 km in the west (Bosshard and Macfarlane, 1970; Araña and Carracedo, 1978). This may reflect variations in the local melt productivity which is consistent with a regional link between melt productivity and the thickness of the lithospheric lid.

1.6.6. General Geology of the Canary Islands

Each of the Canary Islands shows at least two phases of subaerial activity, a primary shield building phase which built the basaltic volcanic centres and a later smaller post-erosional volcanic phase which took place after significant erosion. Only 5% of the total expanse of the islands is exposed and according to Schminke (1982), only 1.1% of the volume of the volcanic edifice of Lanzarote is visible above sea level. The total volume of the province is in the order of 1.4 - 2.0 x 10^5 km^3 (Schmincke, 1982; Coello et al., 1992) which is an order of magnitude greater than the Azores to the NW. The eastern islands of Fuerteventura and Lanzarote are thought to have developed slightly differently to those

islands further west. They differ in structural trends, the dominance of fissure eruptions, which are rarely seen on the other islands, the absence of large volcanic edifices and a lack of highly evolved volcanics such as the Roques Blanco phonolites on Tenerife. Basal Complexes outcrop on three islands (Fuerteventura, Gomera and La Palma). The Basal Complex on Fuerteventura is the finest example, with Cretaceous sediments as well as submarine lavas intruded by basic plutonic rocks (Stillman et al., 1975).

Canarian volcanism tends towards Na-alkaline magmatism with most compositions being moderately undersaturated in silica. However on the whole this magmatism is more alkaline and LILE and REE enriched than most ocean islands. Despite the relative homogeneity of the primitive lavas, each island has a distinct eruptive history. The most evolved salic magmatism (phonolites) is essentially limited to the central islands of Tenerife, Gran Canaria and La Gomera, where shallow magma chambers have developed beneath the large strato-volcanoes (Martí et al., 1994).

The islands of Tenerife and Lanzarote show a contrast in their eruptive style and composition. Lanzarote lavas are amongst the most primitive found in the ocean island intraplate setting and therefore allow the modelling of melt generation and direct comparison with mantle compositions without the hindrance of major fractionation corrections. The Teide-Pico Viejo lavas of Tenerife provide an excellent opportunity to study the effect of magma chamber processes on a suite of differentiated lavas, which range in composition from basanite to phonolite. Canary Islands are also underlain by a plume of low buoyancy flux, and hence the lavas would be expected to have large amount of U-Th-Ra disequilibria present.

1.7. Aims and Objectives of this Thesis

The aims of this work have a significant bearing on a number of different debates. These include the use of U-series isotopes as an approach to understanding the timescales and rates of magmatism in ocean islands and the significance of different melting models used; and in a more localised scenario the nature of the underlying mantle beneath the Canary islands. The rationale behind this research was initially to examine the primitive compositions of the historic and recent pre-historic lavas of Lanzarote, in an attempt to use

melting models designed for MORB for the trace and rare earth elements and U-Series disequilibria found in OIB. The dynamic melting models (e.g. McKenzie, 1985; Williams and Gill, 1992; Spiegelman and Elliott, 1993) developed for MORB, could then be developed (van Calsteren and Hawkesworth, in prep. (1999)) to model OIB from different types of upwelling mantle.

The project was then developed further to investigate the differences between the islands of Lanzarote (primitive compositions, extraction direct from mantle source) and Tenerife (range of compositions from basanite to phonolite, evolution in magma chambers and locally direct extraction from mantle source) to evaluate variations in the underlying mantle beneath the Canary Islands, and to understand the different timescales and processes occurring in the two islands.

Hence the main goals of this work are

a) To establish a dynamic melting model which would model the primitive lava compositions from Lanzarote and Tenerife.

b) To define a source composition for the underlying mantle beneath the Canaries, and the relative contribution from the plume and the overlying lithosphere.

c) To evaluate the rates and timescales of melting processes and their controls in the ocean island setting.

d) To evaluate the rates and timescales of melt differentiation on Tenerife.

Another goal of the laboratory side of this project was to develop an analytical technique suitable for the analysis of Radium, and to establish this as a routine technique to run alongside Uranium and Thorium analyses in the silicate radiogenic isotope laboratories at the Open University. This would allow new constraints on the timescales of processes of less than 8,000 years.

These Figures (i.e. dates) are, as railway timetables say,
subject to change without notice.
Committee on the Measurement of Geological Time (1950)

El Drago

Rule of ACCURACY
When working towards the solution of a problems
it always helps of you know the answer.

Corollary
Provided, of course you know there is a problem.

Plate 2

CHAPTER TWO

Uranium Series Disequilibrium and Analytical Techniques

2.1. Introduction

The aims of this chapter are to provide an overview of radioactive decay and the reasons why the U-Th-Ra system is useful in the understanding of rates and timescales of magmatic processes. This chapter also includes a summary of the techniques used for the measurement of Uranium (U), Thorium (Th) abundances and isotopic ratios and development of the technique for the analysis of Radium (Ra). A summary of the other analytical techniques used during the course of this project, including XRF, INAA, and TIMS for Sr, Nd and Pb isotopic ratios, and general lab techniques such as cleaning, blank monitoring and radiation monitoring can be found in Appendix C.

2.2. U-Series Isotopes

During the mid to late 1800s, many physicists including William Thompson, better known as Lord Kelvin, had been working on the problem of the age of the earth and the sun, using theories and estimates of cooling rates. Lord Kelvin concluded that the age of the earth was probably around 20 to 40 million years. This was too long for some and too short for others. T.C. Chamberlin, a confessed agnostic, added that there might be an as yet unknown source of energy. The discovery of radioactive disequilibria in volcanic rocks came late in the 19th Century, when in 1895 Henri Bequerel, a French physicist, discovered radioactivity in uranium salts, almost at the same time as the German physicist Wilhelm Rontgen discovered x-rays, and soon after Marie Sklodowska-Curie discovered and isolated

radium. In the early 1900s the research into radioactivity continued, Ernest Rutherford had been studying radioactive processes, and he suggested that it might be possible to date rocks using radioactive minerals and within the next few years both uranium and thorium isotopes were used to date minerals. These early ages were improved on by F. Soddy in 1913 when he clarified and increased the accuracy of the methods. The age of the earth was calculated to be in the billions of years, not millions. During a lecture to the Royal Institution on the heat production of radioactivity and its effect on the heat of the Earth, Rutherford was ill at ease to see Lord Kelvin in the audience. He avoided a potential explosive conflict with the old man, by announcing that Lord Kelvin had calculated the age of the Earth from its thermal history, provided no new source of heat was found. Therefore, Lord Kelvin has in fact anticipated the discovery of radioactivity and the heat produced by this phenomenon. Lord Kelvin who had in fact slept soundly through the rest of the talk, just beamed with pleasure (Source: Faure 1986).

The occurrence of radium excesses was first found in volcanics from Vesuvius by Joly in 1909; however it was much later in the century before more work was done on the subject. The importance of U-Series disequilibrium to the study of magmatic processes was only realised some thirty years ago from work by Oversby and Gast (1968) and Allègre (1968), and since that time the subject has been in continuous development. Variations in U-Series isotopes can be used to provide information regarding the timing of different sorts of geological processes giving rise to their formation, as the timescale of decay from parent to daughter isotope is short and relevant to the timescales involved in magmatic (of major importance in this project) and other geological processes, such as sedimentation, erosion and metamorphism. The (^{238}U-^{230}Th) and (^{230}Th-^{226}Ra) systems can also provide indications of the chemical changes occurring during the processes, such as melting, extraction from the source region and differentiation.

Ocean Island Basalts (OIB) and Mid Ocean Ridge Basalts (MORB) often display significant (^{238}U-^{230}Th) disequilibria, which is thought to be generated by melting (e.g. Condomines et al., 1988; Gill and Condomines, 1992). However there are two different end member interpretations which exist to explain U-series disequilibria in igneous rocks. It has been attributed to an overall elemental fractionation of parent-daughter pairs in the erupted melt relative to those in the source, particularly by some of the earlier workers

(Oversby and Gast, 1968; Allègre and Condomines, 1982; Condomines et al., 1988); and subsequentally to the 'in-growth' of the short lived daughter ^{230}Th during partial melting (McKenzie, 1985a; Willliams and Gill, 1989; Spiegelman and Elliott, 1993; Thomas et al, 1999). The large excesses of the daughter nuclide (e.g. ^{230}Th and ^{226}Ra) present in MORB (e.g. Condomines et al., 1981; Goldstein et al., 1989; 1992; 1993; Volpe and Goldstein, 1993; Lundstrom et al., 1995; Bourdon et al., 1996a, b) would appear to require ingrowth of the daughter nuclide. However the importance of ingrowth in OIB which are the products of smaller degrees of melting, is less clear and on the whole the understanding of U-Series systematics in ocean islands is generally less well developed than that in MORB. Part of this project was to analysis U-Th-Ra in Canary Island lavas in an attempt to understand the systematics in a complex ocean island chain.

2.2.1. The Principles of Radioactive Decay

It is necessary to understand the principles of U-series decay (discussed in detail elsewhere, e.g. Ivanovich and Harmon, 1982; Faure, 1986; Dickin, 1997), prior to interpreting the results, so a summary of the main theories follows.

A radioactive nucleus may, at any instant, change spontaneously into a different nuclear type. This process, known as radioactive decay, is one in which the amount of decay of the radioactive parent nuclide to the stable daughter product is proportional to the number of atoms, N, present at time t (Rutherford and Soddy, 1902). The decay constant λ (expressed in units of reciprocal time), also known as the constant of proportionality, is the probability that a given atom of the radionuclide will decay within a stated time. The stability of a nucleus and its preference for decay corresponds to the stability of the proton/neutron ratio. The term dN/dt is the rate of change of the number of parent atoms, and so it would be negative as this rate decreases with time. The equation for radioactive decay gives a negative λN is:

$$\frac{dN}{dt} = -\lambda N = a \qquad [2a]$$

a is the 'activity' in Becquerels (disintegrations per second).

This expression is integrated from $t = 0$ to t, given that the number of atoms present at time $t = 0$ is N_0.

$$\int_{N_0}^{N} \frac{dN}{N} = -\lambda \int_{t=0}^{t} dt \qquad [2b]$$

Hence

$$\ln \frac{N}{N_0} = -\lambda t \qquad [2c]$$

which can also be written as

$$N = N_0 e^{-\lambda t} \qquad [2d]$$

The rate of decay is often measured in terms of the 'half-life', $t^1/_2$, which is the time required for half of the parent atoms to decay. Substituting $N = N_0/2$ and $t = t^1/_2$ into equation 2c and rearranging that equation, equation 2e is obtained.

$$t\frac{1}{2} = \frac{\ln 2}{\lambda} = \frac{0.693}{\lambda} \qquad [2e]$$

D*, the number of radiogenic daughter atoms formed is equal to the number of parent atoms consumed, hence

$$D^* = N_0 - N \qquad [2f]$$

but $N = N_0 e^{-\lambda t}$ (from equation 2d); so substituting for N_0 in equation 2f gives:

$$D^* = N e^{\lambda t} - N \qquad [2g]$$

i.e. $$D^* = N\left(e^{\lambda t} - 1\right) \qquad [2h]$$

If the number of daughter atoms at time $t = 0$ is D_0, then the total number of daughter atoms after time t is given as:

$$D = D_0 + N(e^{\lambda t} - 1) \qquad [2i]$$

This equation is the fundamental equation behind geochronological dating. In the U-series system this is extended, as the daughter products from the radioactive decay (other than the three stable Pb isotopes) are themselves radioactive and decay. Hence the rate of decay of such a daughter product is given by the difference between its rate of production from the parent and its own decay rate:

$$dN_2/dt = N_1\lambda_1 - N_2\lambda_2 \qquad [2j]$$

where N_1, λ_1, N_2 and λ_2 are the abundances and the decay constant of the parent and daughter respectively. N_1 can be substituted from equation [2f] and integrating this equation for a chosen set of initial conditions, setting $N_2 = 0$ at $t = 0$, then:

$$N_2\lambda_2 = \frac{\lambda_1}{\lambda_2 - \lambda_1} N_{1,initial}\left(e^{-\lambda_1 t} - e^{-\lambda_2 t}\right) \qquad [2k]$$

This is known as the Bateman equation and is the basis for much of the mathematics used in the U isotopic system. In a decay chain, where the parent has a much longer half-life than the daugter(s) a state of radioactive or *secular equilibrium* is reached within 4 or 5 half lives of the longest intermediate nuclide. The activities of the nuclides are then equal: $\lambda_1 N_1 = \lambda_2 N_2 ... \lambda_K N_K$. As previously mentioned, a distinctive property of the U-series is that as the daughters are radioactive, hence the decay rate of each daughter in the chain is equal to that of the parent. Thus in secular equilibrium the ratio of the activities of any two nuclides in the decay chain is unity e.g. ($^{230}Th/^{238}U$) = 1, where the parentheses indicate activities.

2.2.2. U-Series Decay

The actinides (whose heavier members include Ac, Pa, Th and U) are the heaviest naturally-occurring elements. Isotopes of the longer lived nuclides are alpha-emitters, and they can be separated into separate decay series. ^{238}U decays to ^{206}Pb via a chain of short lived nuclides, including ^{230}Th and ^{226}Ra which are commonly measured, whilst ^{235}U decays to ^{207}Pb via nuclides such as ^{231}Pa. The Th series includes alpha and beta emitters, during the decay of ^{232}Th to the stable ^{208}Pb. These decay chains are summarised in Figure 2.1.

During geological processes, such as partial melting and fractional crystallisation, nuclides in the decay chain can become fractionated relative to one another, due to variations in their chemistry or the structural site they occupy. This can be utilised as a chronological tool, since the time since such parent-daughter fractionation occurred can potentially be determined. Moreover the range of timescales which can be investigated using U-Th-Ra isotopes is obviously different for the different isotopes systems. The relatively short half-lives of the nuclides make them suitable isotopic tracers for studies of melt segregation from the mantle and magma evolution in the crust. As analytical techniques develop, the shorter-lived nuclides will provide better constrained information about processes taking place on shorter timescales. The half-lives shown in Figure 2.1 give an indication of the timescales which are and may be measurable in the future.

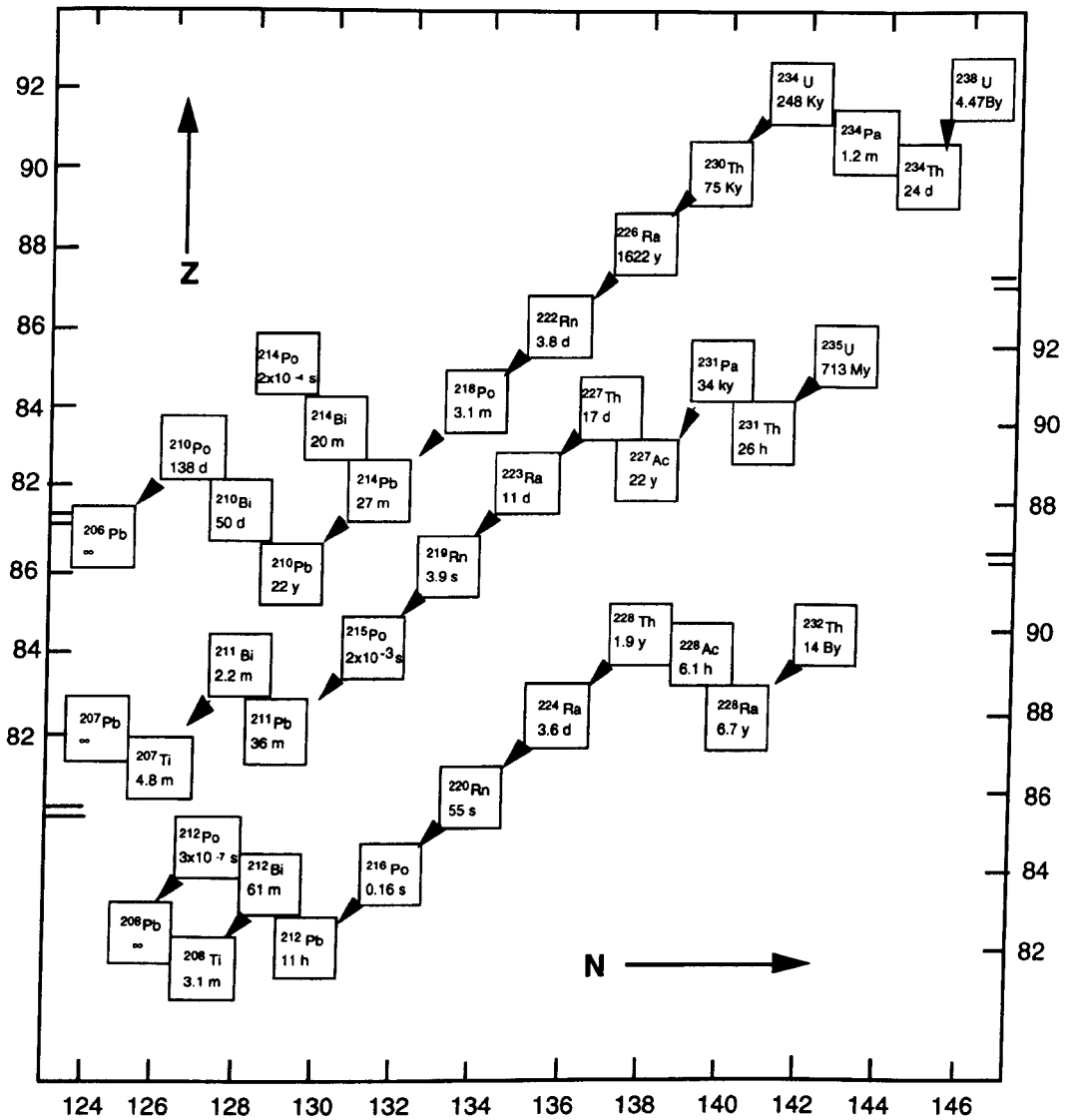

Figure 2.1. ^{238}U, ^{235}U and ^{232}Th decay series with the half-lives of the individual nuclides in the boxes. (After Faure, 1986; Condomines et al., 1988; Dickin, 1997)

2.2.3. Behaviour of Radioactive Nuclides during Partial Melting

Nuclides of U, Th and Ra are thought to behave as incompatible trace elements during partial melting, i.e. they partition between solid and liquid phases at chemical equilibrium according to their partition coefficients, D.

$$Dx = \frac{[X]_{sol}}{[X]_{liq}} \qquad [21]$$

where [X] is the concentration or activity per unit mass of element or radionuclide in the coexisting solid and liquid. The value of D is dependent upon a number of factors including temperature, pressure and the composition of the crystallising mineral and magma.

During partial melting U and Th can be fractionated from one another, as predicted by their partition coefficients and hence their relative incompatibility (Th is typically slightly more incompatible than U in the source of OIB). However both are highly incompatible and hence they are concentrated in the liquid phase relative to less incompatible elements. They tend to concentrated into high SiO_2 rich products, and hence the phonolites of Tenerife (Chapter 4) have higher U and Th contents than the basalts of Lanzarote (Chapter 3). The concentrations of U and Th in igneous rocks vary by approximately three orders of magnitude, but the Th/U ratio is much less variable, ranging between 3.6 and 4.8 in Tenerife and only 3.4 to 4.0 in Lanzarote. Nonetheless, given the small distribution coefficients (e.g. Beattie, 1993a, b) for U and Th during mantle melting, small degrees of melting (1%) are required to fractionate Th/U in the liquid from that in the source. Most mantle sources are unlikely to have been disturbed for millions of years prior to melting, and so they can be assumed to be in radioactive U-series equilibrium.

After U-Th disequilibrium has been generated, the individual parent-daughter pairs decay to re-establish equilibrium over the timescales determined by the half-lives of the daughter nuclei. If no further fractionation occurs after the initial formation, it is possible to date the original fractionation event by measuring the extent to which the radioactive system has returned to the state of secular equilibrium. The longest lived of the ^{238}U-Series nuclides is ^{230}Th with a half-life of 75.4 ky, thus the whole ^{238}U decay chain will have returned to equilibrium in 350 ky, hence the maximum timescale of U-Th isotope disequilibrium. The exception to the rule is ^{234}U which is not fractionated from ^{238}U by high temperature magmatic processes, hence ^{234}U and ^{238}U are always effectively in secular equilibrium in fresh magmatic rocks.

Much of the interpretation of U-series data deals with models of melt generation and melt extraction. These include the simple batch or fractional melting models used for trace element behaviour (e.g. Allègre and Condomines, 1982), and imply instantaneous melting. However, recent work involves dynamic melting models, as the simple batch and fractional melting models do not take account of radioactive decay. Dynamic melting models (discussed in greater detail in chapter 4) take into account the timescales of radioactive decay and of melting, where a melt, residue and matrix continue to interact as they move within the

melting zone (Williams and Gill, 1989), and the different velocities of the individual nuclides in the melt (Spiegelman and Elliott, 1993).

2.2.4 The Equiline or Isochron Diagram

Disequilibrium between the daughter nuclides of ^{238}U give rise to the geochronometers which can, for example, be used to date volcanic rocks younger than 350,000 years. U-series isotopes fill in an important time gap between ^{14}C dating and the K/Ar and Ar/Ar methods. After time t, the ^{230}Th activity in a silicate is the sum of the ^{230}Th growth from the U decay and the residue of the partially decayed initial ^{230}Th. This can be expressed as

$$\left(\frac{^{230}Th}{^{232}Th}\right)_P = \left(\frac{^{230}Th}{^{232}Th}\right)_I e^{-\lambda_{230}t} + \left(\frac{^{238}U}{^{232}Th}\right)\left(1 - e^{-\lambda_{230}t}\right) \quad [2m]$$

and is the equation for a straight line. Subscript P denotes the Present or measured value and subscript I denotes the Initial or original value. This is plotted on a diagram of (^{238}U-^{232}Th) versus (^{230}Th-^{232}Th) (Figure 2.2), which is known as an equiline or isochron diagram (Allègre and Condomines, 1976). Parentheses around the ratios indicate activity ratios, i.e. the concentrations have been multiplied by their decay constants. The slope of the equiline is 1, as it marks the position of the activities of the nuclides in secular equilibrium.

The slope and the intercept of an isochron formed by either whole rocks or co-genetic minerals are equal to:

The slope = $m = 1 - e^{-\lambda t}$: the intercept = $c = \left(\frac{^{230}Th}{^{232}Th}\right)_i e^{-\lambda t}$

A mantle source may produce a melt, which has the same initial (^{230}Th-^{232}Th) as its source, and so is displaced horizontally on Figure 2.2. In the case of OIB, the melts plot to the left of the equiline (i.e. Th excess, relative to source) and as they evolve with time they decay down towards the equiline. Meanwhile the residue would plot to the right of the equiline (U excess relative to source), and so it gradually decays upwards towards the equiline.

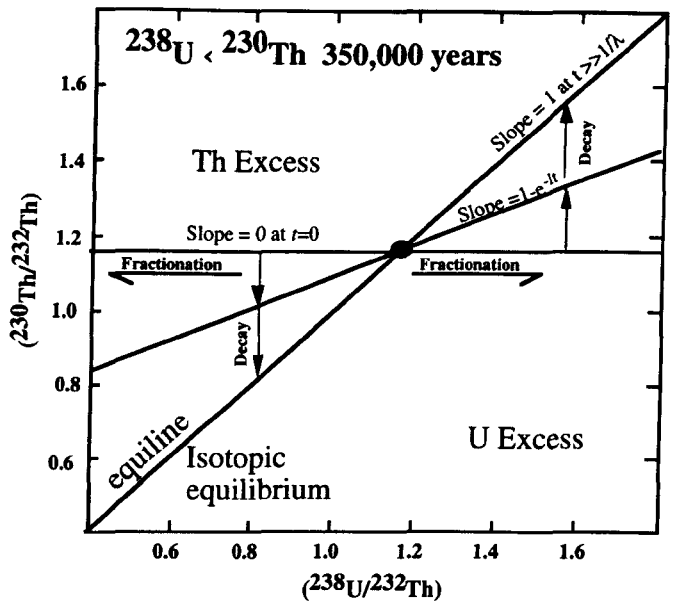

Figure 2.2. An Equiline or Isochron Diagram for (^{238}U-^{230}Th) system. The axes are the activity ratios of ($^{230}Th/^{232}Th$) and ($^{238}U/^{232}Th$).

The decay constants used in the calculations for the U-Series isotopes are listed in Table 2.1.

$\lambda^{238}U$	$\lambda^{234}U$	$\lambda^{232}Th$	$\lambda^{230}Th$	$\lambda^{226}Ra$
1.5513×10^{-10}	2.8350×10^{-6}	4.9475×10^{-11}	9.1952×10^{-6}	4.272×10^{-4}

Table 2.1. Decay Constants ($\lambda\ a^{-1}$) for U-Series Isotopes (from Jaffey et al., 1971; Le Roux and Glendenin, 1963; Lounsbury and Durham, 1971; and Meadows et al., 1980).

When the time of eruption is known t can be entered into the isochron equation and the initial (^{230}Th-^{232}Th) can be calculated, in the following rearrangement of equation 2m.

$$\left(\frac{^{230}Th}{^{232}Th}\right)_I = \left(\left(\frac{^{230}Th}{^{232}Th}\right)_P - \left(\frac{^{238}U}{^{232}Th}\right)_P \left(e^{-\lambda t}\right)\right) e^{\lambda t} \qquad [2n]$$

When time t since U-Th fractionation is not known, we can estimate relative ages from apparent stratigraphy. See Appendix H for examples of these calculations.

2.3. U-Th-Ra Radiogenic Isotope Analysis

The analytical work for this project was carried out in the U-Th silicate laboratory at the Open University over the period March 1995 to March 1998. Most of 1996 and early 1997 was devoted to the development of the Radium technique.

The isotopic abundance and ratios of U and Th were until relatively recently routinely measured by alpha spectrometry, which requires long counting times and relatively large sample sizes due to the typical low concentration of U and Th (0.01 to 10 ppm and 0.03 to 25 ppm respectively) in igneous rocks. Accuracy and precision were limited by chemical recoveries, detector efficiencies, the total number of disintegrations counted and background counts, giving between 2 to 5 % uncertainty at 2σ. With the advancement of TIMS (Thermal Ionisation Mass Spectrometry) it has become possible to analyse much smaller samples with lower concentrations and to a greater accuracy than with alpha spectrometry. The samples are analysed using isotope dilution, which is potentially the most precise and accurate elemental analysis technique available (Thirlwall, 1997).

2.3.1. U-Th-Ra Isotope Technique

The U-Th chemistry was undertaken over a period from March 1995 to March 1998, using two different spiking techniques. Appendix A contains data tables showing all of the U-Th results and Appendix D shows the standards. The first technique used two individual ^{229}Th and ^{236}U spikes, while the second technique, which was used to analyse the majority of the samples used a mixed ^{229}Th-^{236}U spike (AI and AT, two generations of the in-house spike). The initial spiking of the samples was the only difference between these techniques, since the same dissolution and column exchange method was used for both sets of samples. The samples were dissolved in batches of five and every few sets a total procedure blank and/or a rock standard (TML or ATHO) were included. U and Th were separated by a single column using anionic exchange resin with HNO_3, HCl and HBr as eluants, following a method shown below, adapted by Turner et al. (1996) from Chen and Wasserburg, (1981).

The aim was to obtain approximately 500 ng of sample Th on the filament. This was calculated by the following equation using the concentration of Th in the sample from either XRF or preferably INAA analysis.

$$\text{Amount of sample required (in g)} = \frac{500\text{ng}}{\text{ppm in sample} \times 1000}$$

$$\text{Amount of spike required} = \frac{(\text{Wgt of sample} \times \text{Conc of Th (ppm)} \times 1{,}000{,}000)}{(2500 \times \text{Conc of Th in spike})}$$

Between 50 and 500 mg of sample (Th ranged from 1.5 to 33 ppm) were weighed out into cleaned Teflon Savillex beakers (see Appendix A.7) to obtain the amount required on the filament for analysis, and the appropriate amount of spike(s) was added. The following flow chart (Figure 2.3) details the procedure used for the U-Th-Ra dissolution.

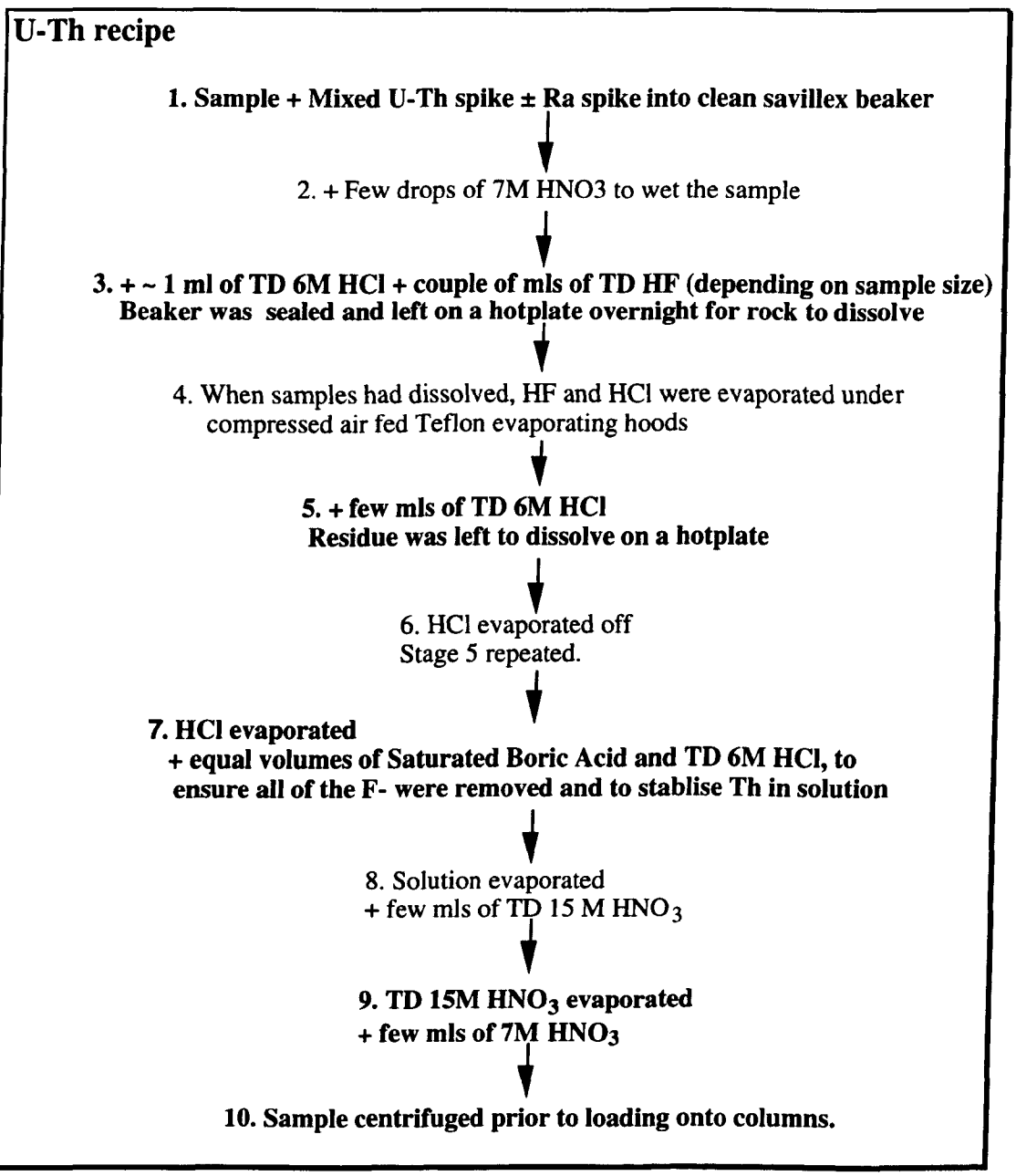

Figure 2.3. The dissolution technique for U-Th-Ra chemistry.

The samples were sealed and left overnight on a hotplate after each addition of acid, to ensure total dissolution, and a clear solution was obtained after each HCl and HNO_3 stage. If the solution remained cloudy after a few days, it was dried down and a couple of ml of 6M HCl were added and the procedure was repeated. The acids were evaporated using

compressed air fed Teflon evaporating hoods that were cleaned with a wipe of dilute acid prior to evaporation of the samples. The amount of acid required at each stage was dependent on the amount of sample dissolved in the first place.

The samples were centrifuged to ensure that any residue was not loaded onto the ion exchange column. The 7M solution being transferred to centrifuge tubes and centrifuged at 4000 rpm for 5 minutes.

The silica columns (stored in 6M HCl) were placed in the column racks and the glass reservoirs were put in place. The following method was used for the elution and collection of the individual U, Th and Ra fractions from the anionic resin.

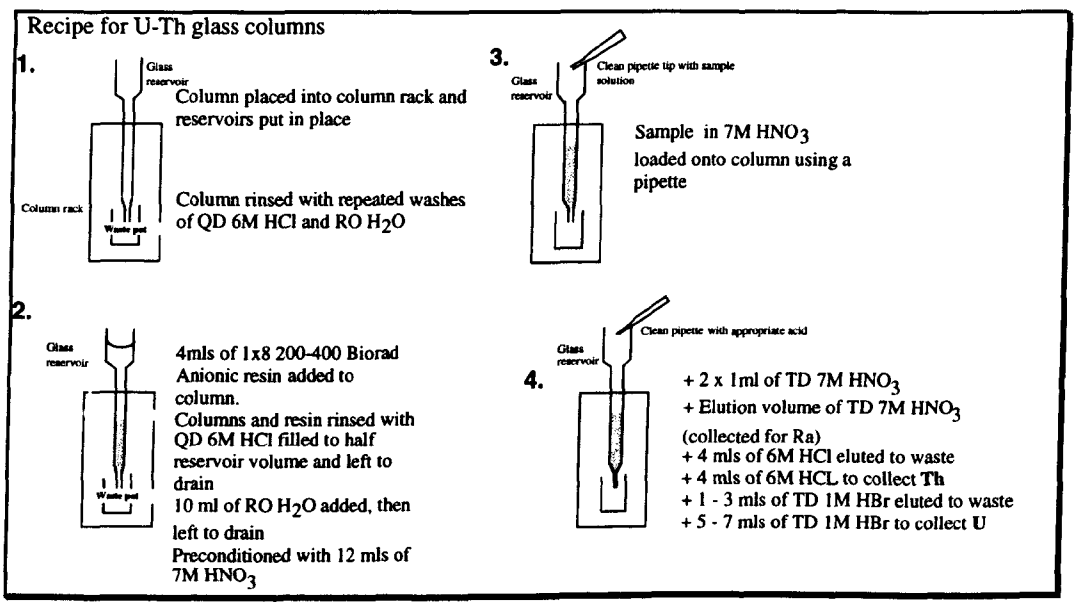

Figure 2.4. showing the procedure for the anionic resin filled silica columns used in the separation of U-Th-Ra chemistry.

Each addition of acid was allowed to drain through the resin, prior to the addition of the next batch. The amount of sample dissolved in the first place dictated the amount of TD 7M HNO_3 that was loaded onto the column and the amount of TD 7M HNO_3 that was eluted through the column. Thus, 0.1g of sample was loaded in 3 ml of TD 7M HNO_3 and had 18 ml of TD 7M HNO_3 eluted. 0.25 g of sample was loaded in 6 ml of TD 7M HNO_3 and had 15 ml of TD 7M HNO_3 eluted. 0.5 g of sample was loaded in 12ml of TD 7M HNO_3 and had 9 ml of TD 7M HNO_3 eluted, and so on.

The Ra fraction (all of the 7M HNO_3) was collected in a 30 ml clean savillex beaker, whilst the U and Th were collected in 7 ml clean beakers. The different amounts of HBr for the U fraction were due to different column calibrations. The fractions collected were

evaporated down to dryness. In some cases a large (> 1 mm in diameter) spot was located in the base of the beaker. This was be due to incomplete separation and a dirty fraction being collected, hence further cleaning up of the sample was necessary. This was done using the same size of anionic columns as used in the Pb procedure (1 ml pipette tips with small teflon frits). The columns were cleaned in 6M HCl and RO H_2O, and 1 ml of the anionic BioRad resin (same resin as for the large columns) was added to the columns. This was cleaned with a repeated wash of TD 6M HCl and TD H_2O and pre-conditioned with 2 resin volumes of TD 7M HNO_3. 0.5 ml of TD 7M HNO_3 were added to the residue of the sample and the sample was left to redissolve. The samples were then loaded onto the column and eluted with 3 column volumes of TD 7M HNO_3. The U and Th fractions were then treated differently. If collecting for Th, 1 resin volume of TD 6M HCl was eluted and 3 resin volumes of TD 6M HCl were collected and dried down. If collecting for U, 3.5 resin volumes of TD 6M HCl were eluted, followed by 0.5 resin volume of TD 1M HBr and finally 3 resin volumes of TD 1M HBr were collected and dried down.

2.3.2. Loading the samples

The samples were now ready to be loaded (either with or without the clean-up columns). The U fractions were redissolved in 2 µl of TD H_2O or TD dilute HNO_3 and were loaded onto 2 µl of dried down graphite aquadag solution on Re single filaments. The aquadag was dried down at up to 0.5 A, whilst the sample was dried down at 0.6 A and the current was turned up to 1 A for a few seconds to ensure that the sample was totally dry. The Th fraction was loaded using a Th loading solution made up from 6 ml of 0.2M HNO_3 and 25 drops of 10% phosphoric acid. 2 µl of loading solution were added to the residue and loaded onto a double Re filament

2.3.3. Standards

Laboratory standards (OU internal standards U456 std, U456 std 2 and Th 'U' std) were run in each magazine to evaluate the reproducibility between the different magazines. U456 std2 was run over the period from June 97 to June 1998 and gave $^{235}U/^{236}U$ = 0.097495 ± 0.00068 yielding two standard deviations of 0.69 %, whilst the $^{234}U/^{236}U$ value was 13.27196 ± 0.02862 yielding two standard deviations of 0.21 % (n = 92). During the

period of analysis (March - September '95) for samples LAN 1 - LAN 17, multiple determinations of the Th 'U' standard (van Calsteren and Schwieters, 1995) gave 6.131 ± 0.021 x 10^{-6} (n = 22) yielding two standard deviations of 1% in the part of this study. There were a number of problems with the quality of the Th 'U' std data over the time of this project. These problems were probably linked to different causes (circuit board, problems with focussing, prior to source clean) with the MAT 262 and in some cases filament geometry or loading, although there were a number of standards which had low abundance, did not run, or gave a number away from the expected value for no obvious reason. At least one of the samples that were run within these magazines was usually repeated to ensure that the number obtained was correct. From November 96 until March 98, multiple determination of the Th 'U' standard gave 6.15783 ± 0.11732 x 10^{-6} (n = 122) yielding standard deviations of 1.91%. The standard deviation was better (0.6 to 1.4 %) in long intervals over this period of analysis. Duplicate determinations of the ATHO Th standard gave ($^{230}Th/^{232}Th$) = 1.015 ± 0.006 (n = 6) and TML gave ($^{230}Th/^{232}Th$) = 1.0883 ± 0.01 (n = 2). On the whole, standards run by the individuals gave better errors than the whole lab compilation (see Appendix C). ((ATHO from Cambridge lab gave ($^{230}Th/^{232}Th$) = 1.015±0.004 (Cohen et al., 1992, 1994); TML from Lundstrom et al., 1995 gave ($^{230}Th/^{232}Th$) = 1.084 (alpha spec.data)). The present procedure is capable of analysing ($^{230}Th/^{232}Th$) ratios to 0.5% 2 sigma precision on 40-60 ng Th (Turner et al., 1997).

2.4. Mass Spectrometry

U and Th concentrations and isotope ratios were determined by thermal ionization mass spectrometry on a high abundance sensitivity Finnigan MAT 262 equipped with an RPQ-II energy filter (van Calsteren and Schwieters, 1995). The software was developed by Peter van Calsteren and David Wright. The U and Th isotopes were collected on isotope specific routines. Most of the Uranium's were measured using 'U456 single' which collected the isotope ratios ($^{234}U/^{236}U$) and ($^{235}U/^{236}U$). The integrated counts collected had to be greater than 100 c.p.s. on ^{234}U and preferably over 1 pA of ^{235}U for a useable number and at least 10 sets of 10 ratios were collected. To achieve precision of less than 0.5% 2 sigma a sample would commonly be collected for 20 sets of 10 ratios. The filament currents

for each sample varied with the variety of Re, but most were collected between 4.2 and 5.5 amps. The total time per isotope varied depending on the isotopes present, but was typically between 4 and 16 seconds. Th was measured on two separate routines, the first (Th'z'229) measured statically the ($^{229}Th/^{232}Th$) ratio, then a second programme (Th) switched dynamic between the Faraday collector and the SEM to measure ($^{230}Th/^{232}Th$). The beam intensity required a minimum of 40,000 counts ^{232}Th for the first routine and greater than 1 pA for the second. The static programme was run until an error of less than 1% 2 sigma error was obtained - usually about 3-4 sets of 10 ratios, then a minimum of 10 sets of 10 ratios each were collected for the dynamic run. The filament current ranged from 2.0 to 5.0 amps on the evaporation filament and 4.4 to 6.0 amps on the ionisation filament for the different routines and different Re batches. Typical abundance sensitivity is $5x10^{-8}$ at 1 amu from the main peaks for ^{238}U and ^{232}Th, and so any tail contributions on ^{230}Th and ^{234}U were insignificant. The dark noise of the multiplier (< 0.1 cps/s) is negligible relative to the typical ^{230}Th beam intensities during analysis (>20 cps/s). Chemical preparation blanks were ~ 50 pg for Th and 100 pg for U, which are negligible compared with the ≥ 100 ng of sample usually loaded and the error of U/Th ratios is ≤ 0.5%. Decay constants used in the calculation of activity ratios were the same as those compiled by Goldstein et al. (1989) (see Table 2.1 for original references).

2.5. Radium Isotope Technique Development and Analysis

A large amount of the analytical work undertaken during this project was dedicated to the development of a technique for the analysis of the abundance and isotopic ratio of Radium (Ra). Disequilibrium between short-lived nuclei in igneous rocks was discovered very early on (Joly, 1909), but has only been subjected to a detailed study relatively recently (e.g. Condomines et al., 1988; Williams and Gill, 1989; Volpe et al., 1991; Gill and Condomines, 1992; Cohen and O'Nions, 1993; Chabaux and Allègre, 1994). ^{228}Ra and ^{228}Th can be used to measure very short period changes in magma chemistry, but due to their very short half-lives of e.g.^{224}Ra, ^{216}Po they are rarely found out of equilibrium. ^{226}Ra is the most widely used short-lived radioactive nuclide, and again it has been routinely measured by alpha counting, but recent developments in TIMS allows its measurement to femtogram

range (10^{-9} ppm) and to a precision of better than 1 % (e.g. Cohen and O'Nions, 1991; Volpe et al., 1991).

The equilibration time for ^{226}Ra is in the order of 8,000 years and so it is obviously useful in studies of geologically rapid, recent and short-lived magmatic processes. However the disadvantage compared to U-Th disequilibria is the lack of a long-lived Ra isotope to normalise against in order to exclude chemical fractionation. Condomines et al. (1988) used both ^{226}Ra and ^{228}Ra with their respective half-lives of 1600 and 5.77 years ratio-ed to ^{230}Th and ^{232}Th respectively. The radioactive pairs reach equilibrium at different rates (in 8,000 and 30 years), and the time of Ra-Th fractionation can be measured by comparing the disequilibrium in each pair. Hence if (^{228}Ra-^{232}Th) disequilibrium is observed the fractionation is less than 30 years old, whilst if this ratio is 1, and yet (^{226}Ra-^{230}Th) is not 1, the fractionation event is older than 30, but less than 8, 000 years. This has been shown effectively by numerous workers including Capaldi et al. (1976) in the Oldoinyo Lengai, and at Stromboli and Etna (Condomines et al, 1987; 1988).

To overcome the lack of long-lived radium nuclide, Williams et al. (1986) suggested using Barium as a proxy. The two elements have similar distribution coefficients and are thought to behave similarly in melting and fractionation processes, since they are a similar size and charge. However it has since been shown that the two elements can have different partition coefficients (Evans et al. 1998), and where one is incompatible, the other can become compatible. Nonetheless the concept of Ra-Ba disequilibrium has been used in the development of thoughts on Ra chemistry. Assuming that Ba behaves as a stable isotope of Ra, an isochron diagram using (^{226}Ra-^{230}Th) and Ba/Th weight ratios is analogous to the (^{230}Th-^{238}U) equiline diagram, as the parent-daughter ratio plots on the y-axis. Another diagram frequently used as an isochron diagram for this system is (^{226}Ra)/Ba versus (^{230}Th)/Ba. These diagrams have been used over the past decade to infer the timescales in magmas including those in MORB from East Pacific, Juan de Fuca and Gorda Rise (Rubin and Macdougall, 1990; Volpe and Goldstein, 1993). If melts develop from a source in secular equilibrium on a Ra equiline diagram, the newly formed melts should lie on a horizontal line, at a constant (^{226}Ra)/Ba ratio. The fractionation of Ra and Ba relative to Th presumed to take place during partial melting, leaves the melt with different ratios from the source, and so the melts gradually move vertically back from positions, both left and right of

the equiline, as in the (^{230}Th-^{238}U) system (Figure 2.2.). Since the half-life of ^{226}Ra is much less than that of ^{230}Th, the latter is considered to be stable and ages are calculated by the intercept of the isochrons on the y axis.

An isochron equation similar to the conventional U-Th isochron can be developed as shown in equation 2o, where () signifies activity ratios and [] signifies concentrations.

$$\frac{\left(^{226}Ra\right)_p}{[Ba]} = \frac{\left(^{226}Ra\right)_l}{[Ba]} e^{-\lambda t} + \frac{^{230}Th}{[Ba]}\left(1 - e^{-\lambda t}\right) \qquad [2o]$$

It can be misleading to rely on two point (glass - phenocryst) isochrons without other supporting evidence, as some minerals such as anorthoclase take up divalent, but not trivalent ions, and so the ratio of the Th and Ba partition coefficients is very small. Assuming secular equilibrium before melting started, a fractionation age for rocks younger than 8 000 years old can be calculated. The most extensive studies have been undertaken on MORB glasses, where high (^{226}Ra/^{230}Th) ratios are found. In the same way as for the U-Th modelling, dynamic melting models have been used to explain the Ra-Th data. Spiegelman and Elliott (1993) estimated that ascending velocities are too low for melt to reach the surface from the depths of U-Th fractionation without Ra decay. Thus, they proposed porosity variations in the melt column ranging from zero at the base to a maximum of 0.5% at the top, which held back the decay of the Ra and allowed some of the Ra to be derived from shallower levels. McKenzie (1985) assumed Ra distribution coefficients of zero and instantaneous melt extraction, with most of the Ra being extracted in very small degrees of melting at depths within the garnet zone. Other models including those of Qin (1992) have invoked disequilibrium melting, assuming this is unavoidable during the generation of ^{226}Ra excesses and argued further that different cations would have different rates of volume diffusion and hence could cause diffusional fractionation. However this overlooks the fact that the source must have spent in the order of 100 k years in the melting zone for an upwelling rate of 5 cm.yr^{-1}.

2.5.1. Development of Analytical Techniques at the Open University

The radiogenic isotope labs at the Open University were able to routinely measure Sr, Nd, Pb, U and Th. However with more work by other groups being done on short-lived isotopes and on the daughters of the decay chains of U and Th, it became necessary to

develop a technique to analyse Radium. This had been worked on with limited success by Marcel Regelous; however a large amount of the laboratory time for this project was spent developing this technique.

Initially the technique used was developed from those of Volpe et al. (1991), Cohen and O'Nions (1991), Cohen and O'Nions (1993), Chabaux et al. (1994) and A. S. Cohen and S.P. Turner (*pers. comm.*). The samples were dissolved as for U-Th analysis and an aliquot of ^{228}Ra spike (calculated from the U concentration of the sample) was added at the initial weighing stage along with the ^{236}U and ^{229}Th spikes. The dissolved sample was added to, washed on and eluted through the anionic resin column in the usual way, but the portion of 7M HNO_3 the loading effluent, washing and elution acid which was usually left for waste was collected as this should contain the Ra fraction. The Ra fraction must be separated from the rest of the elements, such as Fe, Mg, Al, Ca, Sr and Nd, which are also collected in the 7M HNO_3 from the anionic columns. This was done using 2 cation exchange columns of different sizes and it also required the removal of Ba, which behaves in the same way as Ra on the cation columns. The Ra was extracted from Ba using a solution of crown ether (4.4'(5')bis-(tert.-butylcyclohexano)-18-crown-6) in 1-octanol adsorbed on an inert substrate as an extractant: the El Chrom company markets this resin as a Sr Spec® resin (Horwitz et al., 1992; Chabaux et al., 1994). The routine that was initially used yielded no Ra onto the filament and hence into the mass spectrometer, so it was decided to check the yields of the various columns. The Sr Spec® resin was the first column to be checked.

2.5.2 Sr Spec® Resin Experiments

150 µl of the resin was made up in a slurry of 3M HNO_3; this was placed into a small polypropylene column with a teflon frit in place and a mark of 150 µl on the edge of the column, a little above the base of the reservoir. As Ba can be used as a proxy for Ra on the cation columns, the Ra should come off the Sr Spec® columns in the fraction just prior to the Ba. The experiments were undertaken using Ba, to avoid using large amounts of the radioactive Ra. A solution of $BaNO_3$ (1000 ppm) was diluted to give a number of solutions with concentrations ranging from 250 to 5 ppm Ba. An aliquot of the 100 ppm Ba was dried down and taken up in 50 µl of 3M HNO_3 and loaded onto the Sr Spec® column which had

been pre-conditioned with 3M HNO_3. 7 x 150 µl aliquots of 3M HNO_3 were taken through the column and collected in small AA vials.

2.5.3. Atomic Absorption Spectrometry and the VG 54E

The AAS (atomic absorption spectrometer) at the Open University was used for calibrations of the columns for Rb, Sr, and Nd separations. A Ba hollow cathode lamp was placed into the spectrometer and the amount of Ba present in each solution was analysed. This proved to be a time-consuming and cumbersome method, as there were problems with the spectrometer and the Ba lamp was not working correctly. A number of attempts with different concentrations and running techniques failed, and it was eventually decided to try and use the VG 54E to analyse the Ba concentrations instead. The experiment was run as before and the collected fractions were dried down and loaded onto triple Ta beads which had been outgased for 5 minutes at 4.5 A. A test solution of $BaNO_3$ was run as a standard. Although beams were generally unstable, rough analysis of the aliquots was possible and Ba was found in the last couple of aliquots.

2.5.4. Sr Spec® resin (continued)

During these experiments it was discovered that the Sr Spec® resin was best made into a slurry with low molarity (0.2M HNO_3) just prior to loading onto the columns, and that being kept in a slurry for a time (greater than 36 hours) rendered the resin useless. A trial using dilute sulphuric acid to clean the resin was stopped as problems of high blanks developed.

The calibration of the Sr Spec® resin was corrected and finally confirmed using a Ra standard alone, and a mixed of Ra and Ba standards, in aliquots through the column. The Ra eluted as expected prior to the Ba and the calibration as detailed in section 2.6 was used. However when trying actual samples, it became apparent that the Sr Spec® wasn't the sole problem and that there were calibration problems with the other columns, as the recovery of the Ra was still at very low levels (see section 2.6 for running mass spec details). Chabaux et al. (1994) used a much larger Sr Spec® column than has been used here, although G. Zellmer (*pers. comm.*) worked on using the large column when he failed to obtain Ra using

the method used in this project. His calibrations for the large Sr Spec® column can be found in Appendix E.

2.5.5. Cationic Columns Calibrations

Again Ba was used as a substitute for Ra, but in this case their behaviour should have been similar enough for the experiment, because the cationic resin should not distinguish between them. 10 ml polypropylene columns used for the cation columns were soaked in dilute HCl and washed with QD 6M HCl and RO H_2O prior to the addition of the resin. 2ml of the BioRad chromatographic column packed with 2 ml cation-exchange resin (Biorad, 200-400 mesh, 0.8g / ml dry resin) was added to a column. The resin had already been washed in 5 changes of QD 6M HCl and RO H_2O. Once in the column it was further washed with 2 washes of TD 6M HCl and TD H_2O and then the column was then preconditioned with 3 x 2 ml of 3M TD HCl. 50 µl each of the Ca, Sr and $BaNO_3$ 1000 ppm AA standard solutions were weighed into a 15 ml Savillex beaker and gently evaporated. This is roughly equivalent to 50 µg of each element. The dry residue was dissolved in 10 ml of 3M HCl. 0.4 ml of this solution (2 µg of each element) was made up to 3 ml using 3M HCl, then loaded onto the column. The loading solution was collected immediately and each of 4 x 3ml 3M HCl were also collected into individual beakers. 2 x 1ml of TD H_2O was collected and finally 3 x 3ml of 3.75M HNO_3 were collected again in separate beakers. These were dried down and treated with 0.5 ml of 15M TD HNO_3, 10 ml of 0.5M HNO_3 were added to the HCl and H_2O fractions, 50 ml were added to the 1st HNO_3 and 20 ml were added to the 2nd and 3rd HNO_3. This was to allow for the increased concentration as most of the Ba was expected to be in the one fraction. This experiment was repeated with a 0.6 ml BioRad column (a second separation required in the procedure). The Sr spec column, loading 0.4 ml taken up in 0.2 ml to the 0.6 ml cationic resin, and 0.4 ml treated with 0.5ml of 15M TD HNO_3 and redissolved in 50 µl 3M HNO_3 then onto the Sr spec columns. The Sr spec column has been proved to be efficient at separating the Ra and Ba, and Ba came out as expected, as shown in 2.5.4. The sample on the 0.6 ml column was collected in separate fractions of 5 x 2ml HCl, 2 x 1ml H_2O and 2 x 2ml of 3.75M TD HNO_3. These were treated as the 2 ml column fractions.

2.5.6. ICP-MS (Inductively Coupled Plasma-Mass Spectrometry)

The fractions were then ready to be run on the ICP MS in Southampton. ICP-MS is rapidly becoming a routine technique for measuring trace element abundances, amongst other things. The sample is introduced as a solution and converted by a nebuliser into an aerosol and dispersed into Ar gas, which is taken through the sample chamber where larger droplets settle out, and then into the plasma torch, which serves as an ion source for the mass spectrometer. The analyser section of the ICP-MS operates at high vacuum; the most common mass analyser is a quadrupole mass filter which rapidly scans pre-set mass/charge ratios and accumulates ions to give an integrated peak for each mass number. (Jarvis, in Gill (1997) for further information). The ion beam is measured using an SEM. The first attempt at running this experiment failed as all of the Ba appeared to be in the first HCl aliquots; and this was totally unexpected as the Ba should have come out in the change from HCl to HNO_3 on the column. It was discovered that the TD HCl was possibly contaminated with minute amounts of HNO_3 from the cleaning process. This meant that the Ra and Ba were washed straight off the column: nonetheless the problem was solved and for a time HCl direct from the reagent bottle was used, and this gave no apparent problem with the blank. Figure 2.5. shows the results for the 2ml column after a second attempt, the calibration was as expected and the majority of the Ba, and hence Ra came out immediately after the change of acid.

The 1st cationic column calibration was then agreed and is currently being used in the laboratory (See section 2.6). However the 0.6 ml cationic column had further problems: these were eventually solved by using 2ml of Ra standard (AN), the column was treated as before, the standard was loaded in 0.2 ml of 3M TD HCl, then 15 x 1 ml aliquots were taken and each was run through the current Sr spec column to separate the Ba (present in the ^{226}Ra standard from the Ra). They were then run on the MAT 262 on single Re filaments. The calibration in Section 2.6 was achieved from this experiment and the majority of the Ra came out in the 6th to 10th cuts.

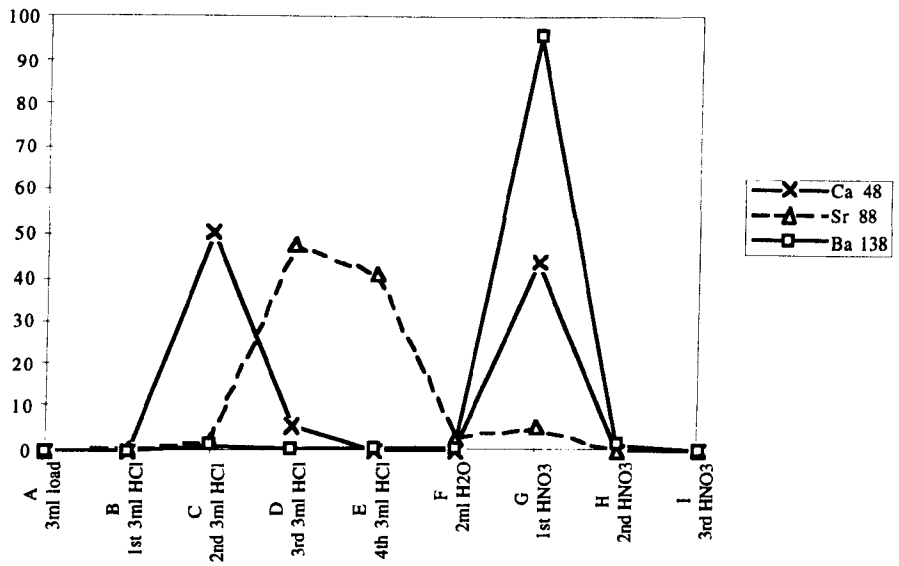

Figure 2.5. Graph showing results from 2 ml cationic resin column.

2.6. Final Procedure for Ra Analysis

The procedure now established for Ra analysis gives a success rate of 90 - 95%. The samples are run in batches of five, similar to the U-Th analysis. The 7M fraction from the U-Th anionic column was collected, dried down, taken up and dissolved in a few mls 6M TD HCl, and dried down again. This was repeated once, to ensure that all the nitrates had been converted to chloride, and then the sample was taken up in 3ml of 3M TD HCl.

2.6.1. 2ml Cationic Resin Column

The first elution was performed on 2 ml cationic resin in a 10 ml polypropylene column, preconditioned with 3 _ 2 ml 3M HCl. Samples were loaded in 3 ml 3M HCl and washed on with 2 _ 1 ml 3M HCl. Subsequently, 8ml 3M HCl followed by 2 _ 1ml H_2O were eluted. Then, the Ra-enriched fraction was collected in 2 _ 1 ml 3.75M HNO_3 followed by 10 ml 3.75M HNO_3. The collected fraction was evaporated to dryness, converted to chloride with 6M HCl, evaporated to dryness again and then taken up in 0.2 ml 3M HCl. The yield on this column is of the order of 95-98%.

A large 10 ml resin column has been developed by D.Peate and T. Kokfelt for the analysis of low level Radium samples, which require large amounts of sample to be dissolved. A summary of this calibration can be found in Appendix E.

2.6.2. 0.6ml Cationic Resin Column

After the first cation separation, a second separation was performed on 10 ml polypropylene cleanup columns packed with 0.6 ml of the same resin, preconditioned with 3 _ 0.6 ml 3M HCl. Samples were loaded in 0.2 ml 3M HCl and washed on with 2 _ 0.6 ml 3M HCl. Subsequently, 4 ml 3M HCl followed by 3 _ 0.6 ml H_2O were eluted. Then, the Ra-enriched fraction was collected in 2 _ 0.6 ml 3.75M HNO_3 followed by 5 ml 3.75M HNO_3. The collected fraction is evaporated to dryness and taken up in 50µl 3M HNO_3. The yield on this column is in the order of 95-96%.

2.6.3 Sr Spec Resin Column

The final and current Sr Spec® procedure developed during my work is as follows.

150 µl of Sr Spec® resin was loaded onto a small polypropylene column containing small teflon frit (these were stored in 6M HCl and washed with RO water and TD HNO_3 prior to the addition of the resin), in a slurry of 0.5M HNO_3. It was necessary to ensure that no air bubbles are present in the resin.

The resin was then washed with 300 µl of 0.5M HNO_3, and preconditioned with 4 x 150 µl 3M HNO_3. The sample was loaded onto the columns in 50 µl of TD 3M HNO_3 and eluted onto the column with 3 x 50µl 3M HNO_3. The Ra fraction was collected in 2 x 150 µl of TD 3M HNO_3 and dried down under compressed air fed evaporating hoods. The yield on this column is of the order of 95%.

2.6.4. Loading Procedure

For Ra isotope analysis, samples were loaded in 2 µl Ra loading solution (which is Ta-HF-H_3PO_4 activator) (Cohen and O'Nions, 1991) onto single Re filaments (outgassed for 15 minutes at 4.5 A, after the filaments have been boiled in repeated RO H_2O washes) and dried down at 1.5 V, 0.6 A. Then, the current was increased to 1.0-1.5 A for ~3 s to remove excess phosphoric acid.

2.6.5. Mass Spectrometry

Problems encountered on the mass spectrometer included insufficient Ra purification, resulting in high Ba count rates and suppressed Ra ionisation, and low concentrations and rapidly dying Ra beams, suggesting that some Ra was lost during separation and that column

yields were variable and could be very low at times. The final Ra procedure gave, on the whole, very good Ra - Ba separation and hence Ba does not suppress the ^{226}Ra and ^{228}Ra peaks, giving an interference pattern over the range of mass units. Interferences from organics (and possibly from Ba) tend to show at peaks at masses 225, 227 and 229. In some cases the interferences were greater than the 'actual' ^{226}Ra peak. For sample runs the interferences had to be below 5% of the smallest peak before a number would be accepted. The ($^{226}Ra/^{228}Ra$) ratio was collected for 10 sets of 10 ratios on the SEM on a beam with an intensity of no less than 100 c.p.s. on the smallest peak. The filament current is dependent on the type of Re used, but was usually no higher than 2.6 A, and no lower than 2.15; however the temperature is relatively constant at around 1250°C. The amount of Ra on the filament, was giving good, generally stable, beams and the reproducibility is approximately 1% (2σ), as determined on an in-house standard. The blank contribution is negligible.

2.6.6. Radium spikes and Standards

The NIST 3159 Th standard solution should contain large amounts of ^{228}Ra, which have decayed from ^{232}Th in the solution over time, hence it is possible to extract the ^{228}Ra from the solution and concentrate it to make a spike. The Ra spike was made by milking a NIST 3159 Th standard solution (9.9mg/ml Th in 10% HNO_3). 10 ml of the NIST 3159 solution and 8 ml of TD 15M Conc. HNO_3 were mixed together in 2 centrifuge tubes to make a 7M HNO_3 solution. A silica column with 8 ml of Biorad anionic resin was preconditioned with 20 ml of TD 7M HNO_3 and the sample was then added to the column, washed on with 2 x 1 ml of TD 7M HNO_3, and eluted with 23 ml of 7M HNO_3: the sample, wash and eluant were collected from the column and dried down overnight. The resin was disposed off (or kept if the Ra concentration was in doubt) since it should contain most of the Th, and the Th should stick to the resin and the Ra should wash straight through. A 4 ml anionic resin column was then made up and pretreated with 12 ml of 7M HNO_3. The dried collect from the first column was redissolved in 4 ml of TD 7M HNO_3 and loaded onto the column; this was washed onto the column with 2 x 1 ml of 7M HNO_3 and then eluted with a further 10 ml. The whole fraction was again collected and dried down overnight, and the resin was disposed off. Another 4 ml resin column was made up, again preconditioned with 12 ml of 7M HNO_3; the dried down collect was taken up in 3 ml of 7M HNO3, and loaded

onto the column. It was then washed and eluted with a further 2 x 1ml and 7 ml of TD 7M HNO_3. An aliquot of this was run on the MAT 262 to test for Th concentration, which obviously must be as low as possible to allow the Ra spike to be used alongside the Th spike. When little or no Th (<1.5 pg Th) was found in the solution, it was then diluted to a usable concentration (usually up to 100 mls) using dilute HNO_3. Three Ra spikes were made and used during the analysis in the project (AL, AR and AU). An attempt to make a new Ra spike using Th oxide powder was abandoned, as firstly the Th oxide powder would not dissolve even in HF and HNO_3 mix, and secondly although some of the ^{228}Ra went into solution, a ratio of ^{226}Ra to ^{228}Ra of 1 was obtained, and this would have caused problems when spiking natural samples.

NIST 4967 was used as a solution standard, until an in-house standard was borrowed from Oxford (^{226}Ra standard -AN). Analyses of the Mt Lassen rock standard gave values (^{226}Ra = 1.080 ± 0.026 pg/g and 1.065 ± 0.010 pg/g) within error of previous published data (Volpe et al., 1991; 1.063 ± 0.010 pg/g and 1.068 ± 0.011 pg/g). Reproducibility is approximately 1% at 2 sigma, as determined on an in-house standard, and the blank contribution is negligible.

There are raging fires at the center of the earth
from which flames can break forth.
Gottfried Wilhelm, Baron von Lhbernitz (1669-1716)
German philosopher and mathematician.

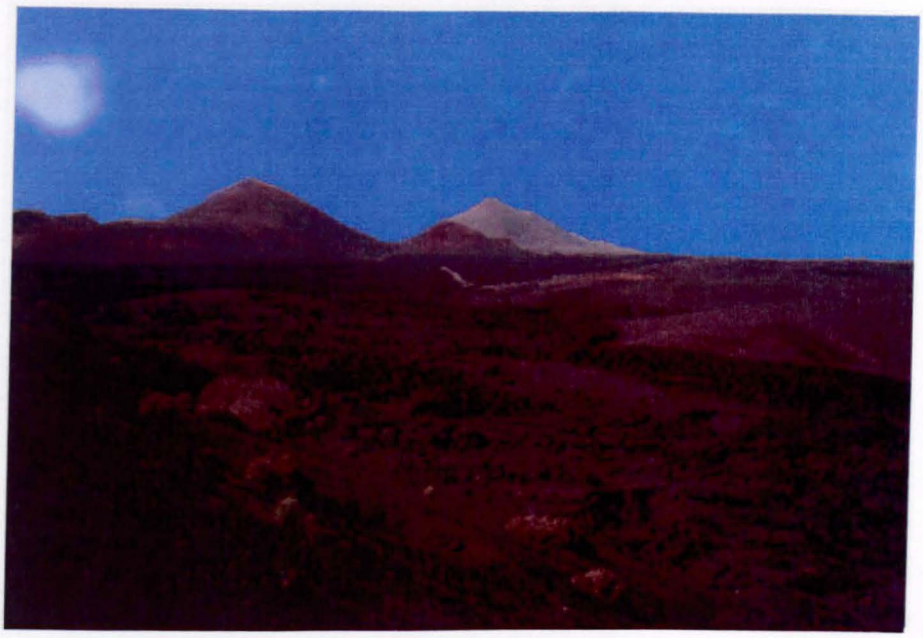

Parque nacional de Timanfaya
1730-36 Eruptions

Montaña de Corona

CHAPTER THREE

Uranium Series, Major and Trace Element Geochemistry of Lanzarote

3.1. Background

This chapter covers the geological background of the island of Lanzarote, Canary Islands and the major, trace and Uranium series geochemistry of historic and recent prehistoric lavas from the island. It is written in a paper format, as it has been submitted in part as a paper titled, 'Melt Generation beneath Ocean Islands; a U-Th-Ra study from Lanzarote in the Canary Islands'. L.E. Thomas, C.J. Hawkesworth, P. Van Calsteren, S.P. Turner and N.W. Rogers, to be published in Geochimica et Cosmochimica Acta in November 1999. One of the primary aims was to model the unusually primitive historic and recent pre-historic lavas sampled from Lanzarote in terms of a model for their melt generation, taking into account the effects of different controls on the melting process and to evaluate the Lanzarote source composition. However, this chapter includes greater details of the general background geology and more detailed geochemical modelling than the paper. Details of the analytical techniques have been covered in Chapter 2. The paper and this chapter conclude with a comparison of the geochemistry of other ocean islands; to evaluate variations in the amount and rate of melting with lithospheric thickness and mantle buoyancy fluxes within the different locations. The geochemistry of Tenerife is dealt with in chapter 4.

3.2. Abstract

The recent historic and prehistoric rocks from Lanzarote range from basanite to alkali basalt, and are from three different age groups in different areas on the island. The youngest are from two of the three 1824 vents, the largest group of samples is from the best known eruption episode, the 1730-36 Timanfaya eruptions, and the oldest samples are from the north-east Corona region (~ 54 ky) (Hoernle (*pers. comm.*). There are individual samples

from the basement and the Famara massif included in the analysis. The rock suites are amongst the most primitive found on intra-plate ocean islands with MgO contents >10.5% and Mg numbers >67. They have some of the characteristics of HIMU OIB, including high Ce/Pb, Nb/Ce and low Nb/U and restricted $^{87}Sr/^{86}Sr$ (0.70306-0.70332) (Weaver, 1991). However, the initial Pb isotope ratios are not as radiogenic as other HIMU OIB ($^{206}Pb/^{204}Pb$ ~19.2), perhaps reflecting a relatively young HIMU signature in the Lanzarote source. There is significant ($^{230}Th/^{238}U$) disequilibrium (^{230}Th excesses range from 6-81%) with the intermediate silica compositions showing the greatest disequilibrium. The younger samples exhibit ^{226}Ra excess, while the Corona rocks are in ^{226}Ra-^{230}Th equilibrium. The major and trace element data have been corrected back to Mg numbers of 70, requiring < 5% olivine fractionation, and these inferred primary compositions are used to evaluate a number of melt generation and mixing models. The results highlight the need for a residual garnet-bearing asthenospheric mantle source, as well as a shallower, oceanic lithospheric mantle signature (phlogopite bearing). The inferred depths and degrees of melt generation (1-4%) do not appear to be correlated with the degree of ^{230}Th-^{238}U disequilibria. Magma mixing plays an important role in controlling the final composition of many of the lavas.

The data are compared with recent results from other OIB to evaluate variations in amounts and rates of melting with lithospheric thickness and mantle buoyancy fluxes. The large ^{230}Th excesses observed in lavas from Lanzarote and other Atlantic OIB are not correlated with the degrees of partial melting or lithospheric lid thickness but are consistent with protracted dynamic melting (Williams and Gill, 1989) coupled with ^{230}Th-ingrowth. The amount of ($^{230}Th/^{238}U$) disequilibrium has an inverse relationship with the underlying buoyancy flux, potential temperature, and the inferred rate of melt generation, in contrast to MORB, in which ($^{230}Th/^{238}U$) disequilibria is greater in areas of higher mantle potential temperature. There is increasing evidence for a contribution from the lithospheric mantle to Lanzarote lavas and other OIB. Source composition may play a far more important role in controlling partial melting processes beneath ocean islands than that inferred for mid-ocean ridges.

3.3. Introduction

As discussed in Chapter 1 ocean island basalts provide an insight into the compositional variations in the Earth's mantle, which in turn constrains models for mantle convection and evolution (e.g. McKenzie and O'Nions, 1995). It remains difficult to determine the depths of source components sampled by OIB, but a number of recent studies have highlighted that some source components are present at comparatively shallow levels in the upper mantle (Class and Goldstein, 1997). If correct, this alters perceptions over the origins of these components, and in particular whether they can be generated by intra-mantle enrichment or metasomatic processes, rather than being due to deeply recycled crust or lithosphere (Hawkesworth et al., 1979; Cohen and O'Nions, 1993; McKenzie and O'Nions, 1995; Hofmann, 1997). However, these geochemical signatures are inferred from surface lavas which have undergone numerous processes, such as partial melting, melt transport, differentiation and crustal contamination. While the effects of some of these processes can be well constrained, the effects of others remain the subject of heated debate. The depths of melt generation can be inferred from both major and trace element compositions (Sims et al., 1995; Shen and Forsyth, 1995), and whilst the depth of origin of the source components is often much greater than the depth of melting, both requires a robust model which is consistent with the constraints from major and trace elements and U-series isotopes. To date these have proved difficult to establish for OIB, and controversies remain over how U-series isotope results can be reconciled with the information available from major and trace elements, and whether dynamic or simpler batch or fractional melting models are most applicable (Williams and Gill, 1989; Chabaux and Allègre, 1994; Sims et al., 1995). This chapter deals with a number of melting models, and their application to the island of Lanzarote. Each melting model was tried in an attempt to get a consistent model that could explain all the geochemical and isotopic data. The main questions in the melt generation of OIB and to a certain extent of MORB, is the degree to which melt generation and transport results in incompatible element fractionation and the decoupling of radiogenic systems and whether these characteristics are transferred to the surface? In this study we report major, trace element, Sr, Nd, Pb and U-Th-Ra isotope results on an exceptionally primitive suite of basalts (Mg * = 67-72) from Lanzarote in the Canary Islands in the eastern Central Atlantic

Ocean. An enriched residual garnet bearing OIB signature together with a shallower lithospheric signature is present in these rocks, and understanding the constraints from the major, trace and rare earth elements allows an informed insight into the causes of the variations in U-Th isotopes.

3.3.1. Partial melting in MORB - Is it better understood than in OIB?

Partial melting processes beneath mid-ocean ridges (MOR) are arguably better understood than those beneath ocean islands, because source composition variations are demonstrably smaller, and there is no lithospheric lid causing variations in the depth at which melting ceases. The broad negative array of Na and Fe at 8% MgO in global MORB implies that the higher average degrees of melting occur at higher average pressures (Klein and Langmuir, 1987). The average degrees and depths of melting increase with increasing temperature and decreasing ridge depth (Klein and Langmuir, 1987; McKenzie and Bickle, 1988; Shen and Forsyth, 1995) which, in turn, requires that melt extraction is very efficient. The degree of ($^{230}Th/^{238}U$) disequilibrium also appears to be greater in MORB from shallower ridge depths, and this has been attributed to more of the melt zone being within the garnet stability field in areas of higher mantle temperatures (Bourdon et al., 1996).

3.3.2. Controls on U-Th disequilibrium in OIB

By contrast, in OIB, the degree of ^{230}Th-^{238}U disequilibrium tends to be less, and the melt fraction higher, particularly in those OIB associated with a high buoyancy flux (i.e. high mantle potential temperature). In other words, ^{230}Th-^{238}U disequilibrium decreases with increasing mantle temperatures (Cohen and O'Nions, 1993; Chabaux and Allègre, 1994; Sims et al., 1995) and so the controls on ($^{230}Th/^{238}U$) disequilibrium would appear to be different in MORB and OIB. Resolving this discrepancy is central to establishing more widely applicable models for melt generation beneath ocean islands.

In intraplate settings the main controls on melt generation are likely to be the thickness of the lithospheric lid (Ellam, 1992), the buoyancy flux of the upwelling mantle plume, which is a function of its potential temperature (Tp), and the volatile content of the source region(s). The onset of partial melting is governed by the depth of intersection with the solidus and so partial melting should start deeper in regions of high buoyancy (i.e. high Tp).

The upper limit on the height of the melt zone will be controlled by the thickness of the overlying lithosphere, and so that will limit the total amounts of melting in any area (McKenzie and Bickle, 1988). The onset of melting is deeper beneath ocean islands than beneath MOR, and this is consistent with the relatively high Fe contents and Sm/Yb ratios of many OIB (Shen and Forsyth, 1995). Increasing the thickness of the overlying lithosphere will lower the cumulative degree of partial melting for a given Tp.

The rate of melting exerts a strong control on ($^{230}Th/^{238}U$) disequilibria since this limits the time for ^{230}Th-ingrowth in the mantle matrix (e.g. McKenzie, 1985). The rate of melt generation depends on the upwelling rate of mantle material through the melt zone, and hence on the buoyancy flux and Tp of the mantle plume (Chabaux and Allègre, 1994). Models to explain variations in ^{230}Th-^{238}U disequilibrium in MORB and OIB vary from the conceptually simple, in which U/Th fractionation is related to melt fraction (Sims et al., 1995), to the more complex which involve chromatographic effects in the melt regime (van Calsteren and Hawkesworth, 1999). However, in general the link between the rates and degrees of partial melting is not well established, although some data from Hawaii indicate that the degree of ^{230}Th-^{238}U disequilibrium increases with the degree of silica undersaturation and decreasing degrees of melting (Sims et al., 1995).

3.4. Background Geology of Lanzarote

A more detailed geological setting of Lanzarote is covered in this section compared to that of the paper. The age of the crust and thickness of the lithosphere is included here, as these are important in later discussions on the effect of lithospheric thickness on melt generation. Appendix A and B provide data tables, fractionation corrections and sample localities.

3.4.1. Crustal and Lithospheric Thicknesses

Lanzarote is the easternmost island in the Canary Island group, situated approximately 100 km from the NW coast of Morocco, Africa. The age of the underlying oceanic lithosphere varies from 150 Ma in the east to 175 Ma in the west (Roest et al., 1992). Oceanic lithosphere becomes thermally stabilised after about 70-80 Ma, at which stage horizontal isotherms occur at depths of 100-125 km (Parsons and Sclater, 1977; Parsons and

McKenzie, 1978). Thus, the 150-175 Ma old lithosphere of the Canaries should have reached a steady state thickness of 100-125 km. The bathymetry for such lithosphere should be ~ 5 km (Parsons and McKenzie, 1978), and yet the water depths around Lanzarote and Fuerteventura are ~ 1.5 km, although these increase to ~ 3 km around the islands further west (Araña and Carracedo, 1979). These shallower depths may reflect either some combination of the dynamic support by the mantle plume, the transition to the African continental lithosphere, or thermal erosion of the lithosphere by the plume (Davies, 1994). The crustal thicknesses beneath the Canary Islands vary systematically from 10-15 km in the east to 7-10 km in the west according to Bosshard and Macfaralane (1970), however 15 km of crust seems to be unexpectedly thick. The relatively constant thickness of the lithospheric lid rules out the observation of variations in the local melt productivity, which may be related to a regional link between melt productivity and the lithosphere thickness. The Canary Islands are generally assumed to have formed since the Miocene, and hence there is no connection with the early opening of the Atlantic Ocean at 200 Ma, and today the islands are ~ 2000 km from the Mid Atlantic Ridge. There is a general E-W progression in the age of the first subaerial activity, but the recent volcanic activity is more randomly scattered across the different islands, with all but one of the islands being active in historic or recent prehistoric times.

3.4.2. Summary of the Samples

Most of the Canary Islands show at least two phases of subaerial activity, a primary shield building phase, and a later smaller post-erosional volcanic phase. The oldest rocks sampled are from the basement underlying the Famara massif and from the Famara massif (see Figure 3.1. for locations), both are relatively weathered and required careful preparation to avoid the altered material. The activity on Lanzarote has been fairly continuous from 2.7 Ma to historic times. The Corona samples from the NE of the island, form part of the Series IV group and are thought to be 54 ka old (Hoernle *pers. comm.*). The most voluminous continuous eruptive episode, and the largest sample group in this study, was the 1730-36 Timanfaya event which erupted over 1 km^3 of basaltic magma (Carracedo et al., 1992). The most recent eruptions took place in 1824, when lavas issued from three small vents in the west of the Timanfaya region. The samples analysed here are from the Volcan Nuevo ~ 1 km

west of the main Timanfaya vent (Volcan Tiguaton: Carracedo et al., 1992), and from Montaña Chinero (Volcan Nuevo del Fuego: Carracedo, 1992; 1994).

3.4.3. Structure of Lanzarote

Lanzarote is an emergent part of the East Canary Rift (ECR), a linear volcanic structure ~ 70 km long by 65 km wide, striking NNE - SSW and located on atypically thick (~ 11 km) oceanic crust (Marinioni, 1991; Marinioni and Pasquarè, 1994). The ECR consists of a number of uplifted blocks of oceanic basement covered by a thick sedimentary sequence (> 10 km) mantled by > 5 km of volcanic rocks, with an intrusive complex between the two layers (Banda et al., 1981). On the submerged western side of the ECR, seismic profiles show evidence of Mesozoic and Tertiary sediments involved in folds and thrust faults, and this sequence is onlapped by undisturbed Plio-Pleistocene layers. Rocks representing submarine 'basement' and Cretaceous marine sediments are exposed in a block of the ECR (>1 km thick) on Fuerteventura. This succession which is commonly vertical or overturned suggests that the island's main structure is due to a major NE facing reclined fold, formed in the late Cretaceous - early Tertiary by motion in a regional shear zone. The occurrence of these sediments on Fuerteventura and the abundance of xenoliths on Lanzarote has been interpreted assuming that oceanic blocks rose individually and were later covered by volcanics from bordering fracture zones (Marinioni and Pasquarè, 1994). The uplifting of these blocks and the related folds and fractures are commonly linked to the SW extension of the S. Atlas fault along the High Atlas in Morocco (Banda et al., 1981). This is a common point for debate, with many believing that the formation of the Canary Islands was not linked to tectonic movements in the Atlas Mountains. There is a general NE-SW trend of the younger Quaternary pyroclastic cones and eruptive vents concentrated in the centre of the island, whilst the oldest eruptions show alignments of E-W and ENE - WSW. The Timanfaya eruptions have two directions of alignment, E-W is the main eruptive fracture direction and NNE - SSW is defined by smaller superimposed vents (Marinoni and Pasquarè, 1994.) These data appear to indicate a progressive rotation of the alignments through time. Dykes associated with the last stages of the shield building activity are common place, and they are often found cross cutting the earlier lava flows in numerous

directions. The emplacement of the dykes are consistent with the alignments of the activity on the island, in that a large percentage of them run NE-SW, whilst in the older areas they are mainly aligned E-W and ENE-WSW (Marinoni and Pasquarè, 1994).

3.4.4. Background Stratigraphy

Lanzarote consists of two edifices, a southern edifice that was active between 15.5 and 12.3 Ma, and a northern edifice active in intervals between 10.2 to 8.3 Ma, 6.6-5.3 Ma and 3.9-3.8 Ma (Coello et al., 1992). These are the best published dates for the island's activity, although N. O. Arnaud and J-M. Cantagrel (*pers comm.*) have more accurate Ar-Ar ages that are younger than the published data. They date the onset of activity at around 9 -10 Ma. Using the ages from Coello et al (1992), these rocks are grouped together as Series I, and there is a large temporal gap between Series I and the Plio-Quaternary Series II, III and IV formed by multi-vent eruptions (Figure 3.1.). The activity on Lanzarote has been fairly continuous from 2.7 Ma to historic times, and the oldest samples analysed for this study are from basement underlying the Famara massif, part of the Series II activity and from the Famara massif itself. The next group of samples are from the Corona region (Volcan Corona) in the NE of the island, where they are part of Series IV and are thought to be 53 ka old (Hoernle *pers. comm.*). The most voluminous continuous eruptive episode, and the largest sample group in this study, was the 1730-36 Timanfaya event which erupted 3 - 5 km^3 of basaltic magma (Carracedo et al., 1992). In 1824, there were eruptions from three small vents on the west of the Timanfaya region, and the samples analysed here are from the Volcan Nuevo vent, ~ 1 km west of the main Timanfaya vent. The lavas are basaltic in composition with limited trachyte outcrops in the older parts of the island. Quaternary cover creates lateral gaps and, unlike on Tenerife, there are no suitable marker horizons within the succession.

Comprehensive work on the stratigraphy and mapping of Lanzarote has been done by Marinoni, (1991); Carracedo et al., (1992); Marinoni and Pasquarè, (1994). Each succession demonstrates several constructive and erosional events, but despite the complexity the island can be divided up into 2 main stages, Pre-erosional and Post-erosional stages separated by an erosive phase, similar to those identified on the other islands.

The oldest eruption and that with the longest duration constructed 2 major structures one in the SW (Los Ajaches), and one in the NE (the Famara massif), and some local lavas in the SE at Morros de Guime. The rocks are mostly extensive basalt flows piled upon one another, but there are also some scoria and tuff cones and a few pyroclastic and trachytic flows. These sequences have undergone severe erosion forming the present day cliffs and precipices. There is thought to have been numerous volcanic cones linking both ends of the island at this time (between 10 and 5 Ma). A period of several million years is thought to have separated the pre-erosional stage that formed the highest part of the island from the following Quaternary shield building stage.

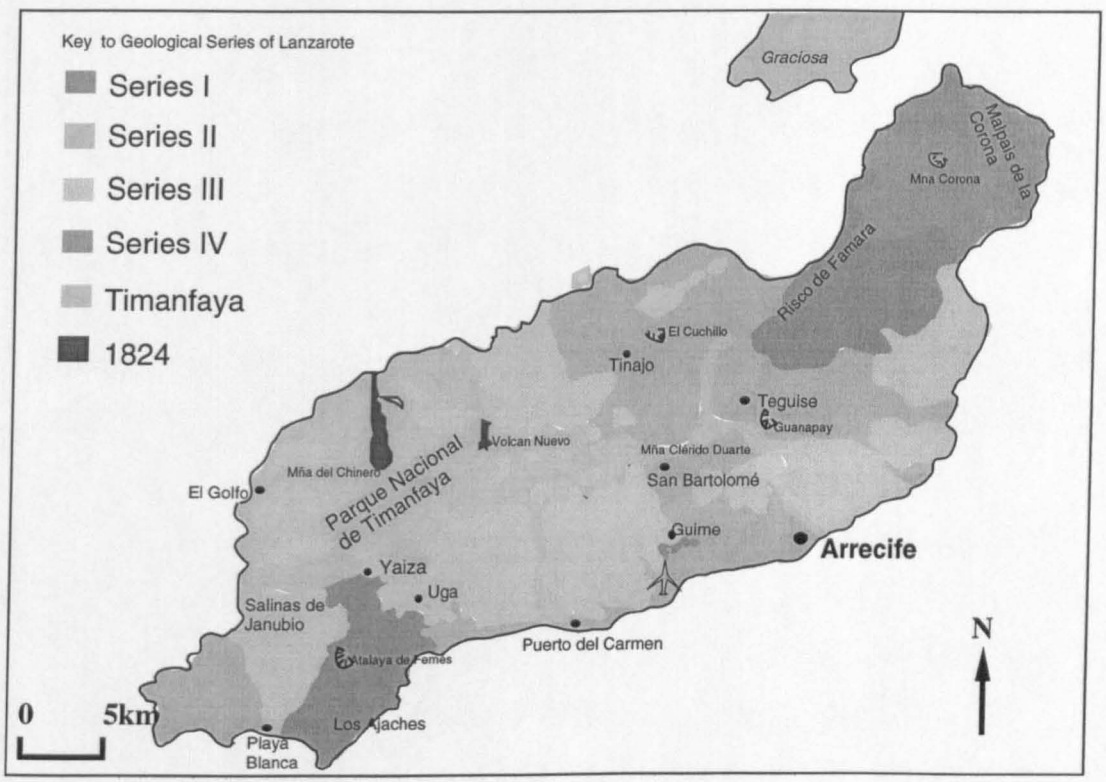

Figure 3.1. is a map which illustrates the geology of the island (after Coello et al., 1992; Marinoni and Pasquarè, 1994.)

In the main Quaternary shield building stage, the highest concentration of volcanics were erupted in the centre of the island and in the south. Numerous shield volcanoes formed such as Guanapay volcano, and there were maars and some doleritic intrusions like those at El Cuchillo. Some parasitic scoria cones and air-fall deposits were also formed.

Gradually through time the eruptive style shifted away from shield volcanoes to be almost completely pyroclastic in origin, with scoria cones, and their associated air fall and

flow deposits and some lava flows. This was again centred on the central sector of the island, although the deposits can be found over most of the island. Some eruptions formed the range of hills extending from the Atalaya de Fermes.

3.4.5. Corona Eruptions

The rocks of the Malpais ('Badlands') de la Corona in the north-east of the island were formed by eruptions in the Series IV phase of activity (~ 54 ka). They include a large area of scoria cones, air-fall deposits and lava flows with one of the major vents being Montaña de la Corona.

3.4.6. The Timanfaya 1730-36 Eruptions

The first eruptive episode to be well documented is the Timanfaya eruption of 1730-1736, in which a series of fissure eruptions created the now famous Timanfaya Park. The eruptive style was still that of scoria cones, air-fall deposits and lava flows, however it is unique compared with the historic (last 500 years) volcanism elsewhere in the Canary Islands. The lavas from these eruptions covered at least 23% of the island, stretching from the central part in the Timanfaya national park near Montana Los Rodeos and Montana Ortiz and to the coast at El Golfo.

The eruptions took place between 1 September 1730 to 16 April 1736, and the extent of the overall eruption was approximately 200 km^2, with between 1 km^3 (Arana, 1995; Thomas et al., 1997) and 3 - 5 km^3 (Carracedo et al., 1992) of material emitted. The magmas evolved from extremely SiO_2 undersaturated lavas (melanephelinites) towards olivine tholeiite compositions with time during the eruption, which is rare in the Earth's historical record of basaltic fissure eruptions.

Eyewitness accounts, include that in the diary of the parish priest of Yaiza, one of the 26 villages which were damaged or destroyed during the eruption, provide important information regarding the different phases of activity. The following is translated from an extract from part of the diary (In Carrecedo and Badiola, 1991; von Buch, 1825).

"Flames issued out of the ground and fragments of red hot rock were thrown through thick clouds of ash, illuminated by the volcanic fire, and resembled a stormy sea." "The darkness produced by the volume of ash and the gases that covered the badly ravaged island caused

the inhabitants of Yaiza to take flight....even on 28 October 1730, the volcanic action occurred in a such a way, that during the following 10 days, the livestock were all asphyxiated due to the poisonous gases in the region." The villages of Timanfaya, Sta Catalina and Mazo were the first to be destroyed by the eruption of lava flows and ash from Caldera de los Cuervos on the 1st -12th September 1730. The destruction of Yaiza by the eruption from Caldera Quemadas was later in December 1731; this is also the last entry in the parish priest's diary, as he left the island. The population was thought have halved during the activity from the approximately 8,000 people at the onset.

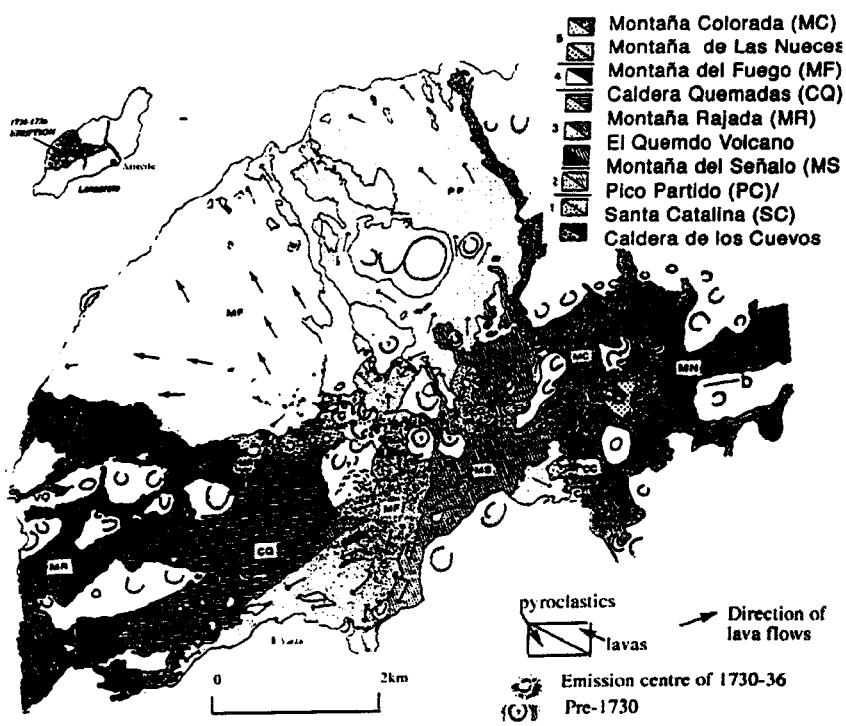

Figure 3.2 Geology of the 1730-36 eruption (after Coello et al., 1992; Carracedo et al., 1992 and Carracedo and Badiola, 1991).

At least nine main eruptive centres can be distinguished within this eruptive episode (Figure 3.2.) and distinctive changes in the eruptive dynamics and magma composition allow five eruptive phases to be described as below (Carracedo et al., 1992; Carracedo and

Badiola, 1991). Some of the dates in Table 3.1 are speculative, pieced together from different bits of evidence by Carracedo et al. (1992).

Phase 1	Caldera de Los Cuervos Sept 1730	Single cinder cone in centre of island, flows went north and west to the coast Non-viscous, extremely silica undersaturated lavas with abundant ultrabasic inclusions
	Pico Partido vent and Caldera de Santa Catalina 10/10/1730 – Feb. (?) 1731	Aligned with previous vent along 3 km NW-SE fissure. Large amounts of lapilli and lava flows. Similar composition and direction of flow to above. Southern vent opened as flows turned southwards threatening Yaiza. Rocks rich in peridotite inclusions. Composition evolving from melanephelinites through basanite to alkali basalt.
Phase 2	Mña del Señalo March -July 1731	Activity resumed near Pico Partido along main E-W fracture. Vent progressed along this fracture. Lavas becoming more silica saturated olivine basalts to olivine tholeiites. Higher viscosity's and lower effusion rates meant shorter flows
Phase 3	Volcán del Quemado – Mña Rajada - 4 Calderas Quemadas June 1731	An abrupt change moved the focus of activity 12 km to the western edge of the fracture. Submarine and phreatomagmatic eruptions on the west coast. El Quemado - a cluster of small elongated cinder cones 1km from coast. Activity migrated east along the fracture from coast forming close alignment of cinder cones. Alkali basanites to olivine tholeiites similar to Phase 2, spread over large part of west of island.
Phase 4	Mña del Fuego Early 1732 - unknown end of eruption as people left island.	Eruption ceased progression along fractures and became stationary. Activity concentrated around Timanfaya. Initially explosive activity formed the overlapping cinder cones of Mña del Fuego. The style changed and lavas were emitted from a cluster of hornitos in the NW and SE. Similar composition to 2 and 3.
Phase 5	Mña de Las Nueces – Mña Colorado Mid March - 16 April 1736	Eruption ended with 2 new centres located at eastern end of fracture resuming W-E progression. Mña de Las Nueces flows entered the sea near Arrecife more than 20 km E. and a separate flow moved north toward Tinajo. Composition evolved from alkali basalts to the most evolved tholeiites seen in the event

Table 3.1. Description of the 5 phases of activity shown in Figure 3.2: 1730-36 Eruption of Lanzarote

3.4.7. 1824 Vents

This final eruptive phase on Lanzarote followed twelve years of earthquakes and began in 1824, with three eruptions that formed three new volcanoes called Clerigo Duarte,

Chinero and Volcan Nuevo. The lavas evolved from basanite to olivine tholeiite and had numerous peridotite inclusions. They flowed north but due to their small volume and low effusion rate did not reach the sea. According to all except Carracedo and Badiola (1991), Volcan Nuevo is a small cone (330 m) Northeast of the Montaña del Fuego on the east of the road halfway towards Mancha Blanca: Carracedo and Badiola (1991) map this flow as Volcan Tiguatón (also 1824). Montaña Chinero is a slightly larger cone (358 m) from which flows extended to the sea; it is situated 0.5 km to the NNE of Mña del Fuego and it was mapped by Carracedo and Badiola as Volcan Nuevo del Fuego. Montaña del Clerigo Duarte is the smallest (303 m) of the 1824 eruptions and it is situated 1 km SE of Tiagua near the road edge.

3.4.8. Xenoliths

Neumann et al. (1995, 1997) reported suites of ultramafic xenoliths containing melt inclusions in the Quaternary and Recent alkaline basalts of Lanzarote. Some of these xenoliths are described by Carracedo et al. (1992) as peridotite inclusions, and they range in size from a few cm to 40-50 cm in diameter. The xenoliths have been separated into two main suites: spinel harzburgites (harzburgites and rare lherzolites) and spinel dunites (spinel dunites and rare spinel-plagioclase dunites). Those collected during this project were dunite compositions with some spinel present. Xenoliths have been used by Neumann et al. (1995, 1998) to study the upper mantle underlying Lanzarote, and to establish a possible composition for the source of the lavas. This chapter deals with the geochemistry of the rocks and comparisons between results published by Neumann et al. (1995, 1997) and those reported here.

The underlying mantle is reported to be highly refractory, old suboceanic lithospheric mantle, modified through a combination of melt extraction and metasomatism by Fe-Ti rich melts and CO_2 rich fluids. Temperatures from the CO_2 inclusions in the xenoliths indicate a high geothermal gradient in the upper mantle and a correspondingly thinned lithosphere (>27 km). These data infer a thinner lithosphere than previously predicted from its age, which may indicate that thermal erosion has thinned the lithosphere in this region.

3.4.9. Sample Locations and Collection

The samples collected from Lanzarote range in composition from basanite to almost olivine tholeiite, with the majority having intermediate alkali basalt compositions. The 1824 and some of the 1730-36 lavas contain large olivine/dunite xenoliths. Most have abundant olivine phenocrysts, and some also contain crustal xenoliths. The petrology and location of each rock can be found in Appendix B. Obvious xenoliths and phenocrysts/xenocrysts were separated from the groundmass prior to rock crushing. The 1824 eruptions tend towards basanitic compositions, while the 1730-36 Timanfaya samples are sub-alkali basalts to tholeiites. Detailed work by Carracedo et al. (1992) on the Timanfaya eruptions shows a gradual trend from silica undersaturated basaltic rocks to olivine tholeiitic compositions with time. This may reflect larger degrees of melting towards the end of an eruption. The third group of samples is from the older Corona region in the northeast of the island (Figure 3.1.).

3.4.10. Mineralogy and Petrology of the Samples from Lanzarote

The majority of lavas sampled have a glassy or very fine-grained matrix and consist of olivine + augite + opaques ± minor plagioclase (see Appendix B for more detailed individual descriptions). Most of the phenocrysts are olivine, although some feldspar is present in some of the more evolved tholeiitic basalts. The xenoliths are largely confined to the historic rocks and composed mainly of olivine, with some opaques (probably chromite) and some spinel.

3.5. Analytical techniques and sample collection

The samples analysed are olivine basanites to basalts, with some containing large olivine/dunite rich xenoliths; most have abundant olivine phenocrysts, and some also contain crustal xenoliths. The xenoliths and phenocrysts were separated from the groundmass prior to rock crushing. The 1824 eruptions trend towards basanitic compositions, while the 1730-36 Timanfaya samples are sub-alkali basalts. Detailed work by Carracedo et al. (1992) and Sigmarsson et al. (1998) on the Timanfaya eruptions shows a gradual trend from silica undersaturated basaltic rocks to olivine tholeiitic compositions with time. This has been interpreted (Carracedo et al., 1992) to reflect an increase in the degree of melting during the

eruptive phase. The third group of samples are from the older Corona region in the north of the island. There are limited trachyte outcrops in the older parts of the island.

The major and trace element abundances and the Sr, Nd, Pb, U, Th and Ra isotopic ratios are given in Appendix A. The major and trace element abundances were measured by XRF, and the REE were measured by INAA. Sr, Nd and Pb were separated following standard ion exchange techniques and isotope ratios were determined statically in multi-collector mode on either a Finnigan MAT 261 or 262 at the Open University. For fractionation corrections and normalising values see Appendix C, and chapter 2 for U-Th-Ra details.

Sr fractionation was corrected to $^{86}Sr/^{88}Sr = 0.1194$ and Nd to $^{143}Nd/^{144}Nd = 0.7219$. Pb was analysed on temperature controlled runs (1255°C) and the ratios corrected for ~1‰ per atomic mass unit mass-fractionation using our values for NBS 981 $^{206}Pb/^{204}Pb = 16.934$ (±2), $^{207}Pb/^{204}Pb = 15.414$ (±2), $^{208}Pb/^{204}Pb = 36.553$ (±2). Sr and Nd isotope ratios were normalised with respect to internally determined values for NBS 987 = 0.71022 (±1) and Johnson and Matthey Nd = 0.511776 (±5). Quoted errors are 1 standard deviation, and errors on individual runs are significantly less than the quoted reproducibility. Blanks for Sr, Nd, and Pb were typically < 0.8 ng, 0.3 ng and 0.3 ng respectively.

Reproducibility of the U456std2 (an in-house solution standard for U) gave ($^{235}U/^{236}U$) = 0.097495 ± 0.00068, yielding two standard deviations of 0.69 %, whilst ($^{234}U/^{236}U$) value was 13.27196 ±0.02862 yielding two standard deviations of 0.21 %. The Th 'U' standard gave two standard deviations of 1% for the first period of analysis and 1.4% for the second. The present procedure is capable of analysing ($^{230}Th/^{232}Th$) ratios to 0.5 % 2 sigma precision on 40-60 ng of Th (see also Turner et al., 1997).

3.6. Analytical Results

3.6.1. Major and trace elements

The lavas from Lanzarote have MgO = 9.81 - 14.64 %, Mg numbers of 67 - 74 and high Cr and Ni contents (383 - 594 ppm and 226 - 442 ppm respectively). They show a wide range in composition from silica undersaturated to silica saturated (SiO_2: 44.1-51.14%) and a range in total alkalis (3.3-5.1%), despite their similar Mg numbers. On the whole the 1730-36 rocks are hypersthene normative and the Corona and 1824 rocks are nepheline normative. The high MgO rocks are not cumulates, as the olivines are in equilibrium with mantle values and the kD's are modal relative to source. The dunite rich xenoliths are more enriched with Mg numbers of up to 93.3 and huge Ni and Cr contents of 2364-2873 ppm and 1831- 3311 ppm respectively.

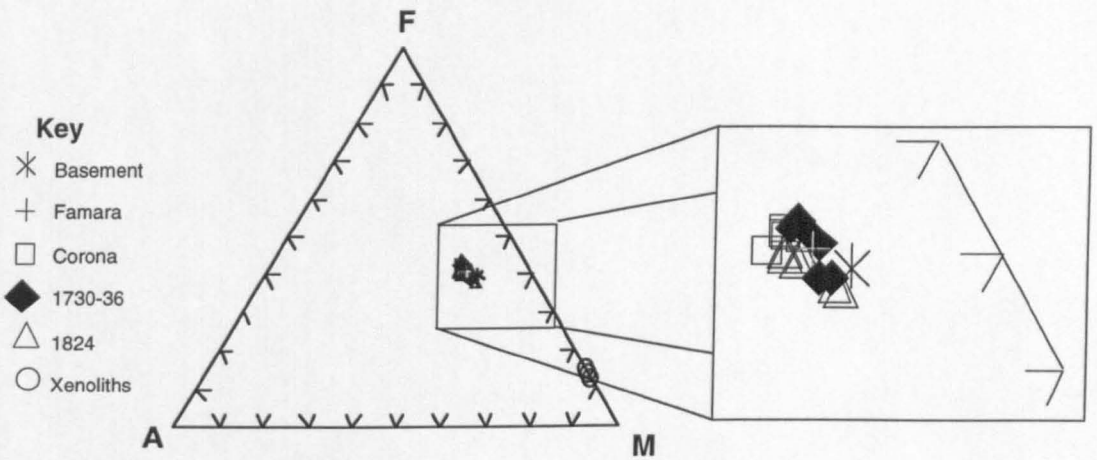

Figure 3.3 is an AFM diagram A = $Na_2O + K_2O$, F = Total Fe as FeO, M = MgO. The lavas have a constricted range of compositions, which as expected, is very different to the xenoliths.

The major compositions have been corrected for olivine fractionation (see Appendix A for description of technique and worked example) to an Mg number of 70 with the Fe^{3+}/Fe^{2+} ratio taken to be 0.15 taken from the range of compositions on the Le Maitre SiO_2-K_2O classification diagram (Cox et al., 1979). This required the addition of up to 5% olivine. Those with a Mg number greater than 70 have been left unchanged. The fractionation

correction does not alter any of the compositions by a substantial amount, as can be seen from figure 3.3a and b.

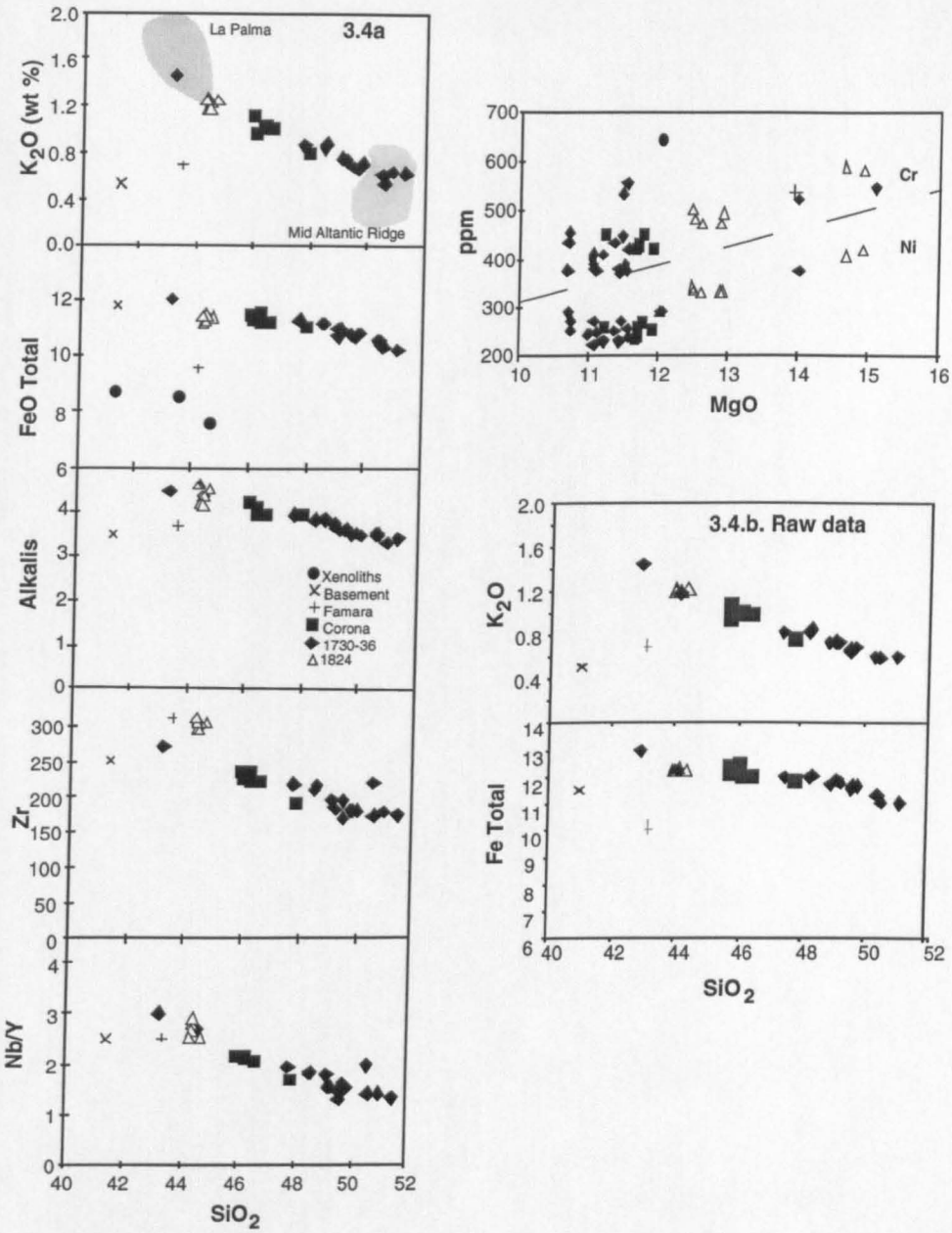

Figure 3.4.a Variations in selected olivine fractionation corrected major and trace element abundances in the Lanzarote lavas: K_2O, $FeO_{Total\ Fe}$, alkalis, Zr and Nb/Y versus SiO_2 and Ni, Cr versus MgO illustrating the primitive signature of the lavas and the range of composition. 3.4.b. show the uncorrected data. The samples analysed in this study are plotted as triangles (1824), diamonds (1730-36) and squares (Corona), Cross + (Famara), Cross × (Basement), Circles (xenoliths) on all the following diagrams. La Palma field is from Elliott, (1991), and MAR is from Langmuir et al., (1992).

Both the corrected and the uncorrected compositions yield striking negative arrays for FeO, alkalis, Zr and Nb/Y versus SiO_2, and positive correlations for MgO versus compatible elements such as Cr and Ni (Figure 3.4.). Such arrays are common in primitive magmas where the MgO content is over 7% and the SiO_2 content is less than 48 wt % (e.g. Weaver, 1991; Turner et al., 1997). In general, the 1824 lavas have lower SiO_2 and higher FeO, incompatible element abundances and ratios such as Nb/Y, than the older rocks. The 1730-36 lavas have relatively high SiO_2 and low FeO and incompatible element abundances (excluding one sample), and Corona samples have intermediate compositions.

Primitive mantle normalised trace element patterns for averages of the three 1824 rocks and of the highest silica 1730-36 rocks are broadly similar to that of average OIB (Sun and McDonough, 1989) (Figure 3.5). The patterns are LREE enriched and HREE depleted when compared with oceanic tholeiites and N-MORB. The patterns peak at Nb and have negative Pb anomalies, while the 1824 rocks additionally have negative Rb and K anomalies not observed in the other rocks.

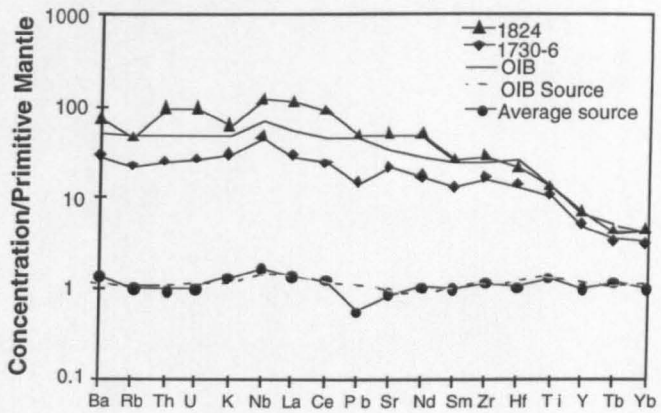

Figure 3.5. Primitive mantle (Sun and McDonough, 1989) normalised diagram showing averages of the 1824 rocks and extremes of 1730-36 Lanzarote rocks. Average OIB is plotted for comparison and the calculated source values for each rock are also shown. D values used are from Halliday et al., (1995) (see Appendix F). Y and Yb should be very similar on a mantle normalised spidergram, but using a published Yb D value the calculated source Yb concentration was well below that of Y. It was therefore necessary to change the D value for Yb in garnet from the published value of Halliday et al. (1995) (6.4) to (3.6) (closer to the Yb D value from McKenzie and O'Nions, 91).

The OIB source composition (from Sun and McDonough, 1989) gave 1 and 4% melts for the rocks, these melts were then taken back to an average source value by removing 1 and 4% partial melts respectively from the lavas (inverse of melting).

The Famara and the basement rocks have very similar trace and rare earth element abundances to the other rocks from the suite, although it is interesting to note that the basement and Famara show a greater depletion in Rb and K than even the 1824 rocks. Thus, the depletion in these elements was not just an artefact of the 1824 rocks, but a long-lived occurrence in the island, and in fact the Timanfaya rocks are the anomaly (Figure 3.6). An explanation for the negative anomalies may be that melting has taken place in the presence of residual phlogopite.

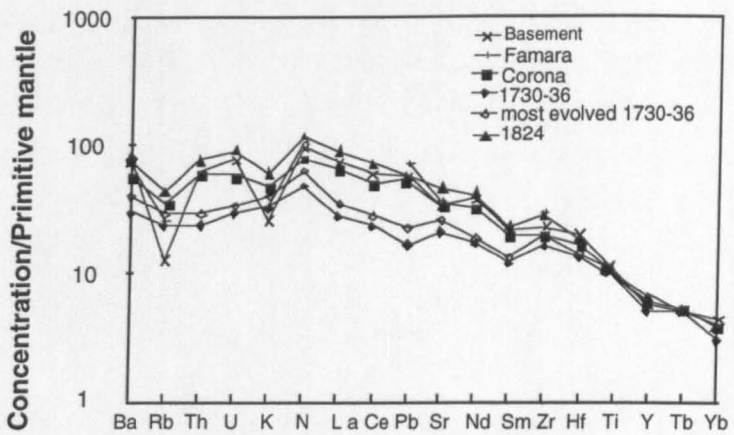

Figure 3.6. A mantle normalised spidergram showing selected samples from all the rock suites from Lanzarote. They are normalised as Figure 3.5.

3.6.2. Sr, Nd and Pb isotopes

The Sr isotopes show a restricted range of 0.70306-0.70332, despite the range in the major and trace elements. The Nd isotopes are relatively low and vary from 0.51274 to 0.51288; however two lavas (one sample from the 1824 lavas and one sample of the Corona lavas) have lower values of 0.51236 and 0.51258 respectively. These represent the lowest $^{143}Nd/^{144}Nd$ ratios yet reported from the Canary Islands (Figure 3.7) and they presumably reflect a contribution from older African lithosphere. The Nd isotope ratios show no obvious trend with major or trace elements, but the rocks are displaced from the Nd-Sr isotope field of MORB towards that of HIMU OIB (Zindler and Hart, 1986).

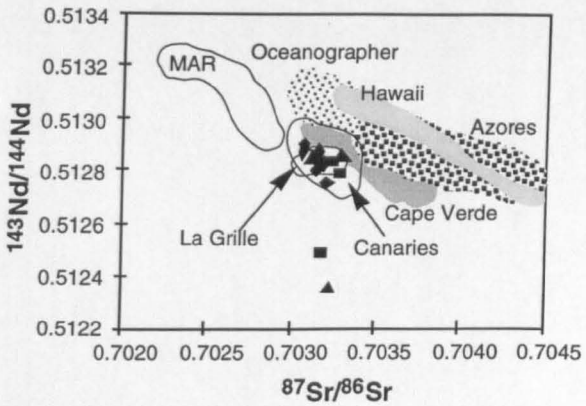

Figure 3.7. *$^{87}Sr/^{86}Sr$ Vs $^{143}Nd/^{144}Nd$ plot showing the isotopic compositions of the Lanzarote lavas together with other data from Atlantic islands including the Canaries, Azores, Cape Verdes and other OIB for comparison (Thirlwall et al., 1997; Hoernle et al., 1991; Sigmarsson et al., 1992; Vance et al., 1989; Turner et al., 1997; Elliott, 1991; McDermott and Hawkesworth, 1991; and the Oceanographer field from Shirey et al., 1987), along with unpublished data from Azores (S Turner, P.King,) and Cape Verde (T. Kokfelt). The majority of the Lanzarote lavas have similar Sr isotopic compositions, whilst a couple of the Corona lavas have lower Nd compositions relative to other data for the Canaries and the Lanzarote samples analysed in this study.*

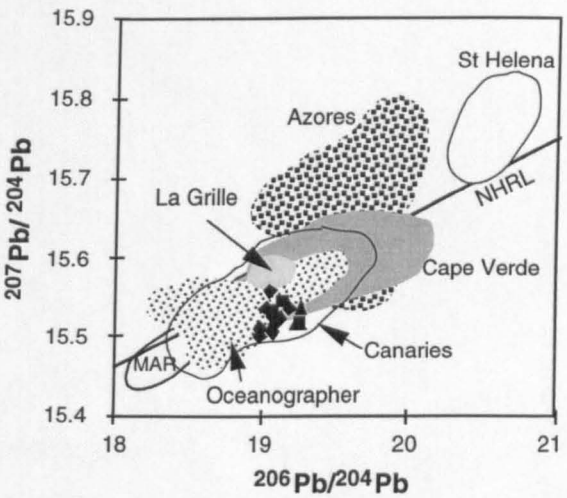

Figure 3.8. *$^{207}Pb/^{204}Pb$ vs. $^{207}Pb/^{204}Pb$ illustrating the Pb isotopic compositions in the Lanzarote samples. Other data from the Canaries, Azores and other OIBs are plotted for comparison (references as for Figure 4.5). The Lanzarote rocks have relatively restricted isotopic ratios which plot between the MAR field on the NHRL (Hart, 1984) and the HIMU OIB e.g. St Helena.*

The Pb isotope ratios of the Lanzarote rocks are also relatively restricted ($^{206}Pb/^{204}Pb$ = 19.1-19.3, Figure 3.8). They plot within the field of published results on rocks from the Canary Islands (e.g. Hoernle et al., 1991; Sigmarsson et al., 1992; Thirlwall et al., 1997) and they overlap with the more radiogenic Pb isotope ratios within the MORB field on the North Hemisphere Reference Line (NHRL) (Hart, 1984). As with Nd and Sr isotopes, there is a slight displacement towards the field of HIMU OIB of Zindler and Hart (1986).

The Lanzarote suite, also show a HIMU trend with the incompatible element ratio Nb/U versus $^{206}Pb/^{204}Pb$ (Figure 3.9). There is a negative correlation of decreasing Nb/U versus increasing isotopic ratio. These rocks also have a high U/Pb ratio ranging from 0.21 to 0.76, further indicating a HIMU source component.

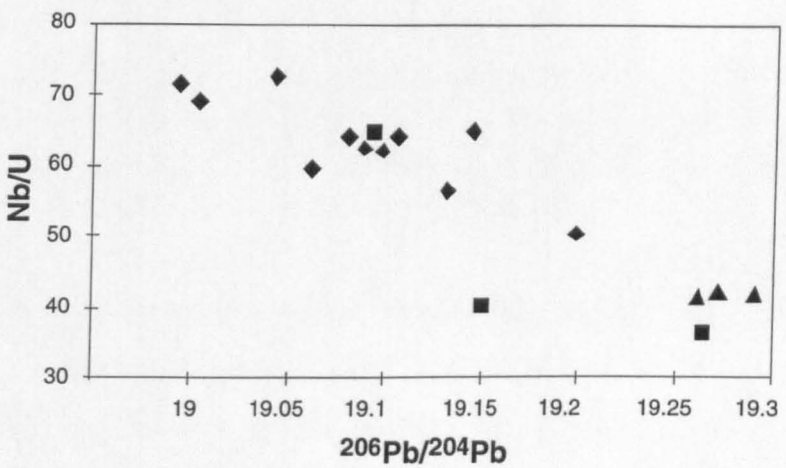

Figure 3.9 shows negative correlation of increasing incompatible element ratio with decreasing $^{206}Pb/^{204}Pb$.

3.6.3. U, Th and Ra isotopes

The Timanfaya basalts have U and Th contents ranging from 0.47 to 1.98 ppm and 1.90 to 7.94 ppm respectively. The U and Th contents of the 1824 rocks are typically 2-3 ppm higher than those in the 1730-36 samples. As with most young OIB, all the samples plot to the left of the equiline in the ($^{230}Th/^{232}Th$) - ($^{238}U/^{232}Th$) isochron diagram (Condomines et al., 1988) (Figure 3.10), and ($^{230}Th/^{238}U$) exhibits a large range from 1.03-1.76. ($^{234}U/^{238}U$) ratios were determined on representative samples (Appendix A) and these all had values of 1 ± 0.004 suggesting that there has been no significant post extrusion

alteration and that the measured U/Th ratios are those of the erupted lavas. The Corona rocks show the greatest ($^{230}Th/^{238}U$) disequilibria, whilst the 1824 and 1730-36 lavas have broadly similar ($^{230}Th/^{238}U$) values.

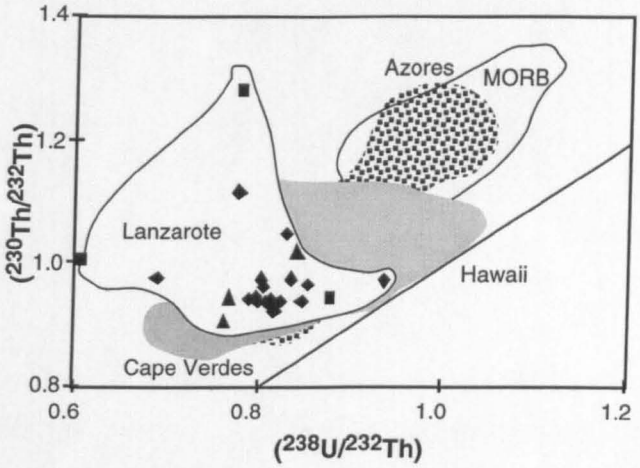

Figure 3.10. ($^{238}U/^{232}Th$)-($^{230}Th/^{232}Th$) equiline diagram illustrating the initial U-Th isotopic ratios of the Lanzarote rocks, and fields for historic to recent pre-historic volcanics from Canaries, Azores, Hawaii and MORB (References as for Figure 3.5. also Cohen and O'Nions, 1993; Hemond et al., 1994; Sims et al., 1995).

Thus, apart from the three Corona samples, very similar ($^{230}Th/^{238}U$) values are observed over a range in SiO_2 contents (40.8-51.1%) (Figure 4.2) and trace element ratios and abundances (e.g. Nb/Y = 1.40-3.41, and Th = 1.90-7.94 ppm). Relative to the Th-Sr isotope correlation observed for many oceanic basalts, the 1730-36 and 1824 rocks are displaced to slightly low ($^{230}Th/^{232}Th$) (Figure 3.11) as seen elsewhere in the Canaries by Sigmarsson et al., (1992).

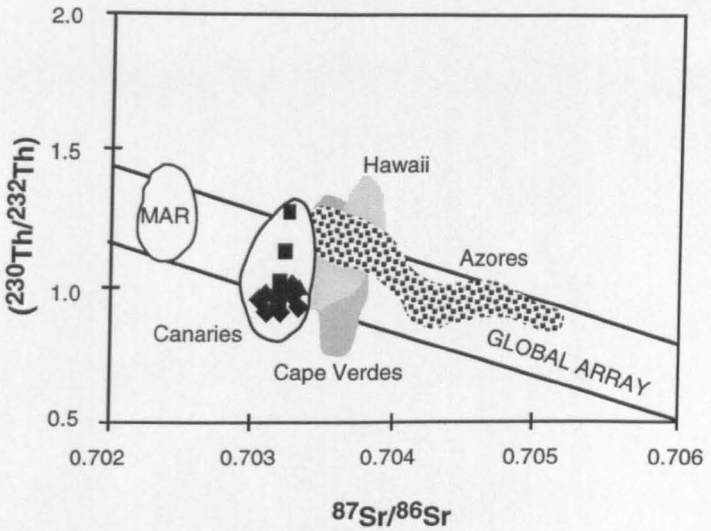

Figure 3.11. ($^{230}Th/^{232}Th$) vs. $^{87}Sr/^{86}Sr$ illustrating the lower ($^{230}Th/^{232}Th$) values observed in the 1730-36 and 1824 lavas relative to other OIB (refs. as in Figure 3.5, and 3.10).

A small subset of samples has been analysed for ($^{226}Ra/^{230}Th$) (Appendix A). All of the younger rocks show Ra excesses (($^{226}Ra/^{230}Th$) = 1.34 ± 0.08 to 1.59 ± 0.13), whilst the older Corona rocks are in $^{226}Ra/^{230}Th$ equilibrium, consistent with their age of >10 ka. The 30-60% ^{226}Ra excesses in the 1730-36 and 1824 lavas require $^{226}Ra/^{230}Th$ fractionation less than 8,000 years prior to eruption.

3.7. Petrogenesis

The rocks from Lanzarote offer an exceptional opportunity to evaluate the depths and conditions of melt generation, because they are amongst the most primitive known from the ocean island setting, and they all exhibit significant ($^{230}Th/^{238}U$) isotopic disequilibrium. In this section the issues addressed include the depths of melt generation, as constrained from both major and trace elements and ($^{230}Th/^{238}U$) disequilibrium, and the conditions of melting and whether they were primarily controlled by the dynamics and temperature of the mantle plume or the thickness of the oceanic lithosphere.

3.7.1. Depths of Melt Generation

The 1824 lavas have similar Sr, Nd and Pb isotope ratios to the 1730-1736 lavas, indicating a similar source region, and yet they have higher incompatible element abundances, and lower SiO_2 and higher FeO* contents (Figure 3.4). In the simplest interpretation, the

silica undersaturated 1824 lavas reflect smaller degrees of melting, and at greater depths, than those erupted between 1730 and 1736.

In Figure 3.12 the fractionation-corrected FeO* and SiO_2 contents of the Lanzarote rocks are compared with experimental data on peridotite melting from Hirose and Kushiro (1993). These experiments were undertaken over a range of pressures, and the melts from both HK-66, an unusually opx-rich lherzolite from Hawaii, and KLB-1, a more typical spinel peridotite with a composition close to that of fertile mantle, exhibit negative FeO*-SiO_2 arrays. FeO increases and SiO_2 decreases with increasing depth of melting and pressure, and this is largely independent of melt fraction and source depletion. FeO can reflect changes in the source. The SiO_2 contents of primitive rocks are widely taken to reflect depths of melting, but a number of suites yield FeO-SiO_2 arrays that are shallower than the experimental data. These include the fractionation-corrected rocks from Lanzarote, and these are broadly similar to the FeO*-SiO_2 array from Hawaii. They exhibit a large range in SiO_2 and little variation in FeO* forming a sub-horizontal array that cuts across the fields for the experimental data (Figure 3.12). This range in SiO_2 strongly suggests that it reflects variations in other parameters, such as the presence of volatiles, in addition to the depths of melting. Comparison of the FeO* contents of the Lanzarote rocks with the experimental data from HK-66, suggests pressures of melting of 1.7 GPa for the 1730-36 lavas, 2.0 GPa for the Corona rocks, and 2.2 GPa for the 1824 rocks, corresponding to melt generation depths of about 58 km, 67 km and 73 km respectively. The possibility that some OIB may be derived from a more orthopyroxenitic source region than typical fertile mantle (c.f. Scarrow and Cox, 1995) is apparent from the similarity in the composition of HK-66 to some of the Canaries rocks. In contrast, the field for average Atlantic OIB is more similar to KLB-1, suggesting that it may be a more likely source composition for the rocks (Figure 3.12).

The reason for the shallower trends on Figure 3.12 is difficult to establish, but they may reflect the presence of volatiles, and/or melting of amphibole veins to generate the low silica compositions. Pyroxenitic veins in the source mantle would infer a more fertile enriched source with the presence of clinopyroxene, whilst HK-66 is an orthopyroxene rich peridotite. The depths of melting inferred for Lanzarote are similar to those inferred for Hawaiian tholeiites and transitional basalts (e.g. Cohen and O'Nions, 1993; Hirose and

Kushiro, 1995), although the Azores field (Turner et al., 1997) has a steeper FeO*-SiO_2 arrays than the Lanzarote data. The lower SiO_2, more alkalic rocks in Lanzarote have lower FeO, and were therefore presumably derived from shallower depths than those from the Azores.

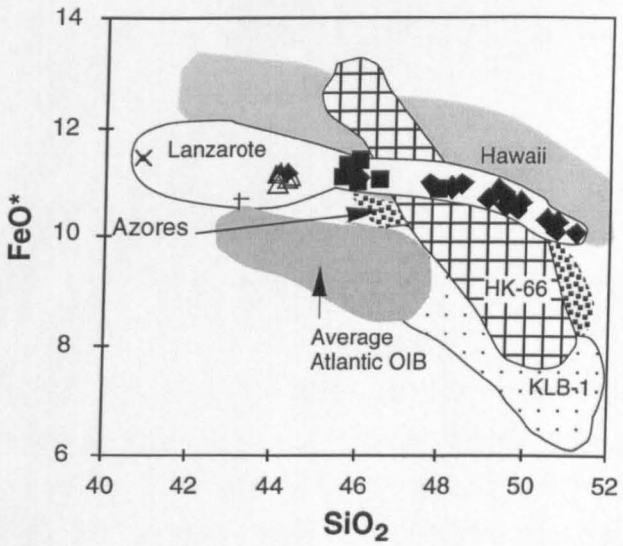

Figure 3.12. SiO2 vs. FeO illustrating the differences between the near horizontal Lanzarote data array and the Hawaiian field (Cohen and O'Nions, 1993; Sims et al., 1995) and the more inclined Azores field (Turner et al., 1997). Fields for the experimental data on HK-66 and KLB-1 (Hirose and Kushiro, 1993) intersect with the Lanzarote data, and the depths of melting can be inferred from the comparison of the FeO* and SiO_2 contents with the experimental data from HK-66.*

Depths of melting can also be inferred from variations in trace element ratios that are sensitive to the presence of residual garnet. Thus Figure 3.13 illustrates the Tb/Yb-La/Yb results for the Lanzarote rocks, and calculated curves for partial melting of a primitive mantle source in both the garnet and spinel peridotite facies. The Lanzarote data define a tight array intermediate between the curves for garnet and spinel facies peridotite, and the increase in La/Yb is accompanied by increasing Yb abundances (see Figures 3.5 and 3.16), which limits the amount of residual garnet which can have been present to < 5% (Table 3.2). The D values for Yb (similar to the McKenzie and O'Nions, 1991 value) does allow the preferred interpretation of melting, although the diagram does not differentiate between mixing and melting, both would provide the array on figure 3.13. These results suggest that partial melting took place close to the garnet-spinel transition, and hence at depths of 60-70 km

(Nicholls, 1974; Ellam, 1992) which is consistent with those inferred from the FeO* abundances above.

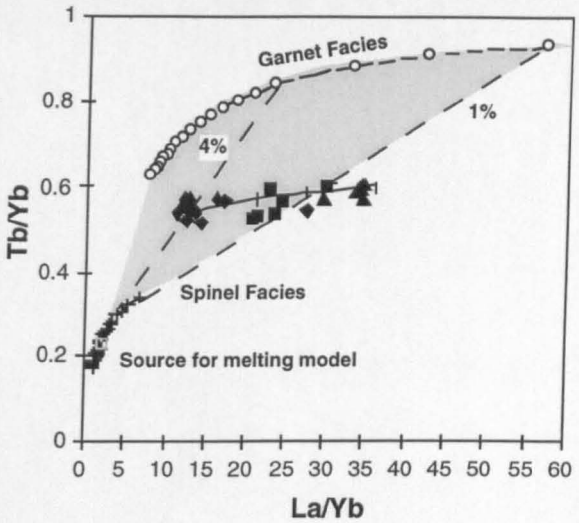

3.13. La /Yb vs. Tb /Yb illustrating the horizontal field for the Lanzarote data which indicates melting took place shallow at small degrees of melting in the presence of residual garnet. The data array plots at intermediate values of Tb/Yb consistent with not much garnet being present. A melting curve using Lanzarote source from table 3.2 plots through the data, giving 1 and 4% melting for the two end member compositions. The shaded field of compositions is generated by non-modal melting of a primitive mantle source, using a range of modal garnet proportions (Class and Goldstein, 1997). Lines for 1 and 4% melting are shown.

3.7.2. Extent of Melting and Source Mineralogy

Simple batch melting calculations indicate that the REE variations within the Lanzarote rocks can be modelled by 1-4 % melting of a source which is slightly LREE enriched relative to primitive mantle, and which contains ~ 5% garnet (Figure 3.13, Table 3.2). The mantle-normalised patterns for the averages of the 1824 and three 1730-36 rocks are best modelled by 1% and 4% batch melts, respectively, of a peridotite with minor and trace element abundances slightly modified from that of primitive mantle (Figure 3.5) (D values used from Halliday et al., 1995 and Rollinson, 1993; see Appendix F). The orthopyroxene was kept constant at 0.2% as the main controlling factor on the melt was the clinopyroxene:garnet ratio. Changing the orthopyroxene value had little effect in the resulting melt. Simple fractional melting was used with a variety of different source compositions including primitive mantle, and the average xenolith composition. The most suitable average source for these rocks is

slightly LREE enriched relative to primitive mantle (La/Yb_N = 1.36), and it has a small negative Pb anomaly reflecting a possible source underlying old oceanic lithosphere.

The 1824, the Famara and the basement rocks contain negative Rb and K anomalies not seen in the Corona or 1730-36 rocks, which might be a source characteristic or else they can be modelled with a small amount of phlogopite in the source during melting. In the Lanzarote suite there are negative K and Rb anomalies, but the Ba and Sr remain constant, suggesting that the residual phase is phlogopite rather than amphibole. Phlogopite is unlikely to be stable at the temperatures and pressures of the convecting upper mantle, or within upwelling thermal plumes, and it may only coexist with garnet at pressures < 3 GPa (97 km depth) and temperatures < 1175 °C (Mengel and Green, 1989). However, experimental evidence suggests that melts in equilibrium with phlogopite should have higher K_2O contents than those observed in the Lanzarote rocks (Edgar et al. 1976; Mengel and Green, 1989).

The depth of melting can be inferred from FeO*, REE, K, and from the modelling, depths are deduced to be within the garnet-spinel transition at 60-70 km. The lower SiO_2 rocks have negative K anomalies, as this is unexpected as it suggests that the melts were derived from shallower depths required for the amphibole/phlogopite to be stable, than the depths previously inferred from their low SiO_2 value. It may be that all the melts in a particular area were derived from similar source compositions and the residual potassic phase was consumed at higher degrees of melting, hence not seen, and that the low SiO_2 melts reflect the presence of amphibole veins rather than deeper depths.

Alternative models to explain the REE and U-Th variations include the presence of residual high pressure clinopyroxene instead of garnet (Blundy et al., 1998), and source rocks containing garnet pyroxenite veins as suggested by Sigmarsson et al. (1998) for the higher La/Yb, more alkalic rocks on Lanzarote. Changes in clinopyroxene compositions close to the lherzolite solidus appear to affect the relative compatibility's of U and Th such that ^{230}Th excesses may be generated by partial melting in the absence of residual garnet (Blundy et al., 1998; Turner et al. in press). However, although the HREE have D values > 1 for these liquidus clinopyroxenes (Blundy et al. 1998), those for Tb and Yb are similar and so melts from garnet-free pyroxenite still produce flat trends on Figure 3.13 with Tb/Yb ratios similar to those in their source rocks.

	SOURCE	MELT COMPOSITIONS			
	Average	Obs. 1824	Calc 1824	Obs 1730-36	Calc 1730-36
Ba	9.8	501	547	192	206
Rb	0.64	28	33	13	13
Th	0.09	8.0	8.3	2.0	2.1
U	0.02	2.0	2.1	0.5	0.5
K	342	15181	18197	7349	7054
Nb	1.21	82	100	32	29
La	0.99	74	67	19	22
Ce	2.23	150	131	41	48
Pb	0.04	3.3	3.7	1.0	1.0
Sr	19	1036	1104	418	403
Nd	1.46	65	56	23	26
Sm	0.44	11	10	6	6
Zr	13	309	297	176	179
Hf	0.33	6	6	4	4
Ti	1680	16734	16789	13328	13194
Tb	0.447	1.3	1.1	0.8	0.9
Y	0.13	30.9	27.8	22.2	24.0
Yb	0.49	2.1	1.8	1.5	1.7

Table 3.2. Calculated source composition for end member melt compositions

The phase proportions are pre-melting modes, hence melt proportions are as in table.

	Ol	**Cpx**	**Opx**	**Garnet**	**Phlogopite**
Phase proportions 1824	0.685	0.059	0.200	0.049	0.007
Phase proportions 1730-36	0.643	0.088	0.200	0.065	0.000
Phase proportions Average	0.664	0.074	0.200	0.057	0.005

The Lanzarote rocks define a slightly inclined array on Figure 3.13, with elevated Tb/Yb ratios consistent with the presence of small amounts of residual garnet (< 5%). Higher residual garnet abundances would result in higher Tb/Yb than those observed, and this also precludes significant contributions from melts of garnet pyroxenite source rocks. Moreover, melts of pyroxenite will be dominated by incongruent melting of orthopyroxene and hence have relatively high silica contents, whereas the high La/Yb rocks on Lanzarote are silica-poor (Fig. 3.13). The garnet pyroxenite of Hirschmann and Stolper (1996) has ~12% garnet and 8% clinopyroxene which yields a bulk D_{Yb} of 0.37 and hence a much smaller range of Yb (6%) with increasing La/Yb in 1-4% partial melts than that observed in the Lanzarote rocks (1.47-2.25 ppm, Figure 3.13). Thus, it seems unlikely that partial melting of garnet pyroxenite was responsible for either the major or the trace element compositions of the Lanzarote basalts. Rather they have been modelled as 1-4 % partial melts of peridotite with ~ 5% garnet, presumably close to the garnet-spinel transition.

3.7.3. Dynamic Melting

Whilst the preceding sections have shown that batch or fractional melting can provide reasonable models for minor and trace elements, they cannot be used to explain ($^{230}Th/^{238}U$) disequilibria, except at unrealistically small degrees of melting < 0.1% (e.g. Elliott, 1997). At higher degrees of melting, the U/Th ratio of the melt will be similar to that of the source, and so the development of ($^{230}Th/^{238}U$) disequilibria requires a broadly vertical shift on the ($^{230}Th/^{232}Th$) - ($^{238}U/^{232}Th$) equiline diagram (Figure 3.10). Such shifts are best modelled by dynamic melting and the continued interaction of the melt and matrix peridotite en-route to the surface (Spiegelman and Elliott, 1993; Elliott, 1997). In a dynamic melting model, the high initial ($^{230}Th/^{232}Th$) in the Lanzarote lavas results from ingrowth of ^{230}Th in a high U/Th mantle matrix following previous melt extraction in the melt column. Ingrowth is linked to the upwelling rate since the matrix must remain in the melting zone for a significant period of time, in order to attain a sufficiently high ($^{230}Th/^{232}Th$). It follows that a low upwelling rate is required beneath Lanzarote and this is consistent with the low buoyancy flux inferred for this plume at 1.0 $Mg.s^{-1}$, compared to the 8.7 $Mg.s^{-1}$ for the high buoyancy flux Hawaiian plume (Sleep, 1990).

The Lanzarote rocks have ^{230}Th excesses ranging from 6-20% for the 1730-36 and 1824 rocks and as high as 80% for the Corona samples (Figure 3.10). Although the Corona rocks lie within the major and trace element arrays defined by the other lavas, their ($^{230}Th/^{232}Th$) isotopic compositions are much more extreme. The reasons for this are unclear and accordingly, the Corona rocks are not considered further in this discussion. However U may have been mobilised by seawater as samples were close to coast and the increased ($^{230}Th/^{232}Th$) is an artefact of this. Mixing with much younger lavas is another possibility, although this is unlikely as the lavas have been erupted for 54 ky. A striking feature of the U-Th isotope results on the 1824 and 1730-36 rocks is that they have broadly similar ($^{238}U/^{232}Th$) and ($^{230}Th/^{232}Th$) values despite having significantly different trace element abundances inferred to reflect different degrees of melting (1-4%).

Following Williams and Gill, (1989) and Spiegelman and Elliott, (1993), a modal dynamic melting model (van Calsteren and Hawkesworth, 1999) has been used. This allows integration of the melt fraction in space and time and also simulates continuing interaction between the melt and the matrix as the melt moves up through the melt zone.

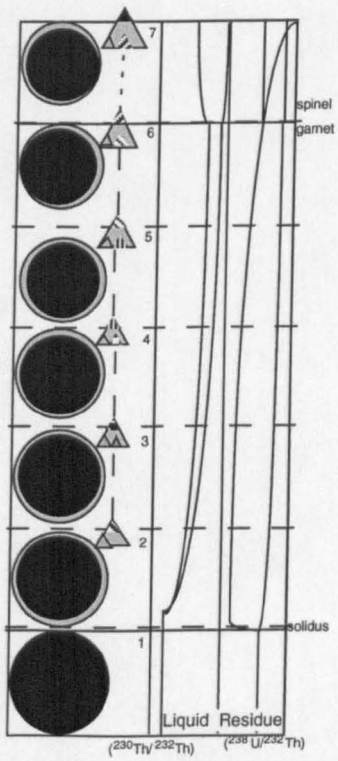

Figure 3.14. A schematic section illustrating modal dynamic melting (after van Calsteren and Hawkesworth, 1999) at 7 arbitrary stages in a melting column. For discussion see text.

In this model melting starts as the mantle crosses the solidus into stage 2, and the new melt is represented by the shaded ring. This melt, which is also indicated by the small triangle in stage 2, collects in the pore volume represented by the larger triangle. However because the volume of the newly generated melt is more than 15% of the volume of the corresponding solid, the melt migrates upwards into the next stage. In stage 3 the newly formed melt is added to the melt expelled from the previous stage, and melting and mixing continues through subsequent stages, allowing melt from the base of the melt column to be mixed with melts from the top of the melt column. The values of ($^{230}Th/^{232}Th$) and ($^{238}U/^{232}Th$) in the combined melt and the matrix are illustrated in the columns on the right hand side of Figure 3.4. At stage 1, the solid mantle is in secular equilibrium and so ($^{230}Th/^{232}Th$) and ($^{238}U/^{232}Th$) are equal. In stage 2 very small degrees of melting form melts with extreme ($^{238}U/^{232}Th$) values, but ($^{238}U/^{232}Th$) remains unchanged in the matrix, and initially ($^{230}Th/^{232}Th$) is also unchanged. As melts are extracted, the ($^{238}U/^{232}Th$) and ($^{230}Th/^{232}Th$) increase in the residue. However with time ($^{230}Th/^{232}Th$) in the melt decreases by radioactive decay, but it is balanced as new melts from residues after initial melting (and therefore with higher ($^{230}Th/^{232}Th$)) are added at higher stages in the melting column. As the melt fractions increase, ($^{238}U/^{232}Th$) in the melt decreases towards its starting value in the solid mantle, while ($^{230}Th/^{232}Th$) increases due to mixing with melts derived from matrix residue higher in the melt column. Above the garnet to spinel transition Th and U do not fractionate noticeably and ($^{238}U/^{232}Th$) remains virtually constant. This is also illustrated on Figure 3.15.

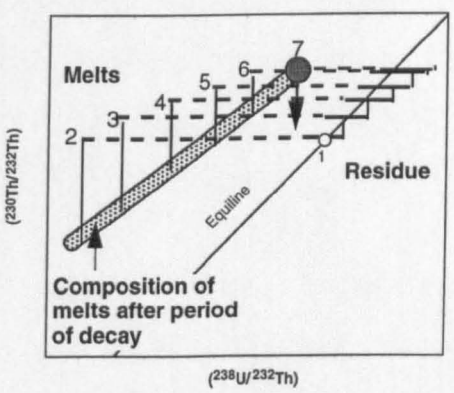

Figure 3.15. A schematic equiline diagram illustrating the effect of progressive partial melting as shown in Figure 3.14 (after van Calsteren and Hawkesworth, 1999).

The U/Th ratio of the source can be constrained by the variation in fractionation-corrected U/Th versus Th (Figure 3.16). As can be seen, there is no systematic change in U/Th with increasing Th, and so it is concluded that these rocks were derived from source regions which had U/Th ratios similar to the mean of those in the erupted magmas.

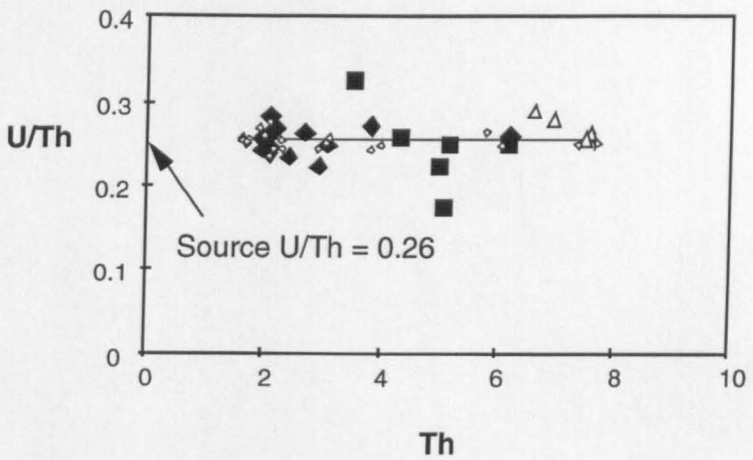

Figure 3.16. U/Th ratios versus Th (ppm) abundance illustrating that the U/Th ratios of the rocks do not change significantly with increasing Th abundance and hence with increasing degrees of melting. The straight line is a melting line between 1 and 4% melts. It is concluded that the U/Th ratio in the source was similar to that in the lavas

We have established that the degrees of melting (F) = 1 and 4%, that U/Th in the source is similar to that of the melts = 0.26, and adopted the D values of shown in Table 3.3 (see Appendix F) from Halliday et al. (1995) and Rollinson (1993). Figure 3.17 illustrates our preferred dynamic melting model for the Lanzarote suite of the 1730-36 and 1824 rocks. As with the trace element modelling, the average of the lowest silica 1824 rocks is taken to represent a 1% melt and the average of the three highest silica 1730-36 rocks is taken to be a 4% melt. The key variables are the distribution coefficients, the U and Th contents of the source and its modal mineralogy, the degrees of melting, the depth and length of the melt zone, the rate of melt generation, and the porosity. These are summarised in Tables 3.2 and 3.3

The modal mineralogy, and the degrees of melting of 1% and 4% for the averages of the three 1824 rocks and the three 1730-36 rocks respectively, are those taken from the trace element modelling summarised in Table 3.2, and Figures 3.6, 3.12 and 3.13. It was assumed that the initial source was in secular equilibrium, and so plotted on the equiline with

a ($^{238}U/^{232}Th$) value of 0.81 corresponding to U/Th = 0.26 estimated from the U/Th-Th variations in Figure 3.16.

	1824	1730-36
Melt column length (km)	3	12
Melt rate at top of column ($kg.m^{-3}.yr^{-1}$)	0.125×10^{-3}	0.125×10^{-3}
Porosity at top of column (%)	0.9	1.5
Matrix transfer time (years)	270,000	1,100,000
U/Th source (ppm)	0.2637	0.2637
D values	**Th**	**U**
Olivine	0.000007	0.000009
Opx	0.00002	0.00004
Cpx	0.015	0.01
Garnet	0.0015	0.015

Table 3.3. Parameters used in dynamic melting model.

The integrated melt fraction is the product of the time that the matrix spends in the melt column and the melt rate which was set constant at 0.125×10^{-3} $kg.m^{-3}.yr^{-1}$. The model assumes 1% melting per 0.1 GPa pressure release (Langmuir et al., 1992). However, the melt rate can be varied, with little or no resultant variation in the calculated U-Th disequilibria, so long as there is a corresponding shift in the time the matrix spends in the melt column so that the integrated melt fraction remains the same.

The porosity from the bottom to the top of the melt column ranges from 0-0.9% for the 1824 lavas and from 0-1.5% for the 1730-36 lavas. Changing these values results in marked changes in the resultant U-Th disequilibrium. Finally, for the melt generation rate assumed, it requires the melt and the matrix to remain in the melt zone for the order of 270 ka to obtain the ^{230}Th-excess observed in the 1% end-member, and approximately 1,100 ka to reproduce the 4% end-member. This corresponds to a matrix upwelling rate of 1 $cm.yr^{-1}$.

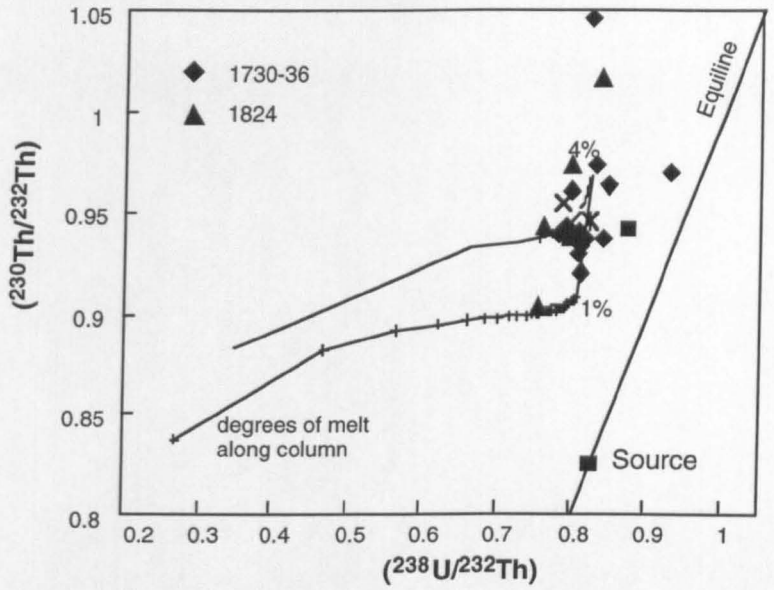

Figure 3.17. *(^{238}U-^{232}Th)-($^{230}Th/^{232}Th$) equiline diagram illustrating MDM model (van Calsteren and Hawkesworth, 1999) to generate the 1 and 4% melts. The Corona samples have been excluded from this diagram. The vertical extent of the data can be modelled using the parameters in Table 3.3. The two lines into the data represent the different melt columns at 1 and 4% melting. The lowest ($^{230}Th/^{232}Th$) can be modelled by 1 % degree of MDM, and 4% melts mixing.*

3.7.4. The Role of Mixing

Dynamic melting models involve mixing between the increments of melt derived from different depths (e.g. Klein and Langmuir, 1987; Langmuir et al., 1992; Spiegelman and Elliott, 1993) and evidence of such mixing may be preserved in suites of primitive rocks. The straight line relations for the fractionation-corrected compositions of the Lanzarote rocks on Figures 3.4, 3.12 and 3.13 are consistent with both variable degrees of melting and magma mixing, but there is even more compelling evidence that the within-suite variations are due to magma mixing. Figure 3.18 illustrates the trends for Sm/Yb - 1/Yb and Sm/Th - 1/Th in the fractionation-corrected compositions for the Lanzarote rocks. The former highlights that Yb increases with increasing Sm/Yb, and by implication with decreasing degrees of melting. In addition, however, the straight line arrays for both Sm/Yb - 1/Yb and Sm/Th - 1/Th are inconsistent with progressive batch melting using the commonly accepted average D values for melting upper mantle peridotite (Halliday et al., 1995). Instead they strongly suggest that the within-suite variations are primarily controlled by magma mixing.

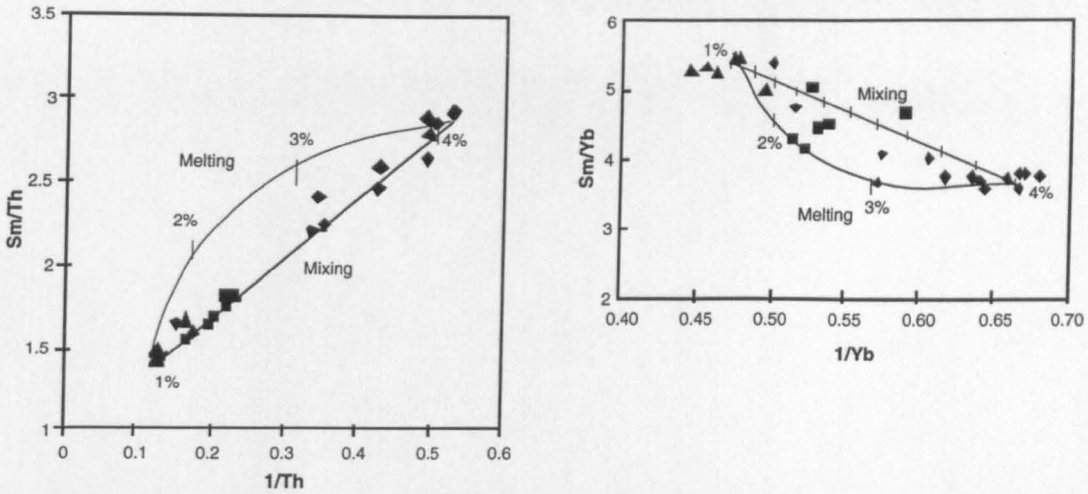

Figure 3.18. Sm/Yb vs 1/Yb and Sm/Th vs 1/Th fractionation-corrected incompatible element arrays for the Lanzarote rocks. Mixing lines and melting curves are plotted and the data scatter around the mixing line. The melting curves were generated by batch melting a primitive mantle source with a range of 1 to 4% degrees of melting with the phase proportions for garnet lherzolite (ol:opx:cpx:grt = 60:25:9:6) (Class et al. 1994).

The straight-line array on the Tb/Yb - La/Yb diagram is therefore interpreted in terms of mixing between the end-members represented by the 1824 and the most depleted 1730-36 lavas, which have been modelled as 1% and 4% melts respectively. It also follows that the Lanzarote FeO*-SiO_2 array reflects mixing as well as melting conditions, and this in part explains why the rocks form a sub-horizontal array that cuts across the fields for the experimental data in Figure 3.12.

If the mixing model is accepted, then the temporal and spatial distribution of the lavas places constraints on the time and length scales of mixing. Although the 1824 and 1730-36 end member lavas erupted adjacent to one another, the Corona rocks, which lie between these end members on the mixing arrays (Figures 3.4 and 3.16), are located 30-40 km further to the NE. The Corona lavas are also inferred to have erupted about 50,000 years prior to these later eruptions, and yet they appear to plot within the tightly defined mixing arrays for all the elements and isotopes, except for ($^{230}Th/^{238}U$). This suggests some variations in the dynamics of the processes responsible for the ($^{230}Th/^{238}U$) values (see previous section), but that the net effects of melting have remained remarkably reproducible over tens of kilometres and for perhaps 50 ka. The preferred interpretation is that such mixing arrays are the major and trace element products of dynamic melting in which the two end members were derived from different depths in the melt column.

3.8. Discussion

The foregoing discussion shows how geochemical data can be used to place a number of constraints on the melt generation processes beneath Lanzarote. We now broaden the discussion to encompass data from other islands within the Canaries and from other North Atlantic OIB, in order to make some more general statements about the controls on melt generation and ($^{230}Th/^{238}U$) disequilibria beneath ocean islands.

3.8.1. Degree of Partial Melting

As discussed in a recent review by Elliott (1997), whilst the case for dynamic melting coupled with ^{230}Th ingrowth to explain observed ^{230}Th-excesses is now generally accepted for MORB, the situation for OIB is less clear and some studies suggest that U-Th disequilibria in OIB can be explained simply by fractionation of U from Th during partial melting. One such study is that of Sims et al. (1995) who observed a broadly negative correlation between ($^{230}Th/^{238}U$) and silica saturation index (hy+4Q-ne)/(hy+di+4Q+ne) in Hawaiian lavas. Smaller degree melts tend to be increasingly silica undersaturated and so these authors argued that this negative correlation reflects an inverse relationship between the degree of partial melting and the amount of U-Th disequilibria. Figure 3.19 is a plot of ($^{230}Th/^{238}U$) versus silica saturation for mafic compositions from a number of different ocean islands. The first observation is that there are no obvious negative trends within OIB from the central Atlantic region, despite variations in lithospheric thickness from 20 to 125 km and lithospheric age from 7 to 175 Ma (see below).

Furthermore, it should be recalled that the inferred degrees of melting on Lanzarote range from 1 to 4% and yet there is no correlated change in the degree of ($^{230}Th/^{238}U$) disequilibria. This strongly argues in favour of dynamic melting coupled with ^{230}Th-ingrowth to explain observed ^{230}Th excesses in at least the central Atlantic OIB (c.f. section 3.7.3). Secondly, it appears that the Atlantic OIB may be separated into two groups, Ne normative and Hy normative. The Tenerife (Thomas, unpublished data), 1824 Lanzarote, La Palma (Elliott, 1991) and Cape Verde (Kokfelt, unpublished data) islands have similar silica saturation over a large range in ($^{230}Th/^{238}U$), whereas the Azores (Turner et al., 1997) exhibit the same range in disequilibria as the Canaries, but a greater range in silica saturation. The

Corona lavas are exceptions in that they have distinctive high ($^{230}Th/^{238}U$) disequilibrium and (hy+4Q-ne)/(hy+di+4Q+ne) values of 0.6 to - 0.2.

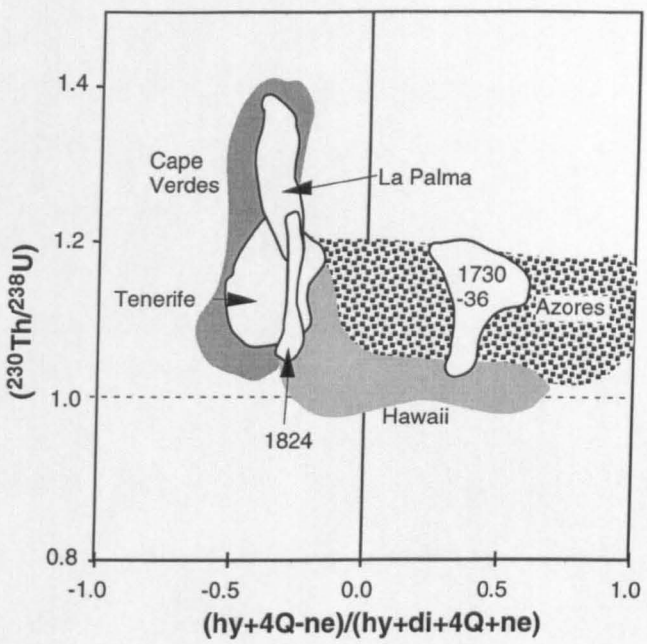

Figure 3.19. Silica saturation index (Sims et al., 1995) versus ($^{230}Th/^{238}U$) disequilibria for La Palma, (Elliott, 1991), Tenerife (chapter 5) and Lanzarote, along with data from other ocean islands. Azores, (Turner et al., 1997), Hawaii (Sims et al., 1995), and unpublished data from Azores (S Turner, P.King) and Cape Verde (T. Kokfelt).

3.8.2. Lithospheric Lid Thickness

The thickness of the lithosphere has often been suggested as an important control on melt generation (e.g. Watson and McKenzie, 1991; Ellam, 1992; Haase, 1996) and it might be expected to affect the development of ($^{230}Th/^{238}U$) disequilibria. The thickness of the lithospheric lid limits the minimum depth of partial melting beneath ocean islands and, for a given mantle potential temperature, it controls the integrated degree of partial melting. Therefore, it is instructive to see how OIB compositions vary with varying lithospheric lid thickness. As discussed above for Lanzarote, the fractionation of LREE from HREE can be used to infer the approximate depths of melting, because it is sensitive to the amount of garnet in the source region (e.g. Ellam, 1992; Haase, 1996). However, ratios such as Ce/Yb reflect both the amount of residual garnet and the degrees of partial melting. In contrast, MREE/HREE ratios, such as Tb/Yb (Figure 3.13) are less sensitive to the amounts of

melting, at least at < 10% melting, and so offer a more robust indication of the amounts of residual garnet present during melting.

Figure 3.20 summarises the variations of Ce/Yb, Ce abundances and Tb/Yb with SiO_2 and lithospheric thickness, for both selected average Atlantic OIB (Haase, 1996) and the fractionation corrected Lanzarote samples. Ce/Yb, Ce and Tb/Yb all increase with decreasing SiO_2 suggesting that there appears to be a general link between the inferred mean depth and amount of melting. In addition, Tb/Yb increases with the age of the underlying lithosphere for the average OIB compositions, consistent with a link between the mean pressure of melting and the thickness of the lithospheric lid (e.g. Haase, 1996).

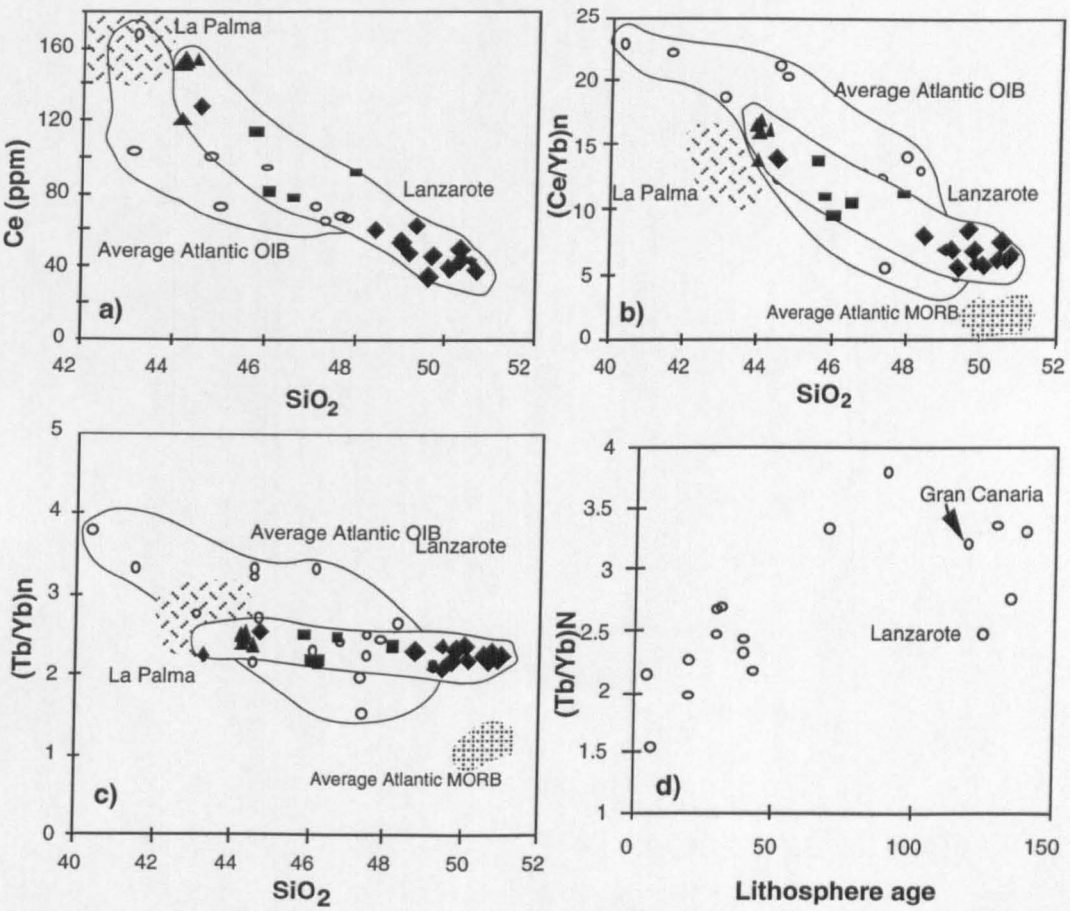

Figure 3.20 a) SiO_2 versus Ce abundance illustrates a negative trend with increasing SiO_2 in Lanzarote, whilst the average Atlantic OIB (Open circles) (Haase, 1996) have a less well defined negative array. b) SiO_2 vs. Ce/Yb illustrates a negative array for the Lanzarote data and average Atlantic OIB fields. c) SiO_2 vs Tb/Yb illustrating negative array for average Atlantic OIB and horizontal array for Lanzarote data. d)Tb/Yb vs lithospheric age (compilation from Hasse, 1996) showing a broadly positive correlation with increasing lithospheric age, at least until greater than 100 Ma.

A striking feature of the arrays in Figure 3.20 is that the Canaries Islands' rocks exhibit such large variations in REE abundances and Ce/Yb, and SiO_2, and yet they were generated in a relatively small area of approximately constant lithospheric thickness (Figure 3.21). In part, this may be a function of the information lost by averaging even relatively primitive OIB compositions from individual islands, but it may also reflect different controls on the SiO_2 contents of the Lanzarote magmas in particular (see also Figure 3.12). The Canaries lavas have a large range in Ce/Yb and Ce abundances, at relatively constant Tb/Yb, consistent with variable degrees of partial melting in the presence of similar amounts of residual garnet, and hence similar depths. However, SiO_2 ranges from 42-51% (Figure 3.20).

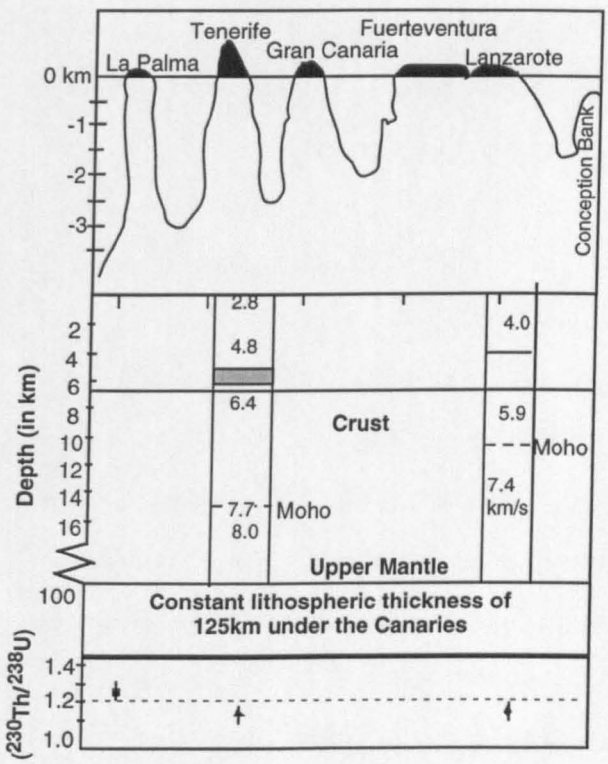

Figure 3.21. Schematic cross-section showing the variation in crustal depths and bathymetry data, similar ($^{230}Th/^{238}U$) disequilibria and constant lithospheric thickness across the Canary Islands. The bathymetry and crustal thickness from Banda et al. (1981). Disequilibria data as for Fig 3.17.

It has been argued above that the data array from Lanzarote is due to mixing between a low SiO_2, high Ce/Yb and a high SiO_2, low Ce/Yb end-member. Moreover, these end-member compositions have SiO_2 contents, which plot respectively below and above the general negative FeO*-SiO_2 arrays observed in basalts from other Atlantic oceanic islands,

and experimental melts of peridotite (Hirose and Kushiro, 1993) (Figure 3.12). The mean depths of melting inferred from the FeO* contents and REE ratios for the Lanzarote magmas are only 60-70 km, which is relatively shallow and likely to be within the lithosphere in areas of >80 Ma old lithosphere. This is also consistent with the presence of a potassic phase during the generation of the low SiO_2, high Ce/Yb 1824 magmas (Table 3.2). It is unexpected that the melts with negative K anomalies have such low SiO_2 values, since low SiO_2 is thought to be due to melting at higher pressures. The trend of increasing undersaturation with pressure does not continue indefinitely. One interpretation is that all the melts in a particular area were derived from similar source compositions and the residual potassic phase is consumed at higher degrees of melting (as in the 1730-36 rocks). The source may have been melting in a veined, possibly amphibole-bearing lithospheric mantle. In contrast, the higher SiO_2 melts might have been derived from the upwelling plume, yet the isotopes are similar in the different rock suites and hence they have been modelled by different degrees of melting of a similar source.

The ($^{230}Th/^{238}U$) disequilibrium has been modelled by decompression dynamic melting; however if melting was in the lithosphere it could not be in response to decompression and it would presumably not be possible to generate the observed ^{230}Th excesses by dynamic melting. The lithosphere in the Canaries should be 100-125 km thick, although there may have been thinning of the lithosphere to allow melting at the 60-70 km depth. For this to be the case a considerable thickness of mantle lithosphere would have to have been thermally eroded (e.g. Davies, 1994), as has been suggested for the shield-building stage of other Canary Islands (Haase, 1996) (see later discussion). Melts generated within the upwelling asthenosphere, hence having ^{230}Th excesses, have mixed with melts generated in shallower conditions, perhaps in the lithosphere. The lithosphere must have been considerably thinned by thermal erosion for the melts to be generated with excess ^{230}Th at the depths modelled from the major and trace elements.

3.8.3. Buoyancy Flux

In MORB the degree of ($^{230}Th/^{238}U$) disequilibria appears to be greater in those from shallower ridge depths where the depth of the solidus is deep and the mean degree of melting

is larger and hence, melt generation rates are higher. This has been attributed to more of the melting zone being within the garnet stability field in areas of higher mantle temperatures (Bourdon et al., 1996). Away from spreading ridges, melt generation rates are much lower (see below) and they appear to be almost independent of lithosphere thickness as discussed earlier. The depth of intersection with the solidus beneath ocean islands will be deeper because of the higher mantle potential temperature (Tp). Buoyancy flux in part reflects Tp and so the variation in buoyancy flux from island to island should correlate with different depths of intersection with the solidus. Intuitively then, a key controlling factor on the amount, rate and conditions of melting beneath ocean islands must be the buoyancy of the underlying plume (Sleep, 1990).

Chabaux and Allègre (1994) noted that regions exhibiting large U-Th disequilibria (e.g. Canaries, Azores) have lower buoyancy flux than regions having small U-Th disequilibria (e.g. Hawaii). Accordingly, they suggested that the rates of melt generation for OIB vary inversely with the buoyancy flux in the underlying mantle. The Canary Islands, Cape Verdes and Azores plumes all have similar buoyancy fluxes (1.0, 1.6 and 1.1 Mg s^{-1} respectively; Sleep, 1990) and exhibit large ($^{230}Th/^{238}U$) isotope disequilibria (Figure 3.17), consistent with the argument that low buoyancy plumes result in magmas with significant U-Th disequilibria. Moreover, if it is accepted that dynamic melting coupled with ^{230}Th-ingrowth is required to explain the U-Th disequilibria, then the data imply that the rates of melt generation are lower beneath the Canaries and Azores than beneath Hawaii. Melt production rates estimated from volcanic output and geophysical calculations, can also provide some measure of melting rates and the Canary Islands, Cape Verdes and Azores plumes all appear to have similar melt production rates of 0.02, 0.03 and 0.01 $km^3\ yr^{-1}$ respectively (White, 1993), despite the location of the Azores close to the axis of the mid-Atlantic ridge. Hawaii has a faster upwelling rate and consequently a faster melting rate than any other ocean island, and so there is less time for ^{230}Th-ingrowth. In the lower buoyancy Iceland plume, ^{230}Th-ingrowth is significant and results in striking disequilibrium in all degrees of partial melting (Condomines et al., 1988; White, 1993; Bourdon et al., 1996; Sigmarsson, 1996).

Melt generation rates are controlled by the rate at which mantle flows through the melting zone and this will be highest for those plumes with the highest buoyancy fluxes.

Plumes may rise beneath lithosphere of any age, and so the rates of melt production, and hence ($^{230}Th/^{238}U$) disequilibria, should be largely independent of lithosphere thickness. In contrast, there is a broad negative correlation between lithosphere thickness and the integrated degrees of melting (Fig 3.18, Ellam, 1992; Haase, 1996). It follows that there should be no link between the ^{230}Th-^{238}U disequilibria, and hence the inferred rates of melt generation, and the integrated degrees of melting. This is observed in the Atlantic OIB considered here (Figure 3.20 and 3.21). The rates of melt generation reflect the deep seated controls on the buoyancy flux of individual mantle plumes, whereas the integrated degrees of melting depend largely on the thickness of the overlying lithosphere.

3.8.4. Source Composition

Finally, it should perhaps be remembered that the lower buoyancy flux OIB just discussed include a number with good evidence for contributions from an old incompatible element enriched source component. Clearly, source composition can affect the depth of intersection with the solidus and presumably, therefore, both the rates and degrees of melting. For example, the low iron contents of many Azores basalts (e.g. Turner et al., 1997) could reflect a major element depleted iron-poor source region that would be naturally buoyant at relatively cool temperatures. Azores basalts plot within the Atlantic OIB field in Figure 4.10 suggesting that this effect is not strong; nevertheless the Azores lavas also show correlations between ($^{230}Th/^{238}U$) disequilibria and indices of source composition, such as $^{87}Sr/^{86}Sr$, suggesting a regional link between source composition and the melting process (Turner et al., 1997).

In the Canaries, the lithosphere is inferred to have a relatively constant thickness, and as discussed above it cannot have been a significant control on the range of inferred degrees of melting. It may also be that the buoyancy flux and the rate of upwelling are relatively invariant beneath the Canaries, and that it is therefore the source composition which is exerting a significant control on the location (60-70 km deep) and degrees of partial melting (1-4% in Lanzarote). The presence of phlogopite in the source, inferred from the trace element modelling and the FeO and REE modelling, both suggest melting occurred at shallow depths around 70 km. Such depths would be well within the lithosphere if the plate has a

thickness of 100-125 km as predicted for its age by the plate model (Parsons and Sclater, 1977). Class and Goldstein (1997) have recently independently reached a very similar conclusion in an analysis of selected OIB. These authors convincingly showed that lavas from La Grille (Grande Comore) and Oahu (Hawaii) contain contributions from a source region which contained small amounts of phlogopite and/or amphibole due to the presence of K, Rb, Sr and Ba negative anomalies. However some recent work by Neumann et al. (1997) and Neumann (*pers. comm.*) has inferred phlogopite to be stable at certain levels in the asthenospheric mantle due to the presence of these negative anomalies in some of the deep xenoliths. If this is the case then it is not a signature for lithosphere. Despite this work a large amount of the published literature persists with the assumption of phlogopite being a lithosphere phase, and being unstable in the asthenospheric mantle, hence, there is increasing evidence for a contribution from the lithospheric mantle to OIB and source composition playing a role in controlling partial melting processes.

However, the Lanzarote lavas exhibit large (^{230}Th-^{238}U) disequilibria and a vertical displacement on the equiline diagram, to elevated (^{230}Th/^{232}Th), relative to that inferred for the source from Figure 3.16. In current models for (^{230}Th/^{238}U) disequilibria, vertical shifts on the equiline diagram can only be produced by dynamic melting and ^{230}Th-ingrowth. However, this in turn requires upwelling of the peridotite matrix which appears unlikely within static lithosphere. At present the only way to reconcile the evidence for shallow melting with the need for dynamic melting is if the plume has thermally eroded the lithosphere to ~70 km depth (e.g. Davies, 1994). This would allow dynamic melting within the plume and contributions from the overlying lithosphere both to occur within a narrow depth range. Such a model is in part supported by the observed bathymetry, which is shallower than would be predicted for the age of the plate (Parsons and McKenzie, 1978).

3.9. Conclusions

A detailed study of highly primitive lavas from Lanzarote indicates the need for a residual garnet bearing asthenospheric mantle source, together with a shallower oceanic lithospheric mantle signature. The small degrees of melting (1 - 4 %) in the Lanzarote suite have similar (^{230}Th/^{238}U), hence the degrees of melting are not linked to the disequilibrium

present or lithospheric lid thickness and require dynamic melting coupled with ^{230}Th-ingrowth. A review of OIB suggests that the lithospheric lid constrains the upper limit of the melting zone and hence the final integrated melt fraction which in turn is linked to SiO_2. Because of the elevated mantle potential temperatures involved, all OIB melt columns extend well into the garnet zone. Therefore, the inverse relationship between disequilibrium generated at depth in the mantle plume and the buoyancy suggests that it is the rate at which material upwells through its solidus which controls the range in U-Th disequilibria in the Canaries. The rate of upwelling in regions of lower buoyancy, e.g. Canaries, is less than in regions of increased buoyancy. The time spent by the melt in the melt column with a slow rate of upwelling is longer and hence there is more time for the ^{230}Th ingrowth to occur, and hence significant disequilibrium is observed. High Tp lowers the solidus and melts are generated more easily. A low upwelling rate and the time spent in the melt zone and the Tp, all appear to exhibit a control on the degree of disequilibrium generated in OIB. In contrast, for MORB the upwelling rate is more or less constant (Richardson and McKenzie, 1994) and the amount of the melt column within the garnet zone is much smaller. Consequently, the time spent in equilibrium with garnet, during which ^{230}Th -ingrowth may occur, is dependent on the length of this part of the melting column rather than the rate at which mantle material upwells. Thus, for MORB, the extent of U-Th disequilibria is positively correlated with mantle temperature whereas for OIB the opposite is true. Although source composition may control the position of the solidus, for MORB source composition, variations are thought to be minor and therefore play less of a role in controlling U-Th disequilibria than variations in mantle temperature (Bourdon et al., 1996). However, in some OIB, there is increasing evidence for a contribution from the lithospheric mantle. Source composition may thus play a far more important role in controlling partial melting processes beneath ocean islands than previously thought or than that inferred beneath mid-ocean ridges. Resolving this discrepancy of different controls on ^{230}Th-^{238}U between MORB and OIB is central to establishing more widely applicable models for melt generation beneath ocean islands.

Hence there is only one volcano on the Canary Islands:
the peak of Teyde. It is a central volcano

Leopold Von Buch (1774-1852) Pomeranian geologist
In: The upheaval of volcanoes 1825

Mt Teide and the lighter coloured 2ka Montaña Blanca eruption
The dark lavas are the 1492 eruption of Teide

Pico Viejo from the west
Las Natrices del Teide - 1798 eruptions

Plate 4

CHAPTER 4

URANIUM SERIES, MAJOR AND TRACE ELEMENT GEOCHEMISTRY OF THE TEIDE-PICO VIEJO COMPLEX

4.1. Background

This chapter provides the detail for a paper on the timescales of magma chamber processes and the isotopic geochemistry of the Teide-Pico Viejo complex of Tenerife. It includes a detailed summary of the geological setting and evolution of the island from early subaerial basalts in the Miocene to the most recent eruption in 1909. The rocks of the Teide-Pico Viejo Complex were sampled using the published stratigraphy of Ablay et al. (1998), although this stratigraphy is currently being amended to include new data from borehole chips and galleries in the complex. The rocks sampled for this project are all from surface exposures of the Teide-Pico Viejo Complex.

The Teide-Pico Viejo Complex rocks provide a contrast to the primitive Lanzarote suite as the complex ranges in composition from basanite to phonolite, reflecting the different effects of various magma chamber processes, such as fractionation, further melting and assimilation.

The rock suites were analysed for majors, trace and rare earth element geochemistry, and their U-series isotopes. Sr and Nd values reported here were done by E-R. Neumann in Oslo (Ablay, unpublished) and the data fields shown are from the larger data set analysed during Ablay's thesis. Comparison between these analysis and those for this project showed only minor differences and most samples were replicated within error of the other laboratory's analysis (see end of Appendix A)

4.2. Introduction

As discussed in Chapter 3, ocean islands provide an insight into the compositional variations within the Earth's mantle and therefore remain central to current debates on the forms of mantle convection and controls on melt generation in intraplate settings (e.g. McKenize and O'Nions, 1995; Hofmann, 1997). Lanzarote provides excellent examples of primitive ocean island basalts, from which it was possible to model depths and degree of melting, and to arrive at a possible source composition for the island, taking into account the different processes which have altered the geochemical signatures. Tenerife, the largest volcanic island in the Canarian archipelago (Schmincke, 1982; Araña and Ortiz, 1991), offers an opportunity to study the effects of shallow level chamber processes in a suite of magmas in a long-lived ocean islands system. The evolution of the most recent activity of the Teide-Pico Viejo Complex lavas from basanite to phonolite is similar to that of older sequences, such as the Las Cañadas. It indicates the existence of magma chambers at different depths in the Earth's crust (Ablay, 1997), which allow the melts to pond and have time to differentiate and mix prior to eruption. Such magma chamber processes do not appear to have affected the samples analysed from Lanzarote; as the erupted lavas are primitive in composition.

4.2.1. Magma Chamber Modelling

Despite numerous studies of active volcanoes, it is only relatively recently that constraints have been developed for assessing the volumes of magma stored in shallow reservoirs, and the mean residence times of magma within such chambers. The main methods used to constrain the underlying magma volumes are improved measurements of the eruptive volumes and geophysical analysis of the underlying area. Such methods include ground deformation, gravity, volcanic tremor and seismic topography (e.g. Schick et al., 1982; Detrick et al., 1987; and Burnett et al., 1989). The techniques have increased in sensitivity over time, but it is still difficult to image small volumes of magma (< 5 km^3). Geochemical constraints on the volumes of magma within magma chambers have included amounts and velocities of volatiles degassing from the magma and effusing from vents and

fumaroles, but these require corrections for melt inclusions and assumptions regarding the pre-degassed concentration of volatiles in the magma (Pyle, 1992).

Physical and chemical modelling of magma chambers based on parameters such as properties of the melt (e.g. percentage of phenocrysts and composition), and the rates of magma supply and transfer has advanced significantly (O'Hara, 1977; Wolff et al., 1990; O'Hara, 1998), but the timescales over which these processes operate are still poorly constrained. Over the last 10 years workers, such as Volpe and Hammond (1991); Volpe (1992); Hemond et al. (1994), Sigmarsson (1996), Heath et al. (1998) and Black et al. (1998) have used U series isotopes to estimate the volumes of magma chambers and, perhaps more importantly, the residence time within individual chambers from volcanoes such as Etna, Kilaeua, Mt. St Helens, Mauna Loa, the Laacher See, Soufriere and Vesuvius.

Reviews of the principles of U-series modelling are provided elsewhere (e.g. Allègre, 1968; Capaldi et al., 1976; Condomines et al., 1988; Gill and Condomines 1992; Elliott, 1997). However briefly the ($^{238}U/^{230}Th$) method is based on the time of equilibrium between the daughter ^{230}Th and the parent ^{238}U after an event which causes U-Th fractionation. Similarly the amount of disequilibrium present between the ^{226}Ra and ^{230}Th (parent) is a measure of time taken for re-equilibration. U-series studies take in account the nuclide activities rather than mass concentrations. The ratios between the different nuclides are by convention reported as activity ratios and are denoted by parentheses. The U-Th-Ra isotopes of whole rocks and co-genetic minerals, which may have different initial degrees of fractionation, may form isochrons described by the isochron equation.

$$\left(\frac{^{230}Th}{^{232}Th}\right)_P = \left(\frac{^{230}Th}{^{232}Th}\right)_I e^{-\lambda t} + \left(\frac{^{238}U}{^{232}Th}\right)_I \left(1 - e^{-\lambda t}\right) \qquad (1)$$

where λ is the decay constant of ^{230}Th (9.1952E-6 Meadows et al., 1980) and ^{232}Th is used for normalising purposes. Ba is used as the normalising factor in the ^{226}Ra - ^{230}Th isochron equation, as there is a lack of a longer-lived radium isotope to normalised against in order to exclude chemical fractionation.

The fractionation age of U from Th or Ra from Th in volcanic rocks can be determined providing that the only change in ratios is due to radioactive decay and not to modification by secondary processes, (e.g. hydrothermal which has mobilised these elements relative to the

initial concentrations). Such isotopes can be used to date trace element fractionation events, but in the case of volcanic rocks, such ages are not necessarily associated with an eruption event. The dating of volcanic rocks by ^{238}U series methods has proved difficult because a number of volcanic rocks record U-Th-Ra fractionation events that are linked to pre-eruption processes in magma chambers, and in some cases even in the upper mantle (Allègre and Condomines, 1976; Capaldi et al., 1982; Hemond et al., 1988 and Pyle et al., 1988). Thus, the rocks do not have homogeneous isotope ratios at the time of eruption, and so they do not yield reliable eruption ages. Many studies describe petrographic and chemical evidence for open-system magma chamber processes, including multiple injections of magma, multiple injections with mixing and fractionation, magma mixing, assimilation, contamination and recycling of crystals in replenished chambers (e.g. Pyle et al., 1988; Volpe and Hammond, 1991 and Heath et al., 1998). Unravelling the effects of such processes is complex, but it is often useful to investigate the age of the crystals separately from the age of the magma, and this can be done by the analysis of mineral separates. In this way U-series isotopes may be used to constrain the timescales and quantify the chemical fractionation in differentiated magmas prior to eruptions (e.g. Condomines et al., 1988). The ability to measure small amounts of ^{226}Ra allows processes on even shorter timescales to be investigated. In this study U-Th-Ra isotopes are used to investigate the timescales of the pre-eruption processes beneath the Teide-Pico Viejo complex, and in particular of the processes of magma differentiation from basanite to phonolite in the last 175 ka (e.g. Condomines et al., 1988 and Gill and Condomines, 1992).

4.2.2. Basanite to Phonolite Assemblages

The association of basanite to phonolite is commonly found in intraplate settings. Evidence for underlying magma chambers, and in some case strongly zoned magma chambers, has been worked on over the last 20 years in areas such as the Laacher See in the Eifel region of Germany (Bourdon et al., 1994); Tristan da Cunha, in the South Atlantic (Le Roex et al., 1990); San Miguel, Azores (Storey et al. 1989); Hut Point Peninsula, Antarctica (Kyle, 1981); and Tenerife, (e.g. Booth et al., 1973; Wolff et al., 1985; Ablay, 1997 and this work). All of these regions are found in the intraplate setting, either associated with ocean island magmatism or rifting (notably the Antarctica example), and their ages range

from 15.4 Ma to the present day at Mount Erebus in Antarctica (Kyle, 1981); 13 to 30 Ka in Laacher See (Bourdon et al., 1994) and from >3 m.y. to present day on Tenerife. In general the largest percentage of the rocks tend to be mafic in composition with only some 10-30 % being salic. Each of these examples has been explained by fractional crystallisation within a zoned magma chamber, although other processes such as assimilation and mixing have also had a role. Different magma batches are unlikely to evolve as isolated entities en route to the surface (Blake and Ivey, 1986).

The gradients of different physical parameters in these zoned chambers may influence both the evolution of the magmas and the causes and mechanisms of eruption (Wolff et al., 1990). Thus, small strongly zoned alkaline magma chambers which evolve by fractional crystallisation of a basaltic or basanitic parent may suffer partial volatile depletion prior to eruption, and this degassing is most likely to be from the upper most layer. Eruption withdrawal mechanisms are dependent on density gradients and therefore the volatile and phenocryst abundances, as well as on any compositional gradients within the magma. In most of the cases listed here, a large percentage of the erupted materials are tephra and pyroclastics, rather than lava. In the case of the Teide-Pico Viejo Complex on Tenerife, the final evolved (phonolite) eruption of a each sequence is linked with a collapse at the issuing vent and a pyroclastic eruption (Martí et al., 1994; Ablay et al., 1998).

The timescales of magma differentiation provide important new insights into the nature of the differentiation processes, and arguable into the causes of eruption. Previous U-series studies on basanite-phonolite suites include that on Laacher See by Bourdon et al. (1994). Some of the younger pumices (13 ±3 ka.) from the main part of the chamber imply a residence time of between 1- 2 ka, while older less precise ages from the lower part of the sequence (~30 ka) suggest either mixing with older cumulate crystals and/or longer residence times. In-situ cumulate formation ages are between 10-20 ka, prior to eruption, whilst the time taken to explain the observed difference in ($^{230}Th/^{232}Th$) between the parental basanite and the phonolite is inferred to be in the order of 100 ka. Such time information favours a slow cooling model in which differentiation of the parental basanite takes place deep in the crust over 100 ka, followed by the emplacement of the resulting magma into an upper crustal chamber and continued differentiation towards the evolved phonolite. The new U-Th-Ra data

presented here on selected 175-0 ka old rocks of the Teide-Pico Viejo Complex are used to evaluate the timescales of differentiation and magma residence times in the chambers beneath this complex.

4.3. Geological Evolution of Tenerife

Tenerife is the largest island (2058 km^2) in the Canaries group (Marti and Mitjavila, 1995a), and it is located in the central group between the islands of Gran Canaria and La Gomera. The island is dominated by the imposing 3718 m Mt Teide, part of the Teide - Pico Viejo complex in the Las Cañadas caldera in the centre of the island. The volcanism is more evolved in composition than the Lanzarote suite. Some 8.4 % of the island is subaerial, compared with much smaller amounts for the rest of the islands. Despite this small amount of subaerial activity, two main phases can be observed, a main pre-erosional shield building phase, followed by a period of quiescence and erosion, and then a smaller post erosional phase.

4.3.1. The Old Basalt Series

The first subaerial volcanism which formed the shield building stage of Tenerife is known as the Old Basalt Series (OBS) and it ranges in age from 16 Ma to 3.3 Ma (Fuster et al, 1968; Ancochea et al., 1990) (Figure 4.1.). N. Arnaud (*pers. comm.*) has discounted the oldest of these dates, due to inaccurate and old analytical techniques, and suggested that the oldest Old Basalt Series activity was at approximately 8 Ma. These rocks outcrop in the Anaga massif to the NE, the Teno massif in the NW and in an isolated window at the Roque del Conde, near Adeje in the south. The OBS tends to be fissure fed and to form accumulations of flows and basaltic pyroclastic deposits. Ankaramites (augite and olivine phyric mafic rocks), basanites and olivine basalt compositions dominate the earlier activity (Araña, 1995), although towards the top of the series more evolved rocks (phonolite and tephrites) appear, often in the form of dykes or plugs. Sedimentary horizons of soils and sands, breccias and baked soils are interbedded with the volcanic units. Considerable amounts of erosion have revealed dyke swarms that follow marked directions in each massif.

The subaerial OBS constitutes only a 1000 - 2000 km^3 cap that rests on basal formations of submarine basalts, probably some 15 - 20,000 km^3 in volume.

The Anaga massif is comprised of a complex sequence of alkali basalt flows with abundant volcaniclastic layers intruded by subvolcanic bodies of basalt, trachyte and phonolite. The series dip roughly seawards and have a total thickness of about 1000 m. Abdel-Monem et al. (1972) published an K-Ar age of 16.1 Ma for the base of this series; however Anchocea et al. (1990) failed to analyse similar samples because of the intense alteration of that layer. The oldest age they obtained within this series was 6.50 Ma ± 0.1. Three successive cycles have been identified in the Anaga region separated by quiet periods of little or no volcanic activity.

The Teno massif is made up of a lower sequence of basaltic lavas and pyroclastics, covered unconformably by a sequence of subhorizontal basaltic flows with some trachytes. The whole massif is cross cut by dykes and salic plugs. The oldest age known from this area is 6.7 Ma, with the youngest age being 4.5 Ma on a phonolitic plug (Anchocea et al., 1990).

There are several outcrops of OBS in the Roque del Conde region, where the sequence is some 1000 m thick. Age determinations from the base to the top of this sequence yield ages between 11.6 and 6.4 Ma (Anchocea et al., 1990), although different ages have again been reported by different authors. Carracedo (1975) obtained an age of 2.4 Ma for one of the samples on which Anchocea et al. (1990) reported 4.8 Ma. The youngest reliable age in this region is 3.8 Ma on a salic plug known as Roque Vento.

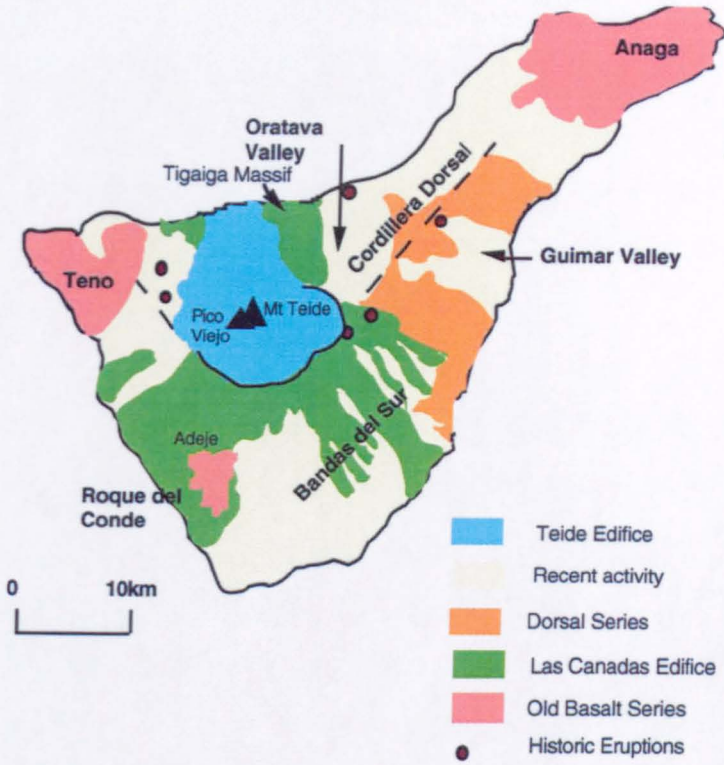

Figure 4.1. Map of Tenerife (After Ancochea et al., 1990)

4.3.2. The Las Cañadas Volcano and Caldera

Following the shield building phase, the next stage of volcanic activity was concentrated in the central part of the island, with the establishment of the Las Cañadas edifice. Differentiated volcanics and basalts formed a large volcanic complex from 3.5 Ma to the present (Martí et al., 1994), and the eruption of evolved peralkaline phonolites indicates the presence of high level (sea-level) magma chambers beneath the complex. Contemporaneous basaltic eruptions resulted in the formation of a SW-NE dorsal ridge linking the Las Cañadas complex and the Anaga massif in the NE, and this is known as the Cordillera Dorsal or Dorsal Series (Fuster et al., 1968; Ancochea et al., 1990). Volcanic activity elsewhere on the island included a large number of monogenetic basaltic cones that constitute the Recent Basalt Series (Fuster et al., 1968). Ancochea et al. (1990) dated the formation of the Las Cañadas volcano at c. 1.8 Ma, and the end of the shield forming stage at c. 3.3 Ma, and suggested an intervening period of quiescence and erosion. However, more recent K-Ar dates (Martí et al., 1994) indicate that some of the Lower Group of the Las Cañadas Volcano is older than 3.5 Ma, suggesting an overlap between the cessation of the

shield building phase and the onset of the central activity. This overlap may be linked to 1-2 km of lithospheric subsidence in the early Pliocene (Watts and Masson, 1995), sustaining the shield building stage and allowing the onset of the central activity at the same time. Morphological reconstruction of the edifice suggests it was less than 3000 m high and elongated in a NNE-SSW direction (Martí et al., 1994.) The series of vents were parallel to the main regional trends of NE-SW and NW-SE.

Two groups have been distinguished in the Las Cañadas volcano, a dominantly mafic Lower Group (>3.5-2.2 Ma), and an Upper Group comprising of three distinct volcanic cycles: the Ucanca (1.59 - 1.18 Ma), the Guajara (0.85 - 0.65 Ma), and the Diego Hernadez formations (0.37 - 0.17 Ma). Each of these groups was separated by periods of dormancy of between 120 and 250 Ka (Anchochea et al., 1990; Martí et al., 1994). Each cycle involved the extrusion of mafic to intermediate magmas followed by voluminous explosive phonolitic eruptions which resulted in the large pyroclastic apron for each cycle preserved today in the Bandas del Sur in the south of the island. This activity created non-welded ignimbrites, pyroclastic surges, fallout deposits, welded ignimbrites and pumice falls with lithic fragments and loose crystals (Booth, 1973; Wolff, 1985: Bryan, 1998). Palaeosols and fossilised wood are found inter and intrabedded. The dispersal of the main pyroclastic deposits to the south and the distribution of the three formations of the Upper Group (Martí et al, 1994), indicate that the focus of volcanic activity migrated systematically northeastwards after caldera collapse occurred. The volume of phonolitic pyroclastic material generated was in the order of at least 130 km^3 (dense rock equivalent) compared with the approximate volume of the caldera of >110 km^3.

The Upper Group of the Las Cañadas volcano is best exposed in the walls of the present caldera. Most of the deposits dip down the outer slopes of the edifice and are truncated by the caldera wall. A large elliptical depression was formed by the collapse of the Las Cañadas volcano (the Las Cañadas caldera) which formed a truncated top to the edifice at an altitude of c. 2 km. The Las Cañadas caldera at present measures some 16 by 9km, with a maximum depth of 600 m of exposed caldera wall at Guajara. It is divided into two unequal sectors by the Roques de Garçia, a spur of pre-caldera material, which abuts against the southern caldera wall. The present caldera rim comprises of several scalloped walls to

the south and east. To the north and west the wall is absent, except for an isolated segment at La Fortaleza, which is part of the Tigaiga Massif. The Tigaiga Massif separates the steep sided Icod and Orotava valleys, which are deep landslide scars incised into the northern flank of the Las Cañadas volcano (Navarro and Coello, 1989; Masson, 1996; Watts and Masson, 1995). Although the chronostratigraphical history of the edifice has been divided into a number of different volcanic units (Hausen, 1956; Ancochea et al., 1990; Martí et al., 1994; Martí and Mitjavila, 1995a), the origin of the caldera is still debated. The two hypotheses preferred are either multiple vertical collapses along ring fractures (Ridley, 1970b; Martí et al., 1994, 1997) or lateral collapse by landsliding (Navarro and Coello, 1989; Carracedo, 1994; and in press). The Las Cañadas caldera is a composite structure (Araña, 1971) comprising three overlapping depressions which young towards the north-east (Martí et al., 1994). Evidence for the association of explosive phonolitic activity with the vertical collapse episodes and the lateral collapse of the northern flank suggest that the caldera resulted from several episodes of vertical collapse combined with lateral failures along the northern caldera wall and flank (Ablay, 1997; Martí et al., 1997).

The Cordillera Dorsal and the scarps of the steep sided landslide valleys of Güimar and La Oratava have been dated at between 0.9 and 0.78 Ma (Ancochea et al., 1990). The thick basaltic sequence accumulated in the valley is less than 0.1 Ma old, with the upper part of the series yielding younger ages of 540 and 560 ka (Ar-Ar, Arnaud, *pers. comm.*) for the flows which cover the scarp of the La Orotava valley. The most recent activity other than the Teide Pico Viejo complex is reflected in numerous small scattered individual basaltic cones, six of which have been active in historic time. These include small cindercones that can be seen dotting along the southern coast.

4.3.3. Teide-Pico Viejo Complex

The Las Cañadas caldera has been partially infilled since 175 ka by the products of the most recent activity on Tenerife, the twin stratovolcano cones of Teide (3718 m) and Pico Viejo (3103 m). The Teide-Pico Viejo complex (Figure 4.2.) comprises a thick sequence of early basanite and alkali basalt, overlain by intermediate and more evolved felsic compositions from the stratovolcanoes of Pico Teide and Pico Viejo, and phonolitic

pyroclastics from the satellite vent of Montaña Blanca, which produced a violent subplinian eruption at around 2 ka (Ablay et al., 1995; Ablay, 1997).

The Roques de Garçia is a sequence of volcanic and sedimentary horizons which form peaks and towers that divide the La Cañadas caldera and separate the exposed products of Pico Viejo to the west from the exposed Teide and Moñtana Blanca rocks to the east (Plate I). The summits of Teide and Pico Viejo are 2700m apart (Ablay, 1997), but the cones overlap to form a WSW-ENE elongated double cone with a saddle at ~3,000 m above sea level. The products of the Teide-Pico Viejo complex extend northwards, where the caldera wall is absent, and to the east and west where the complex is overlain by numerous late Quaternary cinder cones. Pico Teide and Pico Viejo have distinct independent eruptive histories involving alternating eruptive episodes, terminated by summit caldera-forming events associated with phonolitic eruptions.

Pico Teide, Pico Viejo and Montaña Blanca consist of 2 petrologically distinct basanite-phonolite lineages (Ablay, 1997; Ablay et al., 1998): the Teide Series which comprises the products of Pico Teide and the older parts of Pico Viejo, and the Pico Viejo Series which comprises the youngest Pico Viejo and Montaña Blanca. Geochemical modelling suggest that both sequences evolved from similar parental basanite magmas by differentiation and crystal fractionation under different P-T-H_2O conditions. In general, the Teide Series is more crystal-rich and the data exhibit more scatter due to mineral accumulation, magma mixing and contamination, while the Pico Viejo Series is relatively crystal poor, with smooth variations in geochemistry.

Structural evidence for shallow magma chambers, similar to those present beneath the Las Cañadas volcano, include summit caldera collapses at the vents and the radial geometry of the phonolitic Pico Teide satellite vents. Enstatite, wollastonite and ferrosalite pyroxene barometry (based on the strong pressure dependence of Al^{VI} content in igneous pyroxenes) (Grove et al. 1989) and geophysical work by Ablay (1997) suggest that the mafic magmas and intermediate Pico Viejo Series lavas evolved in a deep storage zone in the lower crust at 6-9 kbar P_{total}.

Figure 4.2. (over page) Map of Teide-Pico Viejo complex (after Ablay, 1997; 1998; pers.comm.) Units are colour coded on map, sample locations are labelled. Initials (in alphabetical order) stand for names of vents and localities:

AA: Asientos Altos; AB: Areñas Blancas; AN: Areñas Negras; BH-1-5: Boreholes 1-5; BT: Boca Tauce; DH: Diego Hernadez; EC: El Culaton; ET: El Tabonal Negro; G: La Guajara; HA: Hoya del Abrunco; HC: Hoya del Cedre; LA: Las Pilas; LF: La Fortaleza; LL: Los Llanos de Angostura; Lle: Las Lenguas; LR Los Roquillos; MA: Montaña Abejera; MB: Montaña Blanca; MC: Montaña de la Cruz; MCh (in PV9): Montaña de los Chircheros; MCh: Montaña Chio; MCT: Montaña de la Cruz del Teide; MLC: Montaña de los Corrales; MLL: Montaña las Lajas; MM: Montaña Majua; MMst: Montaña Mostaza; MN: Montaña Negra; MR: Montaña Rajada; MT: Montaña de los Tomillos; MT: Montaña Tapada; N: Las Natrice del Teide; PC: Pico Cabras; PV: Pico Viejo; RB: Roques Blancos; RDG: Roques de Garçia; RV: Riscos Verdes; SC: Siete Cañadas; U: Ucanca; VC: Volcan la Corona

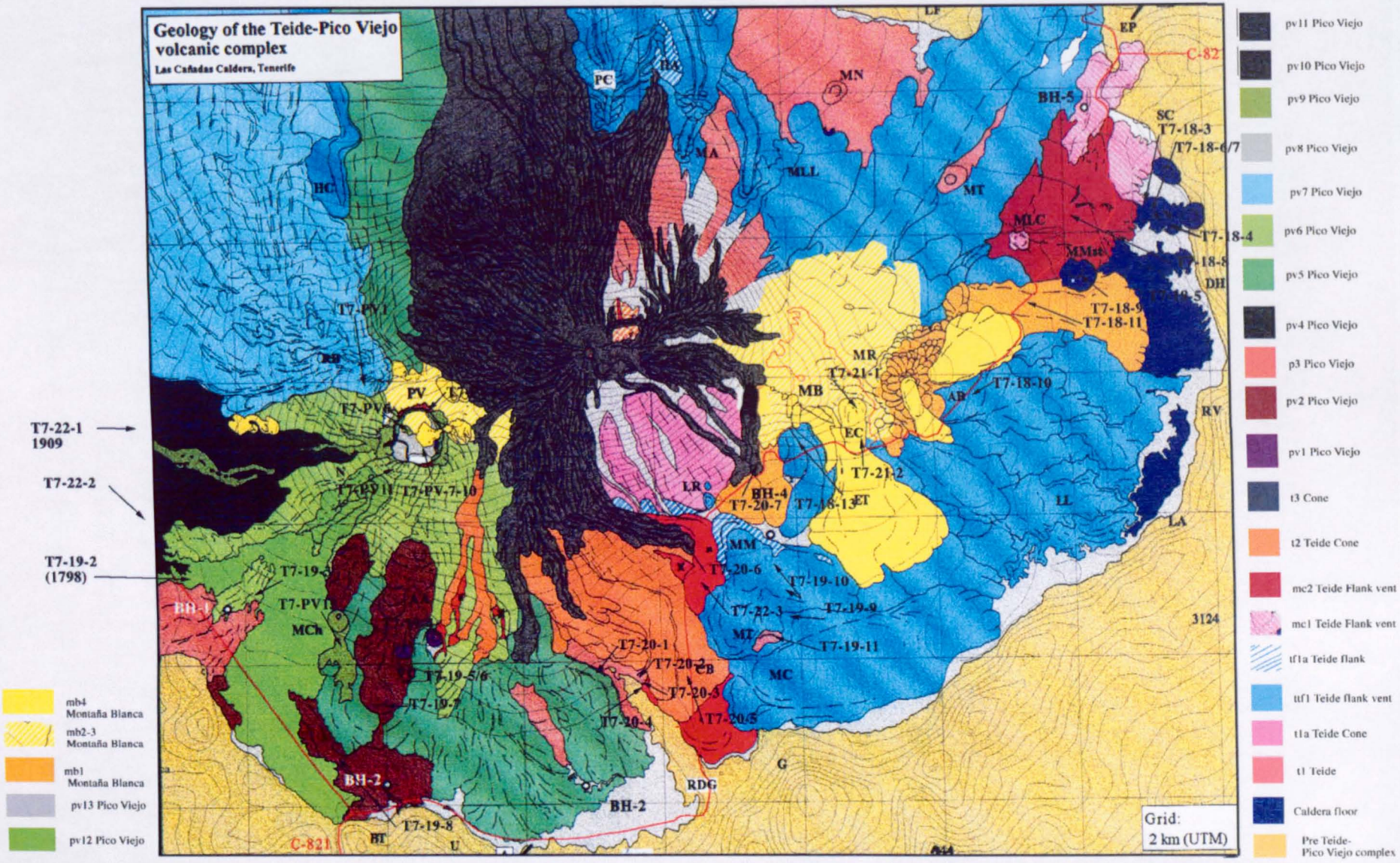
Geology of the Teide-Pico Viejo volcanic complex
Las Cañadas Caldera, Tenerife
T7-22-1 1909
T7-22-2
T7-19-2 (1798)
mb4 Montaña Blanca
mb2-3 Montaña Blanca
mb1 Montaña Blanca
pv13 Pico Viejo
pv12 Pico Viejo
pv11 Pico Viejo
pv10 Pico Viejo
pv9 Pico Viejo
pv8 Pico Viejo
pv7 Pico Viejo
pv6 Pico Viejo
pv5 Pico Viejo
pv4 Pico Viejo
p3 Pico Viejo
pv2 Pico Viejo
pv1 Pico Viejo
t3 Cone
t2 Teide Cone
mc2 Teide Flank vent
mc1 Teide Flank vent
tf1a Teide flank
ttf1 Teide flank vent
t1a Teide Cone
t1 Teide
Caldera floor
Pre Teide-Pico Viejo complex
Grid: 2 km (UTM)
C-821
C-82
PC
HA
MN
MA
MLL
MT
MLC
MMst
BH-5
SC
T7-18-3
T7-18-6/7
T7-18-4
DH
T7-18-9
T7-18-11
T7-18-10
MR
T7-21-1
MB
AB
RV
EC
T7-21-2
LR
BH-4
T7-20-7
T7-18-13
ET
LL
LA
MM
T7-20-6
T7-19-10
T7-22-3
T7-19-9
3124
MT
T7-19-11
MC
T7-20-1
T7-20-2
T7-20-3
T7-20-5
T7-20-4
G
RDG
BH-2
T7-19-8
BT
U
T7-19-5/6
T7-19-7
BH-1
T7-PV1
MCh
T7-19-3
T7-PV11
T7-PV-7-10
T7-PV6
PV
HC
RB
T7-PV1
LP
EP

Intermediate Teide Series lavas are also thought to have originated in the deep storage zone, but they subsequently differentiated in a shallow Teide chamber. Melt inclusion data and biotite-sanidine-magnetite hydrometry suggest this chamber was (and may still be) located at 1.5-2.5 kbars P_{total} (Ablay, 1997; Ablay et al., 1998). The limitations of this hydrometry include the required prior knowledge of temperature and the oxygen fugacity of the system in which biotite must be stable. This chamber and the associated conduits are designated as the Teide sub-system. There is yet another shallow chamber at 1 kbar P_{total}, inferred from the chemistry of Pico Viejo phonolites, and this chamber and its conduits are designated as the Pico Viejo sub-system.

There are six main stages recognised in the evolution of the Teide-Pico Viejo complex that correlate to the stratigraphic groups in Table 4.1.

1) Early mafic compositions erupted from a deep storage zone along a long lived NE-SW extensional lineament.

2) The Teide sub-system must have become more evolved, as phonolites were erupted from radial flank vents (this included the onset of activity at Montaña Blanca) and the chamber was then replenished by mafic lavas from the deep storage zone. Hence the Teide sub-system developed on this NE-SW lineament, and early Pico Teide rocks were erupted with Pico Viejo as its satellite vent. Mixed lava eruptions occurred and the Teide summit collapsed.

3) A NW-SE lineament was activated with intermediate Pico Viejo compositions being erupted: the activity then became phonolitic, and terminated with the summit collapse of Pico Viejo.

4) The Teide sub-system continued to erupt mixed lavas, again terminated by a summit collapse.

5) The Pico Viejo sub-system became reactivated and phonolite evolved at depth. The two lineaments became linked and the phonolite migrated beneath Teide, from Pico Viejo to Montaña Blanca, where the ~2 ka explosive eruption was linked to the second Pico Viejo summit collapse.

6) Historic activity has occurred on both lineaments, and basanites contaminated by phonolitic-mush in the Teide sub-system were erupted in 1430 and 1706. Remobilised phonolite was erupted from Pico Teide in 1492 which forms the striking black lava deposits

cascading over Teide today (Soler et al., 1984) (Plate 1 and 4), and Columbus is believed to have witnessed this eruption en route to America. More contaminated basanite and intermediate lavas were erupted from Pico Viejo in 1798. The youngest eruption was in 1909 when basanitic material was erupted from a small cone at the edge of the caldera. Table 4.1 summaries the stratigraphy and the division of the units of the Teide-Pico Viejo complex, used in this chapter.

Group	Member	Unit	Lithology	Volume (in km^3)
1. Early	Caldera Floor	cf1	Primitive basanite, alkali basalt	~30
2. PTS 1	PT Cone 1	t1	Phonolitic tephrite, tephritic phonolite	~10
	PV Lower Cone	pv2 pv3	Phonolite, Plagioclase phyric basanite Phonolitic tephrite, tephrite	~3
	PT Flank Vents	tf1 tf1a ab1 mc1	Trachy-phonolite, phonolite Phonolite pumice Phonolite crystal rich tephritic phonolite	~1.7
	PT Cone 1	t1a	crystal rich tephritic phonolite	< 0.01
		t1b	phonolitic tephrite-phonolite	<0.01
3. PVS 1	PV Upper Cone	pv4 pv5 pv6 pv7	Plagioclase phyric basanite, phonolitic tephrite Tephritic phonolite Tephritic phonolite Phonolite	~1 ~0.4 ~0.02 ~0.32
	PV Caldera Fill	pv8 pv9	Phonolitic tephrite Plagioclase phyric basanite	~0.1 <0.01
4. PTS 2	PT Cone 2	t2 mc2	Phonolitic Tephrite-phonolite Tephritic phonolite	~1.5
5. PVS 2	Lower MB Upper MB	mb1 mb2-4	Phonolite Phonolite	~0.22 ~.12
6. Historic	PT (1492) PV (1798) Hist. basanites	t3 pv12	Phonolite Phonolitic tephrite, evolved basanite Primitive-evolved basanite	~0.4 <0.01 ~1

Table 4.1. Litho-stratigraphy of Teide-Pico Viejo Complex (After Ablay, 1997)

A new stratigraphy has recently been devised for the Teide-Pico Viejo complex by Giray Ablay (*pers. comm.*), but this is still being modified as new samples from boreholes and underground galleries are added to the database of rocks from his PhD and this project. A summary of the new stratigraphy can be found in Appendix G, however the data in this

chapter are presented in the context of the published stratigraphy summarised in the table above.

4.3.4. Mineralogy and Petrology of Teide-Pico Viejo Complex

See Appendix B for description of individual samples.

The rocks can be split into six main groups as shown in Table 4.1. Group 1, and the caldera floor and historic mafic eruptions from Group 6, tend to be basanitic or basaltic in composition, with MgO ranging from 5 to 10 wt %. The phenocryst phases are olivine and clinopyroxene ± magnetite. The historic 1430, 1704-05 and 1706 eruptions are similar to the caldera floor basanites, while the more evolved historic basanites (1430, 1798 and 1909) contain phenocrysts of olivine, clinopyroxene, magnetite, plagioclase ± apatite and kaersutite. These more silica-rich basanites are termed plagioclase-phyric basanites.

The Pico Viejo Series rocks (PVS1 and PVS2) are generally less crystal rich than those of the Teide Series and they show systematic variations as the compositions become more evolved. They are generally glassy or have relatively fine grained, well crystallised matrices. Plagioclase-phyric basanites contain phenocrysts of plagioclase, apatite and ilmenite with clinopyroxene, magnetite and olivine. The phonolitic tephrites contain phenocrysts of kaersutite, clinopyroxene and plagioclase and apatite in similar proportions, with less magnetite and olivine, whilst the tephritic phonolites contain dominantly kaersutite with clinopyroxene. The more evolved rocks in this series, the phonolites, have mainly alkali feldspar phenocrysts, but they also contain biotite, magnetite, titanomagnetite and ilmenite.

The Teide Series are on the whole more crystal-rich (up to 50 % phenocrysts in some samples) than the Pico Viejo Series, although they have a similar glassy or fine grained groundmass. The lavas range in composition from plagioclase phyric basanite to phonolite, and contain varying amounts of the following phenocryst phases: plagioclase, alkali feldspar, clinopyroxene, magnetite, olivine, apatite and ilmenite. The younger samples are less crystal rich and more fine grained than the older products. Hydrothermal alteration has produced zeolite and carbonate minerals in some of the rocks, but care was taken to avoid these for isotope analysis.

4.4 Sample Collection and Analytical Techniques

Representative samples of all the major exposed units of post caldera age (see Figure 4.2) were collected during a field trip in October/November 1995. The analysed samples range in composition from basanite to phonolite using the total alkalis-silica scheme (Le Bas et al., 1986) with the Le Maitre et al. (1989) nomenclature (Figure 4.3). Some of the mafic lavas from the more recent activity were also collected, in order to compare them with the mafic lavas from Lanzarote. In this chapter the rocks are split either into the 3 separate groups, Teide suite (PTS), Pico Viejo suite (PVS) and mafics, which include the caldera floor mafics and the mafic historic eruptions, or they are divided up into mafics and more evolved compositions with MgO 6% as divider. The different groups (PTS and PVS) gradually evolved in composition through time, with the youngest activity being phonolitic. Gabbro xenoliths from the summit of Pico Viejo were also examined.

The petrology of the historic lavas has been discussed by Garçia-Moral (1989); the petrology and geochemistry of the Las Cañadas edifice has been discussed by Martí et al. (1994, 1997) and the geochemistry of the alkaline shield has been modelled by Ancochea et al. (1990); Martí et al. (1994) and Thirlwall (unpublished). The petrology, stratigraphy and geochemistry of the Teide-Pico Viejo Complex has been discussed by Ablay (1997); Ablay et al. (1998), and this work is on going with Ablay (*pers. comm.*). Isotopic geochemistry provides new insights into the conclusions presented by Ablay (1997), and allows a modified interpretation.

The major and trace element abundances and U, Th and Ra isotopic ratios are given in Appendix A. The major and trace element abundances have been measured by XRF, and the REE have been measured by INAA, (see Chapter 2 and Appendix C for description of the U-Th-Ra analysis). Reproducibility of the U456std2 (in house Uranium solution standard) gave ($^{235}U/^{236}U$) = 0.097495 ± 0.00068, yielding two standard deviations of 0.69 % (No=30); whilst the ($^{234}U/^{236}U$) value was 13.272 ± 0.029, yielding 2 standard deviations of 0.21 %. The Th 'U' standard gave 2 standard deviations of 1.4% for the period of this study. Duplicate analyses suggest that the standard deviations are in fact better for samples than standards. The present procedure is capable of analysing ($^{230}Th/^{232}Th$) ratios to 0.5 % 2 sigma precision on 40 - 60 ng of Th (see also Turner et al., 1997).

4.5. Analytical Results

In each of the following sections the sample suite is divided into three groups and the results are discussed both within and then between groups. The three groups are the mafic rocks (rocks with < 47 % SiO_2, which includes the caldera floor and 1909 eruption), the Pico Teide series (PTS) and the Pico Viejo series (PVS) (the 1798 eruption and a few of Pico Viejo summit eruptions are 'plagioclase phyric basanites' and are included in PVS). The PTS-1 and PTS-2 groups also include some lower silica but high alkalis rocks, which lie at the lower end of the tephrite to basanite field, and have relatively high modal olivine.

4.5.1. Major and Trace Element Geochemistry

The mafic group, which comprises the caldera floor rocks and the most recent historic eruption, are basanite to magnesian alkali basalt in composition. The rocks have MgO = 5.4 -11.3, and Mg numbers ranging from 51 to 65. The historic 1909 eruption (the 1430 and 1706 eruptions have a similar compositions, but they were not sampled for this work) is a plagioclase phyric basanite which has the lowest MgO and Mg number. This rock suite is nepheline normative ranging from 2-16% Ne. They show a range in silica (42.2-46.2 wt %) and in total alkalis (4.39-5.69 wt %), and this variation is most easily modelled by fractional crystallisation.

The rocks of the Pico Viejo series (PVS) are generally glass-rich with lower crystal contents than those of the Pico Teide Series (PTS). Most of the evolved rocks contain kaersutite, whilst olivine is more dominant in the Pico Teide series (PTS). Both series range in composition from basanite to phonolite, although there appear to be fewer tephritic phonolites in the PTS. However the larger database compiled by Ablay et al. (1995; 1998) and Ablay (1997; unpublished data) shows similar numbers of rocks representing each compositional group for the complex (Figure 4.3).

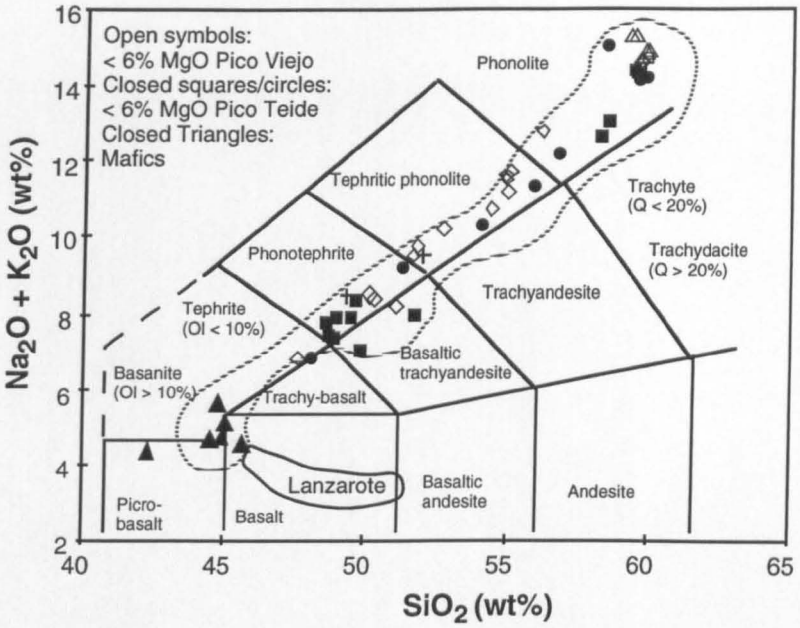

Figure 4.3. Total alkali - SiO_2 diagram (Le Bas et al., 1986), with the nomenclature after Le Maitre et al. (1989). Mafic rocks (closed triangles) include basanites and alkali basalts from caldera floor and 1909 eruption, and the PTS (closed symbols) and the PVS (open symbols) show a range composition from tephrite to phonolite. Both series include rocks termed in text as 'plagioclase-phyric basanites' (Ablay et al., 1997) however they plot in the tephrite to phono-tephrite field. Dotted field (Ablay 1997; Ablay et al., 1995; 1998 and unpublished) gives the extent of the larger Teide-Pico Viejo dataset. The Lanzarote field is from the previous chapter.

The rocks show typical geochemical fractionation trends with decreasing MgO, Fe_2O_3 and CaO with increasing SiO_2 (Figure 4.4). In general the Pico Viejo rocks have slightly lower concentrations of MgO, Fe_2O_3, CaO and P_2O_5 relative to the Teide suite, and there is a greater scatter amongst the Teide rocks, perhaps because of the more porphyritic nature of this suite. The larger dataset (Ablay, 1997; Ablay et al., 1998) shows that the Teide phonolites are poorer in Na_2O and richer in SiO_2 and Al_2O_3 than the Pico Viejo phonolites. Alkalis and Al_2O_3 increase with increasing SiO_2, and there is an inflection in Al_2O_3 at the higher SiO_2 end of the data array, presumably due to the onset of plagioclase fractionation. In the Teide and Pico Viejo suites P_2O_5 decreases with increasing SiO_2, and

the mafic rocks plot on a separate trend with intermediate P_2O_5 values. There is also an inflection in the P_2O_5 trend with MgO as apatite saturation occurs (Figure 4.4).

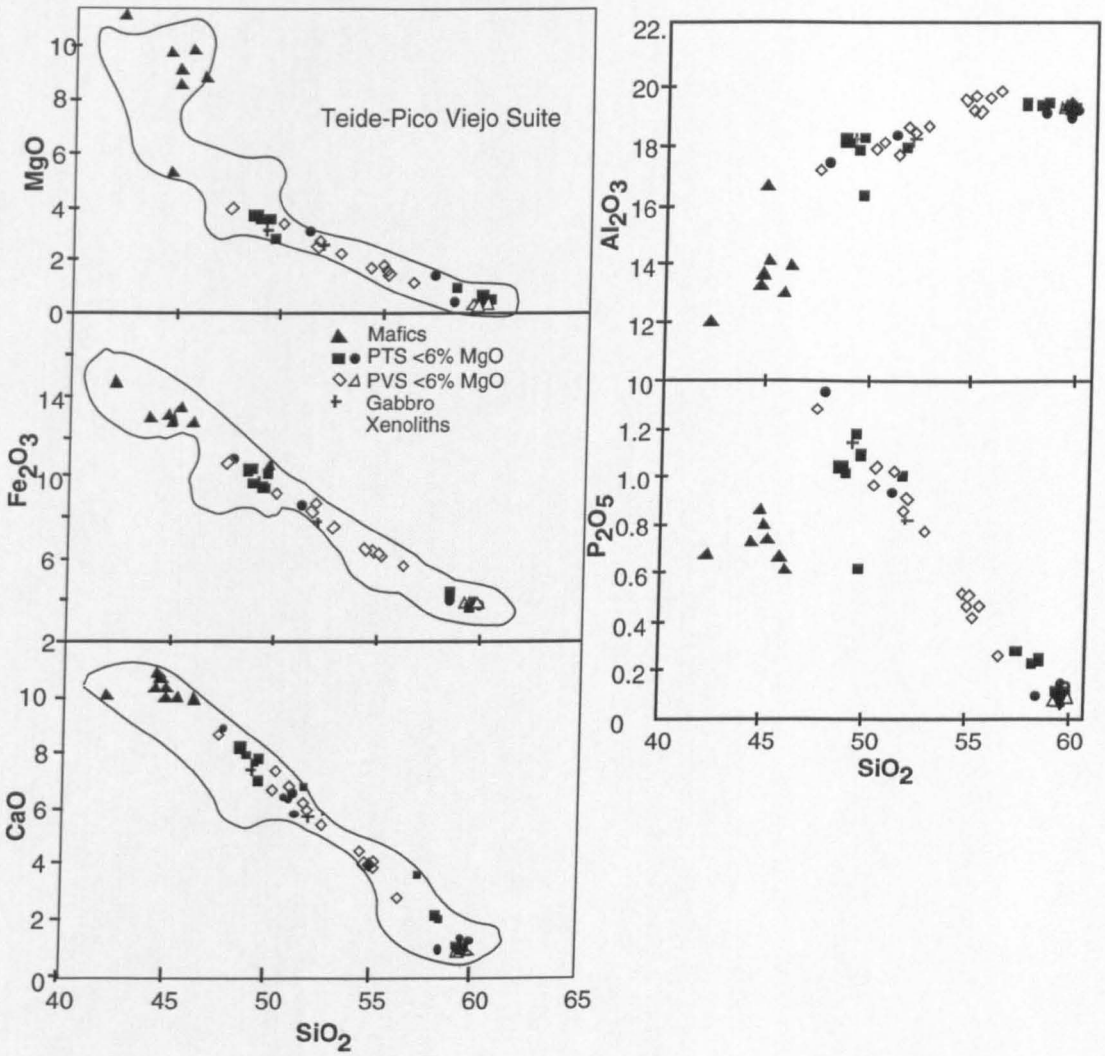

Figure 4.4. Variation of selected major element oxides with SiO_2 (wt %) illustrating the range of composition from basanite to phonolite. The symbols are same throughout this chapter and the background data fields are as for Figure 4.3.

Using MgO as an index of fractionation the two suites have similar fractionation trends shown as total alkalis and Al_2O_3 decrease with increasing MgO, whist Fe_2O_3, TiO_2 and P_2O_5 increase with increasing MgO content (figure 4.5). The TiO_2 and P_2O_5 appear to be lower than expected in the mafic suite of samples, as apatite saturation has been reached in the other suites.

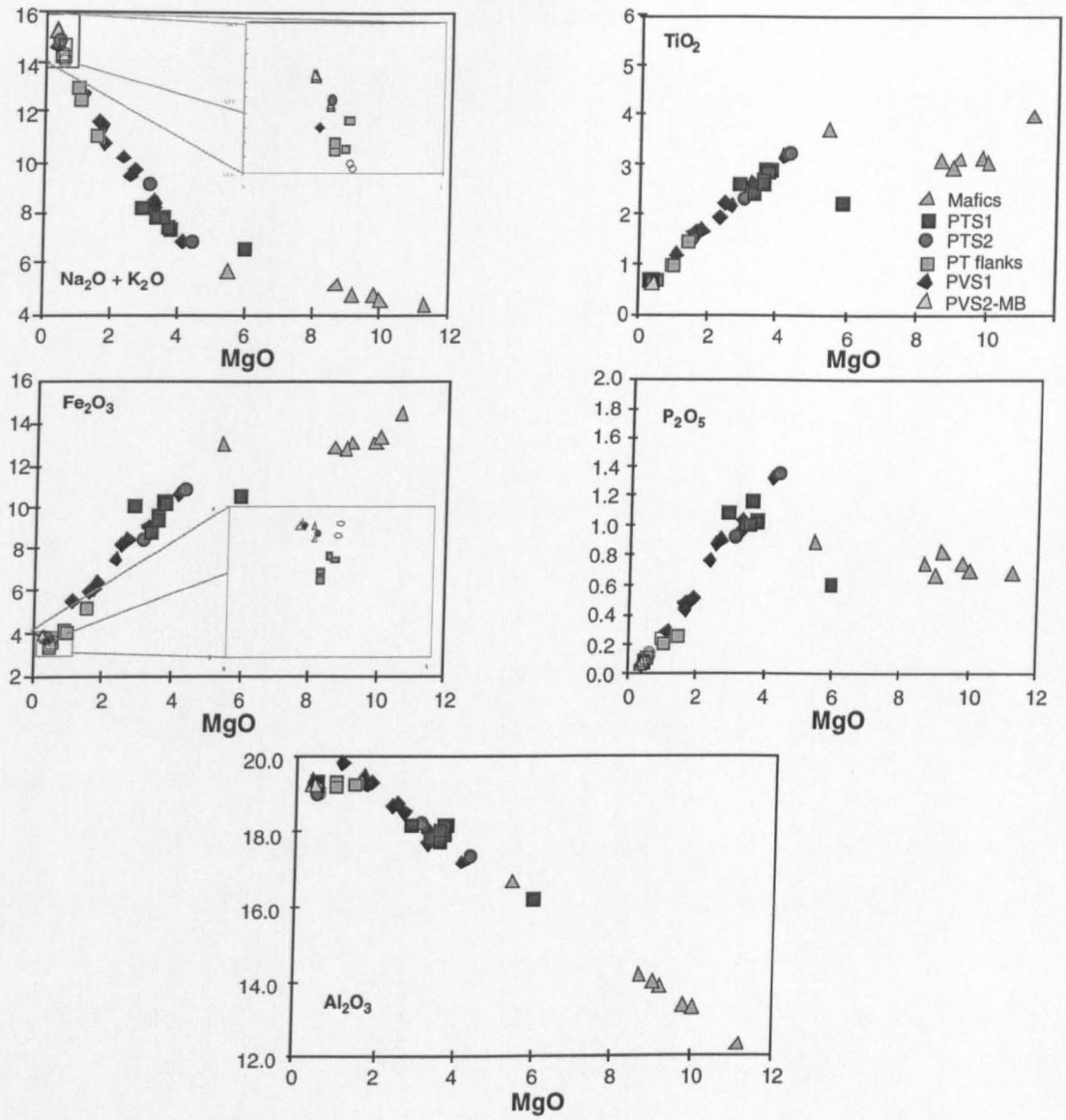

Figure 4.5. Variation of selected major element oxides with MgO (wt %) illustrating the range of composition from basanite to phonolite. The symbols are same throughout this chapter.

Compatible trace elements such as Ni and Cr increase with increasing MgO, as expected from the fractionation of olivine and clinopyroxene, and they have similar concentrations to the primitive Lanzarote rocks (Figures 4.6 and 3.4).

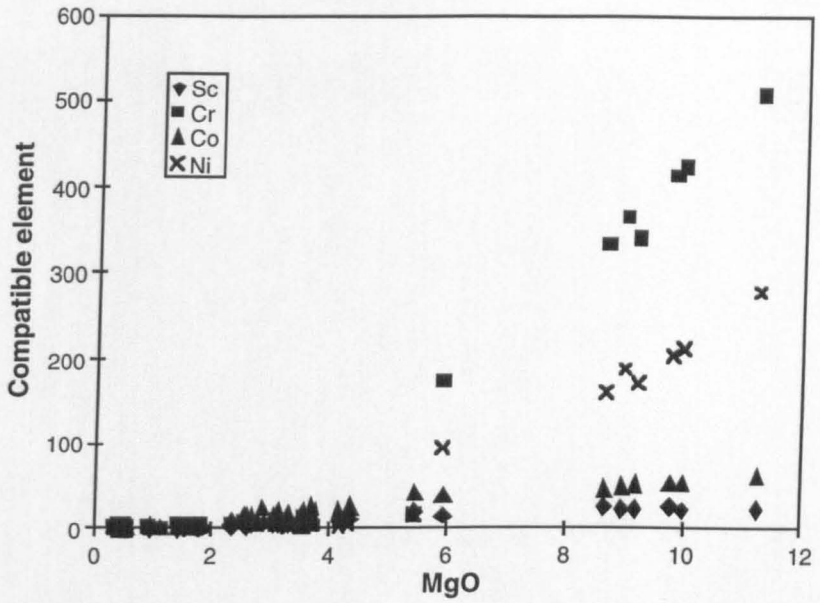

Figure 4.6. A plot of compatible elements against MgO, showing that the concentrations of Cr, Ni, Sc and Co can be up to 500 times higher in the mafic rocks (higher MgO contents) than in the evolved rocks.

Primitive mantle normalised trace element patterns for 7 selected rocks (Figure 4.7.a and b) show that the suite is relatively LREE enriched and HREE depleted when compared to N-MORB (Hart, 1984). The rocks were normalised by dividing by the primitive mantle values and times by 100. Incompatible element contents (Zr, Nb, Rb, Y, U, and Th) are high, with Zr, Nd and Rb enriched throughout relative to N-MORB. The mantle normalised patterns peak at Nb, Pb, Zr and Hf for most samples, whilst there are major negative anomalies in Ba, Sr and Ti for the later Pico Teide series, the late phonolites of Pico Viejo, and the 2 ka Montaña Blanca eruption (Figure 4.7.a). Such anomalies are common in the more evolved rocks in the later part of the suites and reflect onset of crystallisation of feldspars, both sanidines and plagioclases. The mafic rocks to intermediate rocks including the 1909 eruption show similar concentrations and trend.

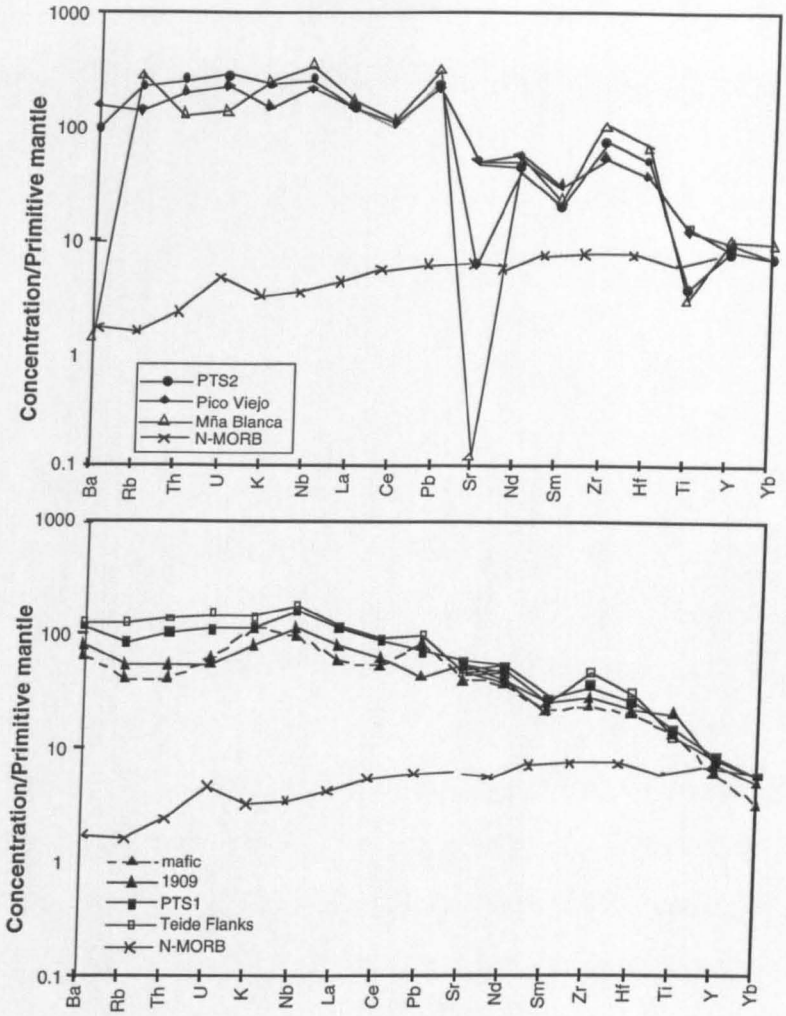

Figure 4.7a and b. Primitive mantle (Sun and McDonough, 1989) normalised diagrams showing selected rocks from each of the series, plus the 1909 eruption. Figure 4.7a shows the evolved data with MgO less than 6%, whilst 4.7b shows the more mafic samples with MgO greater than 6%. Data for N MORB from Rollinson, (1993). The rocks were normalised by taking a characteristic sample for each group and dividing by the concentrations of primitive mantle.

4.5.2. Sr and Nd Isotopes

The Sr and Nd isotopes by E-R Neumann are at present unpublished (Ablay, *pers. comm.*) but they will be incorporated into the paper on the isotope geochemistry of the Teide-Pico Viejo complex. Some of the samples have very low Sr contents (< 2 ppm) and so they are very sensitive to any late stage alteration processes. The majority (22) of the

$^{87}Sr/^{86}Sr$ ratios are restricted to 0.7031 - 0.7034, with a small group (7) between 0.7038 - 0.7042, and an outlier at 0.7078, and the $^{143}Nd/^{144}Nd$ range from 0.51275 to 0.51300. The larger Tenerife field plots within the field for Canaries data; however the smaller group of samples are displaced to higher $^{87}Sr/^{86}Sr$ values, similar to those in the Azores and the Cape Verde islands (Figure 4.8). These samples do not have low Sr contents and hence the values are real. Both fields plot within the Sr-Nd isotope mantle array, with one field displaced towards HIMU OIB and the other closer to BSE (bulk silicate earth) with a slight displacement towards EMII (Zindler and Hart, 1986). This may indicate a mixed source composition for the island, as a mixture of source components, including HIMU and EMII, has been discussed by Hoernle et al. (1991) for the neighbouring island of Gran Canaria. Lanzarote (this work; Neumann et al., 1995) has been modelled as a source with a young HIMU component and some EMII. From the Sr and Nd isotopes reported here (Neumann *pers. comm.*), Tenerife appears to have a HIMU and some EMII component.

The rocks of the higher $^{87}Sr/^{86}Sr$ sample group, which includes samples from Montaña Blanca (PVS2) and some of the more evolved Teide flank vents (PTS1), are phonolitic in composition and they have correspondingly high SiO_2 contents and Rb/Sr ratios (Figure 4.9). These rocks with high Rb/Sr ratios may have undergone some sort of assimilation or mixing with altered material as the $^{87}Sr/^{86}Sr$ is higher than expected and the Rb/Sr ratios are up to 10 times higher than those in from the rest of the samples. These rocks were analysed unleached, it is possible that further analysis ongoing at the current time will give better accuracy of the isotopic ratios at the published values, however a couple of the altered samples were measured at the Open University and gave similar result to those presented here.

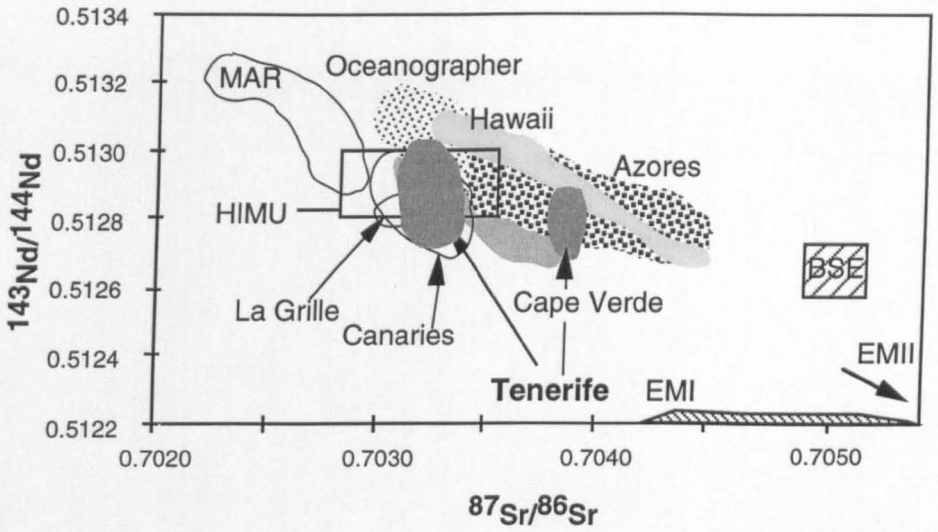

Figure 4.8. $^{87}Sr/^{86}Sr$ vs $^{143}Nd/^{144}Nd$ diagram showing the isotopic composition of the Tenerife lavas together with other Atlantic OIB and MORB, including the Canaries, the Azores, the Cape Verdes and other OIB for comparison (Thirlwall et al., 1997; Hoernle et al., 1991; Sigmarsson et al., 1992; Vance et al., 1989; Turner et al., 1997; Elliott 1991; McDermott and Hawkesworth, 1991) and the Oceanographer field from Shirey et al. (1987), along with unpublished Open University data from the Azores (S Turner, P.King).

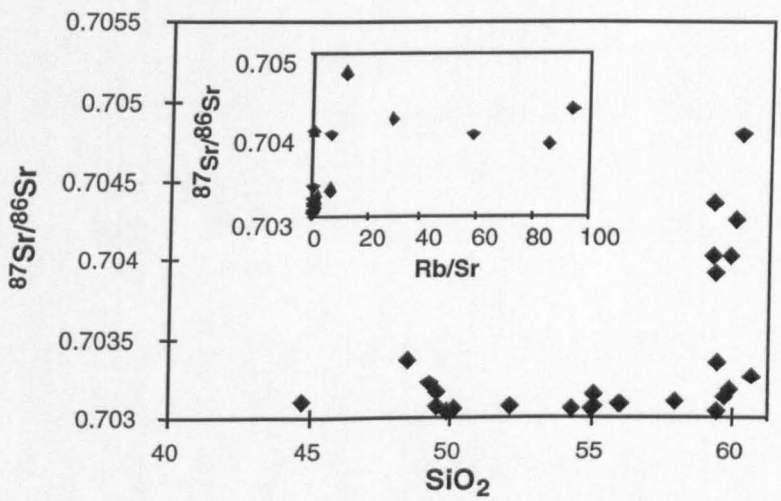

Figure 4.9. SiO_2 vs $^{87}Sr/^{86}Sr$ diagram showing the bimodal isotopic distribution in the more evolved rocks (data: Neumann), whilst the inset shows the higher $^{87}Sr/^{86}Sr$ ratios are associated with a range in Rb/Sr.

4.5.3. U, Th and Ra Isotopes.

The mafic rocks have U and Th contents ranging from 0.82 to 2.80 ppm and 3.42 to 10.97 ppm respectively. The U and Th contents of the evolved rocks range from 2.83 to 8.12 ppm, and 10.98 to 30.19 ppm, respectively, consistent with their higher silica contents. As with most young OIB, all but one of the samples plot to the left of the equiline in the ($^{230}Th/^{232}Th$) - ($^{238}U/^{232}Th$) equiline diagram (Condomines et al., 1988) (Figure 4.10) and there is a large range in ($^{230}Th/^{238}U$) from 1.00 to 1.227. The sample that plots to the right of the equiline is from the summit of Pico Viejo, and it is a cumulate that would appear to have higher U/Th than the host magmas. It is hydrothermally altered and despite having ($^{234}U/^{238}U$) = 1.00, the rock gives a ($^{230}Th/^{238}U$) of 0.8888.

The above isotope ratios, and those plotted in Figure 4.10a, are the present day measured values. However, unlike in the Lanzarote rocks, those from Tenerife have eruption ages ranging from 175 - 0 ka and so it is necessary to back calculate the U-Th isotope ratios to the time of eruption (Figure 4.10b). A fair proportion of the suite have known eruption ages (See Appendix A for ages); however it has been necessary to estimate the age of some of the older rocks. The rocks with uncertain ages were given a best estimate relative to eruptions of known age, and the initial ($^{230}Th/^{232}Th$) isotope ratios for the Teide-Pico Viejo suite of rocks are calculated in appendix H. This is done by rearranging the decay equation to solve for the initial ($^{230}Th/^{232}Th$), then dividing by the ($^{238}U/^{232}Th$). As some of the eruptions ages are uncertain, both the initial and the present day values are referred to in this chapter, because for some processes for related rocks, the present day values can be used.

The initial ($^{230}Th/^{238}U$) values show greater U-Th isotopic disequilibria than the present day values with the initial ($^{230}Th/^{238}U$) values ranging from 1.09 to 1.805. ($^{234}U/^{238}U$) ratios were determined routinely (Appendix A) and, despite the presence of one apparently hydrothermally altered sample with high U/Th, the majority of the rocks had ($^{234}U/^{238}U$) values of 1 ± 0.002. Thus, it appears that there has been no significant post-eruption alteration, and the measured corrected ($^{230}Th/^{232}Th$) and ($^{238}U/^{232}Th$) ratios are those of the erupted lavas.

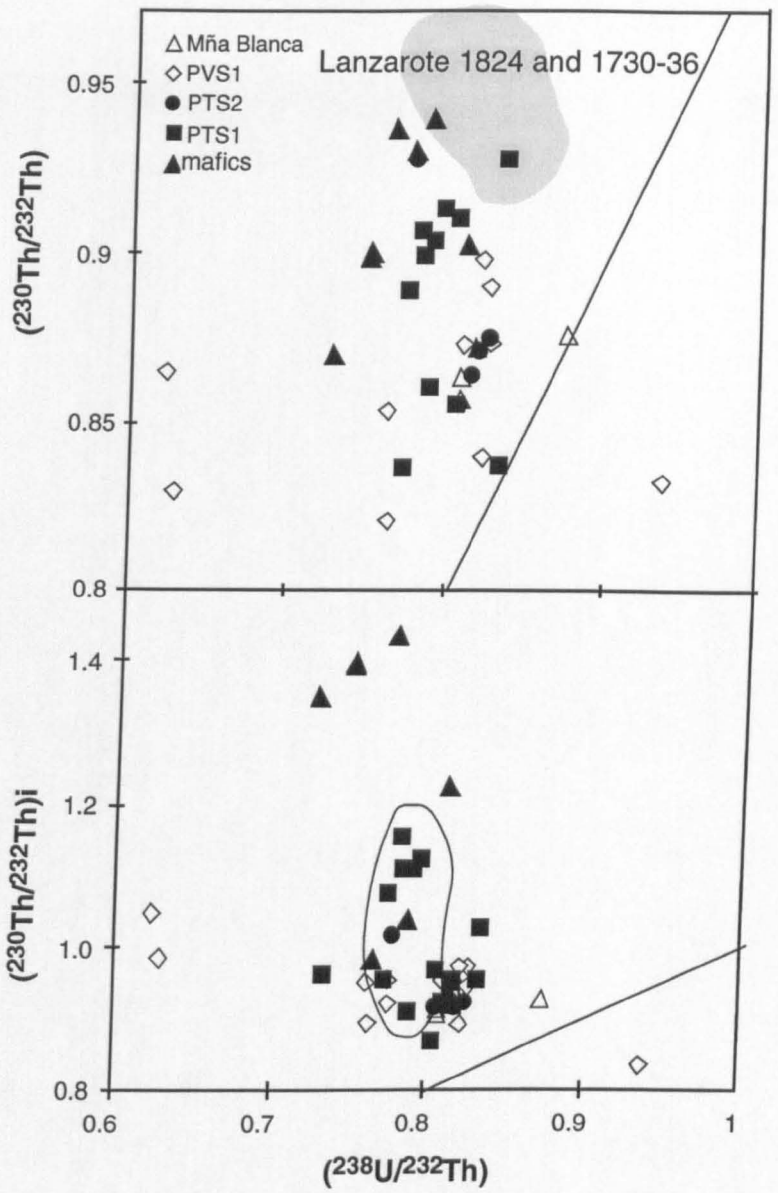

Figure 4.10a and b. The ($^{238}U/^{232}Th$)-($^{230}Th/^{232}Th$) equiline diagram illustrating the measured and calculated initial U-Th isotopic ratios of the Tenerife rocks, with the 1730-36 and 1824 suite of Lanzarote (shaded area) for comparison.

The rocks can be divided in their separate rock compositions and the range of $(^{230}Th/^{238}U)_i$ can be observed within each group. Figure 4.11. shows the frequency of the different composition and the range in $(^{230}Th/^{238}U)_i$ The intermediates or 'tephrites' include both tephrites phonolitic tephrites and tephritic phonolites. This show that there is a range of $(^{230}Th/^{238}U)_i$ within the mafics and the tephrites with and that the average $(^{230}Th/^{238}U)_i$

decreases from 1.35 in the mafics (SiO_2=42-46wt %) to 1.25 in the tephrites (SiO_2= 50-54 wt %) and 1.12 in the phonolites (SiO_2=55.61 wt%).

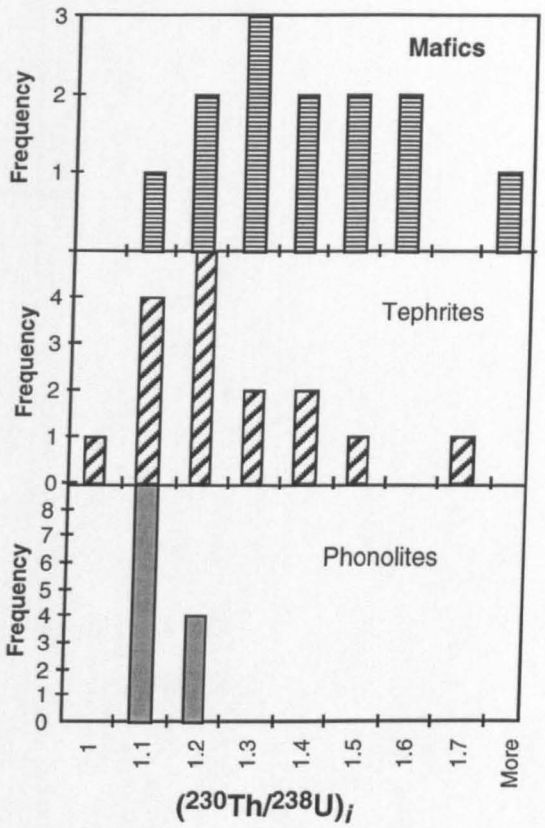

Figure 4.11 illustrates the frequency of the different rock compositions with $(^{230}Th/^{238}U)_i$

A subset of samples has been analysed for ($^{226}Ra/^{230}Th$) (Appendix A). The youngest rocks (i.e. those less than 8,000 years old) show Ra excesses with ($^{226}Ra/^{230}Th$) ranging from equilibrium at 1.01 to 1.54). It is possible to construct an equiline diagram (Condomines et al., 1988) similar to the ($^{238}U/^{232}Th$)-($^{230}Th/^{232}Th$) diagram, for Radium using Ba as the normalising element, assuming that the geochemical behaviour of Ra and Ba is identical (Figure 4.12). The lavas older than about 7500 years confirm the expected $^{226}Ra/^{230}Th$ equilibrium, and lie on the equiline (grouped in field) which is consistent with the time of re-equilibration in the system.

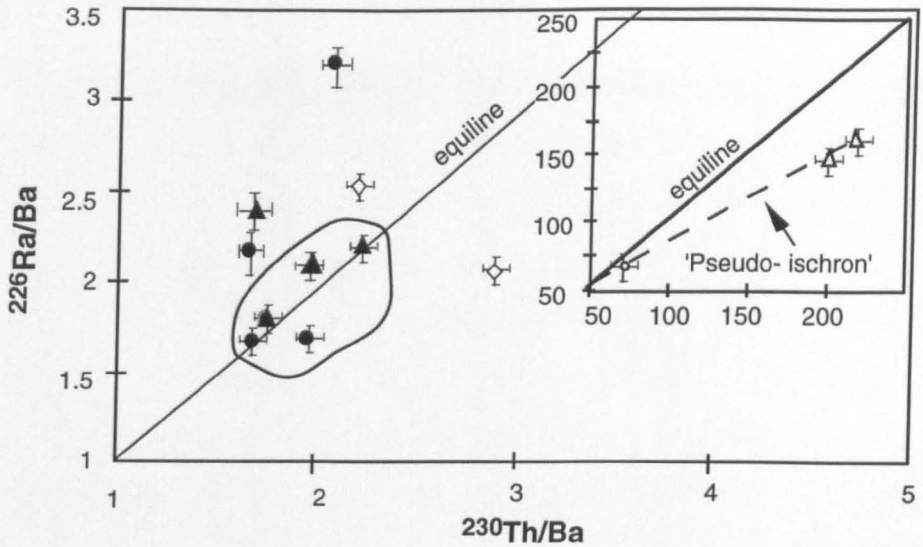

Figure 4.12. (^{226}Ra)/Ba-(^{230}Th)/Ba equiline diagram (Condomines et al., 1988) illustrating a subset of the Teide-Pico Viejo samples. The ^{226}Ra/Ba is almost 100 times greater in the more evolved rocks (open symbols) than in the more mafic and intermediate suites (closed symbols). The 'Pseudo' - isochron is discussed in Section 4.6.7. Units are fmol.μg^{-1}

4.6. Petrogenesis and Interpretations of Majors and Traces

The rocks from the Teide-Pico Viejo Complex offer an excellent opportunity to examine the compositional variations generated by magma chamber processes. Mantle derived magmas have ponded and differentiated, mixed and assimilated perhaps in a number of different chambers at different depths in the Earth's crust. The composition of the erupted magmas will be governed by a number of factors, including the original source composition, the time spent in the individual chambers, the depths of crystallisation (e.g. Kyle et al., 1981;1992 for Mt Erebus) along with contributions from other more mafic or more salic melts. This section deals with 1) the petrogenesis of the mafic rocks, 2) the evolution and processes occurring in the magma chambers and their effect on the compositions of the Teide-Pico Viejo Complex and finally 3) the timescales of differentiation within the complex, as constrained by U-series isotopes.

4.6.1. Mafic Rocks

The erupted compositions of mafic rocks of the Teide-Pico Viejo complex were discussed in the previous chapter; none were in equilibrium with mantle olivine (Roedder and Emslie, 1970) and most have undergone olivine and clinopyroxene fractionation. A simple interpretation of these rocks is that olivine and clinopyroxene fractionated from primary melts which formed the different compositions by different degrees of partial melting of a common mantle source (e.g. Hirose and Kushiro, 1993) similar to that modelled for Lanzarote. There are a number of plagioclase phyric basanites (typically in the historic eruptions of the 1704-6) which have large (2 cm) perfectly formed zoned phenocrysts which appear to be out of place in finely grained mafic rocks. These phenocrysts are not in equilibrium with the melts, and as such these 'phenocrysts' may have been picked up in a chamber beneath the complex. There are mixed magmas and other magmas, which also appear to have incorporated a crystal mush in the Teide-Pico Viejo Complex. It seems likely that in the case of the plagioclase phyric basanites, the speed of the mafic melts was sufficiently rapid for the melts not to have evolved, but they did pick up feldspar crystals that were already crystalline in the chamber, perhaps as side wall cumulates . These were picked up by the melt and as the transport was relatively rapid, they were not reabsorbed before the lavas were erupted.

4.6.2. Previous work on Geochemical Modelling of the Major and Trace elements of the Teide-Pico Viejo Complex

Ridley (1970), Araña et al. (1990), Ablay (1997) and Ablay et al. (1995; 1998) have presented detailed petrology and modelling of the major and trace elements of a larger data set from the Teide-Pico Viejo Complex. This section summarises their findings and section 4.5.3. then briefly covers the additional modelling done as a part of this work and further findings to those published.

Variations diagrams (similar to figures 4.3 and 4.4) show typical geochemical features of oxides compatible in the major ferro-magnesian phase (MgO, Fe_2O_3 CaO) decreasing with increasing SiO_2. Compatible trace elements (figure 4.5.) likewise decrease with MgO due to olivine and clinopyroxene fractionation. The fractionation of Fe-Ti oxides is marked by decreases in TiO_2 at < 8wt% MgO and a strong decrease in P_2O_5 at <6 % MgO

reflects apatite saturation. Plagioclase fractionation is noted by subtle inflections in Al_2O_3 and alkalis at 48 wt% SiO_2 and the inflection in Sr vs Ba. Whilst alkali feldspar fraction is observed by inflections in the trends for Na_2O, K_2O and Al_2O_3 in the phonolites.

The older and younger intermediate compositions from the Pico Teide series show less Ba enrichment than the Pico Viejo series (Figure 4.13). Zr is incompatible in Tenerife lavas which lack zircon (Watson, 1979) (Figure 4.14.). The inflection in Ba as Zr increases rules out mixing between basanites and phonolites (i.e. with > 700 ppm Zr) to model the whole data array. The inflection in La shows the onset of apatite fractionation. The general observations from figure 4.13 show that mixing is not the most important process, there is evidence of changing D values and no evidence for obvious assimilation other than in the highest Zr lavas. Hence fractionation crystallisation is the dominant control.

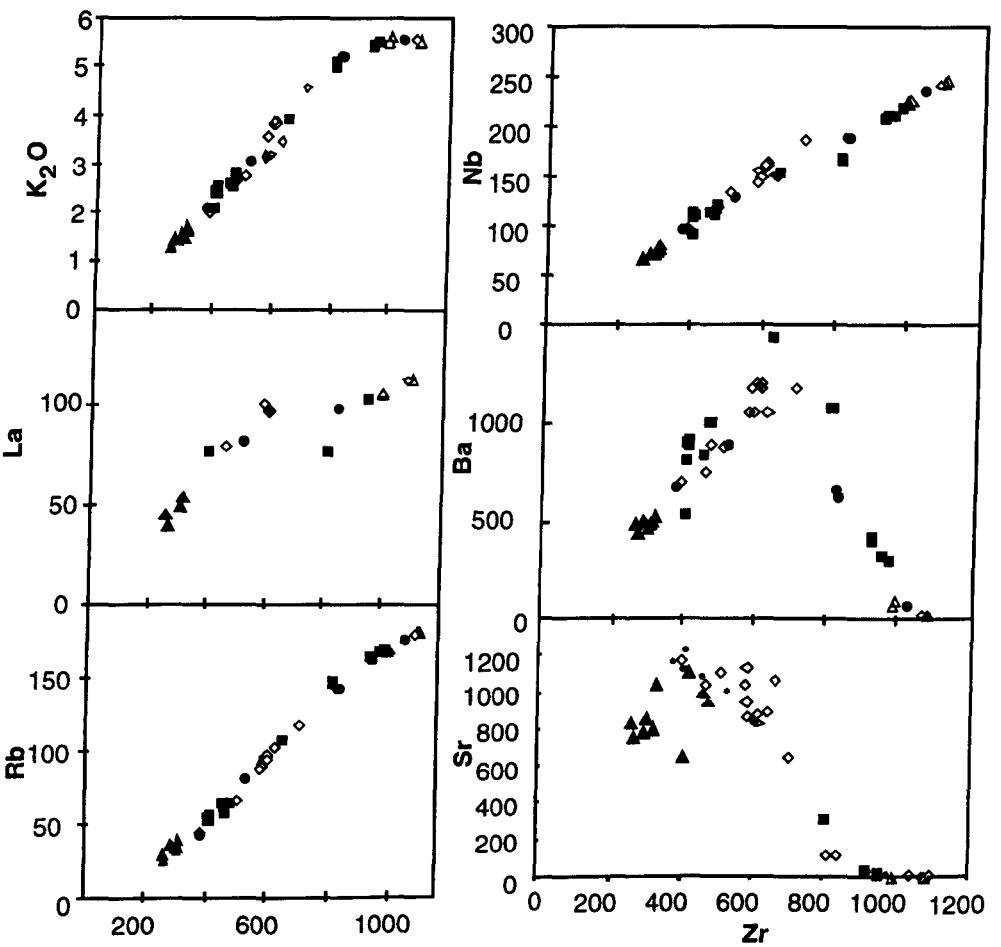

Figure 4.13. Variation of K_2O, La, Rb, Nb, Ba, Sr vs Zr. The Ba decreases at intermediate Zr compositions.

A rapid decline in Ba occurs in lavas with greater than 57 % silica and it seems that this is also the point where an inflection occurs in the Zr - SiO_2 diagram (Figure 4.14). This may be due to the significant increase in the amount of plagioclase and K-feldspar crystallising, and as the inflections are seen in both series, it cannot be solely due to amphibole fractionation.

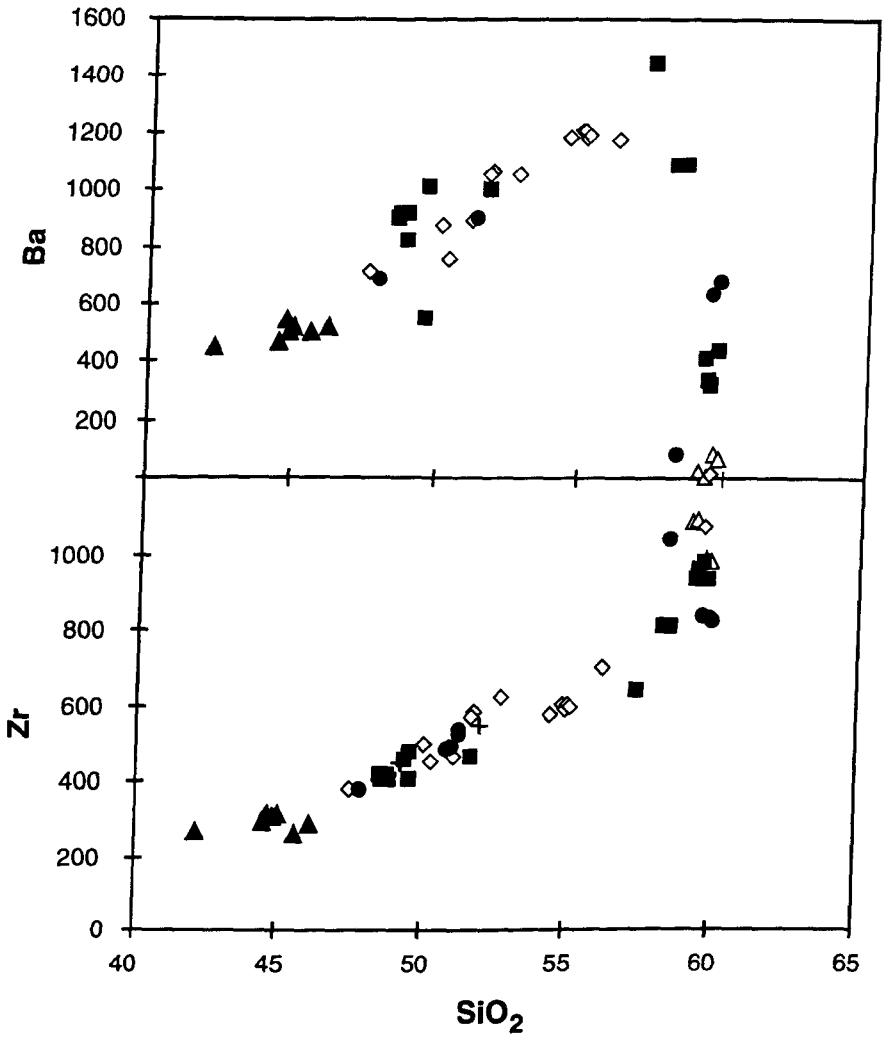

Figure 4.14. Variations in Ba and Zr with SiO_2 illustrating inflections in both trace elements at compositions about 57 % SiO_2. This is seen in both the Teide and the Pico Viejo rocks, and it may be due to increased fractionation of plagioclase, perhaps accompanied by mixing.

All of these observations support fractional crystallisation as the dominant process of differentiation for the Teide-Pico Viejo lavas. However Ablay (1997) and Ablay et al. (1998) suggest that the difference in petrology between the groups of Teide and Pico Viejo may preclude the same fractionation processes from a common basanite parent. Variations in

parental magmas may be amplified by fractionation yielding contrasting suites of rocks (e.g. MacDonald, 1974; Wilson et al., 1995), and further differentiation may be caused by crustal assimilation, magma mixing, the introduction of fluids and the remobilization of solid residues (e.g. MacDonald et al., 1987), for example, crystal mush or side wall rocks.

The fractionation models used by Ridley (1970), Ablay (1997) and Ablay et al. (1995; 1998) include major element least squares mass balance (Bryan et al., 1969) and trace element fractionation models (Arth, 1976). The basanite-phonolite transition was modelled in a series of steps, using analysed mineral compositions to identify possible bulk extracts. These extracts were then used to model Rayleigh fractionation trace element behaviour. The parental magma used by Ablay et al. (1998) is the 1909 evolved basanite. This modelling supports the derivation of both the PVS and PTS by fractional crystallisation of a common evolved basanite parent magma. The geochemical contrasts are accounted for by differences in the composition and proportions of the fractionating mineral assemblages, consistent with systematic modal and mineralogical differences documented between the PVS and PTS. Magma mixing and selective contamination have also been identified.

The models for both the PTS and PVS estimate the most evolved phonolites as 13 % residual liquids of the parental basanite. The main divergence occurs at intermediate compositions, where kaersutite starts to crystallise within the PVS after magnetite, plagioclase and apatite at 50% crystallised. Kaersutite continues to fractionate until the transition from plagioclase to alkali feldspar (~70 % crystallised). In the PTS, kaersutite is absent or in low abundance and plagioclase, clinopyroxene and olivine dominate. Both series have similar calculated proportions of Fe-Ti oxides and apatite. The modelling of Antarctica and Laacher See basanite-phonolite lineages, show a bifurcation of the geochemical data, where amphibole is enters at intermediate compositions.

The presence or absence of amphibole, as discussed in detail in Ablay (1997), depends mainly upon the temperature, oxygen fugacity, melt composition and volatiles present. The activity of H_2O is regarded, in this case, as the main influence on amphibole stability, as there is little evidence for changes in fO_2 for published arguments and the suites have similar major element compositions. In ocean island alkalic systems H_2O and CO_2 are commonly the dominant volatile phases (Gill, 1981) as indicated by the presence of hydrous

minerals. Estimates for the depths of magma chambers from pyroxene barometry, assuming water saturation, place the shallow Pico Viejo chamber approximately at sea level, whilst the intermediate and mafic rocks indicate depths of 18 - 36 km (Ablay, 1997). The Teide phonolites indicate pressures of 1 to 3 kbars which locates their chamber near the foot of the volcanic edifice, a similar depth to the Pico Viejo chamber. The older intermediate lavas are thought to have begun crystallising in the deeper chambers and to have moved into the shallower chamber where they continued to differentiate (Ablay, 1997).

The shallow Teide chamber is thought to have undergone at least three separate replenishment episodes since the flank vent eruptions at around 100 ky; evidence for this includes mingled lavas and crystal-rich tephrites. The mingled lavas show more mafic blobs of melt surrounded by a more salic composition, this infers that the evolved melt has entered a chamber which already contained mafic magmas, the timescale was rapid enough to prevent total mixing of the lava and on eruption the mafic 'blobs' remain within the evolved host. The tephrites magmas may have picked up crystals already formed in the magma chambers. Hence a major problem with modelling magma chamber evolution is that they are not closed systems and they can be replenished, resetting the composition of the melts and the isotopic signatures.

4.6.3. Modelling using MELTS

The MELTS programme (Ghiorso and Sack, 1994) was used to model the major element evolution paths based on phase relations, along with simple mixing modelling similar to that used in chapter 4. The MELTS model has been used here for the major elements for fractionation and assimilation.

MELTS modelling at high (>55 %) SiO_2 contents has been a point of concern, in view of the sparse database that underpins the programme (Ghiorso and Sack, 1994). The presence of amphibole as a crystallising phase also provides problems, as the complex stability of amphibole (Raudsepp et al. 1991) cannot be readily dealt with within the programme. However major element differentiation paths calculated by the MELTS programme from an evolved basanite or primary OIB (Sun and McDonough, 1989) parent reproduce the observed data arrays, until 55 % SiO_2. At this point the modelling appears to break down and the calculated paths diverge from the data array. Magma mixing between

different compositions has been observed in rocks from the Las Cañadas caldera wall (Araña et al., 1994; Martí et al., 1995) and in the Bandas del Sir, the pyroclastics in the south of the island (Wolff et al., 1985; Bryan, 1998). The major and trace elements of the Teide-Pico Viejo complex, fractional crystallisation appears to be the dominant process, however new evidence from Sr and U-series isotopes suggests that mixing and assimilation may have more important roles than suspected by Ablay (1997), especially in the more evolved rocks.

Figure 4.15. provides an example of the MELTS trends and a mixing trend between one of the evolved basanites and an evolved phonolite, and Table 4.3. gives the input data used in the modelling. To obtain the highest SiO_2 compositions it is necessary to mix the 57% SiO_2 rocks with a more evolved product.

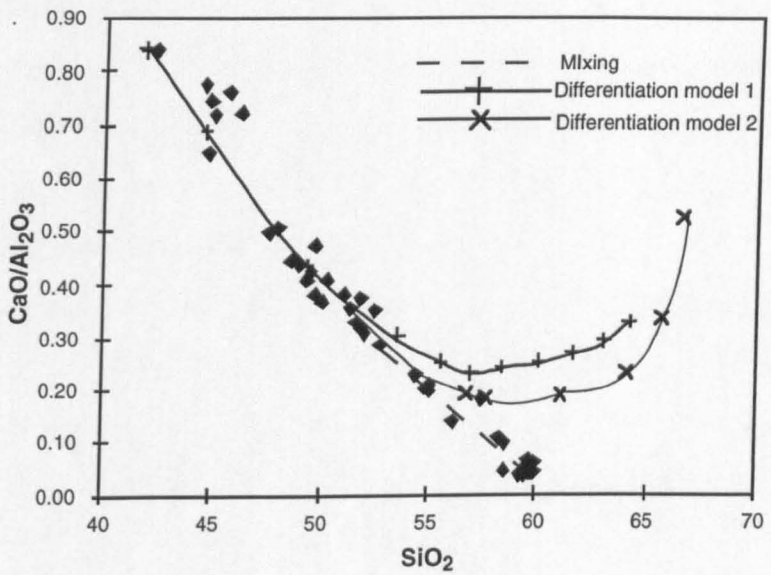

Figure 4.15. SiO_2 vs CaO/Al_2O_3 ratio illustrating that the Teide-Pico Viejo data can be modelled partially by fractionation, with different differentiation models (+ model 1, X model 2) reflecting the presence or absence of amphibole (a crystallising phase in the Pico Viejo lavas). The modelling of the most evolved rocks is by mixing, (DePaolo, 1981) as the MELTS trends do not model this end of the data array.

Model 1 with amphibole crystallising deviates from the data at 52% SiO_2, while the Model 2 without amphibole crystallising improves the fit of the trend, but shows an inflection away from the data at ~ 55% SiO_2 with the onset of K-feldspar crystallisation. A mixing model with the intermediate tephrite T7-18-8 and Montaña Blanca phonolite as end members can explain the data.

MELTS Fractionation	*Model 1*	*Model 2*
Temperature (•C)	1250 -716	1185 - 685
Pressure (kbars)	1 - 0.89	5 - 1
H_2O Content	0.06	0
Oxygen fugacity	QFM	QFM
Phases present	olivine	olivine
	cpx, opx	K-fdsp, plag
	amp,	cpx, opx
	Plag, K-fdsp	mgt
	mgt	±chromite spinel
	±nepheline, apatite	

Table 4.3. Model Parameters used in MELTS Fractionation models (Ghiorso and Sack, 1994).

As MELTS cannot model trace elements, mixing (DePaolo 1981) was used to model the trace elements in an attempt to show that fractionation is not the sole differentiation process. However, as shown in figure 4.13, mixing cannot be the only process. Fractional crystallisation dominates, although it is necessary to use mixing to model the data with SiO_2 contents >55%; the most evolved end member may be pre-existing chamber wall, which is known to have high SiO2 contents (Martí et al., 1994).

The interpretation from modelling in this thesis is that fractionation/differentiation models (e.g. least squares and MELTS) do work up to 55% SiO_2, and problems with 'MELTS' at high SiO_2 values and crystallising amphibole, make models unreliable at higher SiO_2. However it is possible to use mixing to model the complete major element data array and AFC to complete the trace elements and isotope array. It is just as possible for a magma chamber to be differentiating whilst another injection of fresh magma is brought in, which considerably changes the composition and allows the melts to mix back and along a straight-line fractionation trend. There is evidence for some cumulate assimilation in these rocks, such as crystalline mush and 'phenocrysts' in disequilibrium with their melts, suggesting perhaps that the most evolved phonolites evolved from mixing of evolved wallrock compositions with newly generated mafic melts.

4.7. Interpretation of U-Series Data

A number of workers (e.g. Volpe and Hammond, 1991; Bourdon et al., 1994; Hemond et al., 1994; Sigmarsson 1996; Heath et al., 1998) have used U-series isotopes in attempts to model magma chamber processes, and to evaluate the timescales of differentiation, whether it be due to closed or open system processes. Samples from the PTS and the PVS were analysed for U-Th-Ra isotopes to estimate the timescales of differentiation within the magma chambers. There is an established periodicity in the volcanic activity on the island of Tenerife, in that each eruptive cycle (e.g. Diego Hernadez section of caldera wall) (Marti et al., 1994) has lasted between 150 to 200 thousand years. Since the Teide-Pico Viejo complex has been established within this time frame, there is therefore a possibility of relatively long-lived magma residence times.

As discussed in earlier sections, the Teide-Pico Viejo complex ranges in composition from basanite to phonolite and there is a range in the $(^{230}Th/^{238}U)_i$ disequilibrium, although we note that highest values are for the basanites with relatively poor age constraints. It appears that the basanites have the greater disequilibrium and that as SiO_2 increases the amount of disequilibrium drops. This is opposite to what might be expected from the volcanic stratigraphy, the sequence of differentiation for each group goes from basanite to phonolite, with the youngest being the phonolites having the least disequilibrium. Figure 4.16 is a duplicate for figure 4.11 and shows the range of isotope disequilibrium for the different rock compositions. The mafics show a range in $(^{230}Th/^{238}U)_i$ whilst the more evolved rocks increasingly tend towards less disequilibrium, with the 60 % of the tephrites and 90% of the phonolite having $(^{230}Th/^{238}U)_i$ of 1.2 or less.

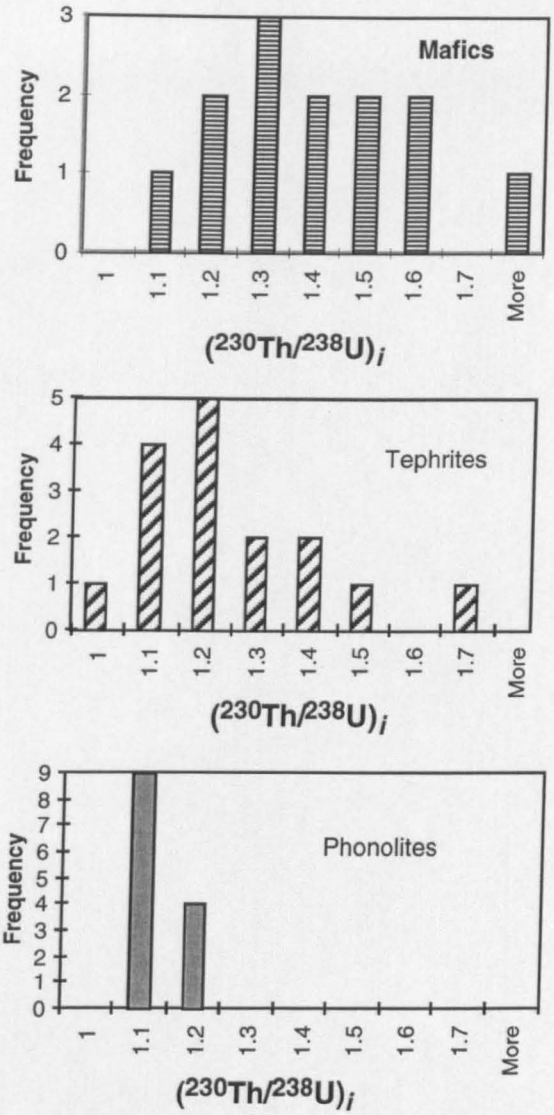

Figure 4.16. illustrates the frequency of $(^{230}Th/^{238}U)_i$ in the different rock compositions

The most mafic rocks, which are the older caldera floor eruptives, have higher $(^{230}Th/^{238}U)_i$ than the younger phonolitic compositions. There appears to have been a relatively continuous supply of basanites with high $(^{230}Th/^{238}U)$ from a deep magma generation zone. Some of these magmas erupted onto the caldera floor and through flank vents, whilst some were stored in the different magma chambers and fractionated, sometimes to phonolite compositions. This takes time and $(^{230}Th/^{238}U)$ decreases over time; also some of the more evolved compositions (e.g. tephritic phonolites and phonolites) may assimilate bits of wall rock or crustal material and evolve further to high $(^{87}Sr/^{86}Sr)$. This may also be the reason for the lower $(^{230}Th/^{238}U)$ in the high SiO_2 rocks. The timescale of decay is exponential which must be taken into account in the modelling.

Figure 4.17 illustrates different rates of differentiation. The light solid line indicates fractionation or mixing with a steep drop due to decay, as the evolved compositions are reached, whilst the dotted line illustrates a model in which the basanite magmas were relatively old prior to the onset of major fractionation. However fractionation appears to speed up, once ($^{230}Th/^{238}U$) has reached a minimum for the basanites. The dotted line follows more of the data, indicating exponential decay and the suite differentiating faster as the compositions evolve (the rate of change of SiO_2 with degrees of melting is variable, however the same diagram can be drawn with Zr, which is not variable of different values of

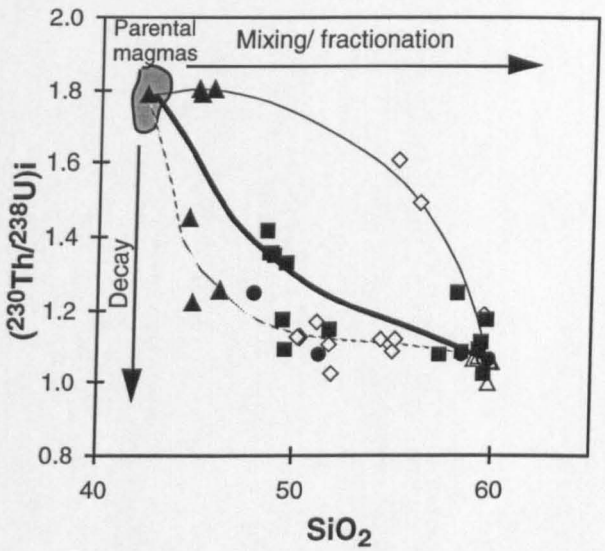

F). The thick solid line indicates mixing between the most mafic and the most evolved compositions. The most evolved compositions still require AFC mixing to end to the very end of the data (highest SiO_2). The PVS1 (diamonds) have relatively constant SiO_2 contents, but a range in $(^{230}Th/^{238}U)_i$, whilst the PTS (squares and circles) show a range in both (Figure 4.17.). This may indicated that the PTS fractionates faster than the PVS.

Figure 4.17. ($^{230}Th/^{238}U$) initial values against SiO_2 illustrating the decrease in disequilibrium from the mafics to the most evolved compositions. The dotted line represents decay then slower fractionation and the solid line indicated decay and more rapid fractionation, and the thick solid line indicates mixing between the most extreme compositions.

It is also interesting to note that the U/Th ratios in the rocks are relatively constant with increasing Th. In Lanzarote, this was used as a way of constraining the source ratio to be similar to that of the melts, whereas in Tenerife, the magma chamber processes would

also appear not to have changed this ratio significantly. The Sr and Nd isotopes argue strongly that the source was similar for both series within the Teide-Pico Viejo suite, and the near constant U/Th ratio supports this idea.

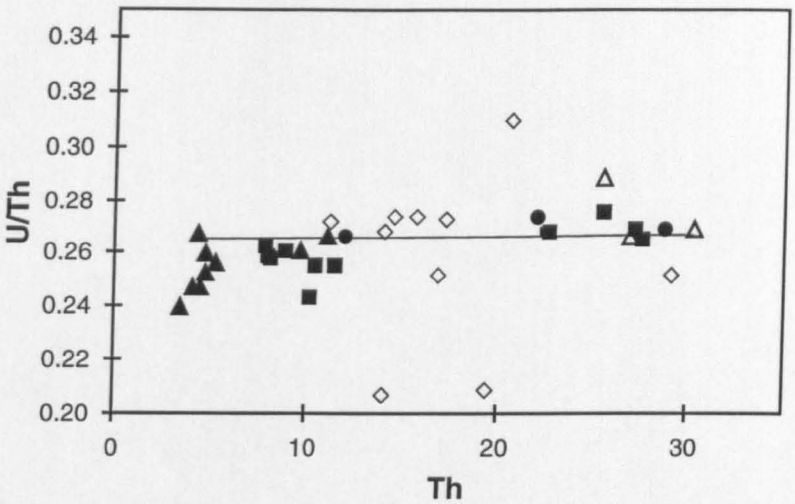

Figure 4.18. U/Th vs Th illustrating that the U/Th ratios change only slightly with increasing Th. Line is mixing trend.

Figure 4.19. shows a trend in the group of older Teide lavas (squares < 55% SiO_2) which has constant ($^{238}U/^{232}Th$) and a range of ($^{230}Th/^{232}Th$). Thus, it is possible to calculate a timescale of differentiation for this group which range in composition from tephrite to phonolite. As the ($^{238}U/^{232}Th$) value is constant in the simplest model, the observed range in $(^{230}Th/^{232}Th)_m$ is all attributed to radioactive decay. This assumes that the highest ($^{230}Th/^{232}Th$) which is observed in the least evolved rock type, is representative of the initial Th isotope ratio of the parental magma. The calculated time period for the highest observed ($^{230}Th/^{232}Th$) value to decay to the lowest is 87044 ± 100 years, and this is a strong indication of how long it may have taken to differentiate from tephrite to phonolite within this group (See Appendix H for calculations). Also this is an indicator that there is no significant contamination in the samples.

It is possible to make a similar calculation for differentiation over the whole of the Teide-Pico Viejo complex, using the highest $(^{230}Th/^{232}Th)_m$, which gives a minimum of 150 thousand years for differentiation from a basanite to a phonolite composition.

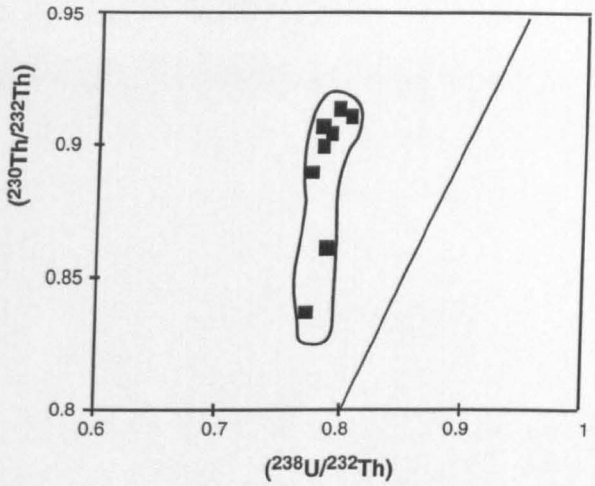

Figure 4.19. PTS1 (filled squares) rocks in field for ease of observation.

The oldest PTS lavas (the filled squares) show a range in $(^{230}Th/^{232}Th)_i$, but the range in Th (ppm) is smaller and a steep negative trend is illustrated on Figure 4.20. This indicates the fractionation rate for these lavas is relatively rapid, which backs up the idea than the PTS1 have fractionated faster than PVS1.

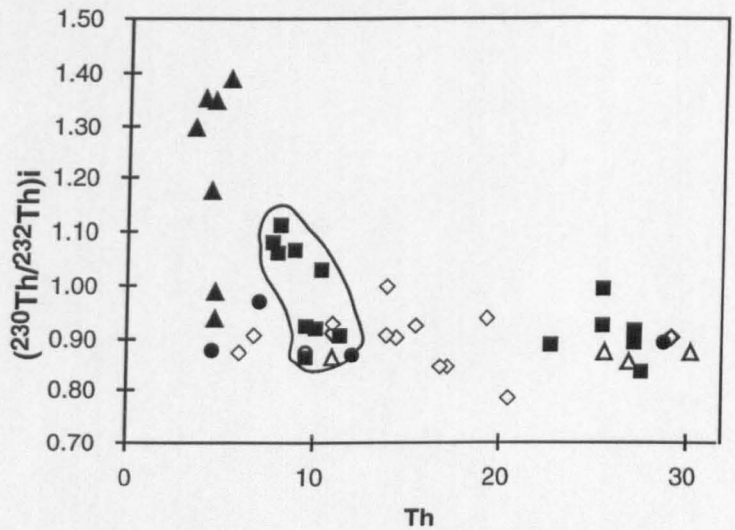

Figure 4.20. $(^{230}Th/^{232}Th)i$ vs Th illustrates the steep decrease in the trend for the older Teide lavas as the rate of fractionation is rapid.

In an attempt to interpret the $(^{230}Th/^{238}U)_i$ vs SiO_2 array (Figure 4.17), a number of scenarios were considered. These include mixing a basanite composition with remelted older salic wallrock, rapid fractionation with radioactive decay, much slower fractionation, and finally fractionation and mixing. The preferred interpretation of the data was that rate of

differentiation increased with time in the evolution from basanite to phonolite, and that mixing with a more evolved melt or solid residue was required to generate the most extreme compositions. This agrees with the presence of commingled lavas (Blake, 1981 and Blake and Ivey, 1986) which involve the presence of near solidified, evolved melt prior to an influx of new melt into a chamber.

The changes in $(^{230}Th/^{238}U)_i$ with stratigraphic position (Figure 4.21.) shows an increase $(^{230}Th/^{238}U)$ in the mafic lavas, whilst the most evolved compositions have the lower disequilibrium. This implies that the differentiation rate increases throughout a cycle, and abruptly drops at the end of one cycle/beginning of next as the melts are more basanitic in composition. The $(^{230}Th/^{238}U)i$ increases in the more mafic early melts, then gradually decreases as the melts differentiate and evolve. It appears that the complex is entering a mafic phase of activity with higher disequilibrium present, similar to that of the oldest caldera floor rocks. It would be interesting to measure $(^{230}Th/^{238}U)$ on the next eruption of the complex, which is due within the next 10 - 20 years, according the volcano's own record. As I would be expected to be mafic in composition with higher disequilibrium than in the 1909 eruption (Figure 4.21).

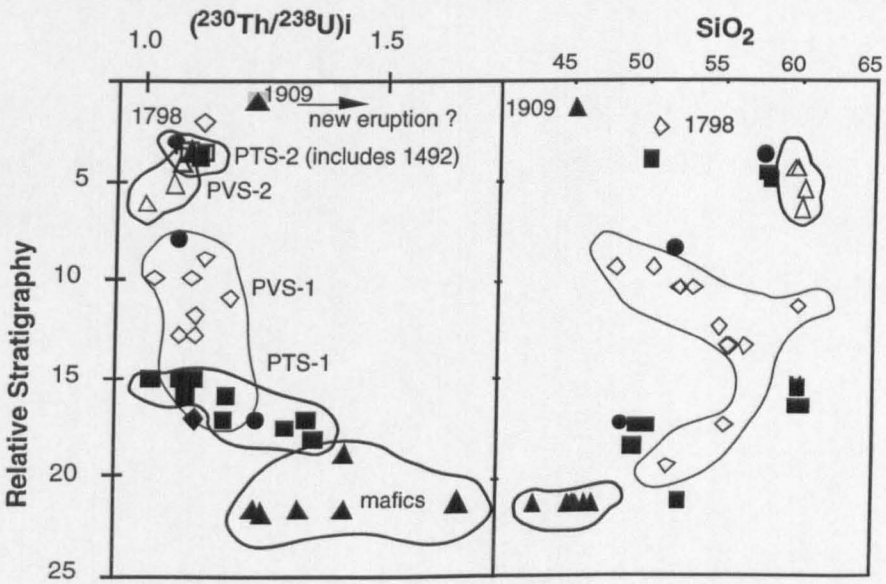

Figure 4.21. Relative stratigraphy vs $(^{230}Th/^{238}U)i$ A trend of decreasing and then gradually increasing disequilibrium.

This would confirm the onset of the next cycle and the conclusion of the previous one, with the caldera collapse at 2ka. It might give an initial measured value of disequilibrium, which may be useful as a check for the high initial ratios for the older mafics. The volume of the different compositions erupted is dominated by the most mafic (62 %) whilst the phonolites make up 11% and the intermediate composition 27 %.

4.7.1. Ra-Th Fractionation prior to Eruption

The highest $^{226}Ra/Ba$ and $^{230}Th/Ba$ are found in the Montaña Blanca phonolites, which have had age determinations done on charcoal at the base of the fallout layer. These ages range from 2105 to 2250 ± 50 years (Ablay, 1997). Despite the whole rock nature of analysis, rather than the more usual mineral isochrons, it is possible to obtain a 'pseudo'-isochron, as a number of these samples plot on a trend to the right of the equiline (Figure 4.12). the lavas must be co-genetic, in the case shown in figure 4.12 the samples are from the Montaña Blanca eruptions, and tied down with a late phonolite from the Teide complex, thought to have come from the same chamber. Calculating an age for this line gives a time of Ra - Th fractionation of 2.3 ka ± 80 years, which is between 50 and 200 years (± 0 - 150) years prior to eruption. Similar fractionation ages from Ra-Th isochron have been discovered in the Longonot volcano in Kenya (Evans, *pers. comm.*). This implies that the pressure build-up as the magma crystallises may be a trigger for an eruption in the not too distant future (Blake, 1984; Tait et al., 1989). The pressure build up caused by fractionation of different phases into minerals, as the mass of magma is crystallising, (in this case, feldspar crystallisation) reaches as optimum level, above which an eruption may be triggered. The crystallising mush causes an increase in pressure, compared with the more molten magma.

4.8. Conclusions

A detailed study of the U-series isotopes from the Teide-Pico Viejo complex aids the understanding of the major and trace elements. The mafic rocks are not primitive compositions, unlike those of Lanzarote and hence as such cannot be treated as primary melts.

The published interpretation of the Teide-Pico Viejo complex (Ablay 1997; Ablay et al. 1995; 1998) relies heavily on fractionation least squares modelling. MELTS modelled differentiation can model the array up to 57 % SiO_2, but the programme runs into problems at high SiO_2 compositions with amphibole crystallising (Ghiorso and Sack, 1994). It may be unreliable for these compositions; however it still predicts the onset of crystallisation of K-feldspar and the early presence of amphibole in the PVS. Multi-step fractionation models have been used by Ablay (1997) to model all the data, fractionating from a basanite parent composition.

A group of some of the most evolved rocks have much higher Sr isotopic ratios than the main group, and these also have greater than 57 % SiO_2, which is further evidence for assimilation of older rock with elevated $^{87}Sr/^{86}Sr$.

U-series isotopes gave information regarding the timescales of differentiation within the Teide and Pico Viejo magma chambers, and the ($^{230}Th/^{238}U$) data led to a greater understanding of the amount of fractionation possible, as the oldest and youngest most mafic rocks have the highest disequilibrium with the most evolved phonolites having the least. The differentiation time for one suite within the Pico Teide suite gave 87 thousand years and differentiation from basanite to phonolite is calculated to be in the region of 150, 000 years, which links nicely with the evolution of the island and the volcanic periodicity. A Ra-Th pseudo whole-rock isochron gave an age of fractionation for the Montaña Blanca eruption of 2.3 ky, which is a maximum of 350 years prior to the eruption, indicating a possible link between the fractionation of Ra-Th into feldspar and eruption.

The source of the Tenerife lavas is indicated by the Sr and Nd isotopes and by a constant U/Th ratio to be similar for the whole of the complex, despite the number of processes which have been involved prior to the eventual eruption of the lavas. The source is thought to be similar to that of Gran Canaria and Lanzarote with contributions from both HIMU and EMII components.

Civilisation exists by geological consent,
subject to change without notice
Philosopher Will Durant

Sunset over the Roques de Garçia

Sunset over the Volcan del Corona

Plate 5

CHAPTER FIVE

CONCLUSIONS

A Summary of Timescales of Melt Generation and Differentiation in lavas from Lanzarote and Tenerife.

The Canary Islands were proposed as a mantle plume by Wilson (1963) and the Ocean Island Basalts that form these islands provide a window into the compositional variations of the underlying mantle, which, in turn, constrain models for mantle convection and evolution. OIB geochemical signatures that arrive at the surface have survived many processes, including partial melting, melt segregation, melt transport and subsequent differentiation. The OIB source has been modelled as a mixture of a number of components (Zindler and Hart, 1986), with different components dominant in different islands. U-series disequilibrium can be used to estimate rates and timescales of melt generation and differentiation (e.g. McKenzie, 1985; Chabaux and Allègre, 1994; Bourdon et al., 1994; Hemond et al., 1994). In this thesis constraints from major and trace elements have been used in conjunction with U-series data to model timescales of melt generation in the primitive lavas from Lanzarote and melt differentiation in the range of compositions from Tenerife.

- The major and trace elements in primitive lavas from Lanzarote can be modelled by mixing two melts.
- These end-member melts, in the simplest interpretation, were a deep smaller degree (1%) melt and a shallower larger degree (4%) melt. The major and trace elements

indicated that the smaller degree melt has negative K anomalies which may be indicate that melt generation continued at a shallow level, perhaps to within the lithospheric mantle with melting in the presence of residual phlogopite, whilst the need for melting within the upwelling asthenospheric mantle was apparent from the ^{230}Th excesses. Depth of melting ranges between 58 and 73 km.

- The Lanzarote source is a mixture of HIMU and EMII asthenospheric mantle, with a contribution from a shallow, perhaps lithospheric, source. This requires thermal erosion of the asthenospheric mantle for melting at the depths modelled from the major and trace elements.
- The two end-member melts were modelled for ($^{230}Th/^{238}U$) disequilibrium by modal dynamic melting (van Calsteren and Hawkesworth, 1998) which allows the calculation of the following physical parameters: a melt rate of 0.125 x 10^{-3} $kg.m^{-1}.yr^{-1}$, the timescale of melt generation (matrix transfer time) of 270 kyrs for the 1% melt and 1,100 kyrs for the 4 % melt, together with an upwelling rate of 1 $cm.yr^{-1}$ and that the melting process has remained consistent over tens of kilometres at depth.
- The Tenerife lavas range in composition from basanite to phonolite, and can be modelled mostly by fractionation from a basanite source with temperatures ranging between 1250 and 685°C. Crystallising phases differ in the Pico Viejo series, where amphibole is dominant in the more evolved lavas, and Pico Teide series, where olivine is the major control.
- The more evolved lavas with high $^{87}Sr/^{86}Sr$ require AFC. Mixing is used to model the evolved lavas for the major elements and AFC is used for the trace elements and isotopes.
- The Tenerife source also appears to be a mixture of HIMU and EMII athenospheric mantle, similar to that modelled from the neighbouring island of Gran Canaria by Hoernle et al. (1991).

- U-Series disequilibrium gave information regarding the timescales of differentiation within the Teide and Pico Viejo magma chamber, not least because the youngest mafic rocks have the highest ($^{230}Th/^{238}U$) and the most evolved phonolites have the lowest. The timescale of differentiation from basanite to phonolite is in the region of 150,000 years, which links to the periodicity of the eruption cycles on the island. A Ra-Th 'pseudo' whole rock isochron gave an age of fractionation for the Montaña Blanca eruption of 2.3 ky, which is a maximum of 300 years prior to eruption, indicating the fractionation of plagioclase as a possible trigger of an eruption.
- Tenerife lavas have undergone differentiation in the underlying magma chambers, hence the range in composition, compared to the restricted basanite to basalt in Lanzarote. The Lanzarote melts appear not to have been stored within magma chambers and in fact there is no seismic evidence for chambers beneath Lanzarote, despite the fact that both Lanzarote and Tenerife are thought to be from a single plume. The island of Gran Canaria, next to Tenerife, has evolved differentiates, but the island of La Palma (Elliott, 1987) at the opposite end of the island chain to Lanzarote has primitive compositions. This may indicate that the centre of plume is more or less aligned underneath the central islands of Tenerife and Gran Canaria, with the islands on the periphery not developing magma chambers and the melts undergoing rapid extraction from the mantle source. It is possible that the plume beneath the Canary Islands stretches the length of the whole chain. Small plumes are tapped off the main plume and melts are either allowed to pond within the lithosphere, forming magma chambers or are directly extracted to the surface (in the case of Lanzarote). The presence of large-scale long-lived magma chamber beneath Lanzarote is a possibility. However the volume of lava erupted, although relatively large, (> $1km^3$ for 1730-36 eruption) does not appear to be large enough, to keep up through-put of magma in the chamber to maintain the primitive composition erupted on Lanzarote.

- Melt generation model parameters can be used to estimate buoyancy flux. The buoyancy flux of the Canaries is low compared with that of Hawaii and it has been observed (Chabaux and Allègre, 1994) that basalts from regions of low buoyancy flux exhibit larger U-Th disequilibria and that the melt generation rates are lower in the Canaries than Hawaii.
- It has been suggested that dynamic melting coupled with ^{230}Th ingrowth is required to explain the observed ^{230}Th excesses in MORB (e.g. Williams and Gill, 1989). However, U-Th isotope disequilibria in OIB have been explained by dynamic melting and by simple U -Th fractionation during melting (Sims et al., 1995).

  In Lanzarote there appears to be no correlated change in the degree of U-series disequilibrium with the degree of melting which argues against a simple fractionation model.
- Source composition can be modelled from the major, and trace elements and the isotopic ratios. It is thought that the composition can affect the depth of intersection of the geotherm with the solidus and presumably, therefore, both the rate and degree of melting. Hence the small degree of melting and low melt rate of the Canaries may be linked to the HIMU asthenospheric source, with the shallow component.
- Depth and degrees of melting have been estimated from the major and trace elements for the island of Lanzarote. The Tenerife lavas are so evolved that it is impossible to estimate the degree of melting for the evolved rocks; however pyroxene barometry has given depth of crystallisation for the suite and indicated the depths of the individual magma chambers
- The thickness of the lithospheric lid beneath the Canaries is relatively constant and as such it is unlikely to have been a controlling factor influencing the degrees of disequilibrium. Although overall average Atlantic OIB show strong links with the age and thickness of lithosphere and hence with mean pressure of melting.

Epilogue

Further work on this thesis would include U-Th mineral separate analysis on the Teide-Pico Viejo lavas, especially the oldest mafic rocks, in an attempt to obtain more accurate ages of crystallisation of phenocryst and eruption of lavas. Ra-Th mineral separate analysis on some of the evolved compositions to model the age of fractionation of the different crystallising phases. Further information regarding the conditions within the magma chamber, such as the fugacity and the presence of volatiles may be gained from analysing zonations in the large (1 cm diameter) plagioclase crystals. These will give the evolution of the Teide-Pico Viejo rocks within the magma chamber. Some further microprobe work and Laser Ablation-MS would give interesting details on the composition and evolution of the individual crystals. There are many feldspars, amphiboles and pyroxenes, which look in thin section (colour changes and differences in twinning) as though they range in composition; analysing these would help in the understanding of the evolution of the magma chambers.

The xenoliths, both from Tenerife and Lanzarote, have not been modelled in this thesis, and they may give important information regarding the mantle source. The range in xenoliths from Tenerife from syenite to gabbro and in Lanzarote spinel lherzolite, harzburgites and dunites may provide further interesting information regarding the comparison between the different islands. The syenite and gabbros are thought to be crustally derived, and hence may give information regarding the conditions within the crust. The lherzolites, harzburgites and dunites will give information regarding the source compositions of the melts.

REFERENCES

Abdel-Monem A., Watkins N. D. and Gast P. W. (1971) Potassium-Argon ages, volcanic stratigraphy and geomagnetic polarity history of the Canary Islands: Lanzarote, Fuerteventura, Gran Canaria and La Gomera. *Am. Jou. Sc.* **271,** 490-521.

Abdel-Monem A., Watkins N. D. and Gast P. W. (1972) Potassium-Argon ages, volcanic stratigraphy and geomagnetic polarity history of the Canary Islands: Tenerife, La Palma and Hierro. *Am. Jou. Sc.* **272,** 805-825.

Ablay G. J. (1997) Evolution of the Teide-Pico Viejo volcanic complex and magmatic system Tenerife, Canary Islands. Ph.D. Thesis Bristol, UK. (unpublished)

Ablay G. J., Ernst G. G. J., Marti J., and Sparks, R. S. J. (1995) The ~2 ka subplinian eruption of Montaña Blanca, Tenerife. *Bull. Volcanol.* **57,** 337-355.

Ablay G. J., Carroll M. R., Palmer M. R., Martí J. and Sparks R. S. J. (1998) Basanite-phonolite lineages of the Teide-Pico Viejo Volcanic Complex, Tenerife, Canary Islands. *Journal of Petrology* **39,** No 5. 905-936.

Albert J. F., Araña V., Diez J. L. & Valentín A. (1990) Physical-chemical conditions of the Teide volcanic system (Tenerife, Canary Islands). *J. Volcanol. Geotherm. Res.* **43** 321-332.

Allègre C . J. (1968) ^{230}Th dating of volcanic rocks: a comment. *Earth and Planetary Science Letters* **5,** 209-210.

Allègre C. J. and Condomines M. (1976) Fine chronology of volcanic processes using ^{238}U-^{230}Th systematics. *Earth and Planetary Science Letters* **28,** 395-406.

Allègre C. J. and Condomines M. (1982) Basalt genesis and mantle structure studied through Th-isotopic geochemistry. *Nature* **299,** 21-24.

Allègre C. J. and Minster J. F. (1978) Quantitative models of trace element behaviour in magmatic processes. *Earth and Planetary Science Letters* **38,** 1-25.

Allègre C. J., Poirier J-P., Humler E., Hofmann A. W. (1995) The chemical composition of the earth. *Earth and Planetary Science Letters* **134,** 515-526.

Allègre, C.J. and Turcotte, D. L. (1985) Geodynamic mixing in the mesosphere boundary layer and the origin of oceanic islands. *Geophysical Research Letters,* **12,** 207-210.

Ancochea E., Fuster J-M. Ibarrola E., Cendrero A., Coello J., Hernan F., Cantagrel J. M. and Jamonde C. (1990) Volcanic evolution of the islands of Tenerife (Canary Islands) in the light of new K-Ar data. *J. Volcanol. Geotherm. Res.* **44,** 231-249.

Ancochea E., Hernán F., Cendrero A., Cantagrel J. M., Fuster J-M., Ibarrola E., Coello J. (1994) Constructive and destructive epsiodes in the building of a young oceanic island, La Palma, Canary Islands and genesis of the Caldera de Taburiente *J. Volcanol. Geotherm. Res.* **60,** 243-262.

Andersen T., Burke E. A. J., Neumann E.- R. (1995) Nitrogen rich fluids in the upper mantle: fluid inclusions in spinel dunites from Lanzarote, Canary Islands. *Contributions to Mineralogy and Petrology* **120,** 20-28.

Anderson D.L. (1979) The upper mantle transition region: ecologite. *Geophys. Res. Lett.* **6,** 433-436.

Anderson D. L. (1998) The scales of mantle convection. *Tectonophysics* **284,** 1-17.

Araña V. (1971) Litología y estructura del Edificio Cañadas, Tenerife. *Estudios Geologicos* **27,** 95-135.

Araña V. (1995) Notes on Canarian volcanism. In: Marti J. and Mitjavila J. (Eds.) *A field guide to the Central Volcainc Complex of Tenerife (Canary Islands) Casa de Los Volcanes No 4* Cabildo Insular de Lanzarote pp 3-17.

Araña V. and Carracedo J. C. (1978) *Los Volcanes de las Islas Canarias. I Tenerife.* Editorial Rueda, Madrid.

Araña V. and Carracedo J. C. (1979) *Los Volcanes de las Islas Canarias. II Lanzarote and Fuerteventura.* Editorial Rueda, Madrid.

Araña V. and Ortiz R. (1991) The Canary Islands: Tectonics, magmatism and geodynamic framework. In Kampunzu A.B. and Lubala R.T. (Eds.) *Magmatism in Extensional Structural Settings. The Phanerozoic African Plate.* Springer-Verlag. Berlin pp 209-249.

Araña V. Diez J. L., Ortiz R & Yuguero J. (1984) Convection of geothermal fluids in Timanfaya volcanic area (Lanzarote, Canary Islands). *Bull Volcanol.* **47** 667-677.

Araña V., Barberi F, and Ferrara G. (1989) El complejo volcanico del Teide-Pico Viejo. In Araña and Coello J. (eds) *Los Volcanes y la Caldera del Parque nacionale del Teide (Tenerife, Islas Canarias)* Madrid; ICONA pp. 101-126.

Araña V., Marti J., Aparicio A., Garîa-Cacho L. and Garçia-Garçia R. (1994) Magma mixing in alkaline magmas: An example from Tenerife, Canary Island. *Lithos* **32,** 1-19.

Arth J. G. (1976) Behaviour of trace elements during magmatic processes - a summary of theoretical models and their applications. *Journal of Research of the US Geological Society* **91,** 6091-9112.

Asimov P. D., Hirschmann M. M., Ghiorso M. S. and Stolper E. M. (1997) Isentropic melting processes in the mantle. *Conference abstract EUG*

Banda E., Dañobeitia J. J., Suriñach E. and Ansorge J. (1981) Features of crustal structure under the Canary Islands. *Earth and Planetary Science Letters* **55,** 11-24.

Beattie P. (1993) U-Th disequilibria and partitioning on melting of garnet peridotites. *Nature* **363,** 63-65.

Beattie, P (1993b) The generation of uranium series disequilibiria by partial melting of spinel peridotite: constraints from partitioning studies *Earth and Planetary Science Letters* **117,** 379-391.

Bedini R. M., Bodinier J-L, Dautria J-M and Morten L. (1997) Evolution of LILE-enirched small melt fractions in the lithospheric mantle; a case study from the East African Rift. *Earth and Planetary Science Letters* **153,** 67-83.

Ben Othman D. and Allégre C. J. (1990) U-Th isotopic systematics at 13°N East Pacific Ridge segment *Earth and Planetary Science Letters* **98,** 129-137.

Bennett V. C., Esat T. M. and Norman M. D. (1996) Two mantle plume components in Hawaiian picrites inferred from correlated Os-Pb isotopes *Nature* **381,** 221-224.

Black S., Macdonald R. and Kelly M. R. (1997) Crustal origin for peralkaline rhyolites from Kenya; evidence from U-series disequilibria and Th-isotopes. *Journal of Petrology* **38,** 277-297.

Black S., Macdonald R., DeVivo B., Kilburn C.R.J. and Rolandi G (1998) U_series disequilibria in young (A.D. 1944) Vesuvius rocks: preliminary implications for magma residence times and volatile addition. *J. Volcanol. Geotherm. Res.* **82,** 97-111.

Blake S. (1981) Volcanism and the dynamics of open magma chambers. *Nature* **289,** 783-785.

Blake S. (1984) Volatile oversaturation during the evolution of silicic magma chambers as an eruption trigger. *J. Geophys Res.* **89,** No B10 8237-8244.

Blake S. and Ivey G. (1986) Magma mixing and dynamics of withdrawal from stratified reservoirs. *J. Volcanol. Geotherm. Res.* **27,** 153-178.

Blundy J.D., Robinson J.A.C. and Wood B.J. (1998) Heavy REE are compatible in clinopyroxene on the spinel lherzolite solidus. *Earth Planet. Sci. Lett.* **160,** 493-504.

Booth B. (1973) The Grandilla pumice deposit of southern Tenerife, Canary Islands. *Proc. Geol. Ass.* **84,** 353-369.

Borley G. (1974) Aspects of the volcanic history and petrology of the island of Tenerife, Canary Islands. *Proc. Geol. Ass.* **85,** Part 2 259-279.

Bosshard E. and Macfarlane D. J. (1970) Crustal structure of the Western Canary Islands from seismic refraction and gravity data. *J Geophys. Res.* **75,** 4901-4918.

Bourdon B., Zindler A. and Wörner G. (1994) Evolution of the Laacher See magma chamber; Evidence from SIMS and TIMS measurements of U-Th disequilibrium in minerals and glasses. *Earth and Planetary Science Letters* **126,** 75-90.

Bourdon B., Langmuir C. H. and Zindler A. (1996) Ridge hotspot interaction along the mid Atlantic Ridge between 37°30 and 40°30 N : the U-Th disequilibrium evidence. *Earth and Planetary Science Letters* **142,** 175-189.

Bourdon B., Zindler A,. Elliott T. and Langmuir, C. H. (1996b) Constraints on mantle melting at mid-ocean ridges from global ^{238}U-^{230}Th disequilibrium data. *Nature* **384,** 231-235.

Bowring S. and Housh T. (1995) The Earth's Early Evolution. *Science* **269,** 1535-1540.

Bryan S. (1998) Pyroclastic rocks of Tenerife - Bandas del Sur and Las Cañadas caldera wall. PhD. Monash University Australia. Unpublished.

Bryan W.B., Finger L.W. and Chayes F. (1969) Estimating proportions in petrographic mixing equations by least squares approximation. *Science* **163,** 926-927.

Burke K.C. and Wilson J.T. (1976) Hotspots on the Earth's surface. *In Volcanoes and the Earth's interior.* R. Decker & Decker B. 31-42, New York: W.H. Freeman (1982).

Burnett M.S., Caress D.W. and Orcutt J.A. (1989) Tomographic image of the magma chamber at 12°50N on the East Pacific rise. *Nature* **339,** 206-208.

Canales J. P. and Dañobeitia J. J. (1998) The Canary Islands Swell; a Coherence Analysis of Bathymetry and Gravity. *Geophys. J. Int.* **132,** 479-488.

Capaldi G., Cortini M., Gasparini P. and Pece, R. (1976) Short-lived radioactive disequilibria in freshly erupted volcanic rocks and their implication for the pre-eruptive history of a magma. *J. Geophys. Res.* **81,** 350-358.

Capaldi G., Cortini M. and Pece R. (1982) Th isotopes at Vesuvius: evidence for open-system behaviour of magma-forming processe. *J. Volcanol. Geotherm. Res.* **14,** 247-260.

Carracedo J. C. (1975) Paleomagnetismo e historia volcánica de Tenerife. Ph.D. Thesis Univ. Complutensis Madrid.

Carracedo J. C. (1994) The Canary Islands: An example of structural control on the growth of large oceanic-island volcanoes. *J. Volcanol. Geotherm. Res.* **60,** 225-241.

Carracedo J. C. (1996) Morphological and structural evolution of the western Canary Islands : hotspot induced 3 armed rifts or regional tectonic trends. *J. Volcanol. Geotherm. Res.***71,** 151-162.

Carracedo J. C. and Badiola E. R. (1991) Lanzarote, La erupicion volcanica de 1730. *Cabildo Insular de Lanzarote.*

Carracedo J.C. and Badiola E. (1991) Mapa geologico de la erupcion de Lanzarote de 1730-36. 1:25,000 Estación Volcanológica de Canarias. In Carracedo J. C. and Badiola E. R. (eds.) Lanzarote, La erupicion volcanica de 1730. *Cabildo Insular de Lanzarote.*

Carracedo J. C., Badiola E. R. and Soler V. (1992) The 1730-36 eruption of Lanzarote, Canary Islands: a long high magnitude basaltic fissure eruption. *J. Volcanol. Geotherm. Res.* **53,** 239-250.

Carracedo J. C. and Badiola E. R. (1993) Evolucion geologica y magmatica de la isla de Lanzarote. *Rev. Acad. Canar. Cienc.* **4,** 25-58.

Carracedo J. C., Day S., Guillou H., Badiola E. R., Canas J. A. and Perez Torrado, F. J. (1998 ?) Geochronological, structural and morphological constraints in the genesis and evolution of an ocean volcanic chain clos to a passive continental margin : The Canary Islands Subm to EPSL 1997.

Cashman K. V. and Marsh B. D. (1988) Crystal size distributions in rocks and the kinetics and dynamics of crystallization. *Contribributions to Mineralogy and Petrology* **99,** 292-305

Chabaux F. and Allègre C. J. (1994) ^{238}U-^{230}Th-^{226}Ra disequilibria in volcanics: a new insight into melting conditions. *Earth and Planetary Science Letters* **126,** 61-74.

Chabaux F., Ben Othman D. and Birck J. L. (1994) A new Ra-Ba chromatographic separation and its application to Ra mass-spectrometric measurement in volcanic rocks. *Chemical Geology* **114,** 191-197.

Chaffey D. J., Cliff R. A. and Wilson B. M. (1989) Characterization of the St Helena source. In Saunders A.D. and Norry M.J.(eds.) *Magmatism in the ocean basins, Geol. Soc. Spec. Publ.* **42,** 257-276.

Chauvel, C. Hofmann, A. and Vidal, P. (1992) HIMU-EM : The French Polynesian connection *Earth and Planetary Science Letters***110,** 99-119.

Chauvel C., McDonough W., Guille G., and Maury M. (1997) Constrasting old and young volcanism in Rurutu Islands, Austral Chain. *Chemical Geology* **139,** 125-143.

Chen J. H. and Wasserburg G. J. (1981) Isotopic determinations of uranium in picomole and subpicomole quantities. *Analytical Chemistry* **53,** 2060-2067.

Christensen U. (1995) Effects of phase transitions on mantle convection *Annual Review of Earth and Planetary Science* **23,** 65-87.

Clarke D. B. and O'Hara M. J. (1979) Nickel and the existence of high MgO liquids in nature. *Earth Planetary Science Letters* **44,** 153-158.

Class C. and Goldstein S. L. (1997) Plume-lithosphere interactions in the ocean basins: constraints from source mineralogy. *Earth and Planetary Science Letters* **150,** 245-260.

Class C., Altherr R., Volker F., Eberz G. and McCulloch M. T. (1994) Geochemistry of Pliocene to Quaternary alkali basalts from Huri Hill, northern Kenya. *Chemical Geology***113,** 1-22.

Coello J., Cantagrel J-M. Hernan F., Fuster J-M., Ibarrola E., Ancochea E., Casquet C., Jamond C., Diaz de Teran J-R and Cendrero A. (1992) Evolution of the eastern volcanic ridge of the Canary Islands based on new K-Ar data. *J. Volcano. Geotherm. Res.* **53,** 251-274.

Cohen A. S., Evensen N. M, Hamilton P. J. and O'Nions R. K. (1980) U-Pb, Sm-Nd and Rb-Sr systematics of mid ocean ridge basalt glasses. *Nature* **283,** 149-153.

Cohen A. and O'Nions R. K. (1991) Precise determination of femtogram quantities of Radium by thermal ionisation mass spectrometry. *Analytical Chemistry* **63,** 2705 -2708.

Cohen A. and O'Nions R. K. (1993) Melting rates beneath Hawaii: Evidence from uranium series isotopes in recent lavas. *Earth and Planetary Science Letters* **120,** 169-175.

Cohen A. S., Belshaw N. S., and O'Nions, R. K. (1992) High precision Uranium, Thorium and Radium isotope ratio measurements by high dynamic range thermal ionisation mass spectrometry *Int. J. Mass Spectrometry and Ion Processes* **116,** 71-81

Collot J-Y et al (1995) Sonic imaging reveals new plate boundary structures offshore New Zealand. *EOS Trans. Am. Geophys. Union.* **76,** (1).

Condomines M. (1994) Comment on : "The volume and residence time of magma beneath active volcanoes determined by decay series disequilibria methods. *Earth and Planetary Science Letters* **122,** 251-255.

Condomines M. and Allègre C. J. (1980) Age and magmatic evolution of Stromboli volcano from ^{230}Th -^{238}U disequilibrium data. *Nature* **288,** 354-357.

Condomines M., Bouchez R., Ma J. L., Tanguy J. C., Amosse J. and Piboule M. (1987) Short-lived radioactive disequilibria and magma dynamics in Etna volcano. *Nature* **325,**

Condomines M., Hemond C. and Allègre C. J. (1988) U-Th-Ra radioactive disequilibria and magmatic processes. *Earth and Planetary Science Letters* **90,** 243-262.

Condomines M., Morand P. and Allegre, C. J. (1981) ^{230}Th-^{238}U radioactive disequilibria in tholeiites from the FAMOUS zone (Mid-Atlantic Ridge, 36 degrees 50'N); Th and Sr isotopic geochemistry. *Earth and Planetary Science Letters* **55,** 247-256.

Condomines M., Tanguy J. C., Kieffer G., and Allègre C. J. (1982) Magmatic evolution of a volcano studied by ^{230}Th-^{238}U disequilibrium and trace element systematics; the Etna case. *Geochimica et Cosmochimica Acta* **46,** 1397-1416.

Condomines M., Tanguy, J.-C. and Michaud V. (1995) Magma dynamics at Mt Etna; constraints from U-Th-Ra-Pb radioactive disequilibria and Sr isotopes in historical lavas. *Earth and Planetary Science Letters* **132,** 25-41.

Cortini M. (1985) An attempt to model the timing of magma formation by means of radioactive disequilibria. *Chemical Geology* **58,** 33-43.

Cousens B. (1990) Isotopic patterns in silicic ignimbrites and lava flows of the Mogan and lower Fatga Formation Gran Canaria, Canary Islands : Temporal changes in mantle source composition. *Earth and Planetary Science Letters* **96,** 319-335

Cousens B. L. and Ludden J. N. (1991) Radiogenic isotope studies of oceanic basalts - A window into the mantle Chp 7. In: Heaman, L and Ludden, J.N. (Eds.) *Short course handbook on application of radiogenic isotope systems to problems in geology, Vol 19 Min.Ass. of Canada*, Toronto.

Cox K. G., Bell J. D. and Pankhurst R. J. (1979) The Interpretation of Igneous Rocks *Chapman and Hall.*

Dañobeitia J. J., Canales J. P., and Dehghani G. A. (1994) An estimation of the elastic thickness of the lithosphere in the Canary Archipelago using admittance function. *Geophys. Res. Lett.* **21**(24), 2649-2652.

Davies G.F. (1994) Thermomechanical erosion of the lithosphere by mantle plumes. *J.Geophys. Res.* **99,** 15,709-15,722.

Davies G.F. (1990) Mantle plume, mantle stirring and hotspot chemistry. *Earth and Planetary Science Letters.* **99,** 94-109.

Davies G. R., Norry M. J., Gerlach D. C. and Cliff R. A. (1989) A combined chemical and Pb-Sr-Nd isotope study of the Azores and Cape Verde hot spots: the geodynamic implications. In Saunders A.S.and Norry M. (eds.) *Magmatism in Ocean basins. Geol Soc Spec Pub* **42,** 231-255.

Davies, G. F. and Richards, M. A. (1992) Mantle convection. *Journal of Geology* **100,** 151-206.

Davies G. R., Halliday A. N., Mahood G. A. and Hall C.M. (1994) Isotopic constraints on the production rates, crystallisation histories and residence times of pre-caldera silicic magmas, Long Valley, California. *Earth and Planetary Science Letters* **125,** 17-37.

Davies G.R. and Halliday A.N. (1998) Development of the Long Valley rhyolitic magma system: Sr and Nd isotope evidence from glasses and individual phenocrysts. *Geochimica and Geochimica Acta* **62,** 3561-3574.

De Natale G., Capuano P., Troise C., Zollo A., Spera F.J., de Vivo B., Ayuso R. and Belkin and, Harvey E. (1998) Seismicity at Somma-Vesuvius and its implications for the 3D tomography of the volcano; Vesuvius. Journal of Volcanology and Geothermal Research 82, 1-4 175-197

DePaolo D. J. (1981) Trace element and isotopic effects of combined wallrock assimilation and fractional crystallisation *Earth and Planetary Science Letters* **53,** 189-202

Detrick R.S., Buhl P., Vera E., Mutter J., Orcutt J., Madsen J. and Brocher T. (1987) Multi-channel seismic imaging of a crustal magma chamber along the East Pacific Rise. *Nature* **326,** 35-41.

Dickin A.P.(1997) Radiogenic isotope geology. Cambridge Scientific Press

Dvorak J. J. and Dzurisin D. (1993) Variations in magma supply rate at Kilauea volcano Hawaii. *J. Geophys. Res.* **98,** (B12) 22,255-22,268.

Dupré B. and Allègre C.J. (1980) Pb-Sr-Nd isotopic correlation and the chemistry of the North Atlantic mantle. *Nature* **286,** 17-22.

Ellam R. M. (1992) Lithospheric thickness as a control on basalt geochemistry. *Geology* **20,** 153-156.

Elliott T. (1991) Element fractionation in the petrogenesis of ocean island basalts, PhD dissertation. Open University

Elliott, T. (1997) Fractionation of U and Th during mantle melting: a reprise. *Chemical Geology* **139,** 165-183.

Evans P., Rogers N.W., Hawkesworth C.J. and Scott S.C. (1998) Rapid magma chamber evolution at Longonot, Kenya. New evidence from U-Th-Ra disequilibria. *Geoscience 1998 Abstract volume,* 135.

Falloon T. J. and Green D. H. (1988) Anhydrous partial melting of peridotite from 8 to 35kb and the petrogenesis of MORB *Journal of Petrology Spec. Lithosphere Issue* 379-414.

Faure G. (1986) Principles of Isotope Geology. 2nd Edition Wiley

Feigenson M. D., Hofmann A. W. and Spera, F. J. (1983) Case Studies on the origin of basalt : II The transition from tholeiitic to alkalic volcanism on Kohala volcano, Hawaii. *Contributions to Mineralogy and Petrology* **84,** 390-405.

Fernandez J., Vieira R., Diez J.l. and Toro C. (1992) Investigations on crustal thickness heat flow and gravity tide relationship in Lanzarote Island. *Physics of the Earth Interiors* **74,** 199-208

Fuster J. M., Araña V., Brandle J. L., Navarro J. M., Alonso U. and Aparicio A. (1968) Geologia y volcanologia de Las Islas Canarias, Tenerife. *Spec. Pub. Instituto Lucas Mallada,* CSIS Madrid 218pp.

Galer S. J. and O'Nions R. K. (1985) Residence times of Thorium, Uranium and Lead in the mantle with implications for mantle convection. *Nature* **316,** 778-782

Gallagher K. and Hawkesworth C. J. (1994) Mantle plumes, continental magmatism and asymmetry in the South Atlantic. *Earth and Planetary Science Letters* **123,** 105-117

Garçia-Moral, R. (1989) Erupciones historicas en Tenerife. In Araña, V. and Coello, J. (eds.) *Los Volcanes y la Caldera del Paques Nacionale del Teide (Tenerife, Canary Islands).* Madrid: ICONA, pp 347-358.

Gariepy C. and Dupre B. (1991) Pb isotope and crust mantle evolution. Chp 6 In: Heaman, L and Ludden, J.N. (eds) *Short course handbook on application of radiogenic isotope systems to problems in geology, 19, Min.Ass. of Canada,* Toronto 1991

George R. M. M. (1997) Thermal and tectonic controls on magmatism in the Ethiopian Province. PhD. dissertation. Open University. July 1997

Ghiorso M.S. and Sack-R.O. (1994) Chemical mass transfer in magmatic processes; IV, A revised and internally consistent thermodynamic model for the interpolation and extrapolation of liquid-solid equilibria in magatic systems at elevated temperatures and pressures. *Contrib. Mineral. Petrol.* **119,** 197-212.

Gill J. B. (1981) *Orogenic Andesites and Plate Tectonics*, Berlin, Springer Verlag 358 pp.

Gill J. B. (1993) Melts and metasomatic fluids: evidence from U-series disequilibria and Th isotopes. *Phil. Trans. R. Soc. Lond. A* **342,** 79-90.

Gill J. B. and Condomines M. (1992) Short lived radioactivity and magma genesis. *Science* **257,** 1368-1376.

Gill J.B. and Williams R. W. (1990) Th isotope and U-series studies of subduction related volcanic rocks. *Geochem. Cosmochem. Acta* **54,** 1427-1442.

Gill J. B., Williams R. W. and Pyle D. M. (1991) Igneous Rocks Chp 9 in: Heaman, L and Ludden, J.N.(eds.) *Short course handbook on application of radiogenic isotope systems to problems in geology, Vol 19 Min.Ass. of Canada,* Toronto.

Gill R. (Ed) (1997) Modern Analytical Geochemistry An introduction to quantitative chemical analysis techniques for Earth, Environmental and materials scientists. *Longman Press*

Gimeno L., Garçia R., and Hernández E. (1998) Precipitations in the Canary Islands in the 17th Century and its relationship with El Niño events. *Bull. Am. Met. Soc.* **79**(1), 89-91.

Goldstein S. J., Murrell M. T. and Janecky D. R. (1989) Th and U isotopic systematics of basalts from the Juan de Fuca and Gorda Ridges by mass spectrometry. *Earth and Planetary Science Letters* **96,** 134-146.

Goldstein S.J., Murrell M.T., Janecky D.R., Delaney J.R. and Clague D.A. (1992) Geochronology and petrogenesis of MORB from the Juan de Fuca and Gorda ridges by ^{238}U-^{230}Th disequilibrium. *Earth and Planetary Science Letters* **109,** 255-272.

Goldstein S.J., Murrell M.T. and Williams R.W. (1993) ^{231}Pa and ^{230}Th chronology of MORB. *Earth and Planetary Science Letters* **115,** 151-159.

Goldstein S.J., Perfit M.R., Batiza R., Fornari D.J. and Murrell M.T. (1994) Off-axis volcanism at the East Pacific Rise detected by U-series dating of basalts. *Nature* **367,** 157-159.

Green D. H. (1973) Experimental melting studies on a model upper mantle composition at high pressure under water saturated and water undersaturated conditions *Earth and Planetary Science Letters* **19,** 37-53.

Green T. H. and Watson E. B. (1982) Crystallisation of apatite in natural magmas under high pressure hydrous conditions with particular reference to Orogenic Rock Series *Contributions to Mineralogy and Petrology* **79,** 96-105.

Griffiths R. W. and Campbell I. H. (1990) Stirring and structure in mantle starting plumes *Earth and Planetary Science Letters* **99,** 66-78

Grove T.L., Kinzler R.J. and Bartels K.S. (1989) Effects of pressure on alumina substitution in igneous augite: an emperical geobarometer. *EOS Transactions AGU* **70,** 1401-1402.

Grove T., Kinzler R. and Bryan W. (1992) Fractionation of MORB In: Mantle Flow and Melt Generation at MOR, *Geophys Monograph* **71,**

Haase K. M. (1996) The relationship between age of lithosphere and the composition of oceanic magmas; constraints on partial melting, mantle source and the thermal structure of the plates. *Earth and Planetary Science Letters* **144,** 75-92.

Halliday A. N., Davidson J. P., Holden T., DeWolf C., Lee D-C. and Fitton J. G. (1990) Trace element fractionation in plumes and the origin of HIMU mantle beneath the Cameroon line. *Nature* **347,** 523-528.

Halliday A. N., Lee D-C, Tommasini S., Davies G. R., Paslick C. R., Fitton J. G. and James D. E. (1995) Incompatible trace elements in OIB and MORB and source enrichment in the sub-oceanic mantle. *Earth and Planetary Science Letters* **133,** 379-395.

Harker A. (1909) The natural history of igneous rocks. *New York, MacMillian.*

Hart S. R. (1984) The DUPAL anomaly: a large-scale isotopic anomaly in the southern hemisphere. *Nature* **309,** 753-756.

Hart S. R. (1988) Heterogeneous mantle domains: signatures, genesis and mixing chronologies. *Earth and Planetary Science Letters* **90,** 273-296.

Hart S. R. and Davies K. E. (1978) Nickel partitioning between olivine and silicate melt *Earth and Planetary Science Letters* **40,** 203-219.

Hart S. R., Hauri E. H., Oschmann L. A. and Whitehead J. A. (1992) Mantle plumes and entrainment: isotopic evidence. *Science* **256,** 517-520.

Hauri E.H. (1997) Melt migration and mantle chromatography 1: simplified theory and conditions from chemical and isotopic decoupling. *Earth and Planetary Science Letters* **153,** 1-19.

Hauri E. H. and Kurtz M. D. (1997) Melt migration and mantle chromatography 2; a time-series Os isotope study of Mauna Loa volcano, Hawaii. *Earth and Planetary Science Letters* **153,** 21-36.

Hauri E., Shimizu N., Dieu J. J. and Hart S. R. (1993) Evidence for hotspot-related carbonatite metasomatism in the oceanic upper mantle. *Nature* **165,** 221-227.

Hausen H. (1956) Contributions to the geology of Tenerife. *Soc Fennica Com Phys Maths.,* **18** (1) 247p.

Hawkesworth C and van Calsteren P. (1994) Trace element and radiogenic isotope constraints on melt generation *Geoscientist* **4,** No. 3, 21-22.

Hawkesworth C.J., Norry M.J. Roddick J.C. and Vollmer R. (1979) $^{143}Nd/^{144}Nd$ and $^{87}Sr/^{86}Sr$ ratios from the Azores and their significance in LIL-element enriched mantle. *Nature* **280,** 28-31.

Hawkesworth C. J. and Norry M. (1983) (Eds.) Continental basalts and mantle xenoliths. *Shiva Geol Series 83 .*

Hawkesworth C. J., Erlank A. J., Marsh J. S., Menzies M. A. and van Calsteren, P. (1983) Evolution of continental lithosphere : Evidence from volcanics and xenoliths, in Southern Africa. In Hawkesworth C. J. and Norry M. (eds.)*Continental basalts and mantle xenoliths* Shiva Geol Series pp 272

Hawkesworth C. J. and van Calsteren P. (1983) Radiogenic isotopes - some applications REE Geochemistry. In Henderson P. (ed.) *Developments in Geochemistry 2* pp 375-421 Elservier Sci. Pub. 83.

Hawkesworth C., Mantovani M and Peate D. (1988) Lithosphere remobilisation during Paraná CFB magmatism. *Journal of Petrology Spec. Iss.* 205-223.

Hawkesworth C. J., Kempton P. D., Rogers N. W., Ellam R. M. and van Calsteren P. W. (1990) Continental mantle lithosphere and shallow level enrichment processes in the Earth's mantle. *Earth and Planetary Science Letters* **96,** 256-268.

Hawkesworth C., Gallagher K., Hergt J. M. and McDermott F. (1993) Trace element fractionation processes in generation of island arc basalts. *Phil. Trans. Roy. Soc. Lon. A.* **342,** 179-191.

Hawkesworth C. J., Gallagher K. Hergt J. M. and McDermott F. (1994) Destructive plate margin magmatism : Geochemistry and melt generation. *Lithos* **33,** 169-188.

Hawkesworth C. J. Hergt J. M., Ellam R. M. and McDermott F. (1994b) Element fluxes associated with subduction related magmatism. *Phil. Trans. R. Soc. Lon.* **335,** 393-405.

Hawkesworth C. Turner S., Gallagher K., Hunter A., Bradshaw T. and Rogers N. (1995) Calc-alkaline magmatism, lithospheric thinning and extension in the Basin and Range. *J. Geophys. Res.* **100,** No B7, 10271-10286.

Hawkesworth C.J., Turner S., Thomas L., van Calsteren P., Cohen A. and Rogers N. (1996) U-Th disequilibria in OIB from the Azores and Canary Islands. Plume Conf abstract

Hawkesworth C., Turner S., Peate D., McDermott F. and van Calsteren P. (1997) Elemental U-Th variations in island arc rocks: implications for U-series isotopes. *Chemical Geology* **139,** 207-221.

Hayes D. E. and Rabinowitz O. D.(1975) Mesozoic magnetic lineations and the magnetic quiet zone off northwest Africa. *Earth and Planetary Science Letters* **28,** 105-115.

Heath E. (1994) ^{238}U-^{230}Th Disequilibria : applications to geochronology and magmagenesis studies in volcanology. Unpub; Research student 1st yr project

Heath E., Turner S.P., MacDonald R., Hawkesworth C. J. and van Calsteren P. (1998) Long magma residence times at an island arc volcano (Soufiere, St Vincent) in the Lesser Antilles: evidence from ^{238}U-^{230}Th isochron dating. *Earth and Planetary Science Letters* **160,** 49-63.

Hemond C., Condomines M., Fourcade S., Allègre C. J., Oskarsson N. and Javoy M. (1988) Th, Sr and O isotopic geochemistry in recent tholeiites from Iceland: crustal influence on mantle drived magmas. *Earth and Planetary Science Letters* **87,** 273-285.

Hemond C., Hofmann A.W., G. Heusser, Condomines M., Raczek I. and Rhodes J.M. (1994) U-Th-Ra systematics in Kilauea and Mauna-Loa basalts, Hawaii. *Chemical Geology* **116,** 163-180.

Hemond C., Hofmann A. W., G. Heusser, Condomines M., Raczek I. and Rhodes J. M. (1995) U-Th-Ra systematics in Kilauea and Mauna-Loa basalts, Hawaii. *Chemical Geology* **120,** 171.

Hildreth W. (1979) The Bishop Tuff: evidence for the origin of compositional zonation in silicic magma chambers. *Geological Society of America Special Paper* **180,** 43-74.

Hildreth W. (1981) Gradients in silicic magma chambers: implications for lithospheric magmatism. *Journal of Geophysical Research* **86,** B10153-10192

Hirose K.and Kushiro I. (1993) Partial melting of dry peridotites at high pressures; determination of compositions of melts segregated from peridotite using aggregates of diamond. *Earth and Planetary Science Letters* **144,** 477-489.

Hirschmann M.M. and Stolper E.M. (1996) A possible role for garnet pyroxenite in the origin of the 'garnet signature' in MORB. *Contributions to Mineralogy and Petrology,* **124,** 185-208.

Hoernle K., Tilton G. and Schmincke H-U. (1991) Sr-Nd-Pb isotopic evolution of Gran Canaria; evidence for shallow enriched mantle beneath the Canary Islands. *Earth and Planetary Science Letters* **106,** 44-63.

Hoernle K. and Schmincke H-U. (1993) The role of partial melting in the 15 Ma geochemical evolution of Gran Canaria: A blob model for the Canary hotspot. *Journal of Petrology* **34,** 599-626.

Hoernle K., Zhang Y-Shen, and Graham D. (1995) Seismic and geochemical evidence for large scale mantle upwelling beneath the eastern Atlantic and western and central Europe. *Nature* **374,** 34-39.

Hofmann A. W. (1988) Chemical differentiation of the Earth: the relationship between mantle, continental crust and oceanic crust. *Earth and Planetary Science Letters* **90,** 297-314.

Hofmann A. W. (1997) Mantle geochemistry: the message from oceanic volcanism. *Nature* **385,** 219-229.

Hofmann A. W. and White W. M. (1982) Mantle plumes from ancient oceanic crust. *Earth and Planetary Science Letters* **57,** 421-436.

Hofmann A. W. and Feigenson M. D. (1983) Case studies on the origin of basalts: I Theory and reassessment of Grenada basalts. *Contributions to Mineralogy and Petrology* **84,** 382-389.

Hofmann A. W., Feigenson M. D. and Raczek I. (1984) Case studies on the origin of basalt: III Petrogenesis of the Mauna Ulu eruption, Kilauea, 1969-1971.*Contributions to Mineralogy and Petrology* **88,** 24-35.

Holik J. S. and Rabinowitz P. D. (1991) Effects of Canary Hotspot volcanism on structure of oceanic crust off Morocco. *J. Geophys. Res* . **96,** 12,039-12,067.

Holik J. S. and Rabinowitz P. D. (1992) Structural and Tectonic evolution of oceanic crust within the Jurassic Quiet zone Offshore Morocco *AAPG Memoir* **53,** Geology and Geophysics of Contintental Margin Chapter 14 259-281.

Horwitz E.P., Chiarizia R and Dietz M.L. (1992) A novel strontium selective extraction chromatographic resin. *Solvent Extr.Ion.Exch.* **10,** 313-336.

Huang Y., Hawkesworth C. J., van Calsteren P., Smith I. and Black P. (1997) Melt generation models for the Auckland volcanics: Constraints from U-Th isotopes. *Earth and Planetary Science Letters* **149,** 67-84.

Huang Y. (1995) U-Th-Pb Fractionation in selected carbonate and silicate systems. PhD Thesis, The Open University. (Unpublished)

Huppert H. and Sparks R. S. J. (1985) Cooling and contamination of mafic and ultramafic magmas during ascent through the continental crust *Earth and Planetary Science Letters* **74,** 371-386.

Irvine T. N. and Baragar W. R. A. (1971) A guide to the chemical classification of common rocks. *Can. J. Earth Sci.* **8,** 523-548.

Ito E., White W. M. and Gopel C. (1987) The O, Sr, Nd, and Pb isotope geochemistry of MORB. *Chemical Geology* **62,** 157-167.

Ivanovich, M and Harmon, R.S. (1992) U-Series disequilibria, Application to Earth, Marine and Environmental Sciences. 2nd Ed. Oxford Sci. Press.

Jaffey A. H., Flynn K.F., Glendenin L. E., Bentley W.C. and Essling A.M. (1971) Precision measurements of half-lives and specific activities of ^{235}U and ^{238}U. *Phys. Rev* **C4,** 1889.

Jarvis K. (1997) Introduction to ICP-MS (In Gill R. (Ed) Modern Analytical Geochemistry An introduction to quantitative chemical analysis techniques for Earth, Environmental and materials scientists. *Longman Press*

Jones S. (1993) Mechanisms of Large silicic magma chamber zonation: the youngest Toba Tuff. *PhD thesis Unpub.* The Open University.

Jochum K. P., Hofmann A. W., Ito E., Seufert H. M. and White W. M. (1983) K, U and Th in MOR basalt glasses and heat production, K/U and K/Rb in the mantle. *Nature* **306,** 431-436.

Joly J. (1909) On the radioactivity of certain lavas. *Philos. Mag.* **18,**

Kelemen P. B. Shimizu N and Dunn T. (1993) Relative depletion of Niobium in some arc magmas and the continental crust: partitioning of K, Nb, La and Ce during melt/rock reaction in upper mantle *Earth and Planetary Science Letters* **120,** 111-134.

Kerr R. A. (1996) Putting stiffness in the Earth's mantle. *Science* **271,** 1053-1054.

Kinzler R. J. and Langmuir C. H. (1995) Minute Mantle Melts. *Nature* **375,** 274-275.

Klein E. M and Langmuir C. H. (1987) Global correlations of ocean ridge basalt chemistry with axial depth and crustal thickness. *J. Geophys. Res.* **94,** 8089-8115

Klügel A., Hansteen T. H., and Schmincke H-U. (1997) Rates of magma ascent and depths of magma reservoirs beneath La Palma, Canary Islands. *Terra Nova* **9,** 117-121.

Kuno H. (1968) Differentiation of basalt magmas. In Hess. H.H., and Poldervaart A. (eds.) *Basalts; The Poldervaart treatise on rocks of basaltic composition.* **2,** Interscience, New York, pp 623-688.

Kushiro I. (1996) Partial melting of a fertile mantle peridotite at high pressures: an experimental study using the aggregates of diamond Earth Processes: Reading the isotopic code. *Geophys Monograph 95* AGU.

Kyle P.R. (1981) Mineralogy and geochemistry of a basanite to phonolite sequence at Hut Point Peninsula, Antartica, based on core from Dry Valley Drilling Project drillholes 1,2 and 3. *Journal of Petrology* **22,** 451-500.

Kyle P.R., Moore J. A. amd Thirlwall M. F. (1992) Petrological evolution of anorthoclase phonolite lavas at Mount Erebus, Ross Island, Antartica. *Journal of Petrology* **33,** 849-875.

Langmuir C. H., Bender J. F., Bence A. E., Hanson G. N. and Taylor S. R. (1977) Petrogenesis of basalts from the famous area: Mid Atlantic Ridge *Earth and Planetary Science Letters* **36,** 133-156.

Langmuir C. H., Vocke R. D., Hanson G. N. and Hart S. R. (1978) A general mixing equation with applications to Icelandic basalts. *Earth and Planetary Science Letters* **37,** 380-392.

Langmuir C., Klein E. and Plank, T. (1992) Petrological systematics of MORB: Constraints on melt generation beneath ocean ridges. In *Mantle Flow and Melt Generation at Mid Ocean Ridges. Geophys. Monogr.* **71.**

Langmuir C.H. (1996) Mantle melting, melt extraction and source heterogeneity: Issues and constraints V.M. Goldschmidt Conf. *J. Conf. Abs.* **1,** 348.

Lawerence Edwards. R., Chen J. H. and Wasserburg G. J. (1986/87) ^{238}U-^{234}U-^{230}Th-^{232}Th systematics and the precise measurement of time over the past 500,000 years *Earth and Planetary Science Letters***81,** 175-192.

Le Bas M.J., Le Maitre R. W., Streckenisen A. and Zanettin, B. (1986) A chemical classification of volcanic rocks based on the total alkali-silica diagram. *Journal of Petrology* **27,** 745-750.

Le Maitre R.W., Bateman P., Dudek A., Keller J. Lameyre Le Bas M.J., Sabine P. A. Schmid R., Sorensen H., Strecheisen A., Woolley A.R. and Zanettin B. (1989) *A classification of igneous rock and glossary of terms.* Blackwell, Oxford.

Le Roux L. J. and Glendenin L.E. (1963) Half-life of ^{232}Th. *Proc. Natl. Mett. Nuclear Energy, Pretoria,* **83.**

Le Roex A.P., Cliff R.A. and Adair B.J.I. 1990 Tristan-Da-Cunha, South-Atlantic - Geochemistry and Petrogenesis of a Basanite Phonolite Lava Series. *Journal of Petrology* **31,**.779-812.

Leat P. T., Thompson R. N., Morrison M. A., Hendry G. L. and Dickin A. P. (1988) Compositionally-diverse recent rift-related magmatism in Northwest Colorado: Partial melting and mixing of mafic magmas from 3 different asthenospheric and lithospheric mantle sources. *Journal of Petrology Spec. Lithosphere iss.* 351-377.

Lounsbury M. and Durham R. W. (1971) The alpha half-life of ^{234}U. In: *Proc. Intl. Conf. Chem. Nucl. Data Measurement and Applications* (ed. M. L. Hurrell) 251. Inst. Civ. Eng.

Lundstrom C. C., Shaw H. F., Ryerson F. J., Phinney D. L., Gill J. B. and Williams Q. (1994) Compositional controls on the partitioning of U, Th, Ba, Pb, Sr and Zr between clinopyroxene and haplobasaltic melts: implications for uranium series disequilibria in basalts. *Earth and Planetary Science Letters* **128,** 407-423.

Lundstrom C. C., Gill J. B., Williams Q. and Perfit M.(1995) Mantle melting and basalt extraction by equilibrium porous flow. *Science* **270,** 1958-1961.

Lundstrom C. C., Williams Q., and B. G. J. (1998) Investigating solid mantle upwelling rates beneath mid-ocean ridges using U-series disequilibria 1: a global approach. *Earth and Planetary Science Letters* **157,** 151-165.

MacDonald R. (1974) The role of fractional crystallisation in the formation of alkaline rocks In Sørensen, H. (ed.) *The Alkaline Rocks.* New York, John Wiley pp 442-459.

MacDonald R., Spark R. S. J., Sigurdsson H., Mattey D. P., McGarvie D. W. and Smith R. I. (1987) The 1875 eruption of Askja volcano, Iceland: combined fractional crystallisation and selective contamination in the generation of rhyolite magma. *Minerological Magazine* **51,** 183-202.

Mapa geografico - Mapa volcanico Lanzarote 1:100,000. (1995) Consejo Superior Geográfico Madrid

Mapa geologico de España 1:50000, (1958) Inst. Geol. Miner. Esp.

Marcantonio F. Zindler A., Elliott T. and Staudigel H. (1995) Os isotope systematics of La Palma, Canary Islands : Evidence for recycled crust in the mantle source of HIMU ocean islands. *Earth and Planetary Science Letters* **133,** 397-410.

Marinoni L. (1991) Evoluzione geologica e strutturale dell'isola di Lanzarote (Islas Canarias). PhD Thesis. Univ Milan.

Marinoni L. and Pasquarè G. (1994) Tectonic evolution of the emergent part of a volcanic ocean island: Lanzarote, Canary Isles. *Tectonophysics* **239,** 111-135.

Martí J. Mitjavila J. and Araña V. (1994) Stratigraphy, structure and geochronology of the Las Cañadas caldera (Tenerife, Canary Islands). *Geol. Mag.* **131,** (6) 715-727.

Martí J. and Mitjavila J. (Eds.) (1995a) A Field Guide to the Central Volcanic Complex of Tenerife (Canary Islands). *Serie Casa de los volcanes No 4* Cabildo Insular de Lanzarote.

Martí J., Mitijavila J.M. and Araña V. (1995b) The Las Cañadas edifice and caldera. In Martí J. and Mitjavila J. (Eds.) (1995) A Field Guide to the Central Volcanic Comples of Tenerife (Canary Islands). *Serie Casa de los volcanes No 4* Cabildo Insular de Lanzarote.

Martí J., Ablay G. J., and Bryan S. (1996) Comment on "The Canary Islands : an example of structural control on the growth of large oceanic volcanoes" by J.C. Carracedo *J. Vol. Geotherm. Res.* **72,** 143-149.

Martí J., Hurlimann M., Ablay G. J., and Gudmundsson A., (1997) Vertical and lateral collapses on Tenerife (Canary Islands) and other volcanic ocean islands. *Geology* **25,** 879-882.

Masson D.G. (1996) Catastrophic collapse of the volcanic island of Hierro 15 ka ago and the history of landslides in the Canary Islands. *Geology* **24,** 231-234.

McBirney A.R. and Noyes R.M. (1979) Crystallisation and layering of the Skaergaard intrusion. *Journal of Petrology* **20,** 487-554.

McDermott F.and Hawkesworth C.J. (1991) Th, Pb and Sr isotope variations in young island arc volcanics and oceanic sediments. *Earth and Planetary Science Letters* **104,** 1-15.

McKenzie D. and O'Nions R. K. (1983) Mantle reservoirs and ocean island basalts. *Nature* **301,** 229-231.

McKenzie D. (1985a) The extraction of magma from the crust and mantle. *Earth and Planetary Science Letters* **74,** 81-91.

McKenzie D. (1985) ^{230}Th-^{238}U disequilibrium and melting processes beneath ridge axes. *Earth and Planetary Science Letters* **72,** 149-157.

McKenzie D. and Bickle M. J. (1988) The volume and composition of melt generated by extension of the lithosphere. *Journal of Petrology* **29,** 625-679.

McKenzie D and O'Nions R.K. (1991) Partial Melt Distribution from inversion of rare earth element concentrations *Journal of Petrology* **32,** 1021-1091.

McKenzie D. and O'Nions K. (1995) The source regions of ocean island basalts. *Journal of Petrology* **36,** 133-159.

McKenzie, D and O'Nions R. K. (1996) Melt production beneath oceanic islands. Submitted to *J ournal of Petrology*

Meadows J. W., Armani R. J., Callis E. L. and Essling A. M. (1980) Half-life of ^{230}Th. *Phys.Rev.* **C22,** 750-754.

Mengel K. and Green D. H. (1989) Stability of amphibole and phlogopite in metasomatised peridotite under water saturated and water undersaturated conditions. In *Kimberlites and Related Rocks, Vol 1. Special Publication, Geological Society of America* **14,** 571-581.

Menzies M. and Murthy V.R. (1980) Nd and Sr isotope geochemistry of hydrous mantle nodules and their host alkali basalts: implications for local heterogenetiies in metasomatically veined mantle. *Earth and Planetary Science Letters* **46,** 323-334.

Morgan W.J. (1972) Plate motions and deep mantle convection. *Geol. Soc. Am. Mem.* 7-22.

Morgan W. J. (1983) Hotspot tracks and early rifting of the Atlantic. *Tectonophysics.* **94,** 123-139.

Morris J. and Tera F. (1989) ^{10}Be and ^{9}Be in mineral separates and whole rocks from volcanic arcs: implications for sediment subduction. *Geochim. Cosmochim Acta* **53,** 3197-3206.

Navarro J.M. and Coello (1989) Depressions originated by landslide processes in Tenerife. Abstract with programme, ESF meeting on Canarian volcanism, Lanzarote, Canary Islands. pp150-152.

Neumann E-R. Wulff-Pedersen E. Johnsen K., Andersen T. and Krogh E. (1995) Petrogenesis of spinel harzburgite and dunite suite xenolith from Lanzarote, eastern Canary Islands: Implications for the upper mantle. *Lithos* **35,** 83-107.

Neumann E-R. and Wulff-Pedersen E. (1997) The origin of highly silicic glass in mantle xenoliths from the Canary Islands. *Journal of Petrology* **38,** (11) 1513-1539.

Newman S., Finkel R.C. and MacDougall J. D. (1984) Comparison of ^{230}Th-^{238}U disequilibrium systematics in lavas from 3 hot spot regions : Hawaii, Prince Edward and Samoa. *Geochim. Cosmochim. Acta* **48,** 315-324.

Nicholls I.A. (1974) Liquids in equilibrium with peridotitic mineral assemblages at high water pressures. *Contributions to Mineralogy and Petrology* **45,** 289-316.

O'Connor J. M. and le Roex A. P. (1992) South Atlantic hot spot- plume systems: 1 distribution of volcanism in time and space. *Earth and Planetary Science Letters* **113,** 343-364.

O'Hara, M. J. (1977) Geochemical evolution during fractional crystallization of periodically refilled magma chamber. *Nature* **266,** 503-507.

O'Hara M. (1998) Volcanic plumbing and the space problem - thermal and geochemical consequences of large-scale assimilation in Ocean Isalnd development. *Journal of Petrology* **39,** 1077-1089.

O'Nions R. K., Evensen N.M. and Hamilton P.J. (1979) Geochemical modelling of mantle differentiation and crustal growth. *J. Geophys Res.* **84,** 6091-9101.

O'Nions R. K. and McKenzie D. (1988) Melting and Continent Generation *Earth and Planetary Science Letters* **90,** 449-456.

O'Nions R. K. and McKenzie D. (1993) Th, U and Pb isotope abundances in basaltic melts *Phil. Trans. Roy. Soc. Lon.A.* **342,** 65-77.

Ormerod D. S., Rogers N.W. and Hawkesworth C. J. (1991) Melting in the lithospheric mantle: Inverse modelling of alkali-olivine basalts from the Big Pine Volcanic field, California. *Contributions to Mineralogy and Petrology* **108,** 305-317.

Ovchinnikova G. V., Belyatskii B. V., Vasil'eva I. M., Leuskii L. K., Grachev A. F., Araña V., and Mithavila J. (1995) Sr-Nd-Pb isotope characteristics of the mantle source of basalts from the Canary Islands. *Petrology* 3(2), 195-206.

Oversby V.M. and Gast P.W. (1968) Lead isotope compositions and uranium decay series disequilibrium in recent volcanic rocks. *Earth and Planetary Science Letters* **5,** 199-206.

Palacz Z. and Wolff J. A. (1989) Sr, Nd, Pb isotope characteristics of the Granadilla Pumice, Tenerife: a study of the cause of Sr isotope disequilibrium in felsic pyroclastic deposits.

In A. Saunders and M. Norry (eds.) *Magmatism in ocean basins. Geol Soc Spec. Pub* **42,** 147-159.

Parsons B. and Sclater J. G. (1977) An analysis of the variation of ocean floor bathymetry and heat flow with age. *J Geophys. Res.* **82,** 803-827.

Parsons B. and McKenzie D. (1978) Mantle convection and the thermal structure of the plates. *J.Geophys. Res.* **83,** 4485-4496.

Plank T. and Langmuir C. H. (1988) An evaluation of the global variation in the major element chemistry of arc basalts *Earth and Planetary Science Letters* **90,** 349-370.

Plank T. and Langmuir C.H. (1992) Effects of the melting regime on the composition of the oceanic crust. *J. Geophys. Res.* **97,** No B13, 19,749-19,770.

Potts P. J., Thorpe O. W. and Watson J. S. (1981) Determination of rare earth element abundances in 29 international rock standards by instrumental neutron activation analysis: a critical appraisal of calibration errors. *Chemical Geology* **34,** 331-352.

Potts P. J., Webb P. C. and Watson J. S. (1984) Energy-dispersive X-Ray-fluorescence analysis of silicate rocks for major and trace-elements. *X-Ray Spectrometry*, **13,** no 1 2-15.

Potts P. J., Thorpe O. W., Issacs M. C. and Wright D. W. (1985) High precision neutron activation analysis of geological samples employing simultaneous counting with both planar and coaxial detectors. *Chemical Geology* **48,** 145-155.

Potts P. J., Webb P. C., and Watson J. S. (1985b) Energy-dispersive X-Ray-fluorescence analysis of silicate rocks - comparisons with wavelength-dispersive performance. *Analyst,* **110,** No.5, 507-513.

Pyle, D. M.; Dawson, J. B.and Ivanovich, M. (1991) Short-lived decay series disequilibria in the natrocarbonatite lavas of Oldoinyo Lengai, Tanzania; constraints on the timing of magma genesis. *Earth and Planetary Science Letters* **105,** 378-396.

Pyle D.M., Ivanovich M. and Sparks R. S. J. (1988) Magma-cumulate mixing identified by U-Th disequilibrium dating. *Nature* **331,** 157-159.

Pyle D. M. (1992) The volume and residence time of magma beneath active volcanoes deteremined by decay series disequilibria methods *Earth and Planetary Science Letters* **112,** 61-73.

Pyle D.M (1994) Isotope disequilibrium studies and magmatic processes. *Geoscientist* **4,** 18-20.

Qin Z. (1993) Dynamics of melt generation beneath mid ocean ridge axes: Theoretical analysis based on ^{238}U-^{230}Th-^{226}Ra and ^{235}U-^{231}Pa disequilibrium. *Geochim. Cosmochim. Acta* **57,** 1629-1634.

Raudsepp M., Turnock A. C. and Hawthorne F. C. (1991) Ti: Amphibole Synthesis At Low-Pressure - What Grows And What Doesnt. *European Journal of Mineralogy*, **3,** 983-1004.

Reinitz I. and Turekian K. K. (1989) $^{230}Th/^{238}U$ and $^{226}Ra/^{230}Th$ fractionation in young basaltic glasses from East Pacific Rise. *Earth and Planetary Science Letters* **94,** 199-207

Richardson C. and McKenzie D. (1994) Radioactive disequilibria from 2D models of melt generation by plumes and ridges. *Earth and Planetary Science Letters* **128,** 425-437.

Ridley I. (1970) The petrology of the Las Cañadas volcanoes, Tenerife, Canary Islands. *Contribution to Mineralogy and Petrology* **26,** 124-160.

Ridley I., (1970b) The origin of some collapse structures in the Canary Islands. *Geological Magazine* **108,** 477-484.

Ridley I. (1971) The field relations of the Las Cañadas volcanoes, Tenerife, Canary Islands. *Bull. Volcanol.* **35,** 318-335.

Robinson J. A. C. and Wood B.J. (1998) The depth of the spinel to garnet transition at the peridotite solidus. *Earth Planet. Sci. Lett.* **164,** No.1-2, 277-284.

Robinson J.A.C., Wood B.J. and Blundy J.D. (1998) The beginning of melting of fertile and depleted peridotite at 1.5 Gpa. *Earth Planet. Sci. Lett.* **155,** 1-2,97-111.

Roedder P. L. and Emslie R. F. (1970) Olivine liquid equilibrium. *Contributions to Mineralogy and Petrology* **29,** 275-289.

Roest W. R., Dañobeitia J. J., Verhoef J. and Collette B. J. (1992) Magnetic anomalies in the Canary Basin and the Mesozoic evolution of the Central North Atlantic. *Marine Geophys. Res.* **14,** 1-24.

Rogers N. W., Hawkesworth C.J. and Palacz Z. A. (1992) Phlogopite in the generation of olivine melilitites from Namaqualand, South Africa and implications for element fractionation processes in upper mantle. *Lithos* **23,** 347-365.

Rogers N. W., Hawkesworth C. J. and Ormerod D. S. (1995) Late Cenozic basaltic magmatism in the Western Great Basin California and Nevada. *J. Geophys.Res.* **100,** No B7, 10287-10301.

Rollinson H. (1993) Using geochemical data: evaluation, presentation, interpretation. Longman.

Rothe P. and Schmincke H-U. (1968) Constrasting origins of the eastern and western islands of the Canarian archipelago. *Nature* **210,** 1151-1154.

Rubin K. H and Macdougall J. D. (1988) ^{226}Ra excesses in mid ocean ridges basalts and mantle melting *Nature* **335,** 158-161.

Rubin K. H. and Macdougll J. D. (1992) Th-Sr isotopic relationships in MORB *Earth and Planetary Science Letters* **114,** 149-157.

Rutherford E. and Siddy F. (1902) The radioactivity of Thorium compounds II. The cause and nature of radioactivity. *J. Chem. Soc. Lond.* **81,** 837-860.

Ryan M.P. (1987) Neutral buoyancy and the mechanical evolution of magmatic systems. In Magmatic Processes: *Physico-chemical Principles,* ed. Mysen B.O. pp 259-87 University Park, Pa. *Geochemical Society of America.*

Saunders A. D., Norry M. J. and Tarney J. (1988) Origin of MORB and chemically-depleted mantle reservoirs: trace element constraints. *Journal of Petrology Special lithosphere issue* 415-445.

Scarrow J. H. and Cox K. G. (1995) Basalts generated by decompressive adiabatic melting of a mantle plume: a case study from the Isle of Skye, NW Scotland. *Journal of Petrology* **36,** 3-22.

Schmincke H-U (1973) Magmatic evolution and tectonic regime in the Canary, Madeira and Azores Island Groups. *Geol. Soc. Am. Bull.* **84,** 633-648.

Schmincke H-U. (1982) Volcanic and chemical evolution of the Canary Islands. In: V.von Rad et al. (eds) *Evolution of the Passive Margin of NW Africa* Springer, Heidelberg 273-306.

Schick R., Cosentino M., Lambardo G. and Patane G. (1982) Volcano tremor at Mount Etna; a brief description. *Mem. Soc. Geol. Ital.* **23,** 191-196.

Shaw D. (1970) Trace element fractionation during anatexis. *Geochem. Cosmochim. Acta.* **34,** 237-243.

Shen Y. and Forsyth D. W. (1995) Geochemical constraints on initial and final depths of melting beneath mid-ocean ridges. *J. Geophys. Res.* **100,** B2 2211-2237.

Shirey S. B., Bender J. F. and Langmuir C. H. (1987) Three component isotopic heterogeneity near the Oceanographer transform, Mid Atlantic Ridge. *Nature* **325,** 217-223.

Sigmarsson O., Carn S. and Carracedo J-C. (1998) Systematics of U series nuclides in primitive lavas from the 1730-36 eruption on Lanzarote, Canary Islands and implications for the role of garnet pyroxenites during oceanic basalt formation. *Earth and Planetary Science Letters* **162,** 137-151.

Sigmarsson O., Condomines M. and Ibarrola E. (1992) ^{238}U-^{230}Th radioactive disequilibria in historic lavas from the Canary Islands and genetic implications. *J. Volcanol. Geotherm. Res.* **54,** 145-156.

Sigmarsson O. (1996) Short magma chamber residence time at an Icelandic volcano inferred from U-series disequilibria. *Nature* **382,** 440-442.

Sims K., DePaolo D. J., Murrell M. T., Baldridge W. S., Goldstein S. J. and Clague D. A. (1995) Mechanisms of magma generation beneath Hawaii and Mid-Ocean Ridges: Uranium/Thorium and Samarium/Neodymium isotopic evidence. *Science* **367,** 508-512.

Sims K.W.W. and DePaolo D.J. (1997) Inferences about mantle sources from incompatible element concentration ratios in oceanic basalts. *Geochim. Cosmochim. Acta* **61,** 765-784.

Sleep, N.H. (1990) Hotspots and mantle plumes: some phenomenology. *J. Geophys. Res.* **95,** B5, 6715-6736.

Soler V., Carracedo J-C. and Heller F. (1984) Geomagnetic secular variation in historical lavas from the Canary Islands. *Geophys. Roy. Astron. Soc.* **78,** 313-318.

Sparks R. S. J., Meyer P. and Sigurdsson H. (1980) Density variations amongst mid ocean ridge basalts; implications for magma mixing and the scarcity of primitive lavas *Earth and Planetary Science Letters* **46,** 419-430.

Spiegelman M. and Elliott T. (1993) Consequences of melt transport for uranium series disequilibrium in young lavas. *Earth and Planetary Science Letters* **118,** 1-20.

Stein M. and Hofmann A. W. (1992) Fossil plume head beneath the Arabian lithosphere ? *Earth and Planetary Science Letters* **114,** 193-209.

Stein, M. and Hofmann, A. W. (1994) Mantle plumes and episodic crustal growth. Nature 372, 63-68.

Stillman C. J., Fuster J., Bennel-Baker M, Muñoz M, Smeweing J and Sagredo J. (1975) Basal complex of Fuerteventura is an oceanic intrusive complex with rift-system affinities. *Nature* **257,** 469-471.

Stillman C. J. (1993) A Canary Islands Dyke Swarm :Implications for the formation of oceanic islands by extensional fissure volcanism. In. Hall H. C. and Fahrig W. F.(eds.) *Mafic Dyke Swarms. Geol Ass of Canada Spec Paper* **34,** 243-255.

Storedtvedt U. M., Sralestad S., Yhomassen K., Langlie A. A., Nergård A. and Gidskehaug, A. (1979) Magnetic discordance in Gran Canaria/Tenerife and its possible relevance to the formation of the northwest African continental margin. *J. Geophys. Res.* **44,** 317-332.

Storey M., Wolff J. A., Norry M. J. and Marriner G. F. (1989) Origin of hybrid lavas from Agua de Pau volcano, San Miguel, Azores. In Saunders,A.D. and Norry, M.J. (eds.) *Magmatism in Ocean Basins Geol.Soc.Spec.Pub.* **42,** 161-180.

Strelow F.W.E. (1960) An ion exchange selectivity scale of cations based on equilirium distribution coefficients. *Analytical Chemistry* **32-9,** 1185-1188.

Sun S-S and McDonough W.F. (1989) Chemical and isotope systematics of oceanic basalts; implications for mantle composition and processes. In Saunders A.D. and Norry M.J. (eds.) *Magmatism in the ocean basins, Geol. Soc. Spec. Publ.* **42,** 313-345.

Tait S., Jaupart C. and Vergniolle S. (1989) Pressure, gas content and eruption periodicity of a shallow crystallising magma chamber. *Earth and Planetary Science Letters* **92,** 107-123.

Thirlwall M. F., Upton B. G. J. and Jenkins C. (1994) Interaction between continental lithosphere and Iceland plume Sr-Nd-Pb isotope geochemistry of Tertiary Basalts, NE Greenland. *Journal of Petrology* **35,** 839-879.

Thirlwall M.F. (1997) Thermal Ionisation Mass spectrometry (TIMS). In *Analytical Geochemistry Techniques* (ed R.Gill) Longman.

Thirlwall M.F. (1997b) Pb Isotopic and elemental evidence for OIB derivation from young HIMU mantle. *Chemical Geology* **139,** 51-74.

Thirlwall M., Jenkins C., Vroon P.Z. and Mattey D.P. (1997) Crustal interaction during construction of ocean islands: Pb-Sr-Nd-O isotope geochemistry of the shield basalts of Gran Canaria, Canary Islands. *Chemical Geology* **135,** 233-262.

Thomas L. Hawkesworth C.J. van Calsteren P., Turner S.P., and Rogers N.W. (1999) in press. Melt Generation beneath ocean islands: a U-Th-Ra isotope study from Lanzarote in the Canary Islands. *Geochimica et Cosmochimica Acta Special Volume for C. Allègre.*

Thompson R. N. (1987) Phase-equilibrium constraints on genesis and magmatic evolution of oceanic basalts. *Earth Science Reviews* **24,** 161-210.

Turner S. (1994) Continetal Basalts Isotope and trace element geochemisty course at O.U.

Turner S. P. and Hawkesworth C. J. (1995) The nature of the sub-continental mantle: constraints from the major element compositions of continental flood basalts. *Chemical Geology* **120,** 295-314.

Turner S., Hawkesworth C. J., van Calsteren P., Heath E., MacDonald R. and Black S. (1996) U-series isotopes and destructive plate margin magma genesis in the Lesser Antilles. *Earth and Planetary Science Letters* **142,** 191-207.

Turner S. and Hawkesworth C. (1997) Constraints on flux rates and mantle dynamics beneath island arcs from Tonga-Kermadec lava geochemistry. *Nature* **389,** 568-573.

Turner S., Hawkesworth C., Rogers N. and King P. (1997) U-Th isotope disequilibria and ocean island basalt generation in the Azores. *Chemical Geology* **139,** 145-164.

Turner S. P., Hawkesworth C. J., Rogers N., Barlett J., Wothington T., Hergt J., Pearce J., and Smith I. (1997b) ^{238}U-^{230}Th disequilibria, magma petrogenesis and flux rates beneath the depleted Tonga-Kermadec island arc. *Geochim. Cosmochim. Acta* **61**(22), 4855-4884.

Turner S. P., Platt J. P., George R. M. M., Kelley S. P., Pearson D. G. and Nowell G. M. (1998 submitted) Magmatism associated with orogenic collapse of the Betic-Alboran domain, SE Spain. Submitted to*Journal of Petrology March 1998*

Valentin A. (1990) Geochemical and geothermal constraints on magma bodies associated with historic activity, Tenerife, Canary Islands. *J. Volc. Geotherm. Res.,* **44,** 251-264.

van Calsteren P. and Schwieters J. B. (1995) Performance of a thermal ionisation mass spectrometer with a deceleration lens system and post-deceleration detector selection, *Int. J. Mass Spec. and Ion Processes*, **146/147,** 119-129.

van Calsteren P. and Hawkesworth C. J. (1999) (in prep) New insights into magmagenesis from a Modal Dynamic Melting model.

Vance D., Stone J. O. H. and O'Nions R. K. (1989) He, Sr and Nd isotopes in xenoliths from Hawaii and other oceanic islands. *Earth and Planetary Science Letters* **96,** 147-160.

Vannucci R., Bottazzi P., Wulff-Pedersen E., and Neumann E.-R. (1998) Partitioning of REE, Y, Sr, Zrand Ti between clinopyroxene and silicate melts in the mantle under La Palma (Canary Islands); Implication for the nature of the metasomatic agents. *Earth and Planetary Science Letters* **158**, 39-51.

Verhoef J. Collette B. J., Dañobeitia J. J. Roeser H. A. & Roest W. R. (1991) Magnetic anomalies off West Africa (20-38°N). *Marine Geophysical Res.* **13,** 81-103.

Villemant B., Boudon G., Komorowski, J-C. (1996) U-Series disequilibrium in arc magmas induced by water-magma interaction. *Earth and Planetary Science Letters* **140,** 259-267.

Volpe A. M. and Hammond P. E. (1991) ^{238}U-^{230}Th-^{226}Ra disequilibria in young Mt. St. Helens rocks: time constraint for magma formation and crystallisation. *Earth and Planetary Science Letters* **107,** 475-486.

Volpe A.M., Olivares J.A. and Murrell M.T.(1991) Determination of Radium isotope ratios and abundances in geological sample by TIMS. *Analytical Chemistry* **63,** 913-916.

Volpe A. M. (1992) ^{238}U-^{230}Th-^{226}Ra disequilibrium in young Mt Shasta andesites and dacites. *J. Volc. Geothermal. Res.* **53**, 227-228.

Volpe A. M. and Goldstein S. J. (1993) ^{226}Ra-^{230}Th disequilibrium in axial and off-axial mid-ocean ridge basalts. *Geochim. Cosmochim. Acta* **57,** 1233-1241.

Von Buch (1825) Physikalische Beschreibung der canarischen Inseln, Berlin. Translated In A source book in geology. (ed. Mather K. F. and Mason S. L.) 1970 - 1st Harvard University Press Printing.

Wager L.R. and Deer W.A. (1939) Geological investigations in East Greenland Part III. The petrology of the Skaergaard intrusion, Kangerdlugssuaq, East Greenland. *Medd, om Grønland* **105,** no 4, 1-352.

Watson E.B. (1979) Zircon saturation in felsic liquids: experimental results and applications to trace element geochemistry. *Contributions to Mineralogy and Petrology* **70,** 407-419.

Watson J.S. (1996) Fast, simple method of powder pellet preparation for x-ray fluorescence analysis. *X-Ray spectrometry* **25,** 173-174.

Watson S. and McKenzie D. (1991) Melt generation by plumes: a study of Hawaiian volcanism. *Joutnal of Petrology* **32,** 501-537.

Watts A. B. and Masson D. G. (1995) A giant landslide on the north flank of Tenerife, Canary Islands. *J. Geophys. Res.* **100**(B12), 24,487-24,498.

Watts A. B., Peirce C., Collier J., Dalwood R., Canales J. P., and Henstock T. J. (1997) A seismic study of lithospheric flexure in the vicinity of Tenerife, Canary Islands. *Earth and Planetary Science Letters* **146**, 431-447.

Weaver B.L. (1991) The origin of oceanic island basalt end member compositions; trace element and isotopic constraints. *Earth and Planetary Science Letters* **104,** 381-397.

Weaver B.L. (1991b) Trace element evidence for the origin of ocean island basalts. *Geology* **19,** 123-126.

White R.S. (1993) Melt production rates in mantle plumes. *Phil. Trans. R. Soc. Lon.* A. **342,** 137-153.

White W. M. and Hofmann A. W. (1982) Mantle heterogeneity and isotopes in oceanic basalts. *Nature* **295,** 363-364.

White W.M. and Hofmann A.W. (1982b) Sr and Nd isotope geochemistry of oceanic basalts and mantle evolution. *Nature* **296,** 821-825.

White W., McBirney A. R. and Duncan R.A. (1993) Petrology and geochemistry of the Galapagos Islands: portrait of a pathological mantle plume. *J. Geophys. Res.* **98,** 19,533-19,563.

White R. S. and McKenzie D. (1995) Mantle plumes and flood basalts. *J. Geophysical Research, B, Solid Earth and Planets,* **100,** 17,543-17,585.

Whitehouse M. J. and Neumann E-R. (1995) Sr-Nd-Pb isotope data for ultramafic xenoliths from Hierro, Canary Islands: Melt infiltration processes in the upper mantle. *Contrib. Min. Pet.* **119**, 239-246.

Widom, E., Schmincke, H. U. and Gill J. B. (1992) Processes and timescales in the evolution of chemically zoned trachyte; Fogo A, Sao Miguel, Azores. *Contributions to Mineralogy and Petrology* **111,** 311-328.

Widom E., Carlson R. W., Gill J. B. and Schmincke H.-U. (1997) Th-Sr-Nd-Pb isotope and trace element evidence for the origin of the Sao Miguel, Azores, enriched source. *Chem. Geol.* **140**, 49-68.

Wilding M., Webb S., Dingwell D., Ablay G. and Marti J. (1996) Cooling rate variations in natural volcanic glasses from Tenerife, Canary Islands. *Contrib. Min. Pet.* **125**, 151-160.

Williams R. W. and Gill J. B. (1989) Effects of partial melting on uranium decay series. *Geochim. Cosmochim. Acta.* **53,** 1607-1619.

Williams R. W. and Gill J. B. (1992) Th isotope and U series disequilibria in some alkali basalts. *Geophys. Res. Lett.* **19,** 139-142.

Wilson J. T. (1963) A possible origin of the Hawaiian islands. *Can. J. Phys.* **41,** 863-870.

Wilson J. T (1965) Evidence from oceanic islands suggesting movement in the earth. *Roy. Soc. Lond. Philos. Trans.* **258,** 145-167.

Wilson M. (1989) *Igneous Petrogenesis: A Global Tectonic approach.* Harper Collins

Wilson M. Downes H and Cebriá J.-M. (1995) Constrasting fractionation trends in co-existing continetal alklaine magma series; Cantal, Massif Central, France. *Journal of Petrology* **36,** 1729-1753.

Wilson, R.M. (1935) Ground surface movement at Kilauea volcano, Hawaii. *Hawaii Res. Publ.* **10.**

Wolff J. A. (1985) Zonation, mixing and eruption of silica undersaturated alkaline magma: a case study from Tenerife, Canary Islands. *Geol. Mag.* **122,** 623-640.

Wolff J. A., Wörner G. and Blake S. (1990) Gradients in physical parameters in zoned felsic magma bodies: implications from evolution and eruptive withdrawal. *J. Volcanol. Geotherm. Res.* **43,** 37-55.

Wulff-Pedersen E., Neumann E.-R., and Jensen B. B. (1996) The upper mantle under La Palma, Canary Islands: formation of Si-K-Na rich melt and its importance as a metasomatic agent. *Contrib. Min. Pet.* **125,** 113-139.

Yang H.-J., Sen G., and Shimizu N. (1998) Mid-Ocean Ridge Melting: Constraints from Lithospheric Xenoliths at Oahu, Hawaii. *Journal of Petrology* **39,** 277-295.

Zellmer G. (1998) Appendix A of Thesis : Radium Analysis. Ph.D., The Open University.

Zindler A. and Hart S. (1986) Chemical geodynamics. *Annu. Rev. Earth and Planetary Science Letters* **14,** 493-571.

Zou H. and Zindler A. (1996) Constraints on the degree of dynamic partial melting and source composition using concentration ratios in magmas. *Geochim et Cosmochim Acta* **60,** 711-717.

List of Appendices

A. Geochemical Data Tables, including calculation of Mg# and fractionation corrections.

A.1. Major, trace element and isotopic data of historic to recent pre-historic lavas from Lanzarote.

A.2. Major, trace element and isotopic data from the Teide-Pico Viejo Complex from Tenerife.

B. Localities, mineralogy and petrology of individual samples

C. Analytical Techniques

D. U-Th-Ra Standards

E. Ra Techniques (extended)

F. Table of partition coefficients, OIB and MORB values used in Chapters 4 and 5.

G. New Straigraphy for Teide-Pico Viejo complex

H. Age Correction calculations for U-series disequilibrium

I. Published abstracts

APPENDIX A

Geochemical Data Tables

The following tables list the whole rock major, trace, rare earth element and Sr, Nd, Pb, U, Th and Ra isotopic data aquired for the Lanzarote and Tenerife suites of lavas. The lavas are divided according to sample location into the separate islands (A.1. Lanzarote; A.2. Tenerife) and then sub-divided into age groups - lithologies.

The total iron content is expressed as Fe_2O_3 throughout, and the Mg # is calculated using the following equation:

$$Mg\# = \left(\frac{Mg^{2+}}{\left(Mg^{2+} + Fe^{2+}\right)} \right) * 100$$

using the molecular weights of MgO and FeO (Wt %) (40.32 and 71.85 respectively) to calculate Mg^{2+} and Fe^{2+}.

The olivine fractionation corrections were as follows

The total Fe_2O_3 was separated into FeO and Fe_2O_3

FeO = ((((Fe_2O_3/159.7) *0.8)*2*71.85)

$Fe_2O_3 = Fe_2O_{3Total}$ * 0.2

The major elements were normalised to 100% and the Mg # was calculated as above.

An olivine composition in equilibrium with a primitive mantle was used and the Fe/Mg ratio and the Mg# of olivine was calculated, then the % of Fosterite to Fayalite was calculated.

This was added to the major element composition (+ Ni, Cr) until an Mg# of 70 (the lowest mantle value) was reached. Each % of olivine added increased the Mg# of the rock. Some of the samples were already above Mg# of 70, a range of Mg# of between 70 and 75 is given for melts in equilibrium with mantle olivines.

Age Group	*Basement*	*Famara Grp*	*Corona*	*Corona*	*Corona*
Volcano		Famara Massif	Mña del Corona	Mña del Corona	Mña del Corona
Sample #	**L1-30-2**	**L1-28-4**	**LAN11**	**LAN12**	**LAN13**
SiO_2	40.84	43.17	45.65	45.77	47.93
TiO_2	3.55	2.92	2.50	2.77	2.38
Al_2O_3	11.97	12.85	12.44	12.72	13.28
Fe_2O_3	12.74	11.89	12.30	12.56	12.05
MnO	0.18	0.18	0.17	0.17	0.17
MgO	13.36	11.54	11.67	11.22	9.97
CaO	11.55	10.68	10.50	10.42	10.18
Na_2O	2.95	3.10	3.23	3.12	3.25
K_2O	0.53	0.69	0.98	1.12	0.82
P_2O_5	0.70	0.64	0.76	0.62	0.57
S%	0.02	0.02	0.00	0.00	0.00
LOI	1.43	2.64	-0.01	0.00	0.00
Total	99.82	100.30	100.19	100.49	100.60
Mg *	72.2	70.6	70.0	69.0	67.0
XRF					
Rb	8	16	22	26	17
Sr	707	769	878	761	736
Y	27	29	29	27	28
Zr	251	325	225	236	195
Nb	68	73	63	58	47
Ba	542	498	470	429	346
Pb	4	5	7	2	4
Th	8	7	6	5	7
Sc	33	26	26	24	20
V	356	278	217	234	209
Cr	544	649	455	435	456
Co	65	62	55	57	55
Ni	302	296	276	261	258
Cu	79	67	79	87	70
Zn	88	92	103	103	115
Ga	18	17	21	20	20
S	34	39	31	27	26
INAA Data					
La			56.9	44.5	45.8
Ce			113	90.3	89.9
Nd			51.4	42.6	43.2
Sm			9.61	8.48	8.46
Eu			3.03	2.74	2.68
Tb			1.14	1.02	1.06
Yb			1.90	1.89	1.86
Lu			0.26	0.25	0.25
Th			6.11	4.99	5.11
U			1.8		1.4
Ta			3.55	3.71	2.79
Hf			4.92	5.20	4.46
Cs			0.36	0.24	0.20
Rb					
Zn			103	133	109
Co			52.2	52.2	48.4
Cr			485	434	396
Sc			23.8	24.1	23.5

Age Group	*Basement*	*Famara Grp*	*Corona*	*Corona*	*Corona*
Volcano		Famara Massif	Mña del Corona	Mña del Corona	Mña del Corona
Sample #	**L1-30-2**	**L1-28-4**	**LAN11**	**LAN12**	**LAN13**
I.D.					
U			1.554	0.883	1.296
Th			6.110	4.990	5.110
Isotopes					
$^{87}Sr/^{86}Sr$			0.703184	0.703274	0.703255
$^{143}Nd/^{144}Nd$			0.512473	0.512783	0.512828
$^{206}Pb/^{204}Pb$			19.150	19.085	19.264
$^{207}Pb/^{204}Pb$			15.545	15.534	15.517
$^{208}Pb/^{204}Pb$			38.906	38.837	38.961
$(^{230}Th/^{238}U)$			1.762	1.637	1.070
$(^{238}U/^{232}Th)$			0.568	0.780	0.879
$(^{230}Th/^{232}Th)$			1.001	1.277	0.941
$(^{234}U/^{238}U)$			1.003	-	1.003
$(^{226}Ra/^{230}Th)$			1.001	1.0001	1.000
^{232}Th (nmol.g-1)					
^{230}Th (fmol.g-1)					
^{226}Ra					

Age Group	*Corona*	*Corona*	*Corona*	*1730-36 Phase 1*	*1730-36 Phase 2*
Volcano	Mña del Corona	Mña del Corona	Mña del Corona	Pico Partido	
Sample #	**L1-25-1**	**L1-25-6**	**L1-25-7**	**L1-27-1**	**LAN17**
SiO_2	46.09	46.53	45.96	50.45	49.07
TiO_2	2.67	2.66	2.64	2.32	2.44
Al_2O_3	12.81	12.85	12.69	13.24	13.14
Fe_2O_3	12.65	12.28	12.20	11.47	11.88
MnO	0.17	0.17	0.17	0.15	0.16
MgO	11.04	10.82	10.79	9.85	10.25
CaO	10.17	10.45	10.40	9.27	9.51
Na_2O	3.16	2.98	2.97	2.91	2.99
K_2O	1.04	1.03	1.04	0.64	0.77
P_2O_5	0.64	0.56	0.58	0.36	0.40
S%	0.02	0.09	0.17	0.02	0.00
LOI	-0.08	0.21	0.45	-0.24	-0.01
Total	100.38	100.62	100.05	100.44	100.59
Mg *	68.3	68.6	68.6	68.1	68.0
XRF					
Rb	23	24	23	18	17
Sr	684	650	663	583	494
Y	27	25	24	24	22
Zr	232	219	221	220	200
Nb	57	51	53	48	40
Ba	408	389	389	314	246
Pb	3	5	2	2	3
Th	4	7	7	6	3
Sc	27	25	21	22	24
V	236	225	224	217	204
Cr	431	431	436	445	431
Co	58	58	55	54	55
Ni	258	243	246	275	256
Cu	85	77	73	76	89
Zn	111	106	108	108	110
Ga	20	20	18	20	19
S	35	977	2207	47	23
INAA Data					
La	41.8	39.0	39.6	22.2	25.3
Ce	81.9	77.3	80.7	45.8	53.5
Nd	41.9	39.9	39.5	25.4	28.9
Sm	8.44	7.98	8.00	6.08	6.39
Eu	2.71	2.54	2.57	2.06	2.13
Tb	1.04	1.01	1.01	0.88	0.90
Yb	1.95	1.70	1.92	1.62	1.75
Lu	0.26	0.24	0.27	0.24	0.24
Th	4.64	4.38	4.53	2.34	2.85
U	1.3	1.5	1.4		0.6
Ta	3.46	3.27	3.30	2.13	2.91
Hf	5.30	5.06	5.36	4.54	4.69
Cs	0.2	0.3	0.3	0.3	0.25
Rb					
Zn	111	112	101	129	119
Co	53.5	51.6	51.6	49.4	49.7
Cr	439	427	441	442	446
Sc	23.7	24.5	24.1	22.4	22.8

Age Group	*Corona*	*Corona*	*Corona*	*1730-36 Phase I*	*1730-36 Phase 2*
Volcano	Mña del Corona	Mña del Corona	Mña del Corona	Pico Partido	
Sample #	**L1-25-1**	**L1-25-6**	**L1-25-7**	**L1-27-1**	**LAN17**
I.D.					
U	1.1162	1.1162	1.1318	0.5794	0.648
Th	4.2415	4.9104	3.4369	2.1245	2.850
Isotopes					
$^{87}Sr/^{86}Sr$					0.703195
$^{143}Nd/^{144}Nd$					
$^{206}Pb/^{204}Pb$					19.090
$^{207}Pb/^{204}Pb$					15.539
$^{208}Pb/^{204}Pb$					38.843
$(^{230}Th/^{238}U)$	1.174	1.416		1.268	1.444
$(^{238}U/^{232}Th)$	0.799	0.690		0.827	0.775
$(^{230}Th/^{232}Th)$	0.938	0.977		1.049	1.119
$(^{234}U/^{238}U)$	1.029	10.304		1.006	-
$(^{226}Ra/^{230}Th)$					-
	18.279				
	92.215				

Age Group	*1730-36 Phase 3*	*1730-36 Phase 3*	*1730-36 Phase 3*	*1730-36 Phase 3*	*1730-36 Phase 3*
Volcano	Mña Rajada	Mña Rajada	Mña Rajada	Mña Rajada	Mña Rajada
Sample #	**LAN1**	**LAN2**	**L1-26-6**	**L1-26-1**	**L1-26-2**
SiO_2	49.34	49.45	43.04	51.14	48.45
TiO_2	2.52	2.51	3.01	2.19	2.72
Al_2O_3	13.30	13.39	11.65	12.68	12.93
Fe_2O_3	12.09	11.98	13.15	11.19	12.19
MnO	0.15	0.16	0.19	0.14	0.16
MgO	9.91	9.81	14.64	10.99	10.52
CaO	9.30	9.37	9.94	8.64	9.53
Na_2O	3.01	2.97	2.97	2.79	3.01
K_2O	0.78	0.77	1.49	0.64	0.89
P_2O_5	0.36	0.35	0.79	0.33	0.45
S%	0.00	0.00	0.03	0.02	0.03
LOI	0.00	-0.01	-0.31	-0.34	-0.34
Total	100.76	100.75	100.58	100.40	100.55
Mg *	67.0	67.0	73.4	70.8	68.1
XRF					
Rb	17	16	35	14	17
Sr	449	448	736	397	518
Y	22	23	26	22	23
Zr	193	191	275	177	216
Nb	35	36	79	30	43
Ba	221	225	536	205	277
Pb	1	2	4	0	1
Th	1	1	7	1	3
Sc	20	23	26	20	21
V	206	199	262	179	206
Cr	386	385	549	537	438
Co	51	50	65	58	57
Ni	231	231	444	373	257
Cu	86	85	70	88	80
Zn	106	107	103	103	104
Ga	21	21	19	18	20
S	36	23	41	27	40
INAA Data					
La	20.3	20.1	54.0		28.8
Ce	43.5	42.4	107		61.2
Nd	24.3	23.8	49.1		32.6
Sm	5.90	5.80	9.19		7.06
Eu	2.03	1.99	2.80		2.36
Tb	0.89	0.85	1.05		0.99
Yb	1.58	1.56	1.94		1.74
Lu	0.22	0.21	0.26		0.26
Th	2.04	2.02	5.73		2.93
U	0.4	0.5	1.3		1.1
Ta	2.48	2.39	4.70		2.97
Hf	4.53	4.53	6.28		5.48
Cs	0.31	0.19	0.4		
Rb	27	23			
Zn	111	93	106		165
Co	49.6	49.8	61.3		52.1
Cr	406	410	573		465
Sc	22.5	22.6	24.2		23.1

Age Group	*1730-36 Phase 3*	*1730-36 Phase 3*	*1730-36 Phase 3*	*1730-36 Phase 3*	*1730-36 Phase 3*
Volcano	Mña Rajada	Mña Rajada	Mña Rajada	Mña Rajada	Mña Rajada
Sample #	**LAN1**	**LAN2**	**L1-26-6**	**L1-26-1**	**L1-26-2**
I.D.					
U	0.586	0.492			
Th	2.040	2.020			
Isotopes					
$^{87}Sr/^{86}Sr$	0.703217	0.703209			
$^{143}Nd/^{144}Nd$	0.512815	0.512740			
$^{206}Pb/^{204}Pb$	19.063	19.045			
$^{207}Pb/^{204}Pb$	15.555	15.534			
$^{208}Pb/^{204}Pb$	38.831	38.808			
$(^{230}Th/^{238}U)$	1.038	1.194			
$(^{238}U/^{232}Th)$	0.935	0.788			
$(^{230}Th/^{232}Th)$	0.971	0.940			
$(^{234}U/^{238}U)$	1.003	1.004			
$(^{226}Ra/^{230}Th)$	-	-			

Age Group	*1730-36 Phase 3*	*1730-36 Phase 4*	*1730-36 Phase 4*	*1730-36 Phase 4*	*1730-36 Phase 4*
Volcano	Mña Quemadas	Mña del Fuego	Mña del Fuego	Mña del Fuego	Mña del Fuego
Sample #	**L1-26-7**	**LAN3**	**LAN4**	**LAN5**	**L1-26-8**
SiO_2	48.21	49.85	49.66	49.74	47.72
TiO_2	2.52	2.42	2.39	2.28	2.43
Al_2O_3	13.03	13.25	13.24	13.43	13.01
Fe_2O_3	12.11	11.82	11.81	11.68	12.20
MnO	0.16	0.15	0.15	0.15	0.17
MgO	10.66	9.79	9.93	9.82	11.02
CaO	9.50	9.26	9.30	9.49	9.88
Na_2O	3.03	2.90	2.90	2.95	3.13
K_2O	0.86	0.73	0.71	0.68	0.87
P_2O_5	0.46	0.32	0.33	0.38	0.55
S%	0.02	0.00	0.00	0.01	0.03
LOI	-0.37	0.00	0.00	0.00	-0.18
Total	100.19	100.48	100.42	100.60	100.83
Mg *	68.5	67.0	68.0	68.0	69.1
XRF					
Rb	17	16	15	15	18
Sr	506	420	430	450	591
Y	23	22	22	22	25
Zr	210	187	189	183	221
Nb	42	34	34	36	49
Ba	288	217	206	221	324
Pb	1	2	0	1	0
Th	5	2	3	3	1
Sc	23	21	27	22	24
V	209	201	202	186	218
Cr	435	407	413	383	450
Co	55	53	54	52	55
Ni	266	243	231	229	272
Cu	79	89	91	96	79
Zn	106	108	108	104	108
Ga	19	20	21	20	18
S	33	23	23	27	42
INAA Data					
La		17.9	18.2	22.5	
Ce		39.4	39.6	47.1	
Nd		22.7	23.4	25.7	
Sm		5.56	5.65	5.80	
Eu		1.95	1.97	2.00	
Tb		0.84	0.82	0.85	
Yb		1.55	1.49	1.57	
Lu		0.22	0.21	0.21	
Th		1.90	1.98	2.35	
U		0.5	0.8	0.7	
Ta		2.33	2.35	2.39	
Hf		4.45	4.57	4.30	
Cs		0.23	0.31	0.25	
Rb		16	29		
Zn		91	92	97	
Co		47.5	48.4	48.7	
Cr		421	425	414	
Sc		22.0	22.2	22.9	

Age Group	*1730-36 Phase 3*	*1730-36 Phase 4*	*1730-36 Phase 4*	*1730-36 Phase 4*	*1730-36 Phase 4*
Volcano	Mña Quemadas	Mña del Fuego	Mña del Fuego	Mña del Fuego	Mña del Fuego
Sample #	**L1-26-7**	**LAN3**	**LAN4**	**LAN5**	**L1-26-8**
I.D.					
U	0.7011	0.470	0.486	0.562	1.0292
Th	2.6167	1.896	1.980	2.350	3.7404
Isotopes					
$^{87}Sr/^{86}Sr$		0.703183	0.703179	0.703169	
$^{143}Nd/^{144}Nd$		0.512851	0.512828	0.512864	
$^{206}Pb/^{204}Pb$		18.995	19.005	19.107	
$^{207}Pb/^{204}Pb$		15.508	15.498	15.514	
$^{208}Pb/^{204}Pb$		38.703	38.686	38.811	
$(^{230}Th/^{238}U)$	1.159	1.145	1.186	1.143	1.168
$(^{238}U/^{232}Th)$	0.813	0.816	0.796	0.813	0.835
$(^{230}Th/^{232}Th)$	0.942	0.934	0.945	0.930	0.975
$(^{234}U/^{238}U)$	1.007	1.003	1.000	1.004	1.000
$(^{226}Ra/^{230}Th)$		-	1.492	1.592	
	11.277				
	57.165				

Age Group	*1730-36 Phase 4*	*1730-36 Phase 5*	*1730-36 Phase 5*	*1730-36 Phase 5*	*1730-36 Phase 5*
Volcano	Mña del Fuego	Mña de Las Nueces	Mña Colorada	Mña Colorada	Mña Colorada
Sample #	**L1-30-1**	**LAN6**	**LAN7**	**LAN8**	**LAN9**
SiO_2	44.29	49.46	50.49	50.75	50.62
TiO_2	2.70	2.43	2.29	2.30	2.30
Al_2O_3	11.83	13.23	13.37	13.34	13.26
Fe_2O_3	12.42	11.75	11.45	11.45	11.39
MnO	0.18	0.15	0.15	0.15	0.14
MgO	13.55	9.78	9.38	9.81	9.89
CaO	10.65	9.47	9.20	9.12	9.15
Na_2O	3.15	3.01	2.96	2.94	2.96
K_2O	1.22	0.70	0.61	0.62	0.61
P_2O_5	0.92	0.43	0.34	0.32	0.34
S%	0.03	0.00	0.00	0.00	0.01
LOI	-0.29	0.00	0.00	0.00	0.00
Total	100.64	100.41	100.23	100.79	100.66
Mg *	71.0	67.0	67.0	68.0	68.0
XRF					
Rb	26	15	13	14	13
Sr	858	550	438	424	436
Y	29	26	23	22	23
Zr	297	201	180	178	180
Nb	79	38	32	31	33
Ba	507	243	196	200	202
Pb	5	1	1	1	2
Th	6	4	3	1	6
Sc	26	22	22	21	26
V	245	191	178	183	185
Cr	529	395	386	405	450
Co	59	49	50	50	54
Ni	374	226	251	268	275
Cu	81	89	83	92	87
Zn	102	100	103	107	112
Ga	17	23	21	22	19
S	70	29	23	21	33
INAA Data					
La	65.0	29.2	18.7	19.1	19.7
Ce	125	60.8	41.2	40.0	41.3
Nd	56.4	30.6	23.1	22.7	23.1
Sm	10.8	6.62	5.68	5.54	5.66
Eu	3.14	2.29	1.99	1.98	1.98
Tb	1.22	0.93	0.85	0.84	0.84
Yb	2.00	1.65	1.50	1.47	1.52
Lu	0.26	0.22	0.22	0.22	0.20
Th	6.54	3.00	1.99	1.90	2.03
U	1.8	1.3	0.5	0.6	0.7
Ta	4.84	2.61	2.03	2.04	2.15
Hf	6.36	4.64	4.18	4.21	4.18
Cs	0.6	0.29	0.24	0.22	
Rb		18			
Zn	111	96	95	92	102
Co	58.5	47.9	46.5	47.5	47.2
Cr	558	405	394	411	444
Sc	25.2	22.4	21.4	21.2	21.3

Age Group	*1730-36 Phase 4*	*1730-36 Phase 5*	*1730-36 Phase 5*	*1730-36 Phase 5*	*1730-36 Phase 5*
Volcano	Mña del Fuego	Mña de Las Nueces	Mña Colorada	Mña Colorada	Mña Colorada
Sample #	**L1-30-1**	**LAN6**	**LAN7**	**LAN8**	**LAN9**
I.D.					
U	1.6263	0.760	0.497	0.495	0.508
Th	6.1434	3.000	1.990	1.898	2.027
Isotopes					
$^{87}Sr/^{86}Sr$		0.703166	0.703158	0.703086	0.703062
$^{143}Nd/^{144}Nd$		0.512844	0.512795	0.512883	0.512860
$^{206}Pb/^{204}Pb$		19.199	19.145	19.098	19.082
$^{207}Pb/^{204}Pb$		15.533	15.522	15.503	15.505
$^{208}Pb/^{204}Pb$		38.964	38.880	38.787	38.781
$(^{230}Th/^{238}U)$	1.198	1.109	1.161	1.128	1.141
$(^{238}U/^{232}Th)$	0.803	0.846	0.808	0.817	0.823
$(^{230}Th/^{232}Th)$	0.962	0.938	0.938	0.922	0.938
$(^{234}U/^{238}U)$	1.006	-	-	-	-
$(^{226}Ra/^{230}Th)$		-	-	-	-
	26.476				
	137.105				

Age Group	*1730-36 Phase 5*	*1824*	*1824Volcan Nuevo*	*1824 Vol Nuevo*	*1824 Vol Nuevo*
Volcano	Mña Colorada	Volcan Nuevo or Tigauton	Volcan Nuevo or Tigauton	Volcan Nuevo or Tigauton	Volcan Nuevo or Tigauton
Sample #	**LAN10**	**L1-26-9**	**L1-28-1**	**LAN14**	**LAN15**
SiO_2	50.68	44.37	44.10	44.09	44.07
TiO_2	2.16	2.76	2.76	2.77	2.76
Al_2O_3	12.64	12.30	12.20	12.27	12.26
Fe_2O_3	11.24	12.35	12.45	12.41	12.41
MnO	0.15	0.18	0.18	0.18	0.18
MgO	11.47	12.41	12.42	12.39	12.53
CaO	8.57	10.79	10.86	10.82	10.73
Na_2O	2.75	3.28	3.12	3.33	3.31
K_2O	0.63	1.25	1.23	1.26	1.25
P_2O_5	0.32	0.95	0.95	0.94	0.93
S%	0.00	0.03	0.01	0.01	0.01
LOI	0.00	-0.37	-0.08	-0.01	-0.01
Total	100.61	100.30	100.19	100.44	100.42
Mg *	72.0	71.3	71.2	71.0	71.0
XRF					
Rb	15	28	27	27	28
Sr	407	994	997	1033	1035
Y	21	32	30	31	30
Zr	178	304	304	309	306
Nb	30	81	80	82	81
Ba	190	528	515	496	517
Pb	0	5	4	4	3
Th	2	8	11	10	9
Sc	25	26	24	26	25
V	173	251	241	242	244
Cr	560	475	498	506	475
Co	60	57	59	59	59
Ni	394	336	336	346	335
Cu	89	84	85	90	92
Zn	107	109	107	112	114
Ga	19	18	20	17	17
S	33	87	57	79	94
INAA Data					
La	18.7	76.1	76.5	74.2	74.4
Ce	39.1	152	153	151	149
Nd	22.0	65.7	67.4	65.3	65.8
Sm	5.37	11.8	11.9	11.5	11.4
Eu	1.87	3.51	3.51	3.50	3.53
Tb	0.79	1.25	1.32	1.27	1.28
Yb	1.50	2.20	2.25	2.10	2.16
Lu	0.21	0.29	0.31	0.28	0.27
Th	2.03	7.90	8.00	7.92	7.94
U	0.7	2.5	2.2	2.0	2.3
Ta	2.02	4.77	4.79	5.04	5.17
Hf	4.17	6.48	6.18	6.32	6.29
Cs	0.35	0.5	0.4	0.25	0.33
Rb					
Zn	98	110	105	94	99
Co	49.9	54.7	54.6	53.8	54.2
Cr	568	488	497	482	481
Sc	20.3	24.6	24.8	24.2	24.1

Age Group	*1730-36 Phase 5*	*1824*	*1824Volcan Nuevo*	*1824 Vol Nuevo*	*1824 Vol Nuevo*
Volcano	Mña Colorada	Volcan Nuevo or Tigauton	Volcan Nuevo or Tigauton	Volcan Nuevo or Tigauton	Volcan Nuevo or Tigauton
Sample #	**LAN10**	**L1-26-9**	**L1-28-1**	**LAN14**	**LAN15**
I.D.					
U	0.539		1.9886	1.968	1.970
Th	2.030		7.5181	7.920	7.940
Isotopes					
$^{87}Sr/^{86}Sr$	0.703201			0.703315	0.703199
$^{143}Nd/^{144}Nd$	0.512827			0.512846	0.512825
$^{206}Pb/^{204}Pb$	19.133			19.272	19.262
$^{207}Pb/^{204}Pb$	15.537			15.513	15.513
$^{208}Pb/^{204}Pb$	38.887			38.987	38.987
$(^{230}Th/^{238}U)$	1.132		1.215	1.229	1.212
$(^{238}U/^{232}Th)$	0.853		0.803	0.768	0.841
$(^{230}Th/^{232}Th)$	0.965		0.975	0.944	1.019
$(^{234}U/^{238}U)$	-		1.000	-	-
$(^{226}Ra/^{230}Th)$	-			-	-
			32.400		
			169.955		

Age Group	*1824 Vol Nuevo*	*1824*	*1824*	*Xenolith*	*Xenolith*
Volcano	Volcan Nuevo or Tigauton	Mña Chinero or Volcan Nuevo del Fuego	Mña Chinero or Volcan Nuevo del Fuego		
Sample #	**LAN16**	**L1-28-2**	**L1-28-3**	**L1-28-3(a)**	**L1-28-3(b)**
SiO_2	44.01	44.07	44.31	44.51	41.11
TiO_2	2.79	2.58	2.61	0.06	0.05
Al_2O_3	12.29	11.42	11.62	0.78	0.34
Fe_2O_3	12.41	12.20	12.28	8.45	9.62
MnO	0.18	0.18	0.18	0.13	0.15
MgO	12.40	14.41	14.23	45.65	48.29
CaO	10.85	10.51	10.64	0.85	0.35
Na_2O	3.30	3.02	3.00	0.22	0.09
K_2O	1.24	1.17	1.19	0.06	0.05
P_2O_5	0.94	0.88	0.90	0.04	0.03
S%	0.01	0.03	0.03	0.04	0.03
LOI	0.00	-0.14	-0.24	-0.17	0.24
Total	100.40	100.31	100.73	100.60	100.34
Mg *	71.0	74.5	74.2	93.3	92.2
XRF					
Rb	28	26	27	1	2
Sr	1040	838	838	65	43
Y	32	28	27	2	1
Zr	311	296	294	9	9
Nb	83	78	79	3	2
Ba	490	519	494	18	36
Pb	3	3	6	0	0
Th	10	8	5	1	0
Sc	24	24	21	8	3
V	237	240	235	38	16
Cr	485	585	594	3311	1831
Co	55	63	65	122	141
Ni	338	422	410	2364	2873
Cu	87	85	80	7	7
Zn	112	100	105	53	79
Ga	18	18	18	1	2
S	73	82	56	118	132
INAA Data					
La	73.9	60.0		5.0	
Ce	150	120		8.8	
Nd	65.2	55.4		3.5	
Sm	11.5	10.1		0.62	
Eu	3.55	3.08		0.18	
Tb	1.27	1.15		0.16	
Yb	2.11	2.02		0.19	
Lu	0.28	0.27		0.04	
Th	8.06	6.03		0.89	
U	2.6	1.5			
Ta	5.28	4.53		0.11	
Hf	6.32	6.23		0.37	
Cs	0.29	0.5			
Rb					
Zn	112	120		50	
Co	54.1	59.7		105	
Cr	503	628		3200	
Sc	24.2	25.0		9.02	

Age Group	*1824 Vol Nuevo*	*1824*	*1824*	*Xenolith*	*Xenolith*
Volcano	Volcan Nuevo or Tigauton	Mña Chinero or Volcan Nuevo del Fuego	Mña Chinero or Volcan Nuevo del Fuego		
Sample #	**LAN16**	**L1-28-2**	**L1-28-3**	**L1-28-3(a)**	**L1-28-3(b)**
I.D.					
U	1.984	1.4999	1.5244		
Th	8.060		7.3358		
Isotopes					
$^{87}Sr/^{86}Sr$	0.703217				
$^{143}Nd/^{144}Nd$	0.512356				
$^{206}Pb/^{204}Pb$	19.290				
$^{207}Pb/^{204}Pb$	15.533				
$^{208}Pb/^{204}Pb$	39.053				
$(^{230}Th/^{238}U)$	1.189		1.516		
$(^{238}U/^{232}Th)$	0.761		0.631		
$(^{230}Th/^{232}Th)$	0.905		0.956		
$(^{234}U/^{238}U)$	1.002		1.008		
$(^{226}Ra/^{230}Th)$	1.341				

Age Group	*Xenolith from 1730-36*
Volcano	
Sample #	**L1-26-6a**
SiO_2	43.30
TiO_2	0.04
Al_2O_3	0.63
Fe_2O_3	9.45
MnO	0.16
MgO	46.36
CaO	0.67
Na_2O	0.10
K_2O	0.07
P_2O_5	0.03
S%	0.02
LOI	-0.36
Total	100.45
Mg *	92.2
XRF	
Rb	2
Sr	20
Y	1
Zr	9
Nb	3
Ba	16
Pb	0
Th	1
Sc	6
V	22
Cr	2328
Co	134
Ni	2622
Cu	6
Zn	77
Ga	1
S	25
INAA Data	
La	
Ce	
Nd	
Sm	
Eu	
Tb	
Yb	
Lu	
Th	
U	
Ta	
Hf	
Cs	
Rb	
Zn	
Co	
Cr	
Sc	

Age Group	*Xenolith from 1730-36*
Volcano	
Sample #	**L1-26-6a**
I.D.	
U	
Th	
Isotopes	
$^{87}Sr/^{86}Sr$	
$^{143}Nd/^{144}Nd$	
$^{206}Pb/^{204}Pb$	
$^{207}Pb/^{204}Pb$	
$^{208}Pb/^{204}Pb$	
$(^{230}Th/^{238}U)$	
$(^{238}U/^{232}Th)$	
$(^{230}Th/^{232}Th)$	
$(^{234}U/^{238}U)$	
$(^{226}Ra/^{230}Th)$	

Mafic Rocks - Basanite/basalts - cf1 and pv1

Unit no	cf1	cf1	cf1	cf1	cf1
Location	*Mña Cerillar - Siete Canadas*	*Arenas Negras - Siete Canadas scoria cone*	*Arenas Negras*	*Arenas Negras*	*Arenas Negras*
Sample #	**T7-18-1**	**T7-18-3**	**T7-18-4**	**T7-18-5**	**T7-18-6**
Rock type	Basalt	Basalt	Basalt	Basalt	Basalt
Ages (years)	100000	150000	100000	100000	100000
SiO_2	42.24	44.99	44.48	44.83	45.59
TiO_2	3.994	3.112	3.175	3.125	3.068
Al_2O_3	12.16	14.18	13.40	13.88	13.31
Fe_2O_3	14.71	12.79	13.08	13.08	13.24
MnO	0.182	0.183	0.182	0.186	0.185
MgO	11.26	8.66	9.80	9.17	9.98
CaO	10.23	10.19	10.44	10.35	10.15
Na_2O	2.93	3.49	3.17	3.26	3.26
K_2O	1.46	1.68	1.56	1.52	1.30
P_2O_5	0.691	0.744	0.744	0.836	0.693
LOI	0.06	0.01	0.50	-0.07	-0.24
Total	99.92	100.02	100.53	100.17	100.53
S%	0.01	0.022	0.07	0.03	0.02
Mg#	0.65	0.63	0.65	0.63	0.65
XRF					
Rb	26	40	35	33	29
Sr	846	818	802	850	758
Y	28	31	30	32	29
Zr	260	308	291	299	254
Nb	69	78	74	75	67
Ba	451	525	473	504	508
Pb	6	3	4	3	2
Th	5	8	6	6	7
U	1	2	2	1	2
Sc	24	28	27	26	23
V	319	275	286	253	253
Cr	508	333	412	342	425
Co	63	48	54	52	56
Ni	280	162	207	173	213
Cu	44	70	71	67	72
Zn	126	117	113	119	112
Ga	21	23	20	22	21
Mo	0	1	1	0	1
As	0	5	2	0	0
S	71	42	477	77	99
INAA					
La	40.60			50.6	46.50
Ce	92.80			110	93.90
Nd	49.10			53.8	47.00
Sm	9.52			10.4	9.43
Eu	3.15			3.33	3.02
Tb	1.14			1.25	1.21
Yb	1.56			2.12	2.18
Lu	0.23			0.30	0.29
Th	3.54			4.68	4.23
U	1.30			1.7	1.20
Ta	4.27			4.42	4.00
Hf	6.27			6.50	5.84
Cs	0.20			0.3	0.30
Rb	-			47	-
Zn	116.00			149	115.00
Co	58.30			45.8	51.80
Cr	482.00			358	417.00
Sc	22.30			24.6	23.60
U/Th INAA	0.367			0.363	0.284

Unit no	cf1	cf1	cf1	cf1	cf1
Location	*Mña Cerillar - Siete Canadas*	*Arenas Negras - Siete Canadas scoria cone*	*Arenas Negras*	*Arenas Negras*	*Arenas Negras*
Sample #	**T7-18-1**	**T7-18-3**	**T7-18-4**	**T7-18-5**	**T7-18-6**
Rock type	Basalt	Basalt	Basalt	Basalt	Basalt
I. D.					
U/Th	0.239	0.256	0.267	0.247	0.247
U (ppm)	0.817	1.333	1.155	1.092	0.983
Th (ppm)	3.415	5.211	4.325	4.428	3.982
Isotopes					
$(^{234}U/^{238}U)act$	1.0097	1.0039	1.0150	1.0058	1.0911
Th/U	4.1786	3.9086	3.7434	4.0549	4.0518
$(^{238}U/^{232}Th)act$	0.7261	0.7763	0.8106	0.7483	0.7489
$(^{230}Th/^{232}Th)act$	0.8706	0.9307	0.9032	0.8995	0.9007
$(^{230}Th/^{238}U)act$	1.1989	1.1989	1.1143	1.2020	1.2027
$^{228}Ra/^{226}Ra$		2.1371		2.0645	
^{226}Ra sample (fmol)		0.1660		0.1748	
^{226}Ra sample (fg/g)		572.62		626.79	
$(^{230}Th/^{232}Th)i$	1.29989	1.38960	1.17843	1.34878	1.35182
$(^{230}Th/^{238}U)i$	1.79017	1.79006	1.45385	1.80249	1.80516

			PV series		
Unit no	cf1	cf1	Historic -1909	< 1ka	pv1
Location	*Mña Mostaza*	*Mña Tapada*	*Mña Chineryo*	*Mña Cangreco*	*Volcan la Corona*
Sample #	**T7-18-9**	**T7-19-11**	**T7-22-1**	**T7-22-2**	**T7-19-4**
Rock type	Basalt	basanite/alk bas	Basanite	Basanite/ph. teph.	basanite
	30000	10500	89	980	
SiO_2	46.16	51.76	44.70	49.63	51.02
TiO_2	2.988	2.458	3.737	2.282	2.611
Al_2O_3	14.01	17.90	16.71	16.29	17.72
Fe_2O_3	12.72	8.90	12.96	10.59	9.04
MnO	0.181	0.190	0.184	0.169	0.194
MgO	8.98	3.30	5.42	5.90	3.27
CaO	10.12	6.73	10.87	7.75	6.75
Na_2O	3.16	5.34	4.02	4.54	5.57
K_2O	1.47	2.54	1.67	2.08	2.67
P_2O_5	0.670	1.009	0.894	0.619	1.044
LOI	0.13	0.45	-0.37	0.27	0.51
Total	100.58	100.59	100.78	100.11	100.39
S%	0.03	0.02	0.04	0.01	0.05
Mg#	0.64	0.48	0.51	0.58	0.47
XRF					
Rb	36	60	35	55	65
Sr	801	1006	1088	654	951
Y	29	41	34	29	41
Zr	279	460	309	400	467
Nb	73	112	82	93	120
Ba	519	1004	550	545	902
Pb	3	8	3	6	7
Th	5	11	6	12	12
U	0	3	0	5	3
Sc	24	11	20	17	12
V	269	126	294	180	137
Cr	364	6	15	174	10
Co	50	16	41	40	19
Ni	190	3	19	96	4
Cu	75	8	34	53	16
Zn	120	118	122	116	124
Ga	20	22	23	22	23
Mo	1	3	1	4	6
As	0	1	0	1	5
S	94	71	187	49	396
INAA					
La			54.70		
Ce			112.00		
Nd			55.90		
Sm			11.10		
Eu			3.50		
Tb			1.41		
Yb			2.43		
Lu			0.33		
Th			4.98		
U			1.70		
Ta			4.88		
Hf			6.65		
Cs			0.50		
Rb			-		
Zn			118.00		
Co			37.20		
Cr			19.00		
Sc			18.70		
U/Th INAA					

Unit no	cf1	cf1	Historic -1909	< 1ka	pv1
Location	*Mña Mostaza*	*Mña Tapada*	*Mña Chineryo*	*Mña Cangreco*	*Volcan la Corona*
Sample #	**T7-18-9**	**T7-19-11**	**T7-22-1**	**T7-22-2**	**T7-19-4**
Rock type	Basalt	basanite/alk bas	Basanite	Basanite/ph. teph.	basanite
I. D.					
U/Th	0.259	0.265	0.252	0.260	0.255
U (ppm)	1.206	2.535	1.166	2.495	2.801
Th (ppm)	4.649	9.552	4.634	9.601	10.965
Isotopes					
$(^{234}U/^{238}U)act$	1.0103	1.0129	1.0219	1.0077	1.0146
Th/U	3.8545	3.7679	3.9728	3.8475	3.9147
$(^{238}U/^{232}Th)act$	0.7872	0.8053	0.7637	0.7886	0.7751
$(^{230}Th/^{232}Th)act$	0.9398	0.9106	0.9370	0.8604	0.8603
$(^{230}Th/^{238}U)act$	1.1939	1.1308	1.2268	1.0909	1.1099
$^{228}Ra/^{226}Ra$					1.7619
^{226}Ra sample (fmol)					0.3417
^{226}Ra sample (fg/g)					1028.20
$(^{230}Th/^{232}Th)i$	0.98833	0.92125	0.93710	0.86100	0.90998
$(^{230}Th/^{238}U)i$	1.25552	1.14400	1.22698	1.09177	1.17405

Unit no	pv2	PV lower cone pv2	PV lower cone pv2	PV lower cone pv2	PV lower cone pv3	PV lower cone pv3
Location	*Asientos Altos*	*Asientos Altos*	*Asientos Altos*	*Asientos Altos - close to BH2*	*PV Flank*	*close to t2*
Sample #	**T7-19-5**	**T7-19-6**	**T7-19-7**	**T7-19-8**	**T7-19-3**	**T7-20-2**
Rock type	Basanite	Basanite	Basanite	Basanite	Ph. teph.	Ph.teph
	105000	95000	95000	95000	25000	
SiO_2	48.60	48.86	48.65	48.94	47.93	54.80
TiO_2	2.901	2.916	2.896	2.772	3.312	1.681
Al_2O_3	17.98	18.21	18.19	18.07	17.41	19.31
Fe_2O_3	10.23	10.25	10.20	9.62	10.82	6.10
MnO	0.189	0.188	0.185	0.201	0.195	0.199
MgO	3.68	3.72	3.69	3.53	4.33	1.67
CaO	8.08	8.16	8.19	7.93	8.84	3.94
Na_2O	5.19	4.97	5.03	5.47	4.80	7.74
K_2O	2.53	2.39	2.44	2.38	2.05	3.88
P_2O_5	1.048	1.046	1.041	1.020	1.360	0.475
LOI	-0.08	0.17	-0.06	0.09	-0.41	0.38
Total	100.34	100.88	100.45	100.02	100.64	100.18
S%	0.03	0.03	0.03	0.014	0.02	0.02
Mg#	0.47	0.47	0.47	0.48	0.50	0.40
XRF						
Rb	58	54	56	54	44	97
Sr	1125	1130	1135	1239	1164	857
Y	39	40	40	38	42	38
Zr	410	411	402	403	372	601
Nb	112	113	110	114	96	165
Ba	896	919	916	822	684	1214
Pb	5	6	4	5	3	13
Th	10	8	9	10	10	18
U	3	1	3	2	3	5
Sc	10	13	12	11	12	4
V	169	169	163	142	196	49
Cr	9	5	6	15	9	7
Co	27	23	23	18	27	7
Ni	6	9	7	4	5	2
Cu	33	31	30	12	12	4
Zn	113	117	115	119	123	117
Ga	23	22	23	22	22	21
Mo	3	3	2	4	3	8
As	4	5	0	3	0	7
S	119	116	120	61	69	91
INAA-						
La	78.90			77.50		97.2
Ce	159.00			160.00		180
Nd	69.80			70.20		64.9
Sm	12.60			12.25		10.7
Eu	3.94			3.97		3.21
Tb	1.53			1.51		1.26
Yb	2.90			2.82		3.25
Lu	0.42			0.41		0.46
Th	8.21			8.99		15.0
U	2.2			2.50		4.1
Ta	6.56			6.67		9.25
Hf	8.08			7.94		10.8
Cs	0.6			0.70		1.20
Rb	-			-		95
Zn	127			104.00		102
Co	22.6			16.30		4.3
Cr	5			6.00		6
Sc	11			7.14		2.34
U/Th INAA						

Unit no	pv2	pv2	pv2	pv2	pv3	pv3
Location	*Asientos Altos*	*Asientos Altos*	*Asientos Altos*	*Asientos Altos - close to BH2*	*PV Flank*	*close to t2*
Sample #	**T7-19-5**	**T7-19-6**	**T7-19-7**	**T7-19-8**	**T7-19-3**	**T7-20-2**
Rock type	Basanite	Basanite	Basanite	Basanite	Ph. teph.	Ph.teph
I. D.						
U/Th	0.258	0.258	0.262	0.260	0.256	0.269
U (ppm)	2.094	2.084	2.051	2.324	1.838	1.825
Th (ppm)	8.115	8.067	7.824	8.926	7.169	6.778
Isotopes						
$(^{234}U/^{238}U)act$	1.0136	1.0164	1.0157	1.0201	1.0056	1.0015
Th/U	3.8762	3.8712	3.8147	3.8401	3.9006	3.7146
$(^{238}U/^{232}Th)act$	0.7828	0.7838	0.7954	0.7901	0.7779	0.8168
$(^{230}Th/^{232}Th)act$	0.9066	0.8991	0.9129	0.9038	0.9277	0.8738
$(^{230}Th/^{238}U)act$	1.1582	1.1471	1.1478	1.1439	1.1926	1.0697
$^{228}Ra/^{226}Ra$	2.1132	2.1677	1.7629		1.6272	
^{226}Ra sample (fmol)	0.1338	0.1432	0.3200		0.2648	
^{226}Ra sample (fg/g)	833.73	797.01	1027.45		1141.12	
$(^{230}Th/^{232}Th)i$	1.10807	1.05991	1.07696	1.06245	0.96644	0.90700
$(^{230}Th/^{238}U)i$	1.41557	1.35229	1.35398	1.34465	1.24238	1.11040

	PTS 1 - PT Flank Vents					
Unit no	PV lower cone pv3	PV lower cone pv3	PT Flanks tfl	Flank Vent tfl	Flank Vent abl	Flank Vent abl
Location	*close to R d G breach*	*Toe of pv3*	*Mña Majua*	*Mña de la Cruz*	*close to Arenas Blancas*	*Arenas blancas*
Sample #	**T7-20-3**	**T7-20-4**	**T7-19-10**	**T7-19-9**	**T7-18-10**	**T7-18-13**
Rock type	Ph. teph.	Phono.teph.	phonolite	Phonolite	phonolite	Phonolite
	85000	80000	75000	75000	75000	60000
SiO_2	49.62	49.47	59.42	59.83	59.61	59.51
TiO_2	2.679	2.691	0.742	0.751	0.728	0.741
Al_2O_3	18.21	17.83	19.28	19.31	19.29	19.26
Fe_2O_3	10.12	9.42	3.68	3.65	3.56	3.52
MnO	0.191	0.184	0.181	0.181	0.184	0.183
MgO	2.86	3.55	0.49	0.51	0.45	0.44
CaO	6.98	7.60	0.99	0.92	0.86	0.90
Na_2O	5.44	5.30	8.93	9.25	8.91	8.80
K_2O	2.83	2.58	5.41	5.48	5.49	5.51
P_2O_5	1.092	1.174	0.117	0.120	0.099	0.097
LOI	0.07	0.18	0.94	0.37	0.77	0.78
Total	100.09	99.98	100.18	100.38	99.96	99.75
S%	0.05	0.025	0.01	0.02	0.02	0.01
Mg#	0.41	0.48	0.25	0.26	0.24	0.24
XRF						
Rb	66	66	164	166	171	169
Sr	944	1095	33	32	20	24
Y	45	39	38	37	38	38
Zr	471	452	932	930	979	955
Nb	123	114	212	210	218	213
Ba	1006	849	411	436	313	335
Pb	7	8	16	17	19	15
Th	15	13	31	29	31	30
U	3	4	7	8	6	8
Sc	9	8	3	0	1	1
V	103	153	13	15	11	11
Cr	7	3	5	6	4	4
Co	24	21	1	2	2	1
Ni	9	5	2	2	1	1
Cu	70	16	4	2	2	2
Zn	127	114	114	115	117	113
Ga	24	24	27	28	27	27
Mo	4	4	16	16	15	14
As	1	3	6	3	5	4
S	201	174	56	60	38	73
INAA						
La	89.2		104.00			
Ce	184		186.00			
Nd	78.5		58.10			
Sm	14.2		8.80			
Eu	4.41		1.96			
Tb	1.67		1.07			
Yb	3.51		3.70			
Lu	0.46		0.52			
Th	10.6		26.60			
U	3.2		7.00			
Ta	7.24		12.80			
Hf	9.25		16.70			
Cs	0.74		2.10			
Rb	68		-			
Zn	116		101.00			
Co	19.3		0.90			
Cr	6		6.00			
Sc	8.60		0.52			
U/Th INAA						

Unit no	pv3	pv3	tf1	tf1	ab1	ab1
Location	*close to R d G breach*	*Toe of pv3*	*Mña Majua*	*Mña de la Cruz*	*close to Arenas Blancas*	*Arenas blancas*
Sample #	**T7-20-3**	**T7-20-4**	**T7-19-10**	**T7-19-9**	**T7-18-10**	**T7-18-13**
Rock type	Ph. teph.	Phono.teph.	phonolite	Phonolite	phonolite	Phonolite
I. D.						
U/Th	0.255	0.255	0.275	0.275	0.265	0.269
U (ppm)	2.654	2.926	7.020	7.041	7.328	7.319
Th (ppm)	10.403	11.477	25.559	25.576	27.620	27.209
Isotopes						
$(^{234}U/^{238}U)act$	1.0140	1.0125	1.0077	1.0063	1.0086	1.0052
Th/U	3.9200	3.9227	3.6411	3.6324	3.7693	3.7178
$(^{238}U/^{232}Th)act$	0.7740	0.7735	0.8333	0.8353	0.8050	0.8161
$(^{230}Th/^{232}Th)act$	0.8892	0.8363	0.8716	0.9081	0.8141	0.8669
$(^{230}Th/^{238}U)act$	1.1488	1.0812	1.0460	1.0872	1.0113	1.0622
$^{228}Ra/^{226}Ra$	1.7684					
^{226}Ra sample (fmol)	0.1353					
^{226}Ra sample (fg/g)	875.94					
$(^{230}Th/^{232}Th)i$	1.02565	0.90455	0.90968	0.98047	0.82312	0.90422
$(^{230}Th/^{238}U)i$	1.32507	1.16943	1.09162	1.17377	1.02254	1.10793

			Historic PV 1798	PVS 1 - PV Upper cone	
Unit no	Flank Vent ab1	Flank Vent mc1	Upper cone pv5	Upper cone pv 5	Upper cone pv 5
Location	*Sample from road section*	*PTS1 flank vent*	*PV summit*	*PV summit*	*PV summit*
Sample #	**T7-18-12**	**T7-18-2**	**T7-PV-2**	**T7-PV-3**	**T7-PV-4**
Rock type	Phonolite	Tephr. Phonolite	Tep. phonolite	Tep. phonolite	Tep. phonolite
	60000	60000	48000	48000	47000
SiO_2	58.54	58.25	54.91	54.98	56.13
TiO_2	1.046	1.045	1.702	1.598	1.243
Al_2O_3	19.40	19.32	19.26	19.44	19.82
Fe_2O_3	4.22	4.22	6.15	6.10	5.48
MnO	0.151	0.147	0.200	0.197	0.189
MgO	0.91	0.94	1.74	1.64	1.12
CaO	1.90	2.07	4.01	4.06	2.77
Na_2O	7.90	7.59	7.69	7.31	8.17
K_2O	5.08	5.01	3.86	3.87	4.60
P_2O_5	0.248	0.229	0.485	0.436	0.283
LOI	0.50	0.95	0.18	0.34	0.33
Total	99.88	99.76	100.19	99.98	100.14
S%	0.023	0.02	0.01	0.01	0.04
Mg#	0.35	0.36	0.41	0.40	0.34
XRF					
Rb	150	148	97	98	118
Sr	316	321	867	889	655
Y	29	28	39	38	36
Zr	808	807	591	601	702
Nb	169	167	160	163	187
Ba	1084	1090	1211	1188	1184
Pb	15	13	12	11	18
Th	26	24	18	19	23
U	7	7	4	4	6
Sc	1	2	2	2	2
V	23	26	49	45	21
Cr	4	4	3	8	3
Co	6	3	5	5	2
Ni	3	2	3	1	2
Cu	4	4	5	7	6
Zn	93	87	111	113	111
Ga	24	25	24	24	25
Mo	13	9	7	4	7
As	5	3	2	3	3
S	45	63	70	52	238
INAA					
La		77.70			97.3
Ce		143.00			179
Nd		44.50			60.2
Sm		6.91			9.59
Eu		2.01			2.77
Tb		0.85			1.12
Yb		3.00			3.30
Lu		0.41			0.47
Th		23.60			20.3
U		5.40			4.3
Ta		10.40			10.4
Hf		14.40			12.4
Cs		1.60			1.34
Rb		-			116
Zn		91.00			94
Co		2.70			3.1
Cr		4.00			5
Sc		1.28			1.22
U/Th INAA					

Unit no	ab1	mc1	pv5	pv 5	pv 5
Location	*Sample from road section*	*PTS1 flank vent*	*PV summit*	*PV summit*	*PV summit*
Sample #	**T7-18-12**	**T7-18-2**	**T7-PV-2**	**T7-PV-3**	**T7-PV-4**
Rock type	Phonolite	Tephr. Phonolite	Tep. phonolite	Tep. phonolite	Tep. phonolite
I. D.					
U/Th	0.267	0.242	0.273	0.205	0.207
U (ppm)	6.068	2.463	3.936	2.869	4.003
Th (ppm)	22.698	10.195	14.436	13.985	19.323
Isotopes					
$(^{234}U/^{238}U)act$	1.0093	1.0079	1.0109	1.0016	1.0179
Th/U	3.7406	4.1386	3.6678	4.8738	4.8269
$(^{238}U/^{232}Th)act$	0.8112	0.7332	0.8273	0.6226	0.6286
$(^{230}Th/^{232}Th)act$	0.8496	0.8372	0.8745	0.8655	0.8297
$(^{230}Th/^{238}U)act$	1.0474	1.1419	1.0571	1.3902	1.3199
$^{228}Ra/^{226}Ra$					
^{226}Ra sample (fmol)					
^{226}Ra sample (fg/g)					
$(^{230}Th/^{232}Th)i$	0.87796	0.91384	0.90069	1.00023	0.93837
$(^{230}Th/^{238}U)i$	1.08235	1.24645	1.08876	1.60664	1.49277

					PVS 1 Caldera Fi
	Upper cone	PV	Upper cone	Lateral eruption	caldera fill
Unit no	pv5	pv6	pv7	pv8	pv8
Location	*Close to R d G*	*Outside PV summit*	*Roques Blancos*	*PV Summit*	*PV Summit*
Sample #	**T7-20-1**	**T7-PV-11**	**T7-PV-1**	**T7-PV-10**	**T7-PV-8**
Rock type	phonolite	teph. ph	Phonolite	ph.teph	ph. teph
	48000	47000	45000	40000	40000
SiO_2	55.03	54.36	59.61	51.76	52.67
TiO_2	1.649	1.735	0.622	2.225	1.956
Al_2O_3	19.39	19.36	19.39	18.53	18.72
Fe_2O_3	6.01	6.44	3.87	8.45	7.53
MnO	0.202	0.201	0.200	0.177	0.164
MgO	1.61	1.83	0.37	2.68	2.35
CaO	3.83	4.43	0.84	5.93	5.36
Na_2O	7.79	7.20	9.03	6.55	6.75
K_2O	3.92	3.57	5.60	3.21	3.48
P_2O_5	0.452	0.510	0.062	0.903	0.766
LOI	0.01	0.38	0.67	0.17	0.28
Total	99.89	100.01	100.26	100.59	100.02
S%	0.02	0.01	0.01	0.03	0.02
Mg#	0.40	0.41	0.19	0.44	0.44
XRF					
Rb	96	92	180	90	104
Sr	833	969	7	1048	1078
Y	38	39	45	43	40
Zr	596	576	1073	584	623
Nb	163	156	244	151	154
Ba	1201	1190	18	1066	1062
Pb	11	12	21	15	19
Th	18	18	33	20	24
U	6	4	6	5	8
Sc	2	2	1	6	4
V	50	47	8	106	93
Cr	6	6	4	11	6
Co	4	7	3	16	13
Ni	3	2	3	10	9
Cu	4	5	3	23	21
Zn	118	108	128	116	95
Ga	22	25	30	26	26
Mo	7	5	12	8	7
As	3	2	6	8	8
S	77	77	60	120	184
INAA					
La			113	101	
Ce			202	191	
Nd			63.0	75.6	
Sm			9.83	13.3	
Eu			1.69	3.85	
Tb			1.22	1.49	
Yb			4.46	3.34	
Lu			0.63	0.46	
Th			30.3	18.0	
U			7.5	5.0	
Ta			14.6	8.62	
Hf			19.5	10.9	
Cs			1.97	1.20	
Rb			173	95	
Zn			106	102	
Co			0.6	14.1	
Cr			5	6	
Sc			0.67	6.55	
U/Th INAA					

Unit no	pv5	pv6	pv7	pv8	pv8
Location	*Close to R d G*	*Outside PV summit*	*Roques Blancos*	*PV Summit*	*PV Summit*
Sample #	**T7-20-1**	**T7-PV-11**	**T7-PV-1**	**T7-PV-10**	**T7-PV-8**
Rock type	phonolite	teph. ph	Phonolite	ph.teph	ph. teph
I. D.					
U/Th	0.272	0.267	0.251	0.271	0.309
U (ppm)	4.242	3.733	7.306	4.673	6.330
Th (ppm)	15.583	13.980	29.113	17.240	20.504
Isotopes					
$(^{234}U/^{238}U)act$	1.0190	1.0063	1.0089	1.0064	1.0201
Th/U	3.6730	3.7445	3.9846	3.6893	3.2390
$(^{238}U/^{232}Th)act$	0.8260	0.8103	0.7615	0.8224	0.9368
$(^{230}Th/^{232}Th)act$	0.8906	0.8741	0.8541	0.8401	0.8326
$(^{230}Th/^{238}U)act$	1.0782	1.0787	1.1217	1.0215	0.8888
$^{228}Ra/^{226}Ra$		1.3008		1.6841	
^{226}Ra sample (fmol)		0.2867		0.2511	
^{226}Ra sample (fg/g)		1558.55		1134.20	
$(^{230}Th/^{232}Th)i$	0.92641	0.90852	0.90160	0.84794	0.78631
$(^{230}Th/^{238}U)i$	1.12157	1.12120	1.18400	1.03102	0.83939

ill				PTS 2	PTS 2 Int.
Unit no	caldera fill pv8	< 1ka pv9	caldera fill pv9	t2	t2
Location	*PV summit*	*PV Summit-*	*Mña de los Chircheros*	*Ieide - collected as t1, now change on newesr map to t2*	*close to R d G*
Sample #	**T7-PV-7**	**T7-PV-6**	**T7-PV-13**	**T7-22-3**	**T7-20-5**
Rock type	ph teph.	Basanite	Plag Basanite	Phono. tephrite.	Phonolite
	40000	35000	40000	25000	25000
SiO_2	51.64	50.06	47.51	51.29	58.47
TiO_2	2.232	2.671	3.209	2.355	0.670
Al_2O_3	18.78	18.02	17.21	18.30	19.09
Fe_2O_3	8.24	9.03	10.64	8.53	3.83
MnO	0.174	0.192	0.196	0.181	0.195
MgO	2.51	3.28	4.14	3.07	0.42
CaO	6.15	6.64	8.65	6.51	0.84
Na_2O	6.31	5.75	4.84	6.07	9.43
K_2O	3.20	2.76	2.01	3.08	5.56
P_2O_5	0.884	1.039	1.323	0.928	0.100
LOI	0.05	0.57	-0.04	0.25	0.59
Total	100.18	100.00	99.69	100.57	99.19
S%	0.02	0.01	0.02	0.03	0.015
Mg#	0.43	0.47	0.49	0.47	0.21
XRF					
Rb	89	67	46	82	178
Sr	1142	1135	1179	1011	11
Y	41	44	42	37	43
Zr	570	499	381	520	1037
Nb	146	135	98	129	237
Ba	1065	879	717	901	73
Pb	14	10	3	7	19
Th	20	13	9	14	33
U	7	4	3	3	8
Sc	7	10	11	6	0
V	102	136	187	124	11
Cr	11	7	8	12	8
Co	16	15	21	17	2
Ni	9	4	3	6	2
Cu	27	12	10	13	4
Zn	103	132	123	111	126
Ga	27	25	24	23	28
Mo	6	6	3	7	18
As	5	0	1	8	4
S	113	100	78	143	46
INAA					
La		91.2		82.8	
Ce		185		162	
Nd		77.0		67.7	
Sm		13.6		11.8	
Eu		4.26		3.62	
Tb		1.60		1.35	
Yb		3.12		2.87	
Lu		0.42		0.41	
Th		11.2		12.4	
U		3.2		3.5	
Ta		7.54		7.40	
Hf		9.39		9.5	
Cs		0.89		1.0	
Rb		66		82	
Zn		116		95	
Co		14.4		14.6	
Cr		6		7	
Sc		7.16		7.42	
U/Th INAA					

Unit no	pv8	pv9	pv9	t2	t2
Location	*PV summit*	*PV Summit-*	*Mña de los Chircheros*	*Teide - collected as t1, now change on newesr map to t2*	*close to R d G*
Sample #	**T7-PV-7**	**T7-PV-6**	**T7-PV-13**	**T7-22-3**	**T7-20-5**
Rock type	ph teph.	Basanite	Plag Basanite	Phono. tephrite.	Phonolite
I. D.					
U/Th	0.252	0.271		0.266	0.269
U (ppm)	4.240	3.001		3.208	7.728
Th (ppm)	16.849	11.089		12.059	28.754
Isotopes					
$(^{234}U/^{238}U)act$	1.0033	1.0161		1.0023	1.0196
Th/U	3.9743	3.6954		3.7589	3.7209
$(^{238}U/^{232}Th)act$	0.7635	0.8211		0.8072	0.8154
$(^{230}Th/^{232}Th)act$	0.8213	0.8984		0.8553	0.8645
$(^{230}Th/^{238}U)act$	1.0758	1.0942		1.0595	1.0602
$^{228}Ra/^{226}Ra$					1.6267
^{226}Ra sample (fmol)					0.4999
^{226}Ra sample (fg/g)					2527.87
$(^{230}Th/^{232}Th)i$	0.84708	0.92774		0.86769	0.87719
$(^{230}Th/^{238}U)i$	1.10953	1.12990		1.07492	1.07572

	PTS2 Phon.	PTS 2	PT (1492)			
	Cone 2 <25ka	Teide Flank	Cone 3 - 1492	Cone 3 - 1492	PV flank	Caldera fill
Unit no	mc2	t3	t3	poss pv4	pv12	mb1
Location	*Mña de los Corrales*	*Toe of flow*	*close to MB*	*Mña Cangreco*	*1798 eruption*	*Mña Rajada*
Sample #	**T7-18-8**	**T7-20-6**	**T7-20-7**	**T7-22-2**	**T7-19-2**	**T7-18-11**
Rock type	Teph. phonolite	phonolite	Phonolite	Plag Basanite	Plag Ph. Tephr.	Phonolite
	25000	507	507		199	4000
SiO_2	57.40	59.60	59.89	49.63	50.25	59.73
TiO_2	1.494	0.756	0.740	2.282	2.633	0.668
Al_2O_3	19.33	19.05	19.17	16.29	18.03	19.35
Fe_2O_3	5.30	3.89	3.82	10.59	9.08	3.87
MnO	0.173	0.177	0.173	0.169	0.193	0.197
MgO	1.40	0.53	0.53	5.90	3.29	0.42
CaO	3.55	1.21	1.18	7.75	7.37	0.82
Na_2O	7.17	8.90	8.93	4.54	5.79	9.23
K_2O	3.96	5.20	5.22	2.08	2.61	5.66
P_2O_5	0.283	0.140	0.136	0.619	0.977	0.105
LOI	0.59	0.42	0.43	0.27	-0.02	-1.38
Total	100.65	99.88	100.22	100.11	100.21	98.67
S%	0.02	0.02	0.02	0.01	0.02	0.023
Mg#	0.39	0.25	0.25	0.58	0.47	0.21
XRF						
Rb	109	144	144	55	60	170
Sr	893	126	130	654	1041	8
Y	35	37	35	29	40	41
Zr	639	833	823	400	454	992
Nb	154	190	189	93	116	228
Ba	1449	634	674	545	762	89
Pb	14	17	17	6	7	19
Th	19	27	25	12	12	32
U	5	7	9	5	4	8
Sc	1	0	1	17	7	0
V	47	16	14	180	147	9
Cr	7	5	4	174	4	4
Co	5	2	3	40	15	0
Ni	3	2	1	96	4	3
Cu	5	3	3	53	9	3
Zn	106	113	110	116	124	123
Ga	25	25	25	22	25	28
Mo	5	13	14	4	4	17
As	5	5	6	1	0	4
S	43	53	107	49	71	59
INAA						
La		99.60	100		80.3	106.00
Ce		172.00	181		161	194.00
Nd		54.60	55.7		68.8	59.60
Sm		8.56	8.78		12.5	9.24
Eu		1.95	2.02		3.87	1.82
Tb		1.03	1.05		1.45	1.15
Yb		3.44	3.58		2.95	3.98
Lu		0.50	0.49		0.41	0.57
Th		23.10	23.4		10.3	27.60
U		6.30	5.6		2.8	7.50
Ta		11.20	11.5		6.83	13.50
Hf		15.20	15.0		8.80	17.80
Cs		1.80	1.72		0.8	2.20
Rb		-	137		65	-
Zn		102.00	98		107	103.00
Co		1.20	1.1		14.1	0.80
Cr		3.00	5		7	4.00
Sc		0.80	0.79		6.99	0.68
U/Th INAA						

Unit no	mc2	t3	t3	poss pv4	pv12	mb1
Location	*Mña de los Corrales*	*Toe of flow*	*close to MB*	*Mña Cangreco*	*1798 eruption*	*Mña Rajada*
Sample #	**T7-18-8**	**T7-20-6**	**T7-20-7**	**T7-22-2**	**T7-19-2**	**T7-18-11**
Rock type	Teph. phonolite	phonolite	Phonolite	Plag Basanite	Plag Ph. Tephr.	Phonolite
I. D.						
U/Th	0.269	0.272	0.270	0.260	0.255	0.288
U (ppm)	7.319	5.970	5.992	2.495	1.499	7.335
Th (ppm)	27.209	21.953	22.201	9.601	5.868	25.490
Isotopes						
$(^{234}U/^{238}U)act$	1.0052	1.0091	1.0074	1.0077	1.0123	1.0261
Th/U	3.7178	3.6774	3.7048	3.8475	3.9152	3.4748
$(^{238}U/^{232}Th)act$	0.8161	0.8251	0.8190	0.7886	0.7750	0.8732
$(^{230}Th/^{232}Th)act$	0.8669	0.8754	0.8715	0.8604	0.8737	0.8768
$(^{230}Th/^{238}U)act$	1.0622	1.0610	1.0641	1.0909	1.1274	1.0042
$^{228}Ra/^{226}Ra$						
^{226}Ra sample (fmol)						
^{226}Ra sample (fg/g)						
$(^{230}Th/^{232}Th)i$	0.87998	0.87568	0.87175	0.86100	0.87386	0.87696
$(^{230}Th/^{238}U)i$	1.07823	1.06130	1.06443	1.09177	1.12760	1.00431

Unit no	Montaña Blanca MB Lower >2ka mb3a	Montaña Blanca MB Upper mb4	Montaña Blanca MB Upper ≈2ka mb4	MB Upper ≈2ka Bomb	PV
Location	*PV Summit (Unit II)*	*El Culaton (Unit III)*	*El Culaton (Unit III)*	*Chio road*	*PV summit*
Sample #	**T7-PV-5**	**T7-21-1**	**T7-21-2**	**T7-19-1**	**T7-PV-9**
Rock type	Phonolite	Phonolite	Phonolite	Scoria and massive	Gabbroic Xenolith
	2000	2000	50000		
SiO_2	59.88	59.20	59.41	52.41	49.25
TiO_2	0.648	0.616	0.607	2.339	2.766
Al_2O_3	19.26	19.27	19.28	18.35	18.18
Fe_2O_3	3.79	3.88	3.87	8.22	9.66
MnO	0.188	0.203	0.202	0.197	0.183
MgO	0.42	0.35	0.34	2.76	3.12
CaO	0.83	0.74	0.73	6.48	7.42
Na_2O	9.38	9.75	9.75	6.01	5.80
K_2O	5.57	5.57	5.58	2.71	2.64
P_2O_5	0.097	0.081	0.078	0.802	1.146
LOI	0.57	0.41	0.35	0.02	0.42
Total	100.62	100.06	100.19	100.30	100.59
S%	0.02	0.02	0.01	0.02	0.01
Mg#	0.22	0.18	0.18	0.45	0.44
XRF					
Rb	168	182	183	65	73
Sr	11	9	3	1079	1203
Y	41	45	45	41	43
Zr	984	1086	1093	488	446
Nb	225	245	248	121	113
Ba	72	26	10	865	974
Pb	19	20	22	5	11
Th	29	33	35	13	13
U	8	10	8	4	4
Sc	2	0	2	8	7
V	9	6	8	115	132
Cr	5	5	5	5	7
Co	2	1	3	11	21
Ni	2	3	3	6	10
Cu	3	4	4	6	29
Zn	122	133	133	125	90
Ga	29	29	30	24	26
Mo	15	18	18	4	4
As	5	7	8	5	4
S	46	62	47	63	81
INAA					
La	107	114	114		
Ce	192	202	204		
Nd	60.0	60.6	61.0		
Sm	9.51	9.79	9.74		
Eu	1.79	1.65	1.64		
Tb	1.16	1.23	1.24		
Yb	4.10	4.37	4.40		
Lu	0.57	0.61	0.64		
Th	27.9	29.6	30.2		
U	7.7	7.8	8.4		
Ta	13.4	13.9	14.4		
Hf	17.7	19.3	19.5		
Cs	2.07	2.26	2.27		
Rb	165	168	170		
Zn	99	110	109		
Co	0.7	0.7	0.6		
Cr	4	4	4		
Sc	0.68	0.69	0.67		
U/Th INAA					

Unit no	mb3a	mb4	mb4	Bomb	
Location	*PV Summit (Unit II)*	*El Culaton (Unit III)*	*El Culaton (Unit III)*	*Chio road*	*PV summit*
Sample #	**T7-PV-5**	**T7-21-1**	**T7-21-2**	**T7-19-1**	**T7-PV-9**
Rock type	Phonolite	Phonolite	Phonolite	Scoria and massive	Gabbroic Xenolith
I. D.					
U/Th	0.266	0.269	0.266	0.248	
U (ppm)	7.146	8.118	2.904	2.561	
Th (ppm)	26.866	30.186	10.915	10.338	
Isotopes					
$(^{234}U/^{238}U)act$	1.0138	1.0136	0.9971	1.0170	
Th/U	3.7595	3.7184	3.7584	4.0370	
$(^{238}U/^{232}Th)act$	0.8071	0.8160	0.8073	0.7520	
$(^{230}Th/^{232}Th)act$	0.8575	0.8733	0.8643	0.8990	
$(^{230}Th/^{238}U)act$	1.0624	1.0702	1.0706	1.1957	
$^{228}Ra/^{226}Ra$		1.3208			
^{226}Ra sample (fmol)		0.3195			
^{226}Ra sample (fg/g)		2208.34			
$(^{230}Th/^{232}Th)i$	0.85840	0.87434	0.86536	0.89861	
$(^{230}Th/^{238}U)i$	1.06360	1.07148	1.07191	1.19569	

Unit no	PV				
Location	*PV summit*	**Comparison between Ablay's Bristol data and OU**			
Sample #	**T7-PV-12**	Ablay 1909	Thomas 1909	Ablay MB	Thomas MB
Rock type	Gabbroic Xenolith	T-1909	**T7-22-1**	T1-20-8	**T7-21-2**
SiO_2	52.00	44.64	44.70	59.4	59.41
TiO_2	1.969	3.73	3.737	0.64	0.607
Al_2O_3	18.18	15.72	16.71	18.83	19.28
Fe_2O_3	7.65	12.72	12.96	3.84	3.87
MnO	0.172	0.19	0.184	0.2	0.202
MgO	2.53	5.39	5.42	0.36	0.34
CaO	5.67	10.7	10.87	0.81	0.73
Na_2O	6.09	4.02	4.02	9.72	9.75
K_2O	3.42	1.66	1.67	5.47	5.58
P_2O_5	0.821	0.92	0.894	0.08	0.078
LOI	1.32	-0.48	-0.37	0.38	0.35
Total	99.82	99.53	100.05	99.73	100.19
S%	0.01		0.04		0.01
Mg#	0.45	0.51	0.51	0.18	0.18
XRF					
Rb	110	34.06	35	181	183
Sr	1081	1130.12	1088	5	3
Y	40	35.07	34	46	45
Zr	546	291.55	309	1112	1093
Nb	152	85.16	82	258	248
Ba	1078		550		10
Pb	16	7.01	3	26	22
Th	21	10.02	6	30	35
U	3	1	0	7	8
Sc	5		20		2
V	107	292.55	294	22	8
Cr	8	33.06	15	10	5
Co	16	43.08	41	14	3
Ni	10	14.03	19	2	3
Cu	18	28.05	34	1	4
Zn	92	79.15	122	86	133
Ga	25	26.05	23	30	30
Mo	2	2	1	15	18
As	6		0		8
S	33		187		47
INAA					
La					
Ce					
Nd					
Sm					
Eu					
Tb					
Yb					
Lu					
Th					
U					
Ta					
Hf					
Cs					
Rb					
Zn					
Co					
Cr					
Sc					
U/Th INAA					

Unit no	
Location	*PV summit*
Sample #	**T7-PV-12**
Rock type	Gabbroic Xenolith
I. D.	
U/Th	0.038
U (ppm)	1.245
Th (ppm)	32.8536
Isotopes	
$(^{234}U/^{238}U)act$	2.5648
Th/U	26.3883
$(^{238}U/^{232}Th)act$	0.1150
$(^{230}Th/^{232}Th)act$	0.7781
$(^{230}Th/^{238}U)act$	6.7667
$^{228}Ra/^{226}Ra$	
^{226}Ra sample (fmol)	
^{226}Ra sample (fg/g)	
$(^{230}Th/^{232}Th)i$	0.77806
$(^{230}Th/^{238}U)i$	6.76674

APPENDIX B

Locality, mineralogy and petrology of individual samples

B.1 Lanzarote Suite

1.1 Basement

L1-30-2 (Oct 1995 - LET) Basement

Grid Reference:	13°28 N; 29°13 W
Location:	Sample from below unconformity below Famara massif. Collected 500m west of Orzola.
Rock Description:	Dark grey, vesicular fine grained rock, with altered olivine phenocrysts.
Rock Type:	Basalt
Mineralogy:	Very fine grained matrix, with high proportion of opaques, olivine, ± clinopyroxene (augite), feldspar, biotite. Phenocryst phases - very altered olivines, with iddingsite rims and along fractures; some weathered biotite, very fractured and broken up, some altered clinopyroxenes.

1.2 Famara Region

L1-28-4 (Oct. 1995-LET) Famara massif

Grid Reference:	13°31 N; 29°08W
Location:	Track up from Playa de Famara into Famara massif. 300m past the last house and the last bit of car worthy track !
Rock Description:	Dark grey fine grained, blocky, very weathered rock, altered olivine phenocrysts
Rock Type:	Alkali basalt
Mineralogy:	Fine grained matrix with high proportion of feldspar laths (sanidine) and opaques, olivine, clinopyroxene. Phenocryst assemblage is weathered olivines with iddingsite around rims and infilling fractured. Some possible chlorite weathering. On the whole very altered unhappy rock.

1.3 Corona Suite

Lan 11 (Dec. 1994- CJH) Corona ~54 Ka old

Grid Reference:	13°27 N; 29°10 W
Location:	Lavas erupted from Mña Corona, several hundred metres north of turning to Cueva de los Verdes and inland from Punta Escarnes.
Rock Description:	Light grey, fine grained slightly vesicular rock with a few olivine phenocrysts
Rock Type:	Alkali basalt
Mineralogy:	Olivine, clinopyroxene (augite), feldspar laths (sanidine), glass and opaques. Zoned olivines range in size from <0.01 mm to 1 mm.

Lan 12 (Dec. 1994- CJH) Corona ~54 Ka old

Grid Reference:	13°27 N; 29°12 W
Location:	Lavas erupted from Mña Corona, on coast road, just south of small lagoon south of Punta Prieta.
Rock Description:	Mid grey, fine grained, vesicular rock with no obvious phenocrysts. No uniform shape to vesicles - mis-shapen

Rock Type: Alkali basalt
Mineralogy: Feldspar laths (sanidine), clinopyroxene (augite), olivine, glass and opaques. Zoned olivines range in size from <0.01mm to 1mm.

Lan 13 (Dec. 1994-CJH) Corona ~54 Ka old
Grid Reference: 13°28 N; 29°13 W
Location: Lavas erupted from Mña Corona, on road south from Orzola to Mirador del Rio. At top of first hill, at the margin of the Corona flow.
Rock Description: Dark grey, fine grained rock, with some small phenocrysts.
Rock Type: Alkali basalt
Mineralogy: Glassy regions with opaques and micro-phenocrysts of olivine and feldspar. Channels of glassy material next to more granular glass with clinopyroxene (augite)

L1-25-1 (Oct. 1995-LET) Corona
Grid Reference: 13°28 N; 29°13 W
Location: Sampled from half way along unsealed track to Casas La Breña, east of Ye. Scoria cone La Quemada de Orzola
Rock Description: Fine grained, dark grey vesicular rock, small phenocrysts of olivine and feldspar (0.5cm diameter).
Rock Type: Alkali basalt
Mineralogy: Fine grained glassy matrix with needle like opaques, clinopyroxene (augite), olivine, feldspar laths (sanidine).

L1-25-3 (Oct. 1995-LET) Corona
Grid Reference: 13°28 N; 29°12 W
Location: Sampled along coast road in Malpais de la Corona between El Arco and Punta de Palo. Outer surface removed as close to sea .
Rock Description: Vesicular basalt flow, fine grained dark grey vesicular rock with some small (<1 mm) crystals visible.
Rock Type: Alkali basalt
Mineralogy: Fine glassy matrix, with feldspar laths (sanidine), olivine phenocrysts, opaques and needle like opaques.

L1-25-6 (Oct. 1995-LET) Corona
Grid Reference: 13°28 N; 29°12 W
Location: Sampled along coast road in Malpais de la Corona between El Arco and Punta de Palo. Outer surface removed as close to sea .
Rock Description: Massive flow, not particularly vesicular. Fine grained dark grey rock with some small (<1 mm) phenocrysts of feldspar.
Rock Type: Alkali basalt
Mineralogy: Mid brown glassy matrix with feldspar laths (sanidine), opaques, clinopyroxene (augite) and olivine.

L1-25-7 (Oct. 1995-LET) Corona
Grid Reference: 13°28 N; 29°12 W
Location: Sampled along coast road in Malpais de la Corona between El Arco and Punta de Palo. Outer surface removed as close to sea .
Rock Description: More vesicular part of same flow as L1-25-6. Vesicular medium grey basalt, very fine grained, no obvious phenocrysts.
Rock Type: Alkali basalt
Mineralogy: Mid brown matrix, vesicular, feldspar laths, opaques clinopyroxene (augite) and olivine.

1.4.1730-36 Timanfaya eruptions
L1-27-1 (Oct. 1995-LET) 1730-36 Phase 1 Pico Partido
Grid Reference: 13°43 N; 29°04W

Location:	Halfway along track west from Tinajo into Los Islotes towards Playa de La Madera. Sampled north of track
Rock Type:	Alkali basalt
Rock Description:	Vesicular, fine grained dark grey rock, with small (< 5 mm) olivine phenocrysts and some crustal xenoliths. Rock sample from a bomb (1.5m in diameter)
Mineralogy:	Glassy matrix with fine grained olivine, clinopyroxene, feldspar (sanidine), opaques. Phenocrysts of olivine with opaque inclusions. Crustal xenolith consisting of plagioclase, anorthoclase, sanidine, some clinopyroxene, and olivine, exsolution lamellae in some of the feldspars

L1-27-2 (Oct. 1995-LET) 1730-36 Phase 1 *Pico Partido*

Grid Reference:	13°43 N; 29°04W
Location:	Same location as L1-27-1, sample from flow
Rock Description:	Vesicular, fine grained dark grey rock, with small (< 5 mm) olivine phenocrysts
Rock Type:	Alkali basalt
Mineralogy:	Glassy matrix with fine grained olivine, clinopyroxene, feldspar (sanidine), opaques. Phenocrysts of olivine with opaque inclusions. Crustal xenolith consisting of plagioclase, anorthoclase, sanidine, some clinopyroxene, and olivine, exsolution lamella in some of the feldspars

Lan 17 (Dec. 1994-CJH) 1730-36 Phase 2 (maybe Phase 4 as units are very mixed in this region)

Grid Reference:	13°45N; 28°57W
Location:	Sampled along halfway along Yaiza to Timanfaya road
Rock Description:	Fine grained, pale grey rock with few olivine and feldspar phenocrysts and few rounded vesicles.
Rock Type:	Alkali basalt
Mineralogy:	Feldspar laths (sanidine), opaques, clinopyroxene (augite) and olivine in fine grained matrix with phenocrysts (< 0.5 cm)

Lan 1 (Dec. 1994-CJH) 1730-36 Phase 3 Mña Rajada

Grid Reference:	13°51N; 28°59W
Location:	Near El Golfo -Freshly broken outcrop, at junction of new road from El Golfo to Yaiza and coast road from El Golfo.
Rock Description:	Fine grained dark grey vesicular rock, Some phenocrysts of olivine (largest 1 cm, most < 0.2 cm). Elongation of vesicles indicates flow movement.
Rock Type:	Alkali basalt
Mineralogy:	Olivine, clinopyroxene (augite), feldspar laths (sanidine) with skeletal oxides, opaques and devitrified glass in groundmass. Phenocrysts of olivine.

Lan 2 (Dec. 1994-CJH) 1730-36 Phase 3 Mña Rajada

Grid Reference:	13°51N; 28°59W
Location:	Near El Golfo -Freshly broken boulder from outcrop, at junction of new road from El Golfo to Yaiza and coast road from El Golfo.
Rock Description:	Fine grained mid grey rock. Ranging amounts of vesiculation with elongation of some areas. Some small phenocrysts of olivine (<1 mm). One large xenolith of green glassy olivine rich material.
Rock Type:	Alkali basalt
Mineralogy:	Olivine, clinopyroxene (augite), feldspar laths (sanidine) with skeletal oxides, opaques and devitrified glass in groundmass. Olivine phenocrysts

L1-26-1 (Oct. 1995-LET) 1730-36 Phase 3 Mña Rajada

Grid Reference:	13°51N; 28°59W

Location:	Near El Golfo -Freshly broken boulder from outcrop, at junction of new road from El Golfo to Yaiza and coast road from El Golfo.
Rock Description:	Fine grained mid grey rock. Ranging amounts of vesiculation with elongation of some areas. Some small phenocrysts of olivine (<1 mm). One large xenolith of green glassy olivine rich material.
Rock Type:	Alkali basalt
Mineralogy:	Olivine, clinopyroxene (augite), feldspar laths (sanidine) with skeletal oxides, opaques and devitrified glass in groundmass. Olivine phenocrysts

L1-26-2 (Oct. 1995-LET) 1730-36 Phase 3 Mña Rajada.

Grid Reference:	13°47N; 28°59W
Location:	From El Golfo main road inland leading towards Yaiza, 1st turning into National Park, then rough track leading east towards Mña del Fuego. Edge of 1730-36 lava flow just past saddle between cinder cones of Pedro Perico and Mña Encantada.
Rock Description:	Medium to dark grey fine grained basaltic rock with some vesicles, dunite xenoliths (1-2cm), with some olivine phenocrysts.
Rock Type:	Alkali basalt
Mineralogy:	Fine grained matrix, some regions more glassy, feldspar laths (sanidine), olivine, clinopyroxene (augite), opaques. Xenoliths, almost entirely olivine with few opaques.

L1-26-4 and L1-26-5 (Oct. 1995-LET) 1730-36 Phase 3 Mña Rajada

Grid Reference:	13°47N; 28°59W
Location:	Lava tube samples beautiful ropy lava and lava stalactites
Rock Type:	Alkali basalt

L1-26-6 (Oct. 1995-LET) 1730-36 Phase 3 Distil end of Mña Rajada

Grid Reference:	13°50N; 28°58W
Location:	Coast from south from El Golfo, sample from kink in road as it turns inland, close to the salt pans.
Rock Description:	Large abundant olivine xenoliths incorporating bits of melt. Very fresh looking dark green olivine and feldspar porphyritic rock.
Rock Type:	Alkali basalt
Mineralogy:	Brown glassy matrix with clinopyroxene (augite), opaques feldspar laths (sanidine), olivine. Xenoliths are almost entirely olivine with glassy material, biotite olivine and clinopyroxene (augite) as small melt type inclusions.

L1-26-7 (Oct. 1995-LET) 1730-36 Phase 3 Mña Quemadas

Grid Reference:	13°48N; 28°58W
Location:	Track heading NW from Yaiza, sample from east of Mña Termesana.
Rock Description:	Medium grey vesicular olivine basalt with some small olivine phenocrysts.
Rock Type:	Alkali basalt
Mineralogy:	Fine grained glassy matrix with olivine, clinopyroxene (augite), opaques, phenocrysts entirely olivine.

L1-26-8 (Oct. 1995-LET) 1730-36 Phase 4 Mña del Fuego

Grid Reference:	13°45N; 28°59W
Location:	Directly east of Mña del Fuego on road side,
Rock Description:	Dark grey, fine grained vesicular basalt.
Rock Type:	Alkali basalt
Mineralogy:	Glassy matrix with lots of feldspar laths (sanidine), olivine, opaques, clinopyroxene (augite), some regions more concentrated in opaques. Olivine phenocrysts.

Lan 3 (Dec 1994-CJH) 1730-36 Phase 4 Timanfaya - Mña del Fuego

Grid Reference:	13°46 N; 28°57 W

Location:	Freshly broken outcrop near edge of lava field at Yaiza. At start of dirt road heading NW from Yaiza, just west of main Timanfaya road.
Rock Description:	Fine grained mid grey finely vesiculated (< 2 mm) rock. Some very small phenocrysts of olivine (< 1 mm).
Rock Type:	Alkali basalt
Mineralogy:	Olivine, clinopyroxene (augite), feldspar laths (sanidine) with skeletal oxides, opaques and devitrified glass in groundmass.

Lan 4 (Dec. 1994-CJH) 1730-36 Phase 4 Timanfaya - Mña del Fuego

Grid Reference:	13°46 N; 28°57 W
Location:	Freshly broken outcrop near edge of lava field at Yaiza. At start of dirt road heading NW from Yaiza, just west of main Timanfaya road.
Rock Description:	Fine grained, Mid light grey, highly vesicular rock with small olivine rich xenolith (2 cm), surrounded by small vesicles. Some small feldspar megacrysts along with olivine phenocrysts (0.5 - 1 cm).
Rock Type:	Alkali basalt
Mineralogy:	Olivine, clinopyroxene (augite), feldspar laths (sanidine) with skeletal oxides, opaques and devitrified glass in groundmass. Xenolith is mainly olivine with few opaques.

Lan 5 (Dec. 1994-CJH) 1730-36 Phase 4 Timanfaya - Mña del Fuego

Grid Reference:	13°46 N; 28°57 W
Location:	Same flow as 3 and 4, several hundred metres east. Just south of the main Playa Blanca road and just west of the turn off to the main Timanfaya road.
Rock Description:	Mid grey, fine grained, highly vesicular rock. Vesicles are rounded ranging in size from <1 mm to 1 cm. Few small phenocrysts of olivine present
Rock Type:	Alkali basalt
Mineralogy:	Randomly aligned olivine phenocrysts in a fine grained matrix of olivine, pyroxene, feldspar and devitrified glass, some small opaques

L1-30-1 (Oct. 1995 - LET) 1730-36 Phase 4 Timanfaya Mña del Fuego

Grid Reference:	13°45 N; 28°09W
Location:	Sample from just before turning west to Timanfaya, on the Tinajo to Yaiza road.
Rock Description:	Very dark grey, vesicular, fine grained rock, with some small olivine phenocrysts.
Rock Type:	Alkali basalt
Mineralogy:	Very vesicular, glassy matrix to very fine grained matrix, occasional phenocrysts of olivine.

Lan 6 (Dec. 1994-CJH) 1730-36 Phase 5 Mña de Las Nueces

Grid Reference:	13°41N; 28°58W
Location:	Base of first flow to cross the Uga to Teguise road travelling North. Between Macher and Tinajo (via Mancha Blanca) turn offs, rocks sampled on west of main road. (Flow erupted to NE)
Rock Description:	Very fine grained, pale grey rock with a few elongated vesicles. No obvious phenocrysts except a small feldspar crystal.
Rock Type:	Alkali basalt
Mineralogy:	No skeletal oxides, few opaques, olivine, clinopyroxene (augite) and feldspar in very fine grained ground mass.

Lan 7 (Dec. 1994-CJH) 1730-36 Phase 5 Mña Colorada.

Grid Reference:	13°41N; 29°01W
Location:	Sampled on road due north from Uga-Teguise road to Tinajo via Mancha Blanca. Taken from top of a sharp break in slope down toward north to west of Mña Ortiz.

Rock Description:	Fairly fined grained, medium dark grey rock with some olivine rich xenoliths. Some vesiculation with some glassy material infilling some of vesicles. Some feldspar megacrysts
Rock Type:	Alkali basalt
Mineralogy:	Olivine, clinopyroxene (augite), glass, opaques and feldspar laths (sanidine) in ground mass. Random alignment of phenocrysts

Lan 8 (Dec. 1994-CJH) 1730-36 Phase 5 Mña Colorada.

Grid Reference:	13°41N; 29°01W
Location:	Sampled on road due north from Uga-Teguise road to Tinajo via Mancha Blanca. Taken from top of a sharp break in slope down toward north to west of Mña Ortiz.
Rock Description:	Medium dark grey, fine grained rock with abundant olivine rich xenoliths (dunite), highly vesicular with feldspar megacrysts.
Rock Type:	Alkali basalt
Mineralogy:	Feldspar laths (sanidine), olivine, clinopyroxene (augite), opaques and glass in matrix, xenoliths are almost entirely olivine with a few opaques.

Lan 9 (Dec. 1994-CJH) 1730-36 Phase 5 Mña Colorada

Grid Reference:	13°40N; 29°01W
Location:	Caldera Colorada (base of cone bulldozed for xenoliths for tourists) sampled on walk from top of eruptive centre (not in situ).
Rock Description:	Very fine grained, dark grey rock, with small megacrysts of feldspar and olivine phenocrysts (1-2 mm).
Rock Type:	Alkali basalt
Mineralogy:	Clinopyroxene (augite), olivine, glass and feldspar. Lots of olivine phenocrysts, with mainly zoned and broken up around edges.

Lan 10 (Dec. 1994-CJH) 1730-36 Phase 5 Mña Colorada

Grid Reference:	13°40N; 29°01W
Location:	Caldera Colorada (base of cone bulldozed for xenoliths for tourists) sampled on walk from top of eruptive centre
Rock Description:	Very fine grained, dark grey vesicular rock, with numerous small megacrysts of feldspar and large numbers of olivine phenocrysts (< 1 mm - 1 cm across). 1 large (3-4 cm) xenolith - crustal (?) - grey crystalline.
Rock Type:	Alkali basalt
Mineralogy:	Glass, some feldspar and some clinopyroxene (augite) and olivine in groundmass, olivine phenocrysts are zoned and fractured. Feldspar laths (sanidine) obvious.

L1-26-10 (Oct. 1995-LET) 1730-36 Phase 5 Mña Colorada

13°40N; 29°01W

Location:	Caldera Colorada (base of cone bulldozed for xenoliths for tourists) sampled on walk from top of eruptive centre (not in situ).
Rock Description:	Very fine grained, dark grey rock, with small megacrysts of feldspar and olivine phenocrysts (1-2 mm).Variety of xenoliths including large (20 cm) dunite xenoliths, 'conglomerate' xenolith; coarse grained crystalline crustal xenolith (gabbroic composition)
Rock Type:	Alkali basalt
Mineralogy:	Clinopyroxene (augite), olivine, glass and feldspar in ground mass Lots of olivine phenocrysts, with mainly zoned and broken up around edges. large quantity of feldspar laths (sanidine). Xenoliths consist of entirely olivine crystal mixed together with very minor opaques, or olivine, clinopyroxene (augite), feldspar with minor opaques and quartz.

1.5 1824 eruptions

Lan 14 (Dec. 1994-CJH) 1824 (Volcan Nuevo or Tigautón) eruption

Grid Reference:	13°43 N; 29°01W
Location:	After much effort found Volcan Nuevo on Tinajo-Yaiza road, few hundred metres west of visitor centre. (On map published by Carracedo et al 1991, this is the Volcan Tigautón (also 1824) - however every other map lists this vent as Volcan Nuevo)
Rock Description:	Dark grey, fine grained rock, with some areas of vesiculation. 1 large xenolith. Phenocrysts of olivine and feldspar and biotite throughout the rock. Some areas are darker on colour and have more vesicles than others.
Rock Type:	Basanite
Mineralogy:	Cryptocrystalline rock, very fine grained matrix made up of glass, clinopyroxene (augite) and opaques. Ranges in grain size, some regions finer grained. Olivine and feldspar phenocrysts

Lan 15 (Dec. 1994-CJH) 1824 (Volcan Nuevo or Tigautón) eruption

Grid Reference:	13°43 N; 29°01W
Location:	As for sample Lan 14, from west rim of vent
Rock Description:	Dark grey, fine grained vesicular rock with olivine phenocrysts. Vesicles elongated in areas.
Rock Type:	Basanite
Mineralogy:	Fine grained matrix of olivine, glass and opaques with some feldspar laths (sanidine). Olivine phenocrysts.

Lan 16 (Dec. 1994-CJH) 1824 (Volcan Nuevo or Tigautón) eruption

Grid Reference:	13°43 N; 29°01W
Location:	Same as for Lan 14.
Rock Description:	Dark grey, fine grained rock, with some areas of elongated vesiculation. Phenocrysts of olivine and feldspar throughout the rock. Some areas are darker on colour and have more vesicles than others.
Rock Type:	Basanite
Mineralogy:	Cryptocrystalline rock, very fine grained matrix made up of glass, clinopyroxene (augite) and opaques. Ranges in grain size, some regions finer grained. Olivine and feldspar phenocrysts

L1-26-9 (Oct. 1995-LET) 1824 (Volcan Nuevo or Tigautón) eruption

Grid Reference:	13°43 N; 29°01W
Location:	Volcan Nuevo on Tinajo-Yaiza road, few hundred metres west of visitor centre. (On map published by Carracedo et al 1991, this is the Volcan Tigautón (also 1824) - however every other map lists this vent as Volcan Nuevo)
Rock Description:	Vesicular, fine grained dark grey rock, with feldspar laths (sanidine) and small (< 5 mm) olivine phenocrysts
Rock Type:	Basanite
Mineralogy:	Cryptocrystalline rock, very fine grained matrix made up of glass, clinopyroxene (augite) and opaques. Ranges in grain size, some regions finer grained. Olivine and feldspar phenocrysts

L1-28-1 (Oct. 1995-LET) 1824 (Volcan Nuevo or Tigautón) eruption

Grid Reference:	13°43 N; 29°01W
Location:	Same location as Lan 14 Volcan Nuevo on Tinajo-Yaiza road, few hundred metres west of visitor centre. Sample from road side, close to visitors centre.
Rock Description:	Dark grey, fine grained rock, with some areas of vesiculation. Some large olivine xenolith. Phenocrysts of olivine and feldspar throughout the rock. Some areas are darker on colour and have more vesicles than

others. Some crustal xenoliths. More porphyritic than previous 1824 lavas

Rock Type: Basanite

Mineralogy: Cryptocrystalline rock, very fine grained matrix made up of glass, olivine, clinopyroxene (augite), feldspar and opaques. Ranges in grain size, some regions finer grained. Olivine and feldspar phenocrysts

L1-28-2 (Oct. 1995-LET) 1824 (Mña del Chinero or Volcan Nuevo del Fuego) eruption

Grid Reference: 13°47 N; 29°04W

Location: Distill flow of Volcan Nuevo (Carracedo et al 1991) or Mña Chinero run reached the sea, directly north of Mña del Fuego. Sample from end of track west from Tinajo through Los Islotes. Youngest flow overlaps 1730-36 flows, followed down from vent.

Rock Description: Dark grey, fine grained rock, with moderate vesiculation. Olivine xenolith. Phenocrysts of olivine and feldspar throughout the rock. Some areas are darker on colour and have more vesicles than others.

Rock Type: Basanite

Mineralogy: Cryptocrystalline rock, very fine grained matrix made up of olivine clinopyroxene (augite), feldspar and opaques. Ranges in grain size, some regions finer grained. Olivine and feldspar phenocrysts. Xenolith made up of almost entirely olivine crystals with fine grained diseminated opaques.

L1-28-3 (Oct. 1995-LET) 1824 (Mña del Chinero or Volcan Nuevo del Fuego) eruption

Grid Reference: 13°47 N; 29°04W

Location: Around the corner from L1-28-2 Distill flow of Volcan Nuevo (Carracedo et al 1991) or Mña Chinero run reached the sea, directly north of Mña del Fuego.

Rock Description: Dark grey, very vesicular fine grained rock with phenocrysts of olivine throughout the rock. Olivine and crustal (biotite rich) xenoliths.

Rock Type: Basanite

Mineralogy: Cryptocrystalline rock, very fine grained matrix made up of olivine clinopyroxene (augite), feldspar and opaques. Ranges in grain size, some regions finer grained. Olivine and feldspar phenocrysts. Xenolith made up of almost entirely olivine crystals with fine grained disseminated opaques.

B.2 Tenerife -Teide-Pico Viejo Complex

Grid Reference for Teide is 16°38 N; 28°40W

2.1 Caldera floor Rocks

T7-18-1 (Oct. 1995-LET) Caldera floor (mafic) rock - Mña Cerillar

Location:	Mña Cerillar on the NE side of the caldera at Siete Cañadas. Loose ejector on side of the cinder cone
Rock Description:	Dark grey, fine grained slightly vesicular rock, rich in phenocrysts of olivine and pyroxene throughout the rock.
Rock Type:	Alkali basalt
Mineralogy:	Glassy to fine grained matrix made up from olivine, cpx and opaques. Lots of very weathered and altered olivine phenocrysts, and alteration (iddingsite) present as infills in vesicles.

T7-18-3 (Oct. 1995-LET) Caldera floor (mafic) rock

Location:	Sampled from scoria cone next to Areña Negras - Siete Canandas scoria cone, in NE of caldera.
Rock Description:	Very dark grey, fine grained rock with some fresh phenocrysts (1-5mm) of olivine and pyroxene throughout the rock. Vesiculation in areas.
Rock Type:	Basanite
Mineralogy:	Dark black-brown (mesocratic) fine grained matrix, with olivine, clinopyroxene and feldspar laths. Olivine and cpx present as phenocrysts (5-10%) (1-5mm) Few vesicles

T7-18-4 (Oct. 1995-LET) Caldera floor (mafic) rock - Areña Negras

Location:	Sampled from Areña Negras, 1km from road in NE of caldera
Rock Description:	Very dark grey, fine grained rock with fresh phenocrysts (1-5mm) of olivine and pyroxene throughout the rock, trending toward 30% ankaramitic . Vesiculation in some areas.
Rock Type:	Basanite
Mineralogy:	Medium grained groundmass olivine, cpx rich, and some feldspar (sanidine), and opaques. exsolution lamination in cpx phenocrysts - shoshenitic texture. Olivine, clinopyroxene and sanidine present and phenocrysts.

T7-18-5 (Oct. 1995-LET) Caldera floor (mafic) rock

Location:	Sampled from flow south of Areña Negras (T7-18-4), on route back towards road.
Rock Description:	Dark grey, fine grained rock with small vesicles and some fresh phenocrysts (1-2 mm) of olivine and clinopyroxene.
Rock Type:	Alkali Basalt
Mineralogy:	Fine grained groundmass consisting of mainly feldspar (sanidine), opaques and devitrified glass. Vesicular. Some olivine and clinopyroxene phenocryst (< 8mm)

T7-18-6 (Oct. 1995-LET) Caldera floor (mafic) rock - Areña Negras

Location:	Walking north from sample T7-1-5, more proximal sample from Areña Negras, 1km from road in NE of caldera
Rock Description:	Very dark grey, fine grained rock with abundant fresh phenocrysts (5-6 mm) of euhedral olivine and some pyroxene. Vesiculation in some areas. Some regions almost cumulative olivine and clinopyroxene
Rock Type:	Alkali basalt

Mineralogy: Groundmass consists of 70% feldspar, 20% opaques and 10% glass. Some fresh looking olivine and clinopyroxene phenocrysts, but some are resorbed and fragmented

T7-18-7 (Oct. 1995-LET) Caldera floor (mafic vent) rock - Areña Negras

Location: Same location as T7-18-6 Sampled from Areña Negras, 1km from road in NE of caldera

Rock Description: A cumulate 'clot' of olivine and clinopyroxene in a very dark grey, fine grained rock. Vesiculation in some areas.

Rock Type: Basanite

Mineralogy: Groundmass consists of 50% feldspar, 40% opaques and 10% glass. Some fresh looking olivine and clinopyroxene phenocrysts, but some are resorbed and fragmented

T7-18-9 (Oct. 1995-LET) Caldera Floor (mafic) rock Mña Mostaza

Location: Sampled from Mña Mostaza , track runs up to summit, sampled from halfway up track. Difficult to get a solid rock, as most is scoria.

Rock Description: Dark grey, highly vesicular, fine grained rock with numerous phenocrysts (2 - 9 mm) of olivine and pyroxene throughout the rock.

Rock Type: Basalt

Mineralogy: Very fine grained, mesocratic rock, alignment of small feldspar laths in groundmass; vesicular in places and some weathered and fresh olivine and clinopyroxene phenocrysts.

T7-19-11 (Oct. 1995-LET) Caldera Floor (mafic) rock Mña Tapada

Location: Small scoria cone (mafic vent) in middle of evolved vent of Mña de la Cruz.

Rock Description: Fine grained dark grey non-vesicular rock, with small plag. and olivine phenocrysts.

Rock Type: Basanite

Mineralogy: Black glassy to fine grained matrix, few vesicles, skeletal olivine, diopside and kaersutite. Feldspar microcrystalline in matrix.

T7-22-1 (Oct. 1995-LET) Mña Chineryo (1909 eruption)

Location: 1909 eruption just outside the western caldera wall.

Rock Description: Two samples - one is more phenocryst rich, and the other is more typical of the rock type. Dark grey fine grained rock with small vesiculated areas. Phenocrysts of olivine and pyroxene.

Rock Type: Basanite

Mineralogy: Fine grained vitric mesocratic rock containing olivine, augite, feldspar and opaques (prob. magnetite) Groundmass contains fine grained feldspar (sanidine laths), olivine, augite, and perhaps anorthoclase.

Pico Viejo

T7-22-2 (Oct. 1995-LET) Mña Cangreco

Location: Recent historic eruption on western edge of caldera.

Rock Description: Dark grey fine grained vesiculated rock, some phenocrysts of olivine and pyroxene (2-mm).

Rock Type: Basanite

Mineralogy: Fine grained vesicular mesocratic rock containing olivine, augite, ± feldspar and opaques (prob. magnetite) Groundmass contains aligned fine grained feldspar (sanidine laths), olivine, and augite.

T7-19-4 (Oct. 1995-LET) Oldest Pico Viejo (pv1)

Location: Sampled alongside track which makes its way up toward Asientos Altos on the SW flank of Pico Viejo. Sample from small scoria cone : Volcan de Corona

Rock Description:	Dark grey, vesicular, fine grained rock with some small phenocrysts (1-5mm) of feldspar throughout the rock.
Rock Type:	Tephrite
Mineralogy:	Glassy matrix with some vesicles, with some microcrystalline feldspar. Phenocrysts of sanidine, opaques and clinopyroxene.

T7-19-5 (Oct. 1995-LET) Asientos Altos (pv2)

Location:	Sampled on track in Asientos Altos on the SW flank of Pico Viejo. Upper part of Asientos Altos.
Rock Description:	Dark grey, vesicular, fine grained rock with large euhedral phenocrysts (1-5mm) of feldspar and sub rounded olivine and pyroxene.
Rock Type:	Tephrite
Mineralogy:	Highly porphyritic with a glassy matrix. Euhedral plagioclase, subrounded olivine and clinopyroxene (diopside) and magnetite Opaque inclusions in resorbed Anorthoclase crystals.

T7-19-6 (Oct. 1995-LET) Asientos Altos (pv2)

Location:	Sampled on track in Asientos Altos on the SW flank of Pico Viejo. Lower part of Asientos Altos.
Rock Description:	Dark grey, vesicular, fine grained rock with some large euhedral phenocrysts (1-5mm) of feldspar and sub rounded olivine and pyroxene.
Rock Type:	Basanite
Mineralogy:	Highly porphyritic with a glassy matrix. 5mm phenocrysts of labradorite, often with inclusions and unhappy edges. 1-2mm sanidine, clinopyroxenes (diopside ?) and opaques. Oligoclase possible ± apatite and olivine

T7-19-7 (Oct. 1995-LET) Asientos Altos (pv2)

Location:	Sampled on track back to road in Asientos Altos on the SW flank of Pico Viejo. Lower part of Asientos Altos.
Rock Description:	Dark grey, slightly vesicular, fine grained rock with large plagioclase phenocrysts. Part of a compound flow, with lots of channels
Rock Type:	Basanite
Mineralogy:	Highly porphyritic with a glassy matrix. 5mm phenocrysts of labradorite, often with inclusions and unhappy edges. 1-2mm sanidine, clinopyroxenes (diopside ?) and opaques. Oligoclase possible ± apatite and olivine

T7-19-8 (Oct. 1995-LET) Asientos Altos (pv1)

Location:	Sampled on track back to rock below Asientos Altos on the SW flank of Pico Viejo. Earliest pv products Lava lake tephrite ! Close to BH-2
Rock Description:	Dark grey, with some elongate vesicles, fine grained rock with small feldspar and olivine phenocrysts.
Rock Type:	Basanite
Mineralogy:	Brown glassy matrix with clear cut vesicles, non porphrytic. Sanidine, anorthoclase, andesine, clinopyroxene and opaques.

T7-19-3 (Oct. 1995-LET) Lower cone Pico Viejo (pv3)

Location:	Sampled between two tongues of the 1798 eruption, 10 m from road which comes into the caldera from the north-west.
Rock Description:	Dark grey, slightly vesicular, fine grained rock with rare phenocrysts (< 5 mm) of feldspar.
Rock Type:	Phonolitic Tephrite
Mineralogy:	Sparsely porphyritic with a glassy trending to fine grained crystalline matrix. Mineralogy consists of amphibole, olivine, clinopyroxene, feldspar and opaques. Phenocrysts include Diopside (1-2 mm), kaersutite (1-2 mm), magnetite (<0.5mm) with some olivine and apatite as inclusions in the amphibole and plagioclase and sanidine laths.

T7-20-2 (Oct. 1995-LET) Lower cone Pico Viejo (pv3)

Location:	Sampled just south of tongue of t2 lava, 0.5km NNE of the top end of Roques de Garçia. Pahoe-hoe
Rock Description:	Dark grey, slightly vesicular, fine grained rock with rare phenocrysts (< 3 mm) of feldspar.
Rock Type:	Phonolitic Tephrite
Mineralogy:	Banded rock with glassy trending to fine grained crystalline matrix with feldspar laths. Phenocrysts include Diopside (1-2 mm), kaersutite (1-2 mm), magnetite (<0.5mm) feldspar (sanidine) with some olivine and apatite as inclusions in the amphibole and feldspar and sanidine laths. More basic regions swirl into ore felsic regions.

T7-20-3 (Oct. 1995-LET) Lower cone Pico Viejo (pv3)

Location:	Sampled on top of the breach of the Roques de Garçia - 25 m from edge.
Rock Description:	Dark grey, fine grained rock with large feldspar phenocrysts (1-2cm). Very weathered
Rock Type:	Phonolitic Tephrite
Mineralogy:	30% feldspar phenocrysts - Ca feldspar (sanidine) often with opaque inclusion, minor clinopyroxene and apatite. Fine grained groundmass with glass, clinopyroxene, apatite, amphibole feldspar laths and opaques, some areas more glassy than others.

T7-20-4 (Oct. 1995-LET) Lower cone Pico Viejo (pv3)

Location:	Sampled just south of tongue of t2, between R.d.G and t2.
Rock Description:	Mid grey, weathered flow, fine grained rock with small feldspar phenocrysts (1-2cm). Very weathered
Rock Type:	Phonolitic Tephrite
Mineralogy:	Fine grained groundmass consisting of feldspar laths, opaques, kaersuitite and clinopyroxene. Phenocrysts include zoned sanidine and oligoclase - andesine. Resorbed olivine with opaque inclusion, clinopyroxene and apatite. On the whole, phenocrysts - unhappy !

Teide Flanks

T7-19-10 (Oct. 1995-LET) Mña Majua (tf1 - previously cf2)

Location:	Sampled from lobe of Mña Majua, SSE of Teide.
Rock Description:	Brown banded rock with feldspar laths and dark brown (mica ?) sheets.
Rock Type:	Phonolite
Mineralogy:	Welded bands, lightly glassy rock, with phenocryst of biotite and feldspar. Resorbed clinopyroxenes and feldspar laths in matrix (Sanidine + oligoclase).

T7-19-9 (Oct. 1995-LET) Mña de la Cruz (tf1 - previously cf2)

Location:	Sampled from lobe of Mña Majua, close to Mña de la Cruz. Just east of Mña Tapada, SSE of Teide.
Rock Description:	Black fine grained rock, coloured sheen, Feldspar phenocryst in an almost pure glass. Current flow obvious on surface.
Rock Type:	Phonolite
Mineralogy:	Welded glassy rock with few phenocryst of feldspar sanidine (5mm) and biotite (1mm) and opaques.

T7-18-10 (Oct. 1995-LET) Teide Flank (ab1) Areña Blancas

Location:	Sampled 0.5 km from road, east of Arenas Blancas pumice deposit,

Rock Description: Medium grey, vesicular, fine grained rock with abundant feldspar laths and pyroxene phenocrysts throughout the rock.
Rock Type: Trachy-phonolite
Mineralogy: Fine to medium grained matrix with brown glassy regions, feldspar laths and opaques in matrix. Feldspar (sanidine, anorthoclase) and (< 3mm) pyroxene phenocrysts.

T7-18-13 (Oct. 1995-LET) Teide Flank (ab1) Areña Blancas
Location: Sampled from tongue of ab1 lava west of El Culaton
Rock Description: medium grey, fine grained rock with some fresh phenocrysts (1-5mm) of feldspar and biotite throughout the rock.
Rock Type: Trachy-phonolite
Mineralogy: Fine to medium grained matrix composed of feldspar laths and opaques and glass. Feldspar (sanidine) and nepheline (6-8mm) kaersutite and some opaques as phenocrysts. No obvious olivine or clinopyroxene phenocrysts.

T7-18-12 (Oct. 1995-LET) Teide Flank (ab1) Areña Blancas
Location: Sampled from east of roadside from Mña Rajada flow
Rock Description: Medium grey, fine grained rock with some feldspar phenocrysts and small pyroxene crystals throughout the rock.
Rock Type: Tephritic phonolite
Mineralogy: Fine to medium grained matrix composed of feldspar laths and opaques. Feldspar (sanidine, anorthoclase) and nepheline and kaersutite (6-8mm) phenocrysts.

T7-18-2 (Oct. 1995-LET) Areña Blancas member (mc1)
Location: Sampled from close to park office in NE of caldera, distill flow from Mña de los Corrales
Rock Description: Mid grey, fine grained rock with some phenocrysts (1-5mm) of olivine, pyroxene and feldspar throughout the rock.
Rock Type: Tephritic Phonolite
Mineralogy: Crystalline fine grained groundmass, with the majority being feldspar (sanidine and anorthoclase), biotite and some opaques. Sanidine and some Kaersutite present as phenocrysts ± nepheline.

T7-18-8 (Oct. 1995-LET) Teide Flank (mc2)
Location: Sampled from flow from Mña de los Corrales, close to roadside. Halfway between vent and distill end of flow (T7-18-2)
Rock Description: Very dark grey, highly vesicular, fine grained rock with some fresh phenocrysts (1-5mm) of olivine and pyroxene throughout the rock.
Rock Type: Tephritic phonolite
Mineralogy: Medium grained groundmass consists of 90% aligned feldspar laths , 5 % opaques and 5 % glass ± amphibole. Vesicles and opaques are also present. Phenocryst phases include opaques and kaersutite.

Pico Viejo Summit (PVS2)

T7-PV-4 (Oct. 1995-LET) Pico Viejo summit (pv5)
Location: Sampled from summit of Pico Viejo
Rock Description: Medium grey, fine grained rock with some dark lath shaped crystal (hornblende) and feldspar phenocrysts.
Rock Type: Tephritic phonolite
Mineralogy: Fine grained matrix with biotite, hornblende, and opaques. Sanidine and amphibole phenocryst with olivine and augite.

T7-PV-3 (Oct. 1995-LET) Pico Viejo summit (pv5)

Location:	Sampled from summit of Pico Viejo
Rock Description:	Dark grey, fine grained rock with aligned feldspar phenocrysts ranging in size from 1cm diameter to 0.5mm.
Rock Type:	Tephritic phonolite
Mineralogy:	Very fine grained matrix composed of feldspar laths (sanidine), biotite, hornblende, augite and olivine and opaques. Feldspar sanidine and kaersutite (6-8mm) phenocrysts.

T7-PV-2 (Oct. 1995-LET) Pico Viejo summit (pv5)

Location:	Sampled from summit of Pico Viejo
Rock Description:	Medium grey, fine grained rock with pyroxene and feldspar phenocrysts ranging in size from 1cm diameter.
Rock Type:	Tephritic phonolite
Mineralogy:	Fine grained matrix with biotite sanidine, augite and hornblende. Needle like feldspar crystals. Ground mass composed of feldspar, biotite, olivine with crushed opaque surrounds and opaques.

T7-20-1 (Oct. 1995-LET) Pico Viejo *summit (pv5)*

Location:	Sampled close to Roques de Garçia, from main flow from Pico Viejo summit. (similar to PV2-4).
Rock Description:	Dark grey, fine grained rock with some vesicles and numerous feldspar phenocrysts ranging in size from 1cm diameter.
Rock Type:	Phonolite
Mineralogy:	Fine grained mesocratic rock with glassy groundmass with laths of sanidine and opaques. Phenocrysts of euhedral kaersuitite and salite, magnetite, clinopyroxene and resorbed feldspar (oligoclase ?).

T7-PV-11 (Oct. 1995-LET) Pico Viejo summit (pv6)

Location:	Sampled from just outside summit crater of Pico Viejo
Rock Description:	Medium grey, fine grained rock vesicular with feldspar phenocrysts
Rock Type:	Tephritic phonolite
Mineralogy:	Dark fine grained matrix with glassy regions. Kinked sanidines, olivine and clinopyroxenes and opaques.

T7-PV-1 (Oct. 1995-LET) Pico Viejo summit (pv7)

Location:	Sampled from NW of summit of Pico Viejo, from largest flow on NW flank.
Rock Description:	Light grey, fine grained vesicular rock with feldspar phenocrysts ranging in size from 1cm diameter.
Rock Type:	Phonolite
Mineralogy:	Fine grained matrix with few phenocrysts of sanidine, needle shaped augite and hornblende. Needle like feldspar crystals.

T7-PV-10 (Oct. 1995-LET) Pico Viejo summit (pv8)

Location:	Sampled from inside summit crater of Pico Viejo
Rock Description:	Dark grey, very vesicular fine grained rock with lath shaped and rounded feldspar phenocrysts.
Rock Type:	Phonolitic tephrite
Mineralogy:	Fine grained dark groundmass with Fe staining. Sanidine, augite and olivine phenocrysts (4mm).

T7-PV-8 (Oct. 1995-LET) Pico Viejo summit (pv8)

Location:	Sampled from summit of Pico Viejo
Rock Description:	Light grey, fine grained rock with numerous feldspar phenocrysts.
Rock Type:	Phonolitic tephrite
Mineralogy:	Fine grained dark groundmass with Fe staining. Sanidine, and plagioclase > 70% of the phenocrysts. Augite, apatite, opaques and olivine.

T7-PV-7 (Oct. 1995-LET) Pico Viejo summit (pv8)

Location:	Sampled from summit of Pico Viejo
Rock Description:	Medium to light grey, fine grained rock with numerous feldspar phenocrysts, vesicles and rounded quartz (?).
Rock Type:	Phonolitic tephrite
Mineralogy:	50% of rock is phenocrysts of plagioclase and sanidine. Olivine and augite (0.2-0.3 cm) in a glassy matrix trending to very fine grained dark groundmass in certain areas.

T7-PV-6 (Oct. 1995-LET) Pico Viejo summit (pv9)

Location:	Sampled from summit of Pico Viejo
Rock Description:	Black very fine grained rock interbedded with red scoria staining. No obvious phenocrysts or vesicles.
Rock Type:	Basanite
Mineralogy:	Banded, some areas with very dark groundmass others more glassy in texture. Fine grained sanidine, plagioclase, augite, olivine in matrix.

T7-PV-13 (Oct. 1995-LET) Pico Viejo summit (pv9)

Location:	Sampled en route down Pico Viejo from Mña de los Chircheros.
Rock Description:	Fine grained, dark grey rock, vesicular with a few feldspar phenocrysts.
Rock Type:	Plag. basanite
Mineralogy:	Dark very fine grained matrix, vesicular with sanidine phenocrysts aligned in rock and opaques.

Teide PTS2

T7-22-3 (Oct. 1995-LET) Teide (t2)

Location:	Sampled from toe of lava from Teide, close to rock, just west of youngest flows from Teide. Opposite Mña Majua.
Rock Description:	Mid grey, fine grained porphyritic vesicular rock with numerous feldspar phenocrysts (up to 7mm)
Rock Type:	Phonolitic tephrite
Mineralogy:	Vesicular fine grained groundmass (streaky microcrystalline) Aligned feldspars, 25% porphyritic with phenocrysts of augite and diopside, kaersuitite, corroded feldspar, anorthoclase, magnetite. Poss. resorbed andesine-oligoclase

T7-20-5 (Oct. 1995-LET) Teide (t2)

Location:	Sampled from Toe of t2 just NW of Roques de Garçia. Bomb sampled just opposite flow front pv3-pv3.,
Rock Description:	Dark grey vitric flow with numerous feldspar phenocrysts.
Rock Type:	Phonolite
Mineralogy:	Vitric dark groundmass, trending toward fine grained in areas. Feldspar phenocrysts with blue hauyne present. Sanidine, and plagioclase.

T7-20-6 (Oct. 1995-LET) Teide (t3)

Location:	Sampled from black vitric flow from Teide , close to roadside opposite Mña Majua.
Rock Description:	Very dark rock, with large elongate feldspar phenocrysts.
Rock Type:	Phonolite
Mineralogy:	Vitric dark rock with large feldspar phenocrysts- 38% phenocryst. Dominant anorthoclase with clinopyroxene, magnetite and occasional apatites in streaky poorly vesicular brown glass. Blue Hauyne also present.

T7-20-7 (Oct. 1995-LET) Teide (t3)

Location:	Sampled from Toe of youngest Teide flow close to road, just before El Tabonal Negras.
Rock Description:	Black vitric lava, highly vesicular, with plagioclase phenocrysts.
Rock Type:	Phonolite
Mineralogy:	Vitric dark rock trending to fine grained in places 30-40% phenocrysts Dominant sanidine and anorthoclase, often resorbed with inclusions, with clinopyroxene, apatite in streaky poorly vesicular brown glass. Blue Hauyne also present. Welded texture in parts.

T7-22-2 (Oct. 1995-LET) Mña Cangreco 1492 eruptions (pv4)

Location:	ed from cone just south of Mña Chineryo just outside caldera.
Rock Description:	Dark grey fine grained rock with large vesicles and some olivine and clinopyroxene phenocrysts.
Rock Type:	Olivine rich basalt
Mineralogy:	Vesicular fine grained mesocratic rock, groundmass of olivine, clinopyroxene, opaques and aligned sanidine laths. Phenocrysts : clinopyroxene and olivine.

T7-19-2 (Oct. 1995-LET) Historic Pico Viejo (pv12) Rock 1798 eruption

Location:	Sampled from 100 m from road which comes into the caldera from the north-west. Sample of the Lavas Negras from Mña Chahorra 1798 eruption
Rock Description:	Medium grey, vesicular, fine grained rock with some fresh phenocrysts (10 mm) of feldspar. Rubbly flow banding on the top.
Rock Type:	Phonolitic Tephrite
Mineralogy:	Fine to medium grained groundmass composed of clinopyroxene, amphibole (Kaersutite) aligned feldspar (sanidine and andesine) laths, opaques and glass. Rare phenocrysts of clinopyroxene, opaques, and some feldspar (plagioclase) with inclusion rims and zonation

T7-18-11 (Oct. 1995-LET) Teide Flank (mb1) Mña Rajada

Location:	Sampled from east of roadside from Mña Rajada flow.
Rock Description:	Very dark grey, glassy rock with some fresh phenocrysts (1-5mm) of feldspar throughout the rock.
Rock Type:	Phonolite
Mineralogy:	Brown glassy (non-crystalline, Feldspar (sanidine, anorthoclase) and nepheline (6-8mm) phenocrysts. No obvious olivine or clinopyroxene phenocrysts, and some vesicles.

T7-PV-5 (Oct. 1995-LET) Mña Blanca Lower (mb3a)

Location:	Sampled from Pico Viejo summit area (Unit II)
Rock Description:	Dark grey rock with greenish weathering, no vesicles and occasional feldspar phenocryst
Rock Type:	Phonolite
Mineralogy:	Glass ! (no obvious minerals)

T7-21-1 (Oct. 1995-LET) Mña Blanca Upper (mb4) El Culaton

Location:	Sampled from 500m up the path to Mña Blanca summit.
Rock Description:	Light grey, glassy, vesicular, fine grained rock.
Rock Type:	Phonolite
Mineralogy:	Welded and banded pumice. Phenocryst poor assemblage, skeletal olivine, magnetite, possible ilmenite, with some anorthoclase/sanidine.

T7-21-2 (Oct. 1995-LET) Mña Blanca Upper (mb4) El Culaton

Location:	Sampled from 250 m up the path to Mña Blanca summit.
Rock Description:	Light grey, glassy, vesicular, fine grained rock, part of a blocky to aa phonolite flow.
Rock Type:	Phonolite
Mineralogy:	Welded pumice. More phenocryst rich than 21-1. Sanidine/Anorthoclase as individual laths and as fragments inside

crystals. No obvious amphibole, olivine or pyroxene. Groundmass is very fine crystals of feldspar..

T7-19-1 (Oct. 1995-LET) Mafic complex Extra-caldera rock

Location:	Sampled from bomb which was part of the western mafic complex, outside caldera on the western side of the Chico road.
Rock Description:	Bomb with beautiful breadcrust texture, scoria and more massive sections.
Rock Type:	Phonolitic Tephrite
Mineralogy:	Vitric black matrix with microphenocrystalline aligned feldspar (sanidine) laths and opaques. Phenocrysts (< 5mm); resorbed kaersutite, sanidine, anorthoclase ± andesine and some opaques (magnetite).

T7-PV-9 (Oct. 1995-LET) Gabbroic bomb from PV summit

Location:	Sampled from Pico Viejo summit.
Rock Description:	Coarse grained, medium grey with altered olivine, phenocrysts. Feldspar and Quartz also present.
Rock Type:	Gabbro
Mineralogy:	Olivine, augite, plagioclase with biotite in coarse grained ground mass. Olivine and clinopyroxene phenocrysts.

T7-PV-12 (Oct. 1995-LET) Gabbroic bomb from PV summit

Location:	Sampled from Pico Viejo summit.
Rock Description:	Gabbroic xenolith -lithics. Weathered light to medium grey rock, medium grained with pyroxene and feldspar obvious.
Rock Type:	Gabbro
Mineralogy:	Olivine, augite, sanidine in coarse grained ground mass.

APPENDIX C:

Analytical Techniques

The samples collected for this project were treated in the following ways, using techniques which are standard for major, trace element and radiogenic isotope analysis in silicate rocks.

C.1 Whole Rock Sample Preparation

The freshest possible samples were collected, which meant that a number were sampled from newly generated road cuttings, and about 1 - 3 kg of sample was collected from each locality. The samples were split into blocks of a few cm^3 using a hydraulic splitter, and all the weathered surfaces and xenoliths bearing areas were removed (using the same hydraulic splitter). Approximately 800 -1000 g of samples was then crushed to < 1 cm chips using a hardened steel jaw crusher. A representative sample of this material was taken using the quartering technique, after any remnants of weathering or phenocryst or xenolith phase were removed. This sample was then powdered to < 200 mesh using either an agate tema swingmill or an agate ball mill.

C.2 X-Ray Fluorescence (XRF) Sample Preparation and Analysis

For major element analysis 0.7000 g of the sample powder (dried overnight at >100°C) was weighed into a platinum (+ 5% Au) crucible with 3.5353 g (± 0.0002 g) of *Johnston Mattey* Spectroflux 100B lithium metaborate-tetraborate fluxing agent, and mixed carefully using a polythene rod. The samples were cooled in a dessicator (containing silica gel) to prevent the reabsorbtion of water prior to weighing. The crucibles containing the mixed flux and sample were heated in a muffle furnace at 1100°C for 15 minutes in batches

of 6, with homogenisation of melt and bubble elimination ensured by swirling the crucibles every 5 minutes. The melt from each crucible was carefully poured in turn, into a pre-heated brass disc mould and a disc press formed a 2.5 cm diameter disc. The discs were cooled slowly under glass covers prior to labelling for analysis.

Loss on Ignition (L.O.I.) calculations were made at the same time by heating 1 - 2 g of sample in pre-heated silica crucibles in a muffle furnace at 1000 °C for 30 minutes. The crucibles were allowed to cool for 10 minutes before being re-weighed. The weight loss (or gain in samples with high Fe contents) was then taken as the volatile content of the sample (mainly CO_2 and H_2O), (or the oxidising potential of the sample for an increase in weight).

The trace elements (Ba, Rb, Sr, Nb, V, Y, Zn, Cu Cr and Ni) of the samples were analysed on powder pellets (Watson J.S. 1996). 8-10 g of powder was weighed into a small polythene bag, to this 6-7 g of PVP (Polyvinylpyrollidone - methyl cellulose binding agent) was added, and the contents were mixed thoroughly following the method of Watson (1996). The mixture was put into a pellet mould and compressed in a hydraulic press at ~ 10 ton/inch^{-2} so that a 3 cm diameter powder pellet was obtained. The pellets were dried at 110°C overnight prior to labelling for analysis.

All analysis were carried out at the Open University using the ARL 8420+ goniometer wavelength dispersive XRF spectrometer, which is equipped with 3 kw Rh anode end-window X-ray tube and diffracting crystals AX06 (multi-layer) PET (Penta-erythrytol), Ge111, LiF200 and LiF220. Elemental intensities were corrected for background and known peak overlaps. Instrumental drift was corrected for using a drift monitor. Standard rock powders were also run as a check on the drift within the run on the spectrometer. The running conditions and calibration lines are described in Potts et al. (1984). Overview of technique can be found in Gill (1997).

C.3. Instrumental Neutron Activation Analysis (INAA)

Neutron activation analysis was carried out at the Open University to determine rare earth element abundances, as well as U, Th, Ta, Rb, Cs, Co, Sc, Cr and W. Analytical

techniques, counting conditions, peak fitting calibrations and corrections are described in full in Potts et al., (1981, 1985a).

0.300±10 g of rock powder was weighed and sealed into a polythene vial. The samples were then placed in batches of nine, along with two standards (Ailsa Craig microgranite and Whinn Sill dolerite) into a polythene cylinder/tube. The vials was separated by pre-weighed and numbered iron foil discs lacquered onto a larger polythene discs, to monitor neutron flux along the cylinder during irradiation at the Imperial College Reactor Centre at Ascot. The samples were subjected to a thermal neutron flux of $5*10^{12}$ ncm^2sec^{-1} for 24 to 30 hours. Measurements were carried out at the Open University after a one week period post irradiation to allow for decay of short lived nuclides or cooling. Counting took place in two sets over a period of a month using a co-axial Ge (li) detector and a planar low energy photon spectrometer (LEPS) either side of the sample vial. Short counts lasted for 800 seconds while long counts took place over 6 to 10 hours.

C.4. Radiogenic Isotope Analysis

Isotope analyses, including both isotope dilution for trace element contents (U, Th, Ra) and isotopic compositions (Sr, Nd, Pb, U, Th, Ra) were carried out in the radiogenic isotope labs over the period from March 1995 to February 1998 in the radiogenic isotope laboratories at the Open University. Clear air is supplied to maintain a positive air pressure. Teflon two bottle distillation is used to distill HF, the HCl is distilled in a Quartz two stage boiling still and HNO_3 is distilled in Quartz subboiling still. Water is purified with Mili-Q-reverse osmosis. Reagents (including water) are purified further by Teflon two bottle distillation to TD standard for the Sr and Nd dissolution and for all the U, Th and Ra chemistry. Whilst Pb isotope analysis requires a further Teflon two bottle distillation to a 2xTD standard for all the reagents . The standard BioRad Cationic and Anionic resins were cleaned in 6 alternating washes of QD HCl and RO H_2O and were left in a final rinse RO H_2O until ready for use. Routine blanks for Sr, Nd and Pb were < 0.8, 0.3 and 0.3 ng, respectively. Standard methods of dissolution are summarised below for the Sr, Nd and Pb analysis.

C.5. Sr and Nd Isotope Preparation

Samples were weighed out into cleaned Savillex teflon beakers (see C7 beaker cleaning) with screw top lids. 100 - 150 mg of samples was used in order to deliver 42,000 to 156,000 ng of Sr (420 -1040 ppm for Lanzarote samples) and 2270 to 9870 ng of Nd to filament. (Nd = 22.7 - 65.8 ppm). The aim was to get a minimum of 750 ng Nd and 5 μg of Sr to the mass spectrometer, hence the amount of sample is increased to over three times to get the amount required. A few drops of TD 15M HNO_3 were added to wet the sample prior to the addition of 2 - 3 ml of TD HF (48%), the sample was then sealed and left to digest (usually overnight on a hotplate). Once the sample was digested ~ 2 ml of TD 15M HNO_3 and ~ 4 ml of Saturated Boric Acid (*see below) were added. This mixture was evaporated under compressed air supply evaporation hoods until a paste consistency was reached, at this stage 2 ml of TD 15M HNO3 were added and after the sample had gone into solution, it was evaporated to dryness. 6 ml of TD 6M HCl were added to the dried residue and a clear solution was obtained after heating on a hotplate. The HCl was evaporated off and a final dissolution was carried out in 2 ml of QD 2.5M HCl for loading onto cation exchange columns.

The sample was transferred from the Teflon beaker into a centrifuge tube and centrifuged at 4000 rpm for 5 minutes to ensure that any undissolved solids were not loaded onto the columns. 1 ml of the resultant solution was loaded onto a pre-conditioned (with 2.5M HCl) cation exchange column containing 10 ml of Biorad® 200-400 mesh AG 50W X8 resin. The sample was washed onto the column using 2 x 1 ml rinse of QD 2.5M HCl and was then eluted using 36 ml of the same acid. The Sr fraction was collected in 14 ml of QD 2.5M HCl, and evaporated to dryness. The Nd fraction was collected by eluting 18 ml of QD 3M HNO_3 and collecting a further 17 ml. This fraction was evaporated to dryness, then redissolved in ~ 0.5 ml QD 0.25M HCl before being loaded onto a pre-conditioned reverse chromatography ion exchange column comprising of 1g of Teflon powder (Voltalef 300 LD PL micro) and 100 g of DEP (di (2-ethylhexyl) phosphate). Again the sample was washed into the resin bed using 2 x 1 ml rinses of QD 0.25 ml HCl, followed by the elution of 18 ml

of QD 0.25M HCl. The Nd fraction was collected in a further 18 ml of the same acid and evaporated to dryness.

* A high blank was traced back to the Saturated Boric Acid and for later analysis this stage was omitted from the procedure. For the few samples measured using the boric acid, the amount of Sr on the filament was significantly large (i.e. high ppm Sr) to prevent the higher blank causing a problem. A selection of these samples were repeated without the boric, and results obtained were within error of those with the boric contamination.

The Sr fraction was loaded onto a single Ta filament which had been outgassed at 4.5A for 5 minutes in a vacuum < 10^{-6} torr. A drop of H_3PO_4 was dried down onto the centre of the filament and the Sr fraction dissolved in 2 µl of TD H_2O, was loaded and dried down at a current of 1.2 A. The H_3PO_4 was evaporated off at 2 A. The Nd fraction was loaded in 2 µl H_2O onto a double Ta filament and dried down at a current of 0.8 A. This was run in the MAT 262 opposite a double Re evaporation filament.

C.6. Pb Isotope Analysis

The Pb dissolution and separation procedure used smaller volumes of cleaner (2 xTD) reagents, so ensure that the blank is minimised, as the samples contain less than 6 ppm Pb. Powders are weighed out into 7 ml Savillex Teflon beakers with screw top lids. Approximately 100 mg was weighed out and wetted with a few drops of 2xTD 15M HNO_3 before < 2 ml of 2xTD HF were added and the samples were left to dissolve on a hotplate overnight. After the samples had gone in solution, they were dried to a paste under compressed air fed evaporating hoods. 2 ml of 2xTD 15M HNO_3 were added and the residue was dissolved before evaporation to dryness. At this point, 2 ml of 2xTD 6M HCl were added, and a clear solution was formed overnight on a hotplate, this was then evaporated to dryness. 1 ml of 1M TD HBr was added, and left to dissolve the sample on a hotplate for twenty minutes and then left to cool overnight.

New columns were made from 1 ml pipette tips by placing small teflon frits inside the tip. The column chemistry was conducted using column volumes as opposed to ml, which allowed the addition of the acids directly from the reagent bottle, hence minimising

contamination. The columns were conditioned by being soaked overnight in QD 6M HCl, then rinsed with QD 6M HCl, and RO H_2O, then were placed into the column racks ready for use. They were given a further rinse in alternate washes of QD 6M HCl and RO H_2O, before the addition of ~ 100 µl (~ 5 drops) of Dowex 200 -400 mesh anionic exchange resin. The resin was washed using a sequence of one column volume (CV) of 2xTD 6M HCl followed by one CV of 2xTD H_2O repeated twice and then the column was pre-conditioned with 0.5 CV of TD HBr.

1 ml of sample solution was loaded onto the column using a 1ml pipette which had been cleaned in TD HBr. The sample was washed onto the column with 0.5 CV TD HBr followed by a further CV of the same acid. The Pb fraction was eluted into a clean beaker using two CV of 2xTD 6M HCl. 50 µl of 2xTD 15M HNO_3 was added to remove any bromine from the sample. This fraction was then evaporated to dryness and redissolved in a few drops of TD HBr for a second pass through the columns. Prior to this second pass the columns were cleaned as before and pre-conditioned with TD HBr. The sample was loaded onto the column and the elution was repeated as before. 2 µls of H_3PO_4 were added to the collected Pb fraction, allowing the residue to be easily located after evaporation.

Loading took place in a laminar flow cabinet, onto single Re filaments by the addition fo 2 µls of silica gel to the H_3PO_4 residue in the base of the beaker using a cleaned pipette. The sample was loaded onto the centre of the filament and dried down at a current of 0.9A. The sample was finally heated to ~1.8A, until a dull red glow and the silica gel had formed a whitish glass.

C.7. Cleaning Procedures

All the radiogenic isotope techniques require strict cleaning procedures to prevent cross contamination of samples and external contamination. All pipettes used are rinsed with the acid to be used for that stage. Care is taken not to disturb resin in the columns and when reagents are added directly from the reagent bottles care is taken to prevent contamination of the tip of the bottles. Reagent blanks, beaker blanks and total procedure blanks are run routinely throughout the time of analysis.

The Savillex Teflon beakers used for dissolution and for collection of the eluted fractions are cleaned in different ways for the different isotopes. Pb, U, Th and Ra require cleaner beakers than Sr and Nd. Beakers for Sr and Nd were first rinsed with RO H_2O to remove any sample residue, left overnight on a hotplate containing a few ml of dilute QD 1.5M HNO_3, rinsed, then left to soak in a beaker of 15M HNO_3 for at least 24 hours on at hotplate. They were then rinsed with RO H_2O and placed into a beaker of warm RO H_2O for 24 hours, then rinsed again and left on a hotplate with a few ml of QD 6M HCl before the final RO H_2O rinse prior to use. The same procedure is used for the Pb, U, Th and Ra beakers with a number of additional cleaning steps. The beakers were half filled with QD 6M HCl before going into the 15M HNO_3 bath, instead of dilute HNO_3. After 24 hours in the RO H_2O bath, the beakers were left containing a few ml of TD 6M HCl for U, Th and Ra and 2xTD 6M HCl for Pb on a hotplate for a few hours. This step was repeated with fresh acid, finally after rinsing with TD H_2O, the U, Th and Ra beakers were left with couple of ml of TD H_2O on a hotplate prior to use. Whilst the Pb beakers were rinsed with 2xTD H_2O before use.

If the same beaker was used for the dissolution and to collect the separated fraction, whilst the sample was being eluted through the columns the beaker were left with a couple of ml of the appropriate standard of 6m HCl acid (QD, TD or 2xTD) on a hotplate. The acid was refreshed at least once, and there was a final rinse with the appropriate H_2O prior to collection.

Filaments were ground and sandblasted to remove any residue Re or Ta ribbon, and the contacts were tested to be greater than 500 MΩ. They were cleaned by boiling in several changes of RO H_2O for ten to fifteen minutes, and dried in a vacuum oven before welding and outgassing.

C.8. Blanks and Yields

Total procedure blanks (TPB)were run alongside the routine samples runs. A known amount of Sr, Nd, Pb, U-Th or Ra spike (depending on which element was being analysed), was weighed out into a clean beaker. This was taken through the procedure with the rest of

the samples, the same amounts of acid were added and evaporated and the same routine was followed on the column procedure. The blank was dried down and loaded onto a filament and run on the respective mass spectrometer, the known ratio and concentration of the standard or spike was then taken away from that analysed. This gave the amount of contamination added to the sample values from the procedure. If the total procedure blank was high, relative to the concentration in the sample, the samples were repeated. The effect of the blanks varied from sample to sample, as the concentration of some samples was much lower than others.

A source of a high TPB may be general contamination through poor lab technique or through a contaminated reagent. To rule out the latter, reagent blanks were run at routine intervals throughout the period of chemistry. This entailed a volume of reagent (not less than 10 ml) being weighed into a cleaned beaker, a volume (usually 0.5 g) of spike was added, and the solution was dried down and loaded onto a filament and run as usual for blanks. (For Boric Acid, it was necessary to dry down a volume of saturated boric acid (as the residue will be crystalline), then take up in 15M HNO_3, dry this down and take up in 7M HNO_3, this was then taken through a 4 ml anionic column, and eluted and collected as normal. Obviously the Boric blank must have the HNO_3 blanks and the column blanks taken away from the total obtained.

Beaker blanks were also run during the period of analysis, to ensure that the beakers were totally clean prior to weighing of samples. An amount of spike or standard was added to a cleaned beaker. This was dried down and loaded onto a filament and run on the machine, any difference from the known spike or standard values should have come solely from the beaker.

Column yields were carried out on the varying cationic and anionic columns. A known amount of a Sr, Nd, Pb, U, Th or Ra (see section 2.6 for greater details on Ra) standard solution was weighed out into a clean savillex beaker. They were dried down and taken up in whichever acid was suitable for the appropriate column. The solution was loaded onto the column and the normal column procedure was followed, the aliquot containing the particular element was collected and then spiked with the appropriate isotope, the solution was

then dried down and loaded onto machine and run as normal samples. If the yield from the column was less than expected (< 90 %), a column calibration was repeated. Individual aliquots were collected from solution and eluant coming through the column, these were spiked separately and the amount of isotope present in each aliquot was calculated from the values run on the MAT 261 or MAT 262.

C.9. Mass Spectrometry

All Sr and Pb analysis were carried out on a Finnigan MAT 261 multi collector mass spectrometer at the Open University, whilst Nd, U, Th and the majority of Ra analyses were carried out on the Finnigan MAT 262. (The software interface was developed for use by David W. Wright and Peter W. C. van Calsteren.)

Sr isotope ratios were fractionation corrected to $^{86}Sr/^{88}Sr = 0.1194$ and Nd to $^{143}Nd/^{144}Nd = 0.7219$. Pb was analysed in temperature controlled runs (1255 °C) and the ratios corrected for ~1‰ per atomic mass unit mass-fractionation using our values for NBS 981, $^{206}Pb/^{204}Pb = 16.934$ (±2), $^{207}Pb/^{204}Pb = 15.414$ (±2), $^{208}Pb/^{204}Pb = 36.553$ (±2).
Pb values were corrected by the equation

$$\left(\frac{20xPb}{20xPb}\right) Meas.Ratio/(1 - fractionation\,factor \times (\text{Diff. in Fractionation})$$

The correction obtained change the measured value by very little.

Sr and Nd isotope ratios were normalised with respect to internally determined values for NBS 987 = 0.710220 (±10) and Johnson and Matthey Nd = 0.511776 (±5). Quoted errors are 1 standard deviation, and errors on individual runs are significantly less than the quoted reproducibility. Total procedure blanks for Sr, Nd and Pb were typically <0.8 ng, 0.3 ng and 0.3 ng respectively. There was a period as previously mentioned with higher Sr blanks up to 100 ng due to the use of 99% pure saturated boric acid (to aid in the dissolution). Its use was discontinued when found subsequently to have a high reagent blank.

C.10. Age corrections

Age corrections for measured $^{87}Sr/^{86}Sr$ and $^{143}Nd/^{144}Nd$ for the historic and recent prehistoric lavas were so small that they were within analytical error of the technique, therefore could not be realistically corrected for.

C.11. Radiogenic monitoring

During the time in the radiogenic U-Th lab, it is necessary to monitor the amount of radiation, for safety and legal reasons, this is done by recorded monthly checks using α and β radiation counters. In the case of a spillage, the spill was cleared up and the area was checked with the counters, any accidents such as a spillage were recorded in a general radiation use lab book. This is also the case, if a new spike was being made up, after preparation the area would be checked to ensure levels of radiation below background.

For legal reasons the lab must submit monthly radiation returns to the radiation officer (Dr Nick Rogers), i.e. the amount of radiation (or in measured terms - the amount of spike used per person) used during that month in the lab. This duty was passed onto myself when David Peate left, and continued from March 97 to October 1998.

APPENDIX D

Rock Standards

Rock standards run in the U-series laboratory over the time period of analysis.

	U (ppm)	Th (ppm)	($^{238}U/^{232}Th$)	($^{230}Th/^{232}Th$)	($^{230}Th/^{238}U$)
ATHO	2.2639 ±3.60% (n = 12)	7.2554 ±3.79% (n = 14)	0.9465 ±1.84% (n =14)	1.0220 ±1.33% (n = 14)	1.0887 ±1.6% (n = 14)
TML	10.7806 ±0.94% (n = 5)	29.3244 ±2.96% (n = 3)	1.1161 ±3.46% (n = 3)	1.1055 ±10.2% (n = 3)	0.9991 ±6.75% (n = 3)
Mt. Lassen	2.7616 ±2.69% (n = 6)	8.3768 ±1.43% (n = 5)	1.0071 ±2.06% (n = 4)	1.0655 ±1.58% (n = 5)	1.0605 ±2.05 (n = 4)

	^{226}Ra	$^{228}Ra/^{226}Ra$
ATHO	1.280 ±0.013 pg/g (n = 2)	884.79 (n= 2)
Mt Lassen	1.07 ± 0.011 pg/g (n = 8)	508.71 ± 5.21 (n = 8)
Mt Lassen	1.063 ± 0.010 pg/g	312.26 ± 5.21
(Volpe et al. 1991)	1.068 ± 0.011 pg/g	311.91 ± 4.62

APPENDIX E

Extensions to the Ra technique

This appendix includes work on the 1ml Sr Spec Resin column by Georg Zellmer and the adaptation of large (10ml) cationic resin columns to do Ra chemistry of low concentration and hence large sample amounts by Thomas Kokfelt and David Peate. The possibility of column capacities too low for more evolved rocks like the Kameni dacites was anticipated. Thus, two modifications of the Ra column procedure were undertaken: Firstly, the second cationic column was scaled up from 0.6 ml to 2 ml. Secondly, the Sr-Spec® column was scaled up to 1 ml, using a 2 ml quartz column, and was recalibrated, starting from the elution procedure outlined by Chabaux et al. (1994).

E.1. Procedure for a 10 ml cationic resin column (TFK and DWP).

10 ml of 200-400 x8 mesh Biorad cationic resin were placed in to a cleaned glass column. The resin was washed with QD 6M HCl and RO H_2O and then preconditioned with 15 ml of 2.5M HCl. The sample was the 7M HNO_3 portion taken from the U-Th columns. This was dried down and converted into HCl, by the repeated addition and drying down of 6M HCl and then taken into 2.5M HCl. The sample was loaded onto the column in 4 ml of 2.5M HCl, 2 x 1 ml of 2.5M HCl were washed through, to wash the sample onto the column and then 36 ml of 2.5M HCl were eluted through. If collecting for other REE at the same time, it is possible to remove the Sr fraction, by the addition of another 14 ml of 2.5M HCl. 5 ml of 3.75M were then eluted and the Ra/Ba fraction were collected in another 4 ml of 3.75M HNO_3. Another 2 ml of 3.75M HNO_3 were eluted and the rest of the REE were collected in a further 12 ml of 3.75M HNO3. (Nd comes off in the first 9 ml).

E.2 Scaling up the second cationic column

2 ml cationic resin was used during the second preconcentration step. After preconditioning, 35 ml 3M HCl were used to load and elute the sample. Then, the Ra-bearing fraction was collected in 15 ml 3.75M HNO_3. Using a larger resin volume also meant that small perturbations of the resin-acid boundary had less effects on separation efficiency.

E.3 Setting up and calibrating the 1 ml Sr-Spec® column

Using a 1ml Sr-Spec® column resulted in a larger resin-acid boundary. To prevent the resin from being disturbed during acid additions, it was topped with ~100 µl of inert Biorad biobeads.

An unspiked sample of known ^{226}Ra concentration was loaded onto the preconditioned column and washed on in a total of 1 ml 3 M HNO3. Subsequently, six 1 ml elutions were collected separately and each was spiked with ^{228}Ra spike and analysed by TIMS. It was found that all ^{226}Ra had been extracted with the first 2 ml eluted immediately after loading the sample. This result differed from the elution systematics of Chabaux et al. (1994) who suggested the sample should be washed on with ca. 3 ml 3M HNO_3 before Ra collection. Clearly, using their procedure all Ra would have been lost.

This was very surprising, and the calibration was repeated: First, the 1 ml Sr-Spec® column was cleaned by ample washing with 3M HNO_3 and 0.5M HNO_3 to ensure complete elution of the Ba and Sr peaks. Cleaning the column was preferred to setting up a new 1 ml column for economical reasons. During the second calibration, which was undertaken using a Ra standard solution to which some Ba spike was added, no Ra was eluted in the first 2 ml, but almost all in the following 2 ml. While this result was still incompatible with observations by Chabaux et al. (1994), it was even more surprising that this second calibration differed so much from the first.

It was concluded that the Sr-Spec® resin changed its adsorption properties during elution of 3M HNO_3. This conclusion was supported by another observation: When the first column calibration was commenced by ample preconditioning with 3M HNO_3, it was noticed

that the resin became light green in colour, a change not observed using 150 µl polyprep columns, probably because of their low transparency compared to the quartz glass columns. Starting from the Sr-Spec® - biobeads interface, the colour slowly migrated downwards through the column and became fainter and fainter throughout the separation procedure, until it was not noticeable any more close to the end of the column cleaning stage. While an immediate explanation of this colour change is not at hand, it may be that the crown ether of the Sr-Spec® resin was modified during HNO_3 elution, resulting in changes of its adsorption properties. All 1 ml Sr-Spec® columns set up subsequently were preconditioned with 3M HNO_3 until the resin's green tint disappeared, and then the second column calibration was used.

Using the modified separation procedure, analyses of Ra by TIMS were slightly more successful as interferences observed on mass numbers 225, 227 and 229 almost always dropped to well below 10% of Ra peaks on mass numbers 226 and 228.

APPENDIX F

Partition Coefficient and OIB and MORB values

Partition Coefficients from compilation by Halliday et al. (1995) and Rollinson (1993).

	Ol	Cpx	Opx	Garnet	phlogopite
Ba	0.000005	0.0003	0.000006	0.00007	1.5
Rb	0.0003	0.0004	0.0002	0.0002	1.7
Th	0.000007	0.0021	0.000020	0.0021	
U	0.000009	0.001	0.00004	0.011	0.00030
K	0.00002	0.001	0.00010	0.013	1.50
Nb	0.00005	0.009	0.003	0.007	0.140
La	0.0002	0.0540	0.0031	0.0007	0.0030
Ce	0.00007	0.0860	0.0021	0.0026	0.0210
Pb	0.0003	0.0075	0.0014	0.0003	0.0043
Sr	0.00004	0.0910	0.0007	0.0007	0.0440
Nd	0.0003	0.1900	0.0023	0.0270	0.0063
Sm	0.0009	0.27	0.0037	0.22	0.0059
Zr	0.001	0.260	0.012	0.200	0.130
Hf	0.0029	0.3300	0.0190	0.2300	
Ti	0.015	0.40	0.086	0.60	0.98
Y	0.0082	0.47	0.015	2.00	0.03
Tb	0.0015	0.0190	0.3100	0.7500	
Yb	0.024	0.430	0.038	3.6 *	0.030

* See note in Chapter 3. KD from McKenizie and n'Nions, 1991

OIB, MORB and Primitive mantle values from Sun and McDonough, (1989)

	Average OIB	N-MORB	E-MORB	Primitive Mantle
Ba	350	6.30	57	6.99
Rb	31	0.56	5.04	0.64
Th	4.00	0.12	0.60	0.09
U	1.02	0.05	0.18	0.02
K	12000	600	2100	250
Nb	48	2.33	8.30	0.71
La	37	2.50	6.30	0.69
Ce	80	7.50	15	1.78
Pb	3.20	0.30	0.60	0.07
Sr	660	90	155	21.10
Nd	38.50	7.30	9	1.35
Sm	10	2.63	2.60	0.44
Zr	280	74	73	11.20
Hf	7.80	2.05	2.03	0.31
Ti	17200	7600	6000	1300
Y	29	28	22	4.55
Tb	1.05	0.67	0.53	0.11
Yb	2.16	3.05	2.37	0.49

APPENDIX G

New Stratigraphy for Teide-Pico Viejo Complex

This stratigraphy is still undergoing modification, so for the purpose of this project the older stratigraphy was used. The differences are outlined below.

The chemical recognition of Teide Series (low pressure evolution) and Pico Viejo Series (high pressure evolution) is retained but not emphasised. Teide is divided into 3 exposed members - El Piton (t3), Canada Blanca (t1b, t2) and crystal-rich tephrite-phonolite (t1a), and 8 members revealed in borehole S-1 (see figure 3.5) (not analysed in this project). Pico Viejo is divided into 2 main groups of products. The Early products are the Teide Series (pv2-3) which have become the Asientos Altos (PV-C) and PV-D respectively. PV-A and PV-B are only found in a gallery excavated into Pico Viejo. El Encerado or PV-E is the youngest of the Teide series lavas erupted from PV and includes plagioclase basanites found in the boreholes, formerly identified as part of pv3 and pv2 respectively.

Young Pico Viejo rocks are changed from pv 4,5 and 6 to PV-F, G and H. Roques Blancos (pv7) becomes tentatively part of the Teide Flank vent group and is denoted as the Roques Blancos member (PV-I). pv8 becomes caldera fill or PV-J, whilst pv9 become PV-K. The Montaña Chircheros member (part of pv9), Montaña Reventada (pv11) and Montaña Chahorra (pv12) members are young flank eruptions (PV-L-M).

Teide Satellite vents are divided into depending on the chemical composition of the eruptions. Intermediate flank vent eruptions including Montaña Negra, Los Tomillos, Volcan Corona, Volcan Tapada and Montaña de los Corrales (mc1-mc2) erupting phono-tephrites, and felsic flank vents including Roques Blancos, Majua and Montaña de la Cruz. Of the mafic vents on the caldera floor (cf1), these are now 4 groups Siete Canadas A, Siete Canadas B, Montaña Cerillar and Montaña Mostaza. SCA and SCB are basanites only seen in

bolehole S-2, whilst Montaña Mostaza is an alkali basalt. T7-18-1, T7-18-3, T7-18-4 and T7-18-5 belong to Montaña Cerillar and are basanitic.

The Montaña Blanca members (mb1-4) are split into Upper and lower series and probably evolved from the last input into the chamber beneath Pico Viejo.

APPENDIX H

U-Series Age Calculations

1. Calculation of the initial ($^{230}Th/^{232}Th$), using a known or estimated age.

Rearrange the decay equation for chapter 2 so that $(^{230}Th/^{232}Th)_i$ is being solved for.

$$(^{230}Th/^{232}Th)_i = (^{230}Th/^{232}Th)_m - (^{238}U/^{232}Th)_m (1-e^{-\lambda})e^{\lambda t}$$

2. Calculation of timescale within older Teide rocks.

$$(^{230}Th/^{232}Th)_i = ((^{230}Th/^{232}Th)_m - (^{238}U/^{232}Th)_m)e^{\lambda(t-T)} + (^{238}U/^{232}Th)_m$$

$(^{230}Th/^{232}Th)_i = 0.78$; $(^{230}Th/^{232}Th)_m = 0.872$; $(^{238}U/^{232}Th) = 0.819$

λ^{230}	9.1952E-6
λ^{232}	4.9475E-11

Therefore the timescale of differentiation in the Teide rocks = 87,044 years

3. Using the decay equation discussed in chapter 2 it is possible to calculate the time taken for the complex to evolve.

$$(^{230}Th/^{238}U)_m = (^{230}Th/^{238}U)_i e^{-\lambda t} - e^{-\lambda t} + 1$$

This can be re-arranged to become

$$(^{230}Th/^{238}U)_m = (^{230}Th/^{238}U)_i - 1)e^{-\lambda t} + 1$$

As an example the age of part of the the complex can be calculated as follows
$(^{230}Th/^{238}U)$ of youngest sample = 1.05, taken as the measured concentration

$(^{230}Th/^{238}U)$ of the oldest sample = 1.2, taken as initial concentration

Therefore

$$1.05 = (1.2 - 1)e^{-\lambda t} + 1$$

$$0.05 = 0.2e^{-\lambda t} + 1$$

$$0.25 = e^{-\lambda t}$$

$$-\lambda t = \ln(0.25)$$

$$t = 150762.82$$

APPENDIX I

Conference Abstracts

AGU Chapman Conference 10-16th November 1996

Shallow level Processes in Ocean Islands

U Series Disequilibria - Melt Generation Beneath Lanzarote

[*L E Thomas*]; C J Hawkesworth; P V Calsteren; S P Turner;

Dept of Earth Science, The Open University, Walton Hall, Milton Keynes

The 1730-35 and 1824 eruptions on Lanzarote include some unusually primitive rocks that range from silica undersaturated to silica saturated. They exhibit striking negative arrays between K_2O, Zr, Nb/Y and SiO_2 that are attributed to variations in the depth and degree of partial melting. $^{87}Sr/^{86}Sr$ is relatively restricted for all compositions (0.7031- 0.7033), ($^{230}Th/^{232}Th$) = 0.92-1.28, and most samples have lower ($^{230}Th/^{232}Th$) than other oceanic basalts with similar Sr isotope ratios. Excess ^{230}Th ranges from 6-80%, but the higher ($^{230}Th/^{238}U$) occur in those rocks which are silica undersaturated and have high Nb/Y and Th abundances. U/Th ratios appear to be unfractionated during partial melting, and ($^{230}Th/^{238}U$) in the silica saturated rocks are consistent with melt generation rates of approximately 10^{-4} kg m^{-3} yr^{-1}. However, the negative trend between ($^{230}Th/^{238}U$) and Th contents in the silica undersaturated rocks requires more complex melting models [Williams and Gill, 1989]. One interpretation is that there was an inverse relation between the degree of melting and the time spent in the melting regime, with the smaller degree melts having been extracted in shorter times than the higher degree melts. These data will be compared with new analysis of more evolved rocks from the Teide-Pico Viejo complex on Tenerife.

VMSG Cambridge January 1997

U-Th Disequilibria and Dynamic melting models - An example from Lanzarote, Canary Islands

L.E.Thomas, C.J.Hawkesworth, P.V.Calsteren, S.P.Turner

Department of Earth Science, The Open University, Walton Hall, Milton Keynes, Bucks,

Simple batch melting models (Shaw, 1970) can be used to model many minor and trace elements, however they cannot reproduce U-series disequilibria except at unrealistically small melt fractions. To successfully model U-Th disequilibria it is necessary to involve dynamic melting. Thus a number of authors (e.g.McKenzie, 1985) have presented detailed dynamic melting models to elucidate the controls and the processes involved in mantle melt generation and extraction from source regions.

The Canary Islands are underlain by a region of low buoyancy flux, it has been argued that the degree of U-Th disequilibria in OIB varies inversely with the buoyancy in the underlying mantle (Chabaux and Allegre, 1994) hence we would expect to find significant disequilibria. The historic lavas analysed from Lanzarote (samples from 1730-36, 1824 and Corona eruptions) are some of the most primitive rocks found in ocean intraplate settings with Mg numbers close to 70 and high Ni and Cr contents. This primitive nature allows comparison with primary mantle melts after only minor correction for olivine fractionation. The rocks range from silica saturated to undersaturated, and exhibit marked negative arrays between K_2O, Zr, Nb/Y and silica, which can be used to constrain the degrees and depth of melting. The source regions for Lanzarote are relatively deep within the garnet melting zone and the overall degrees of melting range from 1-10%. They exhibit significant U-Th isotopic disequilibrium with $^{230}Th/^{238}U$ varying from 1.06 to 1.81 and ^{230}Th excesses of 6-81%: however the restricted ranges of Sr, Nd and Pb isotopes lie within the fields generally accepted for OIB. $^{230}Th/^{238}U$ in the silica saturated rocks are consistent with melt generation rates of approximately $10^{-4}kgm^{-3}yr^{-1}$ but the silica undersaturated rocks require a more complex melting model, perhaps one with smaller degree melts being extracted more rapidly than the larger degree melts.

Rate and Timescales Meeting London November 1997

Rates and Timescales of Melt Generation and Differentiation as inferred from U-series Isotope Variations on Lanzarote and Tenerife, Canaries

L.E.Thomas, C.J.Hawkesworth, P.van Calsteren

Department of Earth Sciences, The Open University, Walton Hall, Milton Keynes, MK7 6AA, UK.

U-Th-Ra disequilibria can be used to constrain the rates and timescales of melt generation and differentiation beneath ocean islands. The islands of Lanzarote and Tenerife provide contrasting eruptive styles and compositions, ranging from exceptionally high MgO basalts and basanites to phonolites. The islands occur very close to the West African continental shelf, and the surrounding water depths increase westwards, even though there appears to be no detectable change in lithosphere thickness. All the islands are underlain by a region of low buoyancy flux, and the magmas exhibit significant ($^{230}Th/^{238}U$) disequilibrium.

Historic and recent prehistoric lavas from Lanzarote have some of the most primitive compositions found on oceanic islands. Samples have been analysed from the 1824, 1730-35 and ~10,000 year old eruptions. These rocks show low silica contents (<50.8%), MgO = 10.7-12.6%, Mg numbers are > 67, Ni and Cr = 232-394 ppm and 383-560 ppm respectively, La/Nb = 0.52-0.97, La/Yb = 11.5-35.5 and Nb/U = 36.2-73.5. The rocks have a restricted range in Sr, Nd and Pb isotopes, which are displaced from MORB towards the HIMU OIB field. The eruptive style on Lanzarote is of fairly low volume, small vent and fissure eruptions which have covered most of the island with basaltic lavas. The primitive compositions are consistent with the lack of evidence for significant magma chambers in the area, and suggest that these magmas were extracted relatively rapidly from the zones of melt generation.

The Teide-Pico Viejo complex of Tenerife has undergone a much more complicated evolution. The rocks show a wide compositional range from basanite to phonolite with silica varying from 42.2 to 59.9%, MgO = 0.34-11.26%, Ni and Cr = 0.5-227 ppm and 0-483 ppm respectively, La/Nb = 0.45-0.7, La/Yb = 21.3-30.2 and Nb/U = 21.1-90.3. Teide and Pico Viejo form a large stratovolcano with high volume eruptions of different compositions tapping different areas in the volcano's plumbing system. Magma generated in the mantle has been partly ponded in the underlying chambers, evolved over time, and mixed with influxes of newly generated magmas from below forming differentiates from basanite to

phonolite compositions. Some primitive melts have however found a route to the surface, as basanite and basalt compositions are found alongside phonolites.

Historic and recent prehistoric lavas analysed from both islands exhibit U-Th disequilibria with ($^{230}Th/^{238}U$) varying from 1.06 - 1.81 for Lanzarote and 1.004 -1.39 for Tenerife. Rocks younger than 8000 years old show ^{226}Ra excesses. On Lanzarote the 1824 lavas have lower SiO_2, higher Fe_2O_3 and incompatible element abundances than the 1730-36 rocks, but with similar radiogenic isotope ratios. Striking trace element arrays in the bulk rock compositions corrected for olivine fractionation cannot be modelled by progressive degrees of partial melting with accepted relative distribution coefficients. Instead they reflect magma mixing processes which appear to have persisted for several thousand years. The end-member compositions have been modelled as ~1 and 5 % melts, with the smaller degree melts generated at greater depths. The inferred source for all the lavas is garnet lherzolite with minute amount of phlogopite mica (<0.5%) and minor and trace elements similar to Sun and McDonoughs' (1989) primitive mantle. Melt generation rates of $5*10^{-4}$ $kg.m^{-3}.yr^{-1}$ are consistent with the disequilibrium data for the island of Lanzarote.

Disequilibrium data for the Teide-Pico-Viejo suite of rocks shows the strong evidence of decay through time within different suites generated in magma chambers. The rocks are modelled by fractionation and mixing with newly generated melts, and one sequence of closed system evolution suggest that basalt to phonolite differentiation took ~ 200Ka.

VMSG 1998 Leicester

Magmatic Processes in Oceanic Islands

A Short Lived Isotope Study from the Canary Isles

L.E.Thomas, C.J.Hawkesworth, P.van Calsteren

Department of Earth Sciences, The Open University, Walton Hall,

Milton Keynes, MK7 6AA, Bucks.

U-Th-Ra disequilibria are used to constrain rates and timescales of melt generation and extraction from the source region beneath ocean islands. The apparent controls on the conditions of melt generation are the thickness of the lithospheric lid, potential temperature and the buoyancy flux of the upwelling mantle plume. The Canary Islands are underlain by a region of low buoyancy flux and consequently relatively low degrees of melting and significant ($^{230}Th/^{238}U$) disequilibrium. Historic and recent prehistoric lavas analysed from Lanzarote and the Teide-Pico Viejo complex of Tenerife exhibit U-Th disequilibria with ($^{230}Th/^{238}U$) varying from 1.06 - 1.81 for Lanzarote and 1.004 -1.39 for Tenerife. Despite this similarity in disequilibria the islands shows different eruptive styles and compositions, with highly primitive melts from deep mantle on Lanzarote to a range from basanite to phonolite compositions influenced by the presence of magma chambers on Tenerife.

For the suites of rocks analysed from Lanzarote, the simplest interpretation is the 1824 lavas reflect smaller degrees of melting (~1%) at greater depths (due to their lower SiO_2, higher Fe_2O_3 and incompatible element abundances) than the 1730-36 rocks which require larger degrees of melting (~8%) at shallower depths. Mixing these end member melt compositions models the data array. All the rocks have similar Sr, Nd and Pb isotopes indicating that the magmas were derived from similar sources.

The Teide-Pico Viejo complex of Tenerife has undergone a much more complicated evolution, requiring numerous fractionation events, melting and mixing in a number of underlying magma chambers.

The bathymetry and seismic data for the Canaries shows the islands closest to the African continent are surrounded by shallower water depths and much thinner crustal thickness', than those further west. However the lithospheric thickness beneath all the islands is a constant 125km, which may mean that lithospheric thickness has influenced the conditions of melt generation within the island group.

Tenerife Workshop May 1998

Rates & Timescales Of Melt Generation And Differentiation In The Teide-Pico Viejo Complex, Inferred From U-Series Isotope Variations

Louise Thomas, Chris Hawkesworth, Peter van Calsteren

Department of Earth Sciences, The Open University, Walton Hall, Milton Keynes UK.

Ocean island basalts provide important windows into the compositional variations of the Earth's mantle, which in turn constrains models for mantle convection and evolution (McKenzie and O'Nions, 1995). These geochemical signals arriving at the surface have been modified by a number of processes, including melting, melt segregation, fractionation, mixing and contamination. Uncertainty remains regarding the contribution from various geochemical components, such as lithospheric contamination, metasomatism and input from recycled crust. U-Th-Ra disequilibria can be used to constrain rates and timescales of melt generation and differentiation beneath ocean islands, and to observe effects from controlling factors, such as the influence of the lithosphere lid, the buoyancy flux or potential mantle temperature and the degree and depth of melting (Thomas et al, 1998). The Canary Islands provide an excellent opportunity to observe U-Th-Ra disequilibrium, because they are underlain by a region of low buoyancy flux (i.e. low mantle potential temperatures) and hence are expected to show significant disequilibrium. Whilst regions of higher mantle temperatures and higher buoyancy flux (e.g. Hawaii) tend towards smaller amounts of disequilibrium and lower melt fractions (Sleep, 1990; Chabaux and Allègre, 1994).

The Teide-Pico Viejo complex has undergone a complicated evolution and lava compositions range from basanite to phonolite with silica varying from 42.2 to 59.9%. Melting at depth in the mantle in the garnet stability field generates ^{238}U-^{230}Th disequilibrium. These melts are in part ponded in magma chambers below the complex, evolving over time and mixing with newly generated magma from below, forming differentiates. Some primitive melts do find routes to the surface as basaltic compositions are found alongside phonolites. Lavas analysed from Teide-Pico Viejo suite exhibit ($^{230}Th/^{238}U$) disequilibrium ranging from 1.004 to 1.39, and hence fractionation took place less than 350K years ago. ($^{230}Th/^{238}U$) increases with decreasing SiO_2 and hence smaller degree melts have larger amounts of disequilibrium. A sequence of closed system evolution for the older Teide rocks suggests that basalt to phonolite differentiation took ~200 Ka. The magma chambers beneath Tenerife are thought to have undergone cyclic removal of magma and refill. ($^{230}Th/^{238}U$) increases in cycles separated by an abrupt decrease as the lavas become younger through the Teide-Pico Viejo sequence. Montaña Blanca eruptions increase in ($^{230}Th/^{238}U$) as they evolve. There is then a sharp decrease prior to the historic eruption of 1492, ($^{230}Th/^{238}U$) then increases until the

most recent activity in 1909. This cyclic behaviour allows inferences regarding melting and subsequent mixing within the magma chambers, as ($^{230}Th/^{238}U$) re-equilibrates after fractionation. ^{226}Ra-^{230}Th disequilibrium is present in rocks younger than 8,000 years. A whole rock isochron gives an age of 2.3 Ka for the Montaña Blanca 2020 b.p. eruption, indicating ^{226}Ra-^{230}Th fractionation into feldspar just prior to eruption and that melt transport was therefore relatively rapid.

References

Chabaux F. and Allègre C.J. (1994) *Earth. Planet. Sci. Lett.* **126,** 61-74.

McKenzie D. and O'Nions R.K. (1995) *J. Pet.* **36,** No 1, 133-159.

Sleep, N.H. (1990) *J. Geophys. Res.* **95,** 6,715-6,36.

Thomas. L. E. et al. (1998) Geochim. et Cosmochim. Acta (submitted)

Goldschmidt August 1998

Rates and timescales of melt generation and differentiation in the Teide-Pico Viejo Complex, Tenerife, inferred from U-series isotopes

Louise Thomas
Chris Hawkesworth
Peter van Calsteren
Department of Earth Sciences, The Open University, Walton Hall, Milton Keynes UK.

Giray Ablay
Consejo Superior de Investigaciones Científicas, Institut de Ciències de la Terra "Jaume Almera", Lluis Solé I Sabaris s/n. 08028 Barcelona, Spain.

U-Th-Ra disequilibria can be used to constrain the rates and timescales of melt generation, differentiation and crustal residence prior to eruption. Ocean island basalts (OIB) provide important windows into the compositional variations in the Earth's mantle, and they are therefore widely used to evaluate models for mantle convection and evolution (McKenzie and O'Nions, 1995). However, the effects of melt generation and migration remain controversial, as do the depths of the source regions sampled by OIB. This study presents new mass spectrometric U-Th-Ra isotope analyses of well characterised samples from the Teide-Pico Viejo complex on Tenerife in the Canary Islands, to investigate the effects and timescales of shallow level basalt-phonolite differentiation, and the conditions of melt generation. The Canary Islands provide an excellent area to observe U-Th-Ra isotope disequilibrium in historic lavas because they are underlain by a region of relatively low buoyancy flux, and so there is sufficient time to develop U-Th-Ra disequilibria during melting (Chabaux and Allegre, 1994). This is in contrast to areas like Hawaii where the faster mantle upwelling rates (Sleep, 1990), and associated melt generation rates, inhibit such isotope disequilibria.

The Geology and Geochemistry of The Teide-Pico Viejo complex, Tenerife

The Teide-Pico Viejo complex of Tenerife has formed in the caldera of the Las Cañadas volcano since 175 Ka. The vent system of Teide, Pico Viejo and Montaña Blanca forms a large stratovolcano complex with high volume eruptions tapping 2 distinct basanite to phonolite lineages (Ablay et al, 1998) from different segments of the volcano's plumbing system. There are believed to be a number of underlying magma chambers at different depths beneath the complex, with lavas ranging from basanite to phonolite, with SiO_2 = 42.2 - 59.9%, MgO = 0.34 - 11.26%, Ni and Cr = 0.5 - 227 ppm and 0 - 483 ppm respectively. The Teide-Pico Viejo complex is divided up into a number of units on the basis of geochemistry (Ablay et al. 98). The group comprising of the caldera floor lavas and the latest historic eruptions are mafic ranging from basanite to trachy-basalt in composition, with the highest MgO (>6 %) Ni and Cr and lowest alkalis and Zr abundances of the samples analysed. The Teide Series comprises of the products of Pico Teide, the oldest parts of Pico Viejo and Montaña Blanca. This suite ranges in composition from plagioclase basanite to phonolite, showing a considerable range in major and trace elements. The youngest Pico Teide and the Teide flank eruptions tend to be the most evolved. Finally the Pico Viejo Series consists of the youngest Pico Viejo and Montaña Blanca rocks, again ranging in composition from plagioclase basanite to phonolite, with the youngest Pico Viejo lavas having more intermediate compositions, while the Montaña Blanca are the most evolved phonolites in the complex. This series show Ba enrichment relative to the Pico Teide series and the Mafic series, despite similarities in most of the other major and trace elements.

U-Th-Ra Isotopes

The lavas analysed range in age from ~ 175 Ka to the most recent eruption in 1909 and the vast majority exhibit ^{230}Th-^{238}U disequilibrium with ($^{230}Th/^{238}U$) = 1.004 - 1.39 (Fig. 1). In addition one cumulate has been analysed and that has excess ^{238}U and ($^{230}Th/^{238}U$) = 0.90.

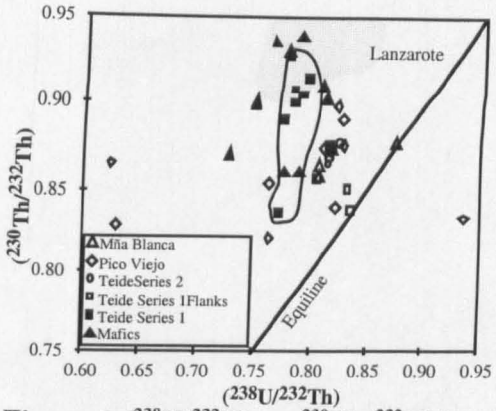

Figure 1 ($^{238}U/^{232}Th$ vs $^{230}Th/^{232}Th$)

In detail the basanites have ($^{230}Th/^{238}U$) = 1.09 - 1.23, and the phonolites have ($^{230}Th/^{238}U$) = 1.004 - 1.09, and so there is a general decrease in the degree of ^{230}Th-^{238}U disequilibrium with increasing SiO_2 (Fig. 2). This might reflect progressive contamination with crustal material that was in or close to isotope equilibrium, but there is no systematic increase in, for example, Sr isotopes with increasing SiO_2. This suggests that contamination with crustal material is unlikely, unless the contaminant was recently crystallised magma from the same system. Alternatively the overall decrease in ($^{230}Th/^{238}U$) with increasing silica might be an indication of the average time for differentiation to phonolite.

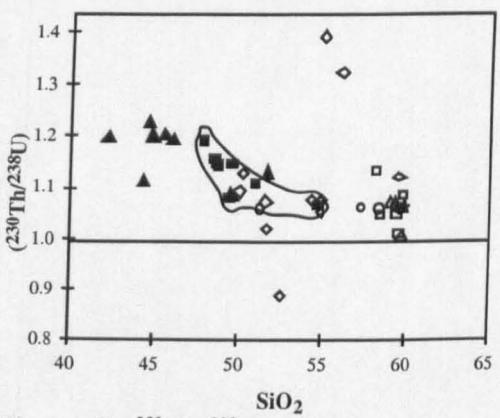

Figure 2 ($^{230}Th/^{238}U$) vs SiO_2

This can be seen in more detail in the Older Teide Series which includes the earliest Teide and the earliest Pico Viejo rocks, in which silica = 47.8 - 54.9 %, but U/Th and Sr and Nd isotopes are constant. ($^{230}Th/^{238}U$) decreases from 1.16 to 1.07 with increasing silica. This suggests basalt to phonolite differentiation took ~200 Ka, even though these magmas were erupted in 50 - 100 Ka. The magma chambers beneath Tenerife are thought to undergo cyclic removal of magma and refill. A possible scenario may have been that the magma evolved in a chamber and some erupted, whilst the rest underwent mixing with newly generated magma and perhaps remelting of more silicic wall rocks, which would have similar Sr and Nd isotopes. This more evolved composition then undergoes further fractionation and decay. The timescale of 200 Ka is significant from a geological and volcanological perspective, since it is the approximate length of time that occurs between the major cycles in the Upper group of the caldera wall, and hence the Las Cañadas volcano.

A residence time of 87 Ka has been determined (Allègre and Condomines, 1976) from the 1492 Teide eruption, consistent with the more rapid stratigraphic evolution of the Teide succession to an evolved intermediate composition which may be parental to the Teide phonolite. The phonolites seem to have separated from the main body of evolving intermediate magmas relatively early on, and were erupted halfway up the succession. Hence we can assume an age of approximately half to a third of the evolution of Teide-Pico Viejo complex (60-90 kys). Furthermore ($^{230}Th/^{238}U$) decreases in cycles as the lavas increase in age throughout the Teide-Pico Viejo sequence. Some of these cycles are close to vertical on an equiline diagram allowing observation of decay through time, whilst the higher ($^{230}Th/^{238}U$) range gives information about conditions of melt generation and mixing.

The mafic compositions (basanite to alkali basalt) in the Teide-Pico Viejo complex can be compared with similar compositions in the historic lavas of Lanzarote (Fig 1). The range of ($^{238}U/^{232}Th$) in the Lanzarote lavas is similar to that in Tenerife, but the ($^{230}Th/^{232}Th$) in Lanzarote tends to be higher than many of the Tenerife mafics (Thomas et al., 1998). The range in ($^{230}Th/^{238}U$) in Lanzarote is attributed to mixing between different melt fractions generated at different depths in the melting zone in the presence of residual garnet, using a constant melt rate of 0.125×10^{-3} $kg.m^{-3}.yr^{-1}$ and varying the matrix transfer time.

$^{226}Ra/^{230}Th$ disequilibrium is present in rocks younger than 8,000 years. A preliminary whole rock isochron gives an age of 2.3 Ka for the Montaña Blanca 2020 b.p. eruption, indicating (^{226}Ra-^{230}Th) fractionation into feldspar just prior to eruption.

References

Ablay, G.J., Carroll, M.R., Palmer M.R., Marti, J. and Sparks, R.S.J. (1998) *J. Pet.* May (In press)

Allegre C.J. and Condomines M. (1976)) *Earth. Planet. Sci. Lett.* **28,** 395-406

Chabaux F. and Allègre C.J. (1994) *Earth. Planet. Sci. Lett.* **126,** 61-74.

McKenzie D. and O'Nions R.K. (1995) *J. Pet.* **36,** No 1, 133-159.

Sleep, N.H. *(1990) J. Geophys. Res.* ***95,*** 6,715-6,36.

Thomas. L. E. et al. (1998) *Geochim. et Cosmochim. Acta* (submitted)